Rozprawa doktorska

# Wpływ parametrów sprężystych skał na proces hydraulicznego szczelinowania dla potrzeb wspomaganych systemów geotermalnych (EGS) na terenie Polski

*Autor:*
mgr Rafał Moska

*Promotor:*
prof. dr hab. Krzysztof Labus

*Opiekun ze strony przedsiębiorstwa:*
dr hab. inż. Piotr Kasza, prof. INiG-PIB

Politechnika Śląska

Dyscyplina naukowa: Inżynieria Środowiska, Górnictwo i Energetyka

Gliwice, 2025

**Autor:**
mgr Rafał Moska
Politechnika Śląska
Wydział Górnictwa Inżynierii Bezpieczeństwa i Automatyki Przemysłowej
Katedra Geologii Stosowanej
ul. Akademicka 2, 44-100 Gliwice
e-mail: rafal.moska@polsl.pl

**Promotor:**
prof. dr hab. Krzysztof Labus
Wydział Górnictwa Inżynierii Bezpieczeństwa i Automatyki Przemysłowej
Katedra Geologii Stosowanej
ul. Akademicka 2, 44-100 Gliwice
e-mail: krzysztof.labus@polsl.pl

**Opiekun ze strony przedsiębiorstwa:**
dr hab. inż. Piotr Kasza, prof. INiG-PIB
Zastępca Dyrektora ds. Eksploatacji Złóż Węglowodorów
Instytut Nafty i Gazu – Państwowy Instytut Badawczy
ul. Lubicz 25A, 31-503 Kraków
e-mail: kasza@inig.pl

**Tytuł w języku angielskim:**

**The impact of rock elastic parameters on the hydraulic fracturing process for Enhanced Geothermal Systems (EGS) in Poland**

*Agnieszce i Lidii*

***Podziękowania***

*Składam serdeczne podziękowania wszystkim osobom, dzięki którym realizacja tej pracy doktorskiej była możliwa.*

*W szczególności chciałbym podziękować Promotorowi pracy Panu prof. Krzysztofowi Labusowi za opiekę naukową, przekazaną wiedzę, zaangażowanie i poświęcony czas.*

*Serdecznie dziękuję także opiekunowi ze strony przedsiębiorstwa, Panu prof. Piotrowi Kaszy. Jego pomoc merytoryczna, opinie i uwagi pozwoliły na osiągnięcie zamierzonych celów pracy.*

*Wyrazy wdzięczności kieruję także do Kierownictwa Instytutu, przede wszystkim Pani Dyrektor prof. Marii Ciechanowskiej, za życzliwość i wsparcie w realizacji celów, a także dla Kierownika Zakładu Stymulacji Wydobycia Węglowodorów Pana dr inż. Marka Czupskiego, za wszelaką udzieloną mi pomoc w trakcie realizacji pracy.*

*Dziękuję pracownikom, Koleżankom i Kolegom z INiG-PIB z którymi miałem przyjemność współpracować, za życzliwość i pomoc na różnych etapach realizacji pracy.*

*Dziękuję także pracownikom Politechniki Śląskiej, przede wszystkim Pani prof. Małgorzacie Labus za wsparcie przy realizacji publikacji naukowych i dysertacji oraz Pani mgr Lindzie Wyżykowskiej za pomoc w realizacji projektu doktoratu wdrożeniowego od strony administracyjno-finansowej.*

*Dziękuję niezmiernie Żonie, Córce oraz Rodzicom za nieocenioną pomoc i wsparcie bez których ta praca nie mogłaby powstać.*

# Spis treści

# Lista publikacji

Niniejsza rozprawa doktorska została zrealizowana w oparciu o pięć spójnych tematycznie publikacji wymienionych poniżej. Wkład współautorów publikacji został zadeklarowany w oświadczeniach przechowywanych przez autora rozprawy oraz współautorów publikacji. Publikacje w pełnej formie zostały dołączone do rozprawy jako załączniki i są w niej oznaczone cyframi rzymskimi.

I. **Rafał Moska**, K. Labus, P. Kasza, *Hydraulic Fracturing in Enhanced Geothermal Systems – Field, Tectonic and Rock Mechanics Conditions – A Review,* Energies, Volume 14, 5725, 2021
DOI:10.3390/en14185725
(**IF**$_{2021}$**=3.252**); 48 cytowań

II. **Rafał Moska**, K. Labus, P. Kasza, A. Moska, *Geothermal Potential of Hot Dry Rock in South-East Baltic Basin Counties – A Review,* Energies, Volume 16, 1662, 2023
DOI: 10.3390/en16041662
(**IF**$_{2023}$**=3.000**); 8 cytowań

III. **Rafał Moska**, K. Labus, P. Kasza, *Dynamic Elastic Properties, Petrophysical Parameters and Brittleness of Hot Dry Rocks from Prospective Areas of Central Europe,* Advances in Geo-Energy Research, Volume 14, 2, 90-105, 2024.
DOI: 10.46690/ager.2024.11.03
(**IF**$_{2024}$**=9.000**); 7 cytowań

IV. K. Labus, **Rafał Moska**, M. Labus, *Potential Enhanced Geothermal System in Western Poland – Petrothermal and Geochemical Issues*, Energies, Volume 18, 876, 2025
DOI: 10.3390/en18040876
**(IF**$_{2025}$**=3,200)**

V. **Rafał Moska**, K. Labus, P. Kasza, *Impact of Rock Elastic Properties on Fracture Geometry in Potential Enhanced Geothermal Systems in Poland,* Energies, Volume 18, 2869, 2025
DOI: 10.3390/en18112869
**(IF**$_{2025}$**=3,200)**

Wkład autora pracy w każdej z publikacji był następujący:

I. **Wkład Rafała Moski**, zgodnie z oświadczeniem autorskim wynosił **60%** i obejmował: opracowanie koncepcji artykułu, wykonanie przeglądu literaturowego, opracowanie manuskryptu i wykonanie wizualizacji.

II. **Wkład Rafała Moski**, zgodnie z oświadczeniem autorskim wynosił **60%** i obejmował: opracowanie koncepcji artykułu, wykonanie przeglądu literaturowego, opracowanie manuskryptu, wykonanie wizualizacji oraz nadzór ogólny.

III. **Wkład Rafała Moski**, zgodnie z oświadczeniem autorskim wynosił **80%** i obejmował: opracowanie koncepcji artykułu, wykonanie przeglądu literaturowego, wykonanie badań laboratoryjnych, opracowanie wyników badań, opracowanie manuskryptu, wykonanie wizualizacji oraz nadzór ogólny.

IV. **Wkład Rafała Moski**, zgodnie z oświadczeniem autorskim wynosił **50%** i obejmował: wykonanie badań laboratoryjnych, przeglądu literaturowego, edycji manuskryptu, oraz jego korekty.

V. **Wkład Rafał Moski**, zgodnie z oświadczeniem autorskim wynosił **80%** i obejmował: opracowanie koncepcji artykułu, wykonanie przeglądu literaturowego, wykonanie badań laboratoryjnych metodą ultradźwiękową, opracowanie wyników badań, wykonanie symulacji numerycznych i opracowanie ich wyników, opracowanie manuskryptu, opracowanie wizualizacji oraz nadzór ogólny.

# Terminologia

**Skróty**

| | |
|---|---|
| EGS | *Enhanced Geothermal Systems* (wspomagane systemy geotermalne) |
| HDR | *Hot Dry Rocks* (gorące suche skały) |
| HF | *Hydraulic Fracturing* (hydrauliczne szczelinowanie) |
| INiG-PIB | Instytut Nafty i Gazu – Państwowy Instytut Badawczy |
| ISRM | *International Society of Rock Mechanics* (Międzynarodowe Towarzystwo Mechaniki Skał) |
| KGD | Kristianovich-Geertsma-de Klerk |
| PKN | Perkins-Kern-Nordgren |
| PŚ | Politechnika Śląska |
| SRV | *Stimulated Reservoir Volume* (objętość złoża objęta stymulacją) |
| XRD | Dyfrakcja rentgenowska |

**Symbole Rzymskie**

| | |
|---|---|
| BI | *Brittleness index* (wskaźnik kruchości), % |
| $c_{ps}$ | Pojemność cieplna objętościowa, J/kg·K |
| $E$ | Moduł Younga, Pa |
| $E_s$ | Moduł Younga statyczny, Pa |
| $E_d$ | Moduł Younga dynamiczny, Pa |
| $e$ | Efuzyjność cieplna, $W \cdot s^{½}/m^2/K$ |
| $G$ | Moduł sprężystości postaci (ścinania), Pa |
| $G_d$ | Moduł sprężystości postaci (ścinania) dynamiczny, Pa |
| $H_f$ | Wysokość szczeliny, m |
| $K$ | Moduł sprężystości objętościowej, Pa |
| $K_d$ | Moduł sprężystości objętościowej dynamiczny, Pa |
| $K_{Ic}$ | Wytrzymałość na pękanie, $Pa \cdot m^{1/2}$ |
| $k$ | Przewodność cieplna, W/m·K |
| $Q$ | Natężenie przepływu, $m^3$/min |
| $W_f$ | Rozwartość szczeliny, cm |
| $V_P$ | Prędkość fali podłużnej, m/s |
| $V_S$ | Prędkość fali poprzecznej, m/s |
| $X_f$ | Długość skrzydła szczeliny, m |

**Symbole Greckie**

| | |
|---|---|
| $\alpha$ | Dyfuzyjność, $m^2$/s |
| $\beta$ | Ściśliwość, $Pa^{-1}$ |
| $\varepsilon$ | Odkształcenie m/m |
| $\nu$ | Współczynnik Poissona, bezwymiarowy |
| $\nu_s$ | Współczynnik Poissona statyczny, bezwymiarowy |
| $\nu_d$ | Współczynnik Poissona dynamiczny, bezwymiarowy |
| $\rho$ | Gęstość objętościowa, $g/cm^3$ |
| $\sigma$ | Naprężenie, Pa |
| $\sigma_V$ | Główne naprężenie pionowe, Pa |
| $\sigma_H$ | Główne maksymalne naprężenie horyzontalne, Pa |
| $\sigma_h$ | Główne minimalne naprężenie horyzontalne, Pa |

# 1. Wstęp

## 1.1 Specyfika wspomaganych systemów geotermalnych

XXI wiek jest czasem globalnej zmiany podejścia do zagadnień związanych z pozyskiwaniem energii. Wykorzystywane dotychczas metody jej wytwarzania, bazujące na paliwach kopalnych takich jak węgiel, ropa naftowa, gaz ziemny, a także pierwiastki radioaktywne, są częściowo zastępowane przez przyjazne dla środowiska technologie niskoemisyjne, w tym energetykę słoneczną, wiatrową, opartą na spalaniu biomasy oraz geotermalną. Wśród wspomnianych technologii, duży potencjał wykazują tzw. wspomagane systemy geotermalne, ang. *enhanced geothermal systems* (EGS) (Lu, 2018). Systemy te tworzone są w specyficznych formacjach skalnych, tzw. gorących suchych skałach, ang. *hot dry rocks* (HDR). Są to skały zalegające na dużych głębokościach, najczęściej poniżej 4000 metrów, w warunkach wysokich temperatur i ciśnień. Charakteryzują się one bardzo niską przepuszczalnością, porowatością i najczęściej nie zawierają wody lub zawierają jej bardzo małe ilości (Wójcicki i inni, 2013). Ze względu na powyższe specyficzne cechy, w warunkach naturalnych tego rodzaju skały nie mogą być wykorzystywane w geotermii klasycznej, ponieważ ich energia termiczna nie może być w technicznie możliwy i ekonomiczny uzasadniony sposób transportowana na powierzchnię w ilości, która umożliwiałaby wykorzystanie jej na skalę komercyjną. Odpowiedzią na problemy z dostępnością do energii skał typu HDR jest sztuczne wytworzenie lub zwiększenie w tych formacjach przewodności hydraulicznej, czemu odpowiada termin „wspomaganie” w nazewnictwie tych systemów. Zasada działania kolektora cieplnego typu EGS polega na wykorzystaniu energii cieplnej formacji HDR, udostępnionej za pomocą szczelin w górotworze, łączących ze sobą odwierty chłonne i produkcyjne, w których ciecz robocza krąży w obiegu zamkniętym (Tester i inni, 2006). Ciecz taka jest tłoczona z powierzchni w sposób wymuszony do odwiertu chłonnego. Na głębokości docelowej nagrzewa się w sieci wytworzonych szczelin, łączących odwiert chłonny z produkcyjnym, a następnie jest transportowana na powierzchnię, gdzie jej temperatura jest wykorzystywana do produkcji energii elektrycznej i cieplnej (figura 1.1). W zależności od temperatury cieczy produkowanej, energia elektryczna może być wytwarzana w systemach binarnych lub bezpośrednich (Sharmin i inni, 2023). Głównymi cechami odróżniającymi wspomagane systemy geotermalne od geotermii konwencjonalnych jest konieczność sztucznego zwiększenia przewodności w górotworze, umożliwiającego połączenie ze sobą kilku otworów na głębokości docelowej, oraz wykorzystanie cieczy roboczej, najczęściej nie będącej cieczą rodzimą dla danej formacji HDR. Pomimo znacząco wyższych nakładów finansowych koniecznych do rozpoczęcia funkcjonowania EGS w porównaniu do klasycznej geotermii, obejmujących wysokie koszty wiercenia, zabiegów stymulacji, infrastruktury powierzchniowej, rozbudowy sieci przesyłowych oraz kontroli wydajności, systemy te charakteryzują unikalne cechy, dzięki którym wydają się one być jednymi z najbardziej perspektywicznych źródeł odnawialnej energii. Skały typu HDR zalegają na pewnej głębokości niemalże w każdym miejscu na ziemi, a energię cieplną naszej planety można określić jako źródło niewyczerpywalne (Lu, 2018). Pozyskiwanie energii z HDR nie jest uzależnione od jakichkolwiek czynników atmosferycznych, a przy produkcji energii nie zachodzą jakiekolwiek procesy spalania i nie są wykorzystywane na dużą skalę urządzenia charakteryzujące się stosunkowo krótkim okresem użyteczności i przez to wymogiem ich utylizacji (takie jak panele fotowoltaiczne i łopaty turbin wiatrowych). Co więcej, EGS po okresie przygotowania i testów, wymagają minimalnej obsługi ludzkiej. Elektrownie dostarczające stałą, z góry przewidywalną ilość energii odnawialnej, przez dziesiątki lat wydają się być bardzo dobrym dopełnieniem rozwijanych obecnie systemów energetyki wiatrowej i słonecznej. Nie dziwi więc znaczący wzrost zainteresowania systemami geotermii wspomaganej w ostatnich latach na niemal wszystkich kontynentach, co zaowocowało rozpoczęciem realizacji projektów badawczych mających na celu dopracowanie detali tej technologii w drodze do zwiększenia opłacalności ekonomicznej.

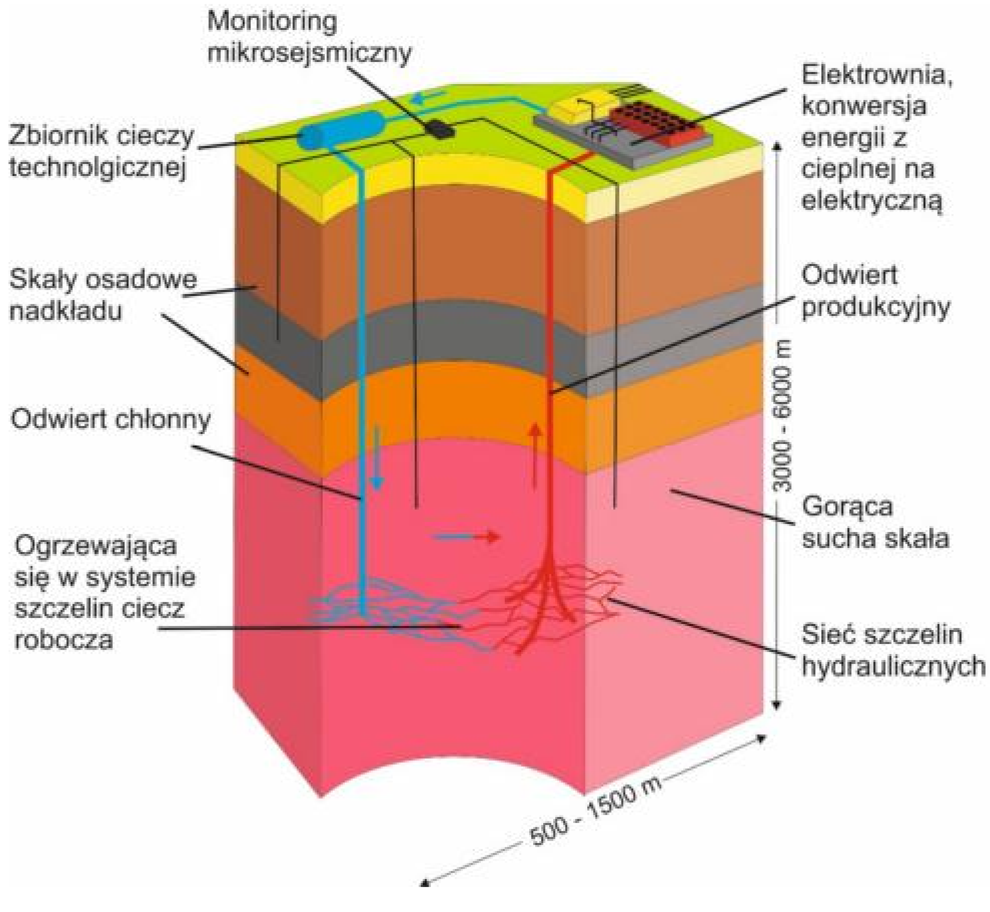


Figura 1.1: Schemat działania wspomaganego systemu geotermalnego.

## 1.2 Zabiegi stymulacyjne w geotermii wspomaganej

Zwiększenie przewodności hydraulicznej w skałach HDR jest realizowane za pomocą zabiegów stymulacyjnych znanych z przemysłu naftowo-gazowniczego. Zabiegi te można podzielić na trzy główne typy: termiczne, chemiczne oraz hydrauliczne (Economides i Martin, 2007). Podczas stymulacji termicznej zimna ciecz wprowadzana do górotworu powoduje mikropęknięcia ziaren, matrycy skalnej i materiału wypełniającego szczeliny naturalne. Efekty termoelastyczne zmniejszają naprężenie normalne w obrębie szczelin naturalnych ułatwiając ich otwieranie się. Stymulacja chemiczna polega na pompowaniu do górotworu roztworów kwasów rozpuszczających materiał powodujący ograniczenie przepuszczalności skał, taki jak m. in. ziarna skał, spoiwo, zwierciny, pozostałości płuczki oraz wytrącone minerały hydrotermalne. Do tego celu wykorzystuje się kwasy nieorganiczne i organiczne, takie jak: HCl, HF i $CH_3COOH$, w zależności o rodzaju skał w formacji i od rodzaju ograniczenia przepuszczalności, zwanego także uszkodzeniem przepuszczalności. Obydwie opisane powyżej metody stymulacyjne są skuteczne jedynie w strefie przyodwiertowej lub w stosunkowo niewielkiej odległości od otworu wiertniczego. W geotermii wspomaganej wykorzystywane są one zazwyczaj jako metody wtórne, pozwalające na usunięcie uszkodzenia i poprawę przepuszczalności w tej strefie. Główną metodą stymulacji wykorzystywaną w EGS jest hydrauliczne szczelinowanie, ang. *hydraulic fracturing* (HF). Technologia ta polega na zatłoczeniu do otworu cieczy roboczej pod ciśnieniem wyższym od ciśnienia szczelinowania formacji docelowej na danej głębokości, czego skutkiem jest spowodowanie pęknięcia skały i zainicjowanie propagacji szczeliny, indukowanej w ściśle określonym kierunku. Tego rodzaju szczelina lub system szczelin może osiągać długości i wysokości rzędu setek metrów, przy rozwartości od kilku mm do kilku cm i przewodności rzędu setek mD. Pozwala to na uzyskanie przewodności hydraulicznej w skałach HDR na odległości od kilkudziesięciu metrów do ponad kilometra, a tym samym zdolność do transportu stosunkowo dużej objętości cieczy roboczej pomiędzy odwiertami w systemie geotermalnym. Odpowiednio zaprojektowany system typu EGS w dobrze dobranej lokalizacji, w formacji w której prawidłowo zostały wykonane odwierty i zabiegi stymulacyjne, może stabilnie funkcjonować przez wiele lat, czego przykładem są przede wszystkim projekty zrealizowane w Rowie Renu w Europie Zachodniej, takie jak Soultz-sous-Forêts, Landau i Rittershoffen (Held i inni, 2014; Schill i inni, 2017; bestec-for-nature.com)

## 1.3 Hydrauliczne szczelinowanie gorących suchych skał

Zabiegi HF w HDR różnią się zasadniczo pod względem oczekiwanego efektu od zabiegów w konwencjonalnych oraz niekonwencjonalnych złożach węglowodorów. W niekonwencjonalnych akumulacjach gazu ziemnego celem HF jest wytworzenie jak najbardziej efektywnego połączenia hydraulicznego pomiędzy jak największą częścią stymulowanej formacji a odwiertem. Im większa część formacji objęta zostanie zabiegiem HF, tym większa objętość uwolnionego gazu może pod wpływem ciśnienia złożowego przedostać się poprzez szczeliny do odwiertu i zostać wyeksploatowana. Objętość stymulowanego złoża odzwierciedla parametr SRV (ang. *stimulated reservoir volume*), który jest obliczany na podstawie monitoringu mikrosejsmicznego podczas trwania zabiegu i po nim. Ogniska zdarzeń mikrosejsmicznych są wtedy rejestrowane przez geofony w odwiertach obserwacyjnych, a miejsca ich występowania i odległości od odwiertu w którym jest prowadzona stymulacja pozwalają stwierdzić, na jakie odległości w danej płaszczyźnie propagują szczeliny (King, 2010). W skałach typu HDR celem stymulacji hydraulicznej jest natomiast wytworzenie optymalnego połączenia pomiędzy co najmniej dwoma otworami wiertniczymi, z których jeden pełni funkcje chłonną i jeden produkcyjną. Optymalne połączenie oznacza w tym przypadku wytworzenie w szczelinach hydraulicznej przewodności o takiej wielkości, która umożliwi jak największą sprawność całego systemu, tj. najwyższą temperaturę cieczy produkowanej przez jak najdłuższy okres czasu, ale jednocześnie nie spowoduje niepożądanego zjawiska zwarcia termicznego (ang. *thermal short circuiting*) (McClure i Horne, 2014). Jest to zjawisko tworzenia się preferowanej ścieżki przepływu w formacji prowadzące do zbyt szybkiego jej schładzania, co z kolei skutkuje znacznym spadkiem temperatury produkowanej cieczy i wydajności całego systemu. Jednym z powodów zwarcia jest „przestymulowanie” formacji, tj. zastosowanie zbyt dużych ciśnień i wydatków zatłaczania podczas zabiegu HF. Zwarcie termiczne może być trudne do likwidacji, czego przykładem jest projekt EGS Rosemanowes w Wielkiej Brytanii (Batchelor, 1986, 1987).

Wyróżnia się trzy główne mechanizmy zwiększające przewodność podczas stymulacji hydraulicznej (Park i inni, 2020):

(1) hydrauliczne szczelinowanie tzw. czyste – tworzenie nowych szczelin w górotworze w wyniku oddziaływania na skałę sił tensyjnych podczas pompowania cieczy zabiegowej pod ciśnieniem wyższym od ciśnienia szczelinowania formacji (ang. *pure opening mode*). Po spadku ciśnienia poniżej wartości ciśnienia zamknięcia szczeliny ulegają zaciśnięciu w wyniku dominacji naprężeń złożowych.

(2) ponowne otwieranie zamkniętych naturalnych szczelin w wyniku oddziaływania sił tensyjnych cieczy zabiegowej i zamykanie ich po spadku ciśnienia (ang. *hydraulic jacking*).

(3) hydrościnanie - indukowanie poślizgu i dylatacji na powierzchni szczelin naturalnych w wyniku oddziaływania sił ścinających (ang. *hydraulic shearing*).

Niektórzy badacze sugerują również występowanie mechanizmów mieszanych (ang. *mixed mechanism*) (McClure and Horne, 2014). Mechanizmy te bezpośrednio wpływają na kluczowe aspekty technologii szczelinowania, takie jak dobór cieczy roboczej, materiału podsadzkowego oraz zakres stosowanych ciśnień i wydatków pompowania. W skałach osadowych typu HDR, najbardziej zbliżonych do niekonwencjonalnych, macierzysto-zbiornikowych skał gazu ziemnego dominują mechanizmy tzw. czystego szczelinowania oraz otwierania szczelin naturalnych w wyniku działania sił tensyjnych. Są to zazwyczaj formacje zbite, monotonne, charakteryzujące się mniejszą ilością naturalnych płaszczyzn nieciągłości. Szczeliny indukowane oraz ponownie otwarte w tych skałach, podobnie jak w formacjach złożowych gazu ziemnego, zamykają się pozostając nieprzewodne po spadku ciśnienia do poziomu ciśnienia zamknięcia szczeliny, dlatego też do ich podparcia konieczne jest zastosowanie materiału podsadzkowego. To z kolei determinuje użycie cieczy zabiegowej o lepkości na tyle wysokiej aby możliwy był jego transport. W praktyce najczęściej wykorzystuje się do tego ciecze liniowe na bazie polimerów naturalnych oraz ciecze sieciowane (Kasza, 2019).

W magmowych formacjach HDR, takich jak granity, w których występują strefy szczelin i spękań naturalnych, głównym mechanizmem jest hydrościnanie, co potwierdzają obserwacje mikrosejemiczne (Jung, 2013; Xie i inni 2015) W tym przypadku ciśnienie pompowania podczas zabiegu zazwyczaj nie przekracza minimalnego naprężenia głównego. Ze względu na poślizg ścian szczelin podczas hydrościnania, po spadku ciśnienia pozostają one przewodne. Te cechy sprawiają, że zastosowanie materiału podsadzkowego w takich formacjach do podtrzymania rozwartości i tym samym przewodności często nie jest konieczne, a to z kolei pozwala na wykorzystanie cieczy zabiegowej o bardzo niskiej lepkości. W praktyce do tego celu najczęściej stosowana jest woda wodociągowa.

Indukowana hydraulicznie szczelina charakteryzuje się wymiarami mierzonymi w trzech płaszczyznach: długością, wysokością oraz rozwartością (figura 1.2). Jej wymiary oraz powiązana z nimi przewodność zależą od: litologii szczelinowanej strefy docelowej, przepuszczalności formacji, wielkości naprężeń w tej strefie oraz strefach otaczających, współczynnika efektywności cieczy szczelinującej oraz parametrów sprężystości skał: modułu Younga oraz współczynnika Poissona.

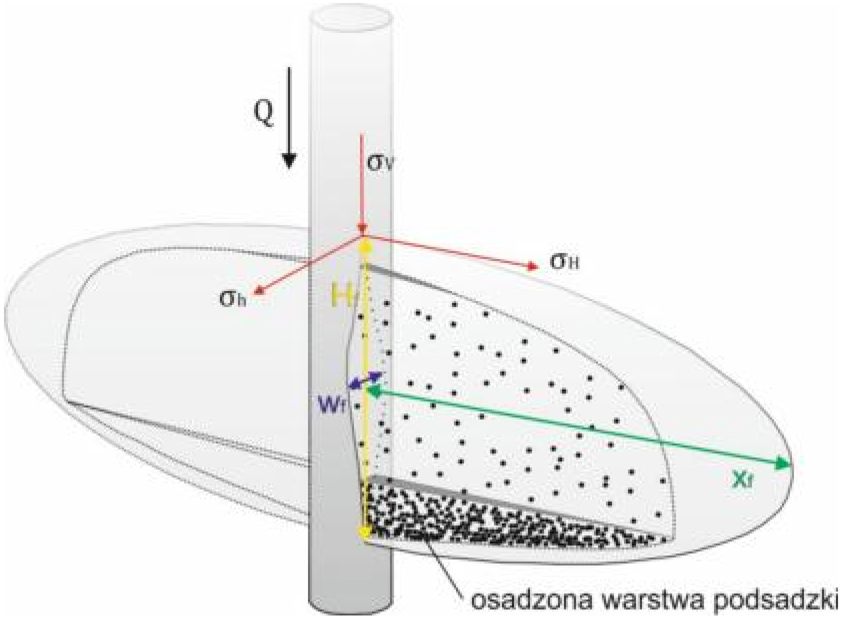


Figura 1.2: Wymiary szczeliny indukowanej. $X_f$ – długość, $H_f$ – wysokość, $W_f$ – rozwartość. Q – kierunek przepływu cieczy w odwiercie podczas szczelinowania.

W zależności od mechanizmu powodującego propagację szczelin podczas stymulacji hydraulicznej, może się to odbywać na dwa główne sposoby. W skałach osadowych gdzie mechanizmem jest szczelinowanie tzw. czyste, propagacja szczelin zależy w głównej mierze od kierunków naprężeń głównych w górotworze. Szczeliny propagują zawsze w kierunku prostopadłym do minimalnego naprężenia głównego. W reżimach tektonicznych ekstensyjnym i przesuwczym, gdzie dominującym jest naprężenie pionowe pochodzące od skał nadkładu ($\sigma_V$), szczeliny propagują równolegle do maksymalnego naprężenia horyzontalnego ($\sigma_H$) i prostopadle do minimalnego naprężenia horyzontalnego ($\sigma_h$). W reżimie kompresyjnym, gdzie $\sigma_V$ ma wartość niższą niż $\sigma_h$, szczeliny propagują w kierunku horyzontalnym (figura 1.3).

W formacjach o dobrze rozwiniętej sieci szczelin naturalnych, w których głównym mechanizmem stymulacji hydraulicznej jest hydrościnianie, płaszczyzny osłabienia są stymulowane jako pierwsze. Dlatego w trakcie zabiegu HF propagacja następuje po naturalnym śladzie zamkniętej szczeliny, a powstające nowe szczeliny są w mniejszości. Nowe szczeliny, jeśli są inicjowane i propagują zgodnie z stanem naprężenia w formacji, stają się jedynie łącznikami pomiędzy szczelinami naturalnymi (McClure and Horne, 2014). Zatem propagacja zgodna ze stanem naprężeń ma miejsce jedynie w okresie inicjacji nowej szczeliny i jej propagacji we wczesnym stadium.

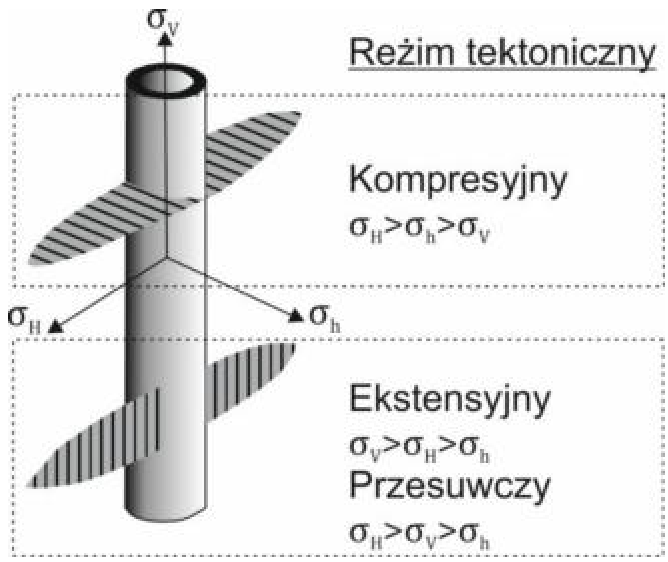


Figura 1.3: Uproszczony model szczeliny hydraulicznej w zależności od reżimu tektonicznego (na podstawie Dixit i inni, 2017).

## 1.4 Parametry sprężystości skał i ich wpływ na geometrię szczeliny

Moduł Younga ($E$) definiuje ilość energii potrzebną do osiągnięcia przemieszczenia i wywodzi się z klasycznej koncepcji liniowej mechaniki pękania. Wraz ze wzrostem $E$ wzrasta długość oraz wysokość szczeliny, a spada jej rozwartość. Spada również ciśnienie netto (ciśnienie różnicowe pomiędzy ciśnieniem propagacji szczeliny a ciśnieniem zamknięcia szczeliny). Skały o wysokim $E$ wymagają więcej energii do ich przemieszczenia podczas tworzenia szczeliny. W takich formacjach, definiowanych jako „twarde", szczeliny charakteryzują się niewielką rozwartością (Economides i Martin, 2007). Współczynnik Poissona ($v$) odzwierciedla stosunek deformacji skały w kierunku zgodnym z kierunkiem naprężenia, do deformacji w kierunku do niego prostopadłym. Wartość $v$ dla substancji nieściśliwej jest równa 0,5 (Zoback, 2007). W złożu, $v$ określa zdolność do zniszczenia skały pod wpływem naprężenia (Rickman i inni, 2008). W skałach o wysokim $v$ zwiększa się także ryzyko wystąpienia niepożądanego zjawiska embedmentu, tj. wgniatania ziaren podsadzki w skałę w szczelinie, która jest nią podsadzana. Zjawisko to powoduje zmniejszenie przewodności szczeliny (Masłowski i inni, 2019; Masłowski i Labus 2021). Moduł sprężystości objętościowej ($K$) jest miarą odporności materiału izotropowego na zmianę objętości, gdy jest ono poddane kompresji izometrycznej. Jego odwrotnością jest ściśliwość ($\beta$). Moduł sprężystości postaci ($G$), nazywany modułem ścinania, to miara odporności materiału na naprężenie ścinające. Dla cieczy wynosi on zero (Zoback, 2007). W praktyce, w projektowaniu zabiegów HF, wykorzystywane są zazwyczaj jedynie $E$ oraz $v$ (Kasza, 2019).

## 1.5 Laboratoryjne metody wyznaczania parametrów sprężystości skał

Właściwości mechaniczne skał mogą być wyznaczane niszczącymi lub nieniszczącymi metodami laboratoryjnymi. W metodzie niszczącej parametry sprężystości są obliczane na podstawie zależności między naprężeniem a odkształceniem skały w różnych warunkach obciążenia statycznego. Odkształcenie jest mierzone do chwili zniszczenia próbki, a uzyskiwane parametry sprężystości są nazywane statycznymi. Statyczny moduł Younga $E_s$ odzwierciedla związek pomiędzy zadanym obciążeniem $\sigma$ a odkształceniem $\varepsilon$, w osi obciążenia (1):

$$E_s = \sigma/\varepsilon \tag{1}$$

Statyczny współczynnik Poissona $v_s$ opisuje stosunek odkształcenia poprzecznego $\varepsilon_t$ do odkształcenia osiowego $\varepsilon_a$ (2):

$$v_s = -d\ \varepsilon_t/d\ \varepsilon_a \tag{2}$$

Zakłada się, że statyczne parametry sprężystości próbek skał są bliższe wartościom dla tych skał in situ (Shen i inni, 2024).

W metodzie nieniszczącej właściwości mechaniczne skał, tj. dynamiczny moduł Younga $E_d$ i dynamiczny współczynnik Poissona $v_d$, określa się pośrednio, na podstawie zależności między prędkościami fal ultradźwiękowych podłużnych i poprzecznych (odpowiednio $V_P$ i $V_S$) oraz gęstością objętościową próbki $\rho$ (3, 4).

$$E_d = \rho\frac{{V_P}^2(1+v_d)(1-v_d)}{(1-v_d)} \tag{3}$$

$$v_d = \frac{1/2-(V_S/V_P)^2}{1-(V_S/V_P)^2} \tag{4}$$

Dynamiczny moduł Younga $E_d$ jest zazwyczaj wyższy od odpowiadającego mu modułu statycznego $E_s$ (Eissa i Kazi, 1988). W skałach spękanych o niskiej wytrzymałości, stosunek $E_d/E_s$ może znacznie przekraczać 2 (Brotons i inni, 2016; Bukowska i inni 2022). Obserwowane różnice są spowodowane przez czynniki związane z warunkami obciążenia, składem mineralnym i temperaturą, ale główną przyczyną jest obecność płaszczyzn osłabień i nieciągłości – mikropęknięć, szczelin i porów. Korelacje między $E_s$ i $E_d$ są opisywane przez kilka typów równań empirycznych. Najczęściej używane są równania regresji liniowej ($E_s = aE_d + b$) oraz potęgowej ($E_s = \alpha E_d^{\beta}$). Dla skał magmowych oraz metamorficznych najlepsze wyniki daje najczęściej korelacja potęgowa, natomiast dla formacji osadowych liniowa i logarytmiczna (Shen i inni, 2024).

Moduły $E$ dla nienaruszonych i niezmienionych hydrotermalnie granitów mogą dochodzić do 80 GPa (Meller i Ledesert, 2017; Villeneuve i inni, 2018). Wraz ze wzrostem liczby płaszczyzn nieciągłości obserwowane są spadki $E$ i większe rozbieżności pomiędzy wartościami dynamicznymi oraz statycznymi. W badaniach przeprowadzonych przez Lama i Vutukuriego (1978) określono, że moduły sprężystości statyczny $E_s$ i dynamiczny $E_d$ dla nienaruszonych granitów mają podobne wartości, około 65–70 GPa. Natomiast w granicie przeobrażonym zarówno $E_s$ jak i $E_d$ wyraźnie spadają, przy czym średnia wartość $E_d$ jest trzykrotnie wyższa od $E_s$ (odpowiednio 15,0 GPa i 5,0 GPa).

Zależności pomiędzy dynamicznymi i statycznymi współczynnikami Poissona w literaturze opisywane są w różny sposób. Van Heerden (1987) sugeruje, że w większości przypadków $v_d$ jest niższy od $v_s$. Z kolei Shen i inni (2024) pokazują, że korelacje pomiędzy nimi różnią się w zależności od typu litologicznego skały. Dla skał magmowych najlepszy współczynnik dopasowania zapewnia krzywa wykładnicza: dla skał osadowych wielomianowa, a dla metamorficznych logarytmiczna. Jednakże, bez względu na typ litologiczny skały, podawane w literaturze współczynniki dopasowania są niskie (0,3-0,7), co oznacza, że proste modele korelacyjne słabo opisują zależności pomiędzy dynamicznym i statycznym współczynnikiem Poissona (Shen i inni, 2024).

## 1.6 Symulacje numeryczne geometrii szczeliny hydraulicznej

Modelowanie numeryczne geometrii szczelin w kolektorach EGS umożliwia testowanie różnych wariantów konfiguracji systemu geotermalnego przed wdrożeniem ich w realnych warunkach terenowych. Podstawowymi modelami formowania szczeliny hydraulicznej są modele dwuwymiarowe: KGD (Kristianovich-Geertsma-de Klerk), PKN (Perkins-Kern-Nordgren) i model radialny. W modelach tych zakłada się, że formacja skalna jest nieskończonym, izotropowym, liniowym ośrodkiem sprężystym, charakteryzującym się pewnym modułem Younga $E$ oraz współczynnikami Poissona $v$ i wytrzymałości $K_{Ic}$. W modelu KGD zakłada się ponadto, że szczelina ma stałą wysokość, a jej długość i rozwartość w funkcji długości są zmienne. Wytwarzająca ją ciecz szczelinująca jest płynem newtonowskim, zatem nie zmienia lepkości pod wpływem zmian naprężenia ścinającego, jest pompowana ze stałym natężeniem przepływu laminarnego i nie zachodzi zjawisko filtracji. W modelu PKN szczelina ma kształt wydłużony w osi długości, sięgającej setek metrów, oraz ograniczoną ale stałą wysokość, osiągającą rząd dziesiątek metrów. Jej rozwartość jest mała, mierzona w milimetrach i zmienna wraz z wysokością i długością szczeliny. Model radialny opisuje sytuację, w której nie uwzględnia się barier propagacji szczeliny na wysokość lub propagująca szczelina ich nie osiąga. Model ten zazwyczaj trafnie opisuje wstępny etap tworzenia szczeliny w formacji skalnej (Economides i Nolte, 2000). Wspólną cechą tych modeli jest to, że wymagają założenia stałej wysokości szczeliny lub radialnej jej propagacji. Bardziej zawansowanymi modelami formowania szczeliny są modele 3D oraz planar 3D, nie wymagające założeń dotyczących orientacji szczeliny, jednakże ze względu na złożoność obliczeniową są rzadziej stosowane w praktyce przemysłowej. Modele P3D (Pseudo 3D) łączą zachowanie modeli 3D oraz prostotę obliczeniową. Model P3D skupiony zakłada pionowy profil szczeliny, składający się z dwóch półelips połączonych w środku, przy czym długość szczeliny i wysokość obliczane są w krokach czasowych. Modele P3D wykorzystują dane na temat właściwości formacji ograniczających strefę perforacji od stropu i spągu, aby oszacować szybkość propagacji szczeliny w ich obrębie. Do modelowania zabiegów HF w EGS wykorzystywano jak dotąd zarówno mniej zaawansowane modele formowania szczelin 2D (Legarth i inni, 2003; 2005; Zimmerman i inni, 2010; Zimmermann i Reinicke 2010), jak i modele bardziej zaawansowane: formowania szczelin klastrowych i dyskretnych (Lei i inni, 2020), model uszkodzeń termo-hydro-mechanicznych (Guo i inni, 2019; 2020; Aliyu i Archer 2021) oraz sprzężone modele termo-poro-elastyczne (Cheng i inni, 2019).

## 1.7 Motywacja i cele pracy

Niniejsza dysertacja została przygotowana ramach programu Doktorat Wdrożeniowy edycja V, we współpracy pomiędzy Politechniką Śląską (PŚ) a Instytutem Nafty i Gazu – Państwowym Instytutem Badawczym (INiG-PIB). Działalność INiG-PIB zgodnie z polityką rozwoju firmy na lata 2020-2025 ukierunkowana jest na rozwój usług związanych z energetyką bazującą na surowcach odnawialnych, w tym energetyką geotermalną. Realizacja tej dysertacji jest odpowiedzą na potrzebę pogłębienia wiedzy INiG-PIB w aspekcie niekonwencjonalnych, odnawialnych technologii energetycznych, jakimi, między innymi, są EGS. Jej efekty pozwolą na poszerzenie oferty badawczej przedsiębiorstwa, w szczególności w aspekcie badań wytrzymałościowych skał z dużych głębokości oraz projektowania elementów technologii HF w HDR.

Tematyka pozyskiwania energii cieplnej skał systemami geotermalnymi typu wspomaganego, na wzór projektów prowadzonych w Europie Zachodniej, jest od kilkunastu lat dyskutowana w polskich kręgach naukowych. Dotychczasowe publikacje na ten temat mają charakter rozważań teoretycznych (Sapińska-Śliwa i inni, 2015; Niezgoda i inni, 2018), lub omawiają szczegółowe, stosunkowo wąskie elementy tej bardzo rozległej tematyki (Labus i inni, 2023). Wyjątek stanowi raport wykonany na zlecenie Ministerstwa Środowiska (Wójcicki i inni, 2013) oraz zbiór publikacji wydanych w ramach projektu *Energisers* (energisers.agh.edu.pl). Prace te miały na celu ocenę możliwości wykorzystania struktur geologicznych typu HDR na obszarze Polski do budowy systemów EGS (Wójcicki i inni 2013) oraz modelowania systemu $CO_2$-EGS poprzedzone badaniami laboratoryjnymi wraz z analizami właściwości nadkrytycznego $CO_2$ i oceną ekonomiczno-środowiskową. Pomimo szerokiego spektrum badawczego obydwu tych prac, ich efekty nie były ukierunkowane na opracowanie jakichkolwiek elementów technologii HF, takich jak: schematy pompowania, skład cieczy zabiegowych oraz materiałów podsadzkowych, mimo że ich prawidłowy dobór jest podstawą późniejszego optymalnego funkcjonowania EGS w tych strukturach. Nie analizowano również wpływu poszczególnych elementów technologii HF na geometrię kolektora geotermalnego oraz wpływu właściwości mechanicznych HDR na wymiary wytwarzanych szczelin. Co więcej, wyraźna luka poznawcza w aspekcie relacji pomiędzy parametrami mechanicznymi HDR a geometrią kolektora geotermalnego występuje nie tylko w odniesieniu do konkretnych, specyficznych dla danego obszaru formacjach skalnych, lecz do ogólnego problemu badawczego dotyczącego tego zagadnienia. Jak dotychczas jedyną publikacją podejmującą tę tematykę była praca Lei i innych (2023), w której zaprezentowano m. in. analizę wrażliwości rozwartości szczelin i ich powierzchni na zmiany parametrów wytrzymałościowych skał w kolektorze geotermalnym w basenie Gonghe w Chinach.

Podane powyżej powody skłoniły autora do podjęcia badań nad wpływem parametrów sprężystości gorących suchych skał na proces hydraulicznego szczelinowania w EGS. Przyjęto założenie, że na podstawie laboratoryjnie wyznaczonych dynamicznych parametrów sprężystości skał, danych petrofizycznych, a także danych dotyczących naprężeń złożowych można wyznaczyć geometrię szczeliny powstałej w hipotetycznym zabiegu hydraulicznego szczelinowania, w strukturze geologicznej perspektywicznej z punktu widzenia wspomaganego systemu geotermalnego.

Sformułowano następujące cele badawcze:

• określenie wpływu parametrów sprężystości skał formacji docelowej na geometrię szczeliny tworzonej w procesie HF, w warunkach ciśnienia i temperatury typowych dla obszarów perspektywicznych dla systemów geotermalnych typu EGS na terenie Polski,

• określenie zależności pomiędzy zmianami ciśnienia podczas testów geomechanicznych a parametrami sprężystości skał,
• określenie korelacji pomiędzy parametrami wyznaczonymi metodami ultradźwiękową oraz wytrzymałościową.
• dopracowanie metodyki badań ultradźwiękowych próbek skał reprezentujących kolektory HDR w warunkach wysokiego ciśnienia i temperatury, poprzedzone modyfikacją oprzyrządowania badawczego, dostosowującą je do bezpiecznej pracy w tych warunkach,
• wykonanie symulacji numerycznych geometrii szczelin w wybranych obszarach perspektywicznych dla EGS w Polsce,
• przygotowanie ogólnych rekomendacji technologicznych do zabiegów HF w analizowanych formacjach.

Cele te zrealizowano na podstawie dogłębnej analizy literaturowej, samodzielnie przeprowadzonych badań laboratoryjnych na próbkach skalnych oraz symulacji numerycznych.

## 1.8 Zakres pracy

Praca została podzielona na następujące części:

**Rozdział 1** stanowi wstęp obejmujący: opis specyfiki wspomaganych systemów geotermalnych EGS, charakterystykę zabiegów stymulacji w geotermii wspomaganej, parametrów sprężystości skał, sposobów ich wyznaczania oraz podstawowych modeli geometrii szczeliny hydraulicznej. Rozdział ten opisuje także motywację do podjęcia zagadnienia oraz cele i zakres pracy.

**Rozdział 2** jest przeglądem najważniejszych projektów EGS prowadzonych na świecie, pod kątem parametrów geologicznych, petrofizycznych, tektonicznych oraz elementów technologii hydraulicznego szczelinowania w nich wykorzystywanych. Porównano w nim informacje na temat projektów już istniejących z dostępnymi danymi dotyczącymi potencjalnych obszarów HDR na terenie Polski.

**Rozdział 3** rozbudowuje zagadnienia dotyczące obszarów perspektywicznych dla technologii EGS w Europie Środkowej o kraje bałtyckie, oraz porównuje ich warunki geologiczne do panujących na obszarze Polski.

**Rozdział 4** obejmuje charakterystykę parametrów petrofizycznych, geomechanicznych i cech petrograficznych wybranych perspektywicznych formacji typu HDR w Polsce, opracowaną w oparciu o wyniki własnych badań laboratoryjnych. Zawiera również zmodyfikowaną interpretację, mającego duże znaczenie dla doboru technologii szczelinowania hydraulicznego, wskaźnika kruchości skał BI, która może być wykorzystywana do oceny podatności na HF w magmowych formacjach HDR.

**Rozdział 5** przedstawia potencjał termiczny i geochemiczny wybranych perspektywicznych dla EGS obszarów w zachodniej Polsce. Zawiera on wyniki badań termicznych próbek skalnych z bloku Gorzowa i bloku karkonoskiego oraz ocenę parametrów termicznych tych formacji. Zawiera także wyniki numerycznego modelowania zmian temperatury formacji i zasięgu jej chłodzenia podczas długotrwałej eksploatacji energii termalnej oraz wyniki modelowania geochemicznego reakcji zachodzących w tych skałach w trakcie eksploatacji ciepła.

**Rozdział 6** składa się z dwóch części, z których pierwsza zawiera charakterystykę dynamicznych parametrów sprężystości analizowanych skał nasyconych cieczą, charakterystykę statycznych parametrów sprężystości skał nienasyconych oraz korelacje dynamicznych i statycznych parametrów wytrzymałości skał. Druga część obejmuje wyniki symulacji numerycznych geometrii szczelin hydraulicznych w funkcji parametrów sprężystości skał, wykonanych w oparciu o dane archiwalne i wyniki własnych badań laboratoryjnych. W rozdziale tym przedstawiono również analizę wrażliwości parametrów geometrii szczeliny oraz jej przewodności, w zależności od parametrów sprężystości skał.

**Rozdział 7** zawiera rekomendacje technologiczne do zabiegów HF w warunkach charakterystycznych dla obszarów perspektywicznych dla EGS w Polsce, opracowane na podstawie wszystkich prac przeprowadzonych w ramach realizacji doktoratu.

# 2. Hydrauliczne szczelinowanie we wspomaganych systemach geotermalnych – przegląd uwarunkowań tektonicznych, geomechanicznych i powiązanych z nimi aspektów technologicznych – Artykuł I

Początki stosowania technik intensyfikacji wydobycia na potrzeby instalacji geotermalnych w głęboko zalegających gorących skałach sięgają połowy lat 70 XX wieku (Tester i inni, 2006). W kolejnych latach elementy tych technik były intensywnie rozwijane i usprawniane (Zimmermann i inni, 2010; McClure and Horne, 2014: Blöcher i inni, 2016; Olasolo i inni, 2016). Metody intensyfikacyjne, nazywane również metodami stymulacji produkcji, wywodzące się z przemysłu naftowo-gazowniczego, obejmują kilka głównych grup technologii pozwalających na zwiększenie powierzchni kontaktu pomiędzy odwiertem a złożem i w konsekwencji poprawę chłonności i produktywności odwiertu. Technologie obejmujące różne typy kwasowań matrycowych, jak również stymulacji termicznych, są skuteczne jedynie w strefie przyodwiertowej, sięgającej maksymalnie kilku metrów od osi odwiertu, dlatego w geotermii wspomaganej wykorzystywane są jedynie jako wtórne metody stymulacyjne lub sposoby na udrożnienie uszkodzonej strefy przyodwiertowej. Technologią pozwalającą na zwiększenie przewodności hydraulicznej skał na odległości rzędu setek metrów od odwiertu – co ma podstawowe znaczenie z punktu widzenia efektywności wspomaganego systemu geotermalnego - jest szczelinowanie hydrauliczne. Artykuł I zawiera oryginalny, wykonany przez doktoranta przegląd najważniejszych elementów technologii hydraulicznego szczelinowania wykorzystanych we wspomaganych systemach geotermalnych na świecie. Zebrane w nim szczegółowe charakterystyki formacji docelowych HDR w prowadzonych projektach EGS, dane z badań laboratoryjnych skał oraz informacje z dotychczas wykonanych zabiegów szczelinowania hydraulicznego w tych projektach, umożliwiły określenie najbardziej perspektywicznych obszarów badawczych, przewidzianych do realizacji w ramach doktoratu oraz zdefiniowanie zakresu badań laboratoryjnych w artykule III i IV. W konsekwencji, pozwoliły one także na opracowanie założeń symulacji numerycznych zabiegów hydraulicznego szczelinowania dopasowanych do konkretnych warunków geologiczno-złożowych perspektywicznych obszarów w Polsce (artykuł V).

## 2.1 Projekty EGS realizowane na świecie

Dla zaprojektowania skutecznego zabiegu szczelinowania hydraulicznego istotne jest rozpoznanie warunków geologiczno-tektonicznych obszaru perspektywicznego, które będą determinowały szczegóły projektowanej technologii intensyfikacji. W artykule I przedstawiono wybrane, najistotniejsze i najdokładniej opisane w literaturze światowej projekty EGS, w których wykonywano zabiegi stymulacyjne metodą hydrauliczną i scharakteryzowano ich krytyczne elementy związane z przeprowadzonymi operacjami szczelinowania hydraulicznego (figura 2.1).

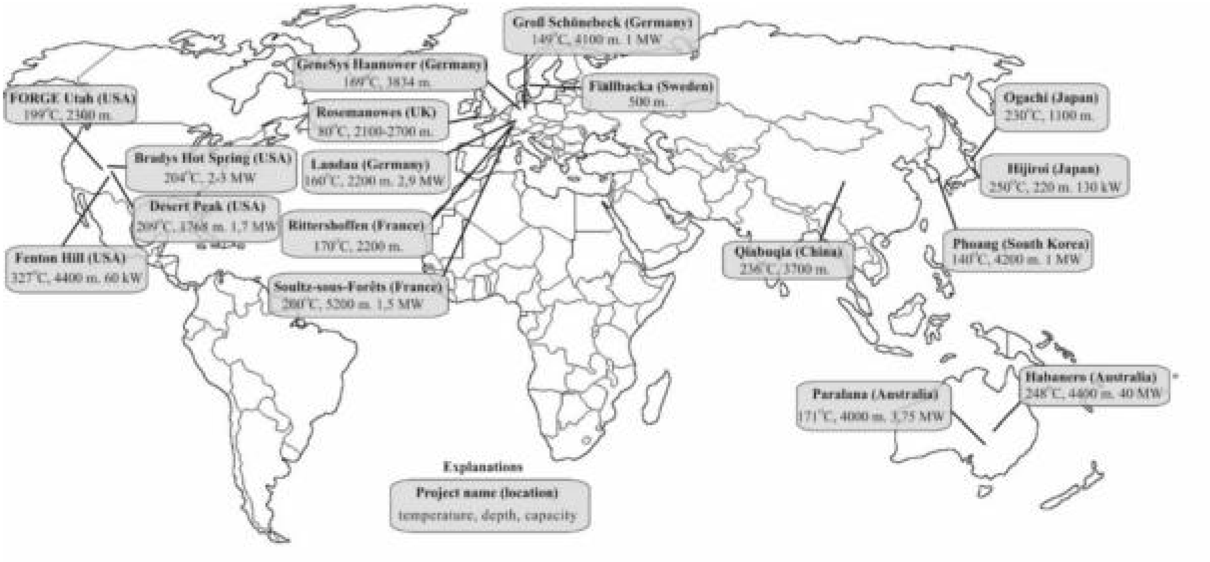


Figura 2.1: Wybrane projekty EGS realizowane na świecie.

Analizowane dane dotyczyły warunków geologicznych, w tym: głębokości zalegania strefy docelowej, temperatury w tej strefie, litologii skał, a także parametrów tektonicznych i geomechanicznych, tj. reżimu tektonicznego, wartości naprężeń głównych, parametrów Younga i Poissona skał oraz prędkości propagacji fal sejsmicznych i ultradźwiękowych. Powyższe dane zostały również uzupełnione o informacje technologiczne dotyczące przeprowadzonych zabiegów szczelinowania i obejmujące: ciśnienia szczelinowania, wydajności pompowania, cechy stosowanych płynów zabiegowych i materiałów podsadzkowych oraz wymiary wytworzonych szczelin hydraulicznych. Tego rodzaju kompleksowa charakterystyka projektów EGS, pod kątem najważniejszych cech geologicznych, tektonicznych i technologicznych, nie była wcześniej publikowana.

## 2.2 Przegląd uwarunkowań geologicznych, tektonicznych, geomechanicznych oraz powiązanych z nimi aspektów technologicznych zabiegów hydraulicznego szczelinowania

Strefami docelowymi w większości dotychczas przeprowadzonych projektów EGS są skały krystaliczne, najczęściej granity (projekty Fenton Hill, Rosmanowes, Habanero, Phoang, Qiabuqia, FORGE oraz projekty w Rowie Renu), charakteryzujące się przepuszczalnością poniżej 0,01 mD i porowatością nie przekraczającą kilku %. W utworach tych występuje naturalna szczelinowatość związana ze zjawiskami tektonicznymi oraz przeobrażeniem skał na skutek oddziaływania hydrotermalnego. Te naturalnie zaciśnięte szczeliny są najczęściej głównym celem stymulacji hydraulicznej – podczas zabiegu zostają rozwierane w pierwszej kolejności. Po zwiększeniu przewodności w wyniku zabiegu pełnią one rolę przepuszczalnych arterii, łączących odwierty chłonne i wydobywcze. Strefy docelowe znajdują się na głębokościach od 2000 do 5000 metrów, a ich lokalizacja jest wybierana głównie w oparciu o analizy gradientu geotermicznego. Temperatury w tych strefach wynoszą od 150°C do ponad 300°C, co determinuje bezpośrednio rodzaj systemu pozyskiwania energii, jego moc i efektywność. Do eksploatacji zasobów o umiarkowanej entalpii (120-175°C) wykorzystuje się technologię binarną, w której płyn geotermalny ogrzewa płyn roboczy o niższej temperaturze wrzenia niż woda. Przy wyższej entalpii złoża, powyżej 175°C, często stosowana jest technologia impulsowa – flash, w której płyn dwufazowy z odwiertu zasilającego jest separowany na parę bezpośrednio zasilającą generator i ciecz, która albo jest przesyłana do instalacji binarnej albo od razu jest ponownie zatłaczana do górotworu.

Podczas wyboru potencjalnej lokalizacji kryteria tektoniczne nie mają najwyższego priorytetu. Systemy EGS tworzone były zarówno w formacjach poddanych reżimom ekstensyjnym i przesuwczym (np. Soultz-sous-Forêts, Landau), jak i kompresyjnym (np. Habanero, Fjällbacka). Prędkości fali podłużnej w skałach krystalicznych stref docelowych zazwyczaj znajdują się w granicach 4400-5500 m/s. Dynamiczne moduły Younga oraz współczynniki Poissona dla tego rodzaju formacji są najczęściej raportowane w granicach odpowiednio 45-75 GPa i 0,12-0,25, przy czym w strefach spękanych i przeobrażonych hydrotermalnie moduły Younga osiągają znacznie niższe wartości w porównaniu do analogicznych skał nienaruszonych.

Zabiegi HF wykonywane w skałach magmowych to najczęściej zabiegu typu Massive Hydraulic Fracturing (MHF), w których pompuje się co najmniej 1000 $m^3$ cieczy zabiegowej w danym etapie zabiegu lub co najmniej 10 000 $m^3$ podczas całej operacji. Z uwagi na fakt, że większość projektów EGS była pierwotnie projektami naukowo-badawczymi, stosowano w nich także innego rodzaju schematy pompowania, w tym stymulację cykliczną, a także opartą o możliwie niskie ciśnienia różnicowe, mające na celu zmniejszyć ilość rejestrowanych zdarzeń sejsmicznych zachodzących podczas prac. W skałach krystalicznych, jako główną ciecz zabiegową najczęściej stosowano czystą wodę, bez dodatków polimerów zwiększających lepkość, reduktorów tarcia, inhibitorów minerałów ilastych i innych składników powszechnie stosowanych w przemyśle naftowym. W zabiegach tych nie stosowano materiałów podsadzkowych, ze względu na zdolność szczeliny stymulowanej hydrościnaniem do samopodsadzenia.

Systemy geotermalne typu wspomaganego są tworzone również w formacjach osadowych lub w strefach przejściowych pomiędzy formacjami osadowymi a krystalicznymi, czego przykładem jest projekt Groß Schönebeck w Niemczech, gdzie stymulowane były horyzonty w piaskowcach czerwonego spągowca oraz niżej ległych permskich skałach wulkanicznych (andezytach). W skałach osadowych w zabiegu HF tworzone są głównie nowe szczeliny. Ponieważ skały te charakteryzują się zazwyczaj niższą wytrzymałością mechaniczną niż granity, a na płaszczyznach nowo wytworzonych szczelin nie jest indukowany poślizg, formacje te wymagają wykonywania zabiegów z wykorzystaniem podsadzki o wysokiej wytrzymałości i o wymiarach najczęściej 20/40 mesh (425-850 µm). Determinuje to użycie cieczy zabiegowych zdolnych do jej transportu. W tym celu wykorzystywane są płyny na bazie naturalnych lub sztucznych polimerów liniowych lub usieciowanych, zwiększających lepkość. Podejmowane były również nieliczne próby wykonywania szczelinowania typu MHF w piaskowcach. W analizowanych projektach EGS, monitorowano zdarzenia mikrosejsmiczne zachodzące zarówno podczas zabiegów HF jak i po ich zakończeniu. W większości przypadków nie odnotowano zdarzeń o magnitudzie, która mogłaby zagrozić przebiegowi prac oraz bezpieczeństwu osób i mienia. W dwóch projektach miały miejsce zdarzenia odczuwalne na powierzchni ziemi: Phoang (magnituda 5,5) oraz Basel (magnituda 3,4) (Ladner i inni, 2009;

Ellsworth i inni, 2019). W efekcie tych zdarzeń obydwa projekty zostały wstrzymane, a następnie przedwcześnie zakończone.

## 2.3 Obszary perspektywiczne dla geotermii wspomaganej w Polsce

Na podstawie danych literaturowych dotyczących geotermii wspomaganej na świecie, a także dotychczas wykonanych analiz potencjalnych lokalizacji w Polsce, w artykule I wskazano również perspektywiczne obszary, w których mogłyby powstać tego rodzaju systemy geotermalne (figura 2.2). Obszary te obejmują rejon Karkonoszy (karbońskie granity), blok Gorzowa (permskie skały wulkaniczne), rejon niecki mogileńsko-łódzkiej (formacje osadowe triasu dolnego), a także karbońskie formacje osadowe Górnośląskiego Zagłębia Węglowego i permsko-karbońskie skały osadowe niecki szczecińskiej. Perspektywiczne formacje występują na głębokościach poniżej 4000 m i osiągają temperatury powyżej 150°C. Reżim tektoniczny na tych obszarach jest opisywany jako ekstensyjny lub ekstensyjny z elementem przesuwczym, a główne naprężenie pionowe, przy założeniu średniej gęstości skał nadkładu wynoszącej 2,4 g/cm$^3$, wynosi od 96 od 156 MPa, w zależności od rozpatrywanej głębokości.

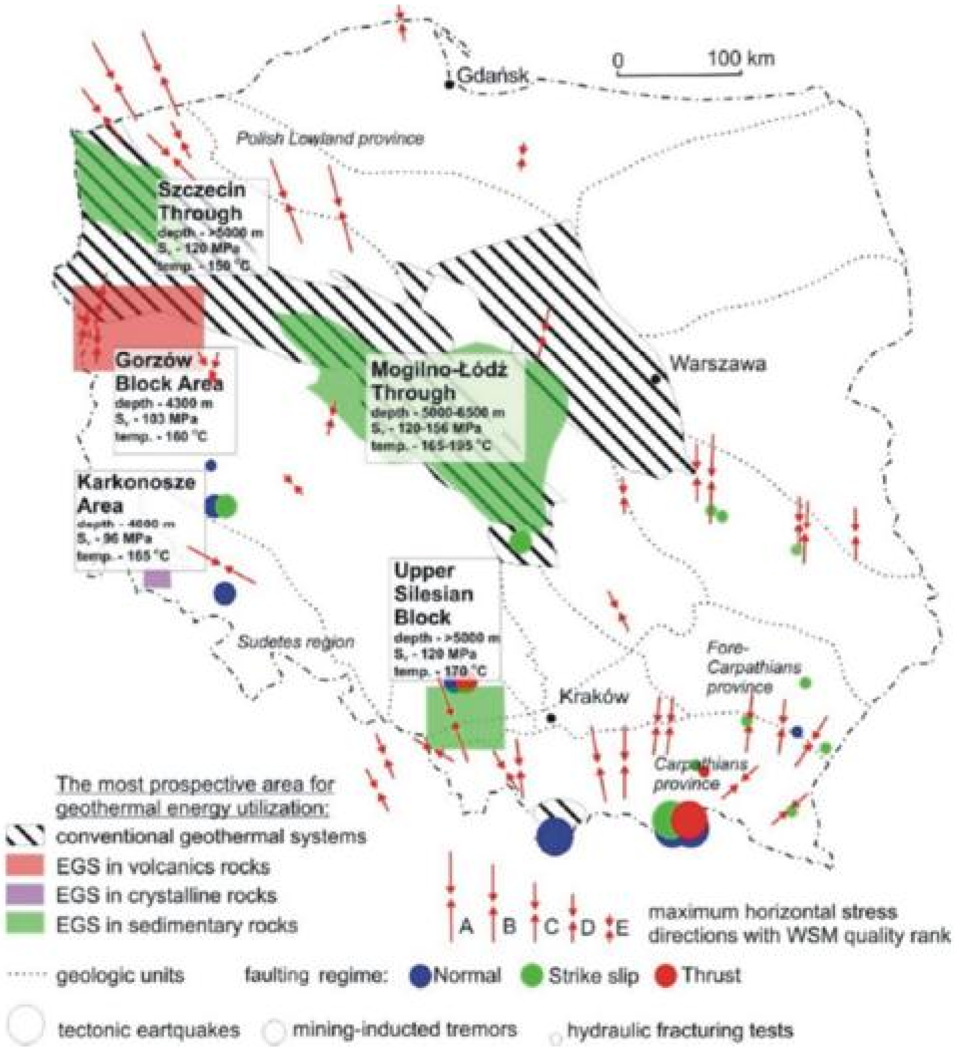


Figura 2.2: Obszary perspektywiczne dla geotermii wspomaganej w Polsce, scharakteryzowane w artykule I.

## 2.4 Podsumowanie

W artykule I zaprezentowano wyniki przeglądu literaturowego obejmującego najważniejsze uwarunkowania geologiczne, złożowe oraz elementy technologii hydraulicznego szczelinowania w najistotniejszych projektach EGS prowadzonych na świecie. Przeanalizowane publikacje naukowe oraz sprawozdania z projektów badawczych jasno wskazują, że hydrauliczne szczelinowanie jest najczęściej używaną i najskuteczniejszą metodą tworzenia kolektorów geotermalnych w skałach typu HDR, zarówno osadowych jak i magmowych. Jednymi z najistotniejszych kwestii dotyczących stymulacji hydraulicznej formacji HDR są różnice w mechanizmie stymulacji w zależności od typu litologicznego skały. Formacje osadowe są stymulowane w mechanizmie tensyjnym. Powstają w nich najczęściej nowe indukowane szczeliny, propagujące w kierunku prostopadłym do minimalnego naprężenia horyzontalnego. W formacjach magmowych zaś, głównymi arteriami przewodności są reaktywowane w mechanizmie hydrościnania szczeliny naturalne. Na obszarze Polski zidentyfikowano kilka regionów o podwyższonym potencjale dla systemów EGS, charakteryzujących się korzystnym gradientem geotermalnym. Do najbardziej perspektywicznych zalicza się m.in. rejon Karkonoszy, blok Gorzowa, nieckę szczecińską, nieckę mogileńsko-łódzką oraz blok Górnośląski. Zebrane w publikacji dane umożliwiły określenie najbardziej perspektywicznych obszarów badawczych, przewidzianych do szczegółowej analizy w ramach doktoratu oraz zdefiniowanie zakresu badań laboratoryjnych opisanych w artykułach III i IV. Pozwoliły one także na opracowanie założeń symulacji numerycznych zabiegów hydraulicznego szczelinowania dopasowanych do konkretnych warunków geologiczno-złożowych perspektywicznych obszarów w Polsce zaprezentowanych w artykule V.

# 3. Potencjał geotermalny gorących suchych skał w krajach południowo-wschodniej części basenu bałtyckiego – Artykuł II

Początek drugiej dekady XXI wieku był czasem istotnych zmian w postrzeganiu dostępności i bezpieczeństwa energetycznego w krajach europejskich. Destabilizujący europejską gospodarkę konflikt pomiędzy Rosją i Ukrainą, a także postępujące wycofywanie się z wykorzystywania paliw kopalnych, wzmocniły działania na rzecz rozwoju technologii energetycznych opartych o źródła odnawialne i bez emisyjne. Energetyka geotermalna jest jednym z najbardziej stabilnych źródeł energii odnawialnej, a wykorzystanie ciepła gorących suchych skał pozwala na czerpanie korzyści z jej potencjału niemalże w każdym miejscu na ziemi. Artykuł II będący autorskim przeglądem literatury wykonanym przez doktoranta, ma charakter pracy uzupełniającej publikację I, rozbudowując zagadnienia dotyczące obszarów perspektywicznych dla technologii EGS w Europie o kraje bałtyckie oraz porównanie warunków geologicznych w ich perspektywicznych obszarach do warunków Polskich. Kraje te są obecnie w dużym stopniu uzależnione od dostaw energii z zewnętrznych źródeł. Rozwój technologii wspomaganych systemów geotermalnych mógłby spowodować zwiększenie udziału energii produkowanej lokalnie w krajowym miksie energetycznym tych państw oraz zwiększyć dywersyfikację dostaw energii. Tego rodzaju opracowanie dotyczące potencjału geotermii wspomaganej krajów południowo-wschodniej części basenu bałtyckiego nie było dotychczas opublikowane. Informacje zgromadzone w artykule II umożliwiły wyznaczenie najbardziej perspektywicznych obszarów badawczych, które zostały szczegółowo zanalizowane w artykułach III, IV i V.

## 3.1 Potencjał gorących suchych skał w krajach bałtyckich.

W analizowanym rejonie Europy występuje obniżona gęstość strumienia ciepła ziemskiego, będąca rezultatem efektu paleoklimatycznego związanego z najmłodszą epoką lodowcową. Mimo to, zarówno rozkład gradientu geotermicznego, jak i gęstości strumienia ciepła, nie różnią się znacząco od wartości mierzonych w Europie Zachodniej (w szczególności w Rowie Renu) i znacznie przewyższają parametry termiczne w Finlandii, gdzie realizowany jest obecnie projekt EGS (Vidal i Genter, 2018; Kukkonen i Pentti, 2021). W krajach bałtyckich (Litwa, Łotwa oraz Estonia) potencjał HDR leży w podłożu krystalicznym. Strop perspektywicznych intruzji magmowych występuje tam stosunkowo płytko, od ok. 2500 m na Litwie do ok. 500 m w Estonii. Temperatury zbliżone do tych w Niemczech i w zachodniej Polsce (ok. 150°C) są osiągane na Litwie i Łotwie na głębokościach rzędu 4000-5000 m, a w Estonii, ze względu na najniższy gradient geotermiczny (26-28°C/1000 m) jeszcze głębiej.

Perspektywicznymi obszarami na Litwie jest rejon intruzji Zemaiciu Naumiestis, na południe od Kłajpedy, gdzie gradient geotermiczny osiąga 35-40°C/1000 m, a temperatura rzędu 150°C w sjenogranitach jest osiągana na głębokości 4500-5000 m (Motuza i inni, 2003; Sliaupa i inni, 2010), (tabela 3.1). Na Łotwie można wyróżnić dwa obszary o podwyższonym potencjale, w obszarach o gradiencie geotermicznym do maksymalnie 35°C/1000 m: prekambryjski batolit na południe od Lipawy oraz batolit w centralnej oraz południowej części kraju, w którym temperatura na głębokości 4000 m powinna wynosić ok. 140°C (Borodinecs i inni, 2020). W Estonii najwyższy potencjał mają granity rapakivi prekambryjskiego cokołu krystalicznego, występujące w centralnej części kraju. Jednakże ze względu na niski gradient geotermiczny i strumień ciepła w tym rejonie, na głębokości rzędu 4000 m spodziewane temperatury nie przekraczają 73°C (Joeleht i Kukkonen, 2002; Nurmi, 2022).

Odrębną kwestią jest słabe rozpoznanie lokalnych warunków tektonicznych państw bałtyckich, a w szczególności rozwoju sieci naturalnych szczelin i stref uskokowych, wpływających na kierunek propagacji szczelin w trakcie zabiegów HF. Stanowi to główną barierę rozwoju wysokotemperaturowej geotermii wspomaganej w tych krajach.

Tabela 3.1: Porównanie wybranych obszarów perspektywicznych dla EGS w obszarze południowo-wschodniego basenu bałtyckiego.

| Obszar perspektywiczny dla EGS | | Gradient geotemiczny, °C/1000 m | Gęstość strumienia cieplnego, $mW/m^2$ | Głębokość strefy docelowej, m temperatura,°C | Litologia, stratygrafia |
|---|---|---|---|---|---|
| Litwa | intruzja Zemaiciu Naumiestis na południe od Kłaipedy | 35-40 | 83-100 | 4500-5000, 150 | sjenogranity, porfirowo-kwarcowe monzodioryty prekambru |
| Łotwa | batolit na południe od Lipawy | do 35 | brak danych | poniżej 1740, 140 na głębokości 4000 | intruzywne skały magmowe prekambru |
| | batolit w centralnej i południowej części kraju | do 35 | brak danych | poniżej 1500, 140 na głębokości 4000 | intruzywne skały magmowe prekambru |
| Estonia | północna i centralna część kraju, cokół prekambryjski | 26-28 w pokrywie osadowej, 14 w cokole | 40-50, 42 | 4000, 58-73 w zależności od obszaru | granity rapakivi, prekambru |
| Polska | rejon Karkonoszy | 44 | 75-80 | 4000, 165 | intruzywne skały magmowe karbonu |
| | blok Gorzowa | 35-40 | 105 | 4300, 160 | trachyandezyty permskie |
| | niecka mogileńsko-łódzka | do 34 | 75-90 | 5000-6500, 165-195 | piaskowce pstrego piaskowca, trias dolny |
| | niecka szczecińska | do 27 | 85-100 | >5000, 150 | skały osadowe, karbońskie i permskie |
| | blok górnośląski | do 45 | 80-95 | >5000, 170 | klastyczne osady karbońskie |

## 3.2 Potencjał gorących suchych skał w Polsce na tle krajów bałtyckich

Najwyższy strumień cieplny na obszarze Polski jest obserwowany we wschodniej i centralnej części kraju (Szewczyk i Gientka, 2009). Jego wartości dobrze korelują z temperaturami skorupy ziemskiej obserwowanymi na głębokości 2 km (Szewczyk, 2010). Gradienty geotermalne są wyższe w porównaniu do najbardziej perspektywicznych obszarów w krajach Bałtyckich i osiągają wartości od 34 do 45°C/1000 m, w zależności od konkretnego perspektywicznego obszaru. Jedynie w obszarze niecki szczecińskiej gradient geotermiczny nie przekracza 27°C/1000 m. Natężenie strumienia cieplnego przewyższa wartości obserwowane w Estonii i dorównuje tym zanotowanym na Litwie 65-105 mW/m$^2$, w zależności od konkretnego perspektywicznego obszaru (figura 3.1).

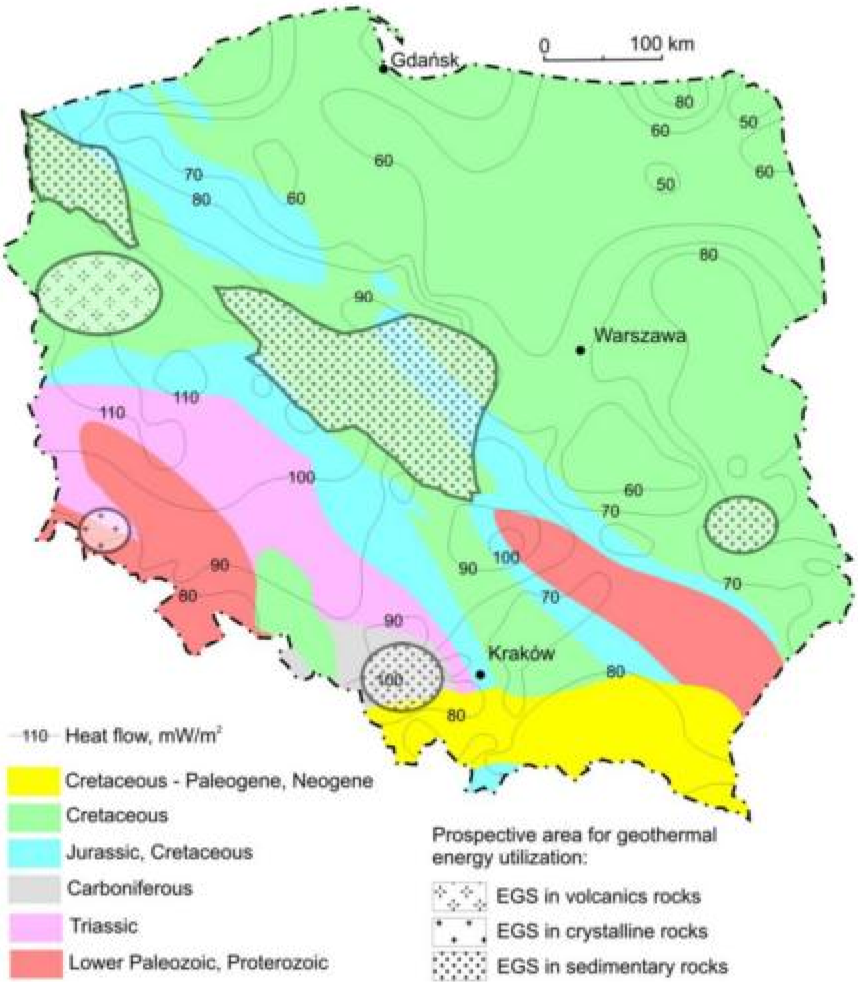


Figura 3.1: Perspektywiczne rejony EGS w Polsce na tle uproszczonej budowy geologicznej i gęstości strumienia cieplnego.

## 3.3 Podsumowanie

Artykuł II stanowi uzupełnienie przeglądu literatury, rozbudowując zagadnienia dotyczące obszarów perspektywicznych dla technologii EGS w Europie o kraje bałtyckie oraz zawierając porównanie warunków geologicznych w ich perspektywicznych obszarach do warunków Polskich. W scharakteryzowanych w artykule krajach południowo-wschodniej części basenu bałtyckiego (Litwa, Łotwa, Estonia) rozkład gradientu geotermalnego oraz gęstości strumienia cieplnego nie odbiega znacząco od wartości obserwowanych w Europie Zachodniej. Potencjał HDR w tych regionach związany jest głównie z obecnością podłoża krystalicznego, jednakże niewystarczające rozpoznanie lokalnych warunków tektonicznych, w szczególności rozwoju naturalnych stref szczelinowych i uskokowych, mających duże znaczenie podczas stymulacji hydraulicznej, stanowi główną barierę rozwoju technologii EGS. Informacje i dane zgromadzone w artykule II umożliwiły wyznaczenie najbardziej perspektywicznych obszarów badawczych, które były szczegółowo analizowane w artykułach III, IV i V.

# 4. Charakterystyka petrofizyczno-geomechaniczna gorących suchych skał z perspektywicznych obszarów w Polsce – Artykuł III

Informacje niezbędne do zaprojektowania zabiegu hydraulicznego szczelinowania na potrzeby geotermii wspomaganej, podobnie jak w przypadku wydobycia węglowodorów, można podzielić na dwie główne grupy (Kasza, 2019):

- dane otworowe: głębokość, konstrukcja otworu (w tym zarurowanie i zacementowanie), dotychczasowe prace i pomiary wykonywane w otworze (np. rekonstrukcje),
- dane złożowe: miąższość strefy docelowej oraz stref wyżej i niżej ległych, porowatość, przepuszczalność, skład mineralny, temperatura, nasycenie przestrzeni porowej, ciśnienie złożowe, uszkodzenie przepuszczalności strefy przyodwiertowej, parametry geomechaniczne skał, wartości naprężeń głównych.

Dane dotyczące parametrów mechanicznych skał strefy złożowej, nadkładu oraz formacji niżej ległych, wraz z kierunkami i wartościami naprężeń głównych pozwalają wyznaczyć ilość energii potrzebną do wytworzenia szczelin hydraulicznych lub otwarcia szczelin naturalnych w procesie hydraulicznego szczelinowania. W artykule III, na podstawie wykonanych przez doktoranta badań laboratoryjnych na próbkach skalnych, dokonano charakterystyki parametrów petrofizycznych oraz petrograficznych wybranych perspektywicznych formacji typu HDR w Polsce. Przedstawiono również wyniki samodzielnych badań geomechanicznych, przeprowadzonych na zmodyfikowanym przez doktoranta urządzeniu do testów ultradźwiękowych. Wskazano także, w jaki sposób wskaźnik kruchości skał (*Brittleness index,* BI), wykorzystywany dotąd w przemyśle naftowo-gazowym, może być używany do oceny podatności na hydrauliczne szczelinowanie w tychże formacjach. Tego rodzaju charakterystyka obszarów perspektywicznych w Polsce oraz sposób wykorzystania wskaźnika kruchości nie zostały wcześniej opublikowane. Przedstawione w artykule III dane i informacje dotyczące perspektywicznych formacji skalnych zostały wykorzystane w dalszych pracach ukierunkowanych na osiągnięcie głównych celów rozprawy doktorskiej, czyli wyznaczenie wpływu parametrów sprężystości na geometrię kolektora geotermalnego i opracowanie uogólnionych rekomendacji technologicznych do wykonania zabiegów w warunkach polowych. Rezultaty tych prac omówiono w artykule V.

## 4.1 Analizowane obszary perspektywiczne

Na podstawie omówionego wcześniej rozpoznania warunków geologicznych i analizy projektów geotermii wspomaganej (publikacje I i II), wytypowano trzy perspektywiczne dla technologii EGS obszary na terenie Polski. Za najkorzystniejsze uznano lokalizacje znajdujące się w strefach o podwyższonych parametrach termicznych, w zachodniej i centralnej części kraju. Każda z tych lokalizacji charakteryzuje inną budową geologiczną i innym typem skały docelowej. Wytypowanie karbońskich granitów karkonoskich, triasowych piaskowców niecki mogleńsko-łódzkiej oraz dolnopermskich wulkanitów bloku Gorzowa pozwoliło na uzyskanie pełnego przekroju typów formacji, w których są realizowane projekty geotermii wspomaganej na świecie. Podczas realizacji pracy przeanalizowano profile 29 otworów wiertniczych z trzech wymienionych lokalizacji pod kątem litologii strefy docelowej, miąższości poszczególnych formacji oraz dostępności materiału rdzeniowego. Na tej podstawie wytypowano cztery odwierty, z których pobrano próbki skał. Były to: Czerwony Potok-PIG-1 (rejon Karkonoszy), Piotrków Trybunalski IG-1 (niecka mogileńsko-łódzka) oraz Gorzów Wielkopolski-2 i Jeniniec-4 (blok Gorzowa).

## 4.2 Metodyka badań laboratoryjnych

Z pobranych próbek skalnych wycięto 96 próbek rdzeniowych o średnicy 2,54 cm (1,0 cal) i długości 5,08 cm (2,0 cale), w kierunku prostopadłym do warstwowania (równoległym do osi otworów wiertniczych), zgodnie z metodami sugerowanymi przez ISRM (Ulusay i Hudson, 2007). Dla każdej z próbek wykonano podstawowe badania petrofizyczne i analizy składu mineralnego. Wyznaczono gęstości szkieletowe oraz objętościowe próbek, współczynniki porowatości efektywnej metodą helową oraz współczynniki przepuszczalności absolutnej dla azotu. Skład mineralny poszczególnych próbek wyznaczono w oparciu o metodę dyfrakcji rentgenowskiej (XRD), z analizą ilościową metodą Rietvelda. Dynamiczne parametry sprężystości zostały wyznaczone dla 64 próbek skał, przy wykorzystaniu elementów metodyki zalecanej przez ISRM (Ulusay i Hudson, 2007) oraz metodyki stworzonej przez doktoranta na potrzeby wykonywania badań metodą ultradźwiękową. Pomiary wykonywano przy pomocy urządzenia Vinci AVS-700 do wyznaczania prędkości propagacji fal sprężystych w skałach, w warunkach złożowych. Wyznaczono prędkości propagacji fali podłużnej (P) oraz poprzecznej (S) przy częstotliwości pracy przetworników 500 kHz. Testy zostały przeprowadzone w zakresie ciśnienia 0 – 55 MPa, dla próbek, których przestrzeń porowa była nasycona powietrzem (próbki suche). W pierwszej fazie przykładano ciśnienie osiowe oraz obwodowe o takich samych wartościach – do 15 i 30 MPa, a następnie zwiększano ciśnienie osiowe, stopniowo do 55 MPa (figura 4.1). Dla wszystkich trzech konfiguracji ciśnienia obwodowego, tj. 15, 30 i 55 MPa, wykonywano pomiary dla co najmniej czterech próbek rdzeniowych. Każda próbka była ściskana w komorze urządzenia tylko jeden raz. Temperatura badań wynosiła 140°C, co jest górną granicą możliwości urządzenia.

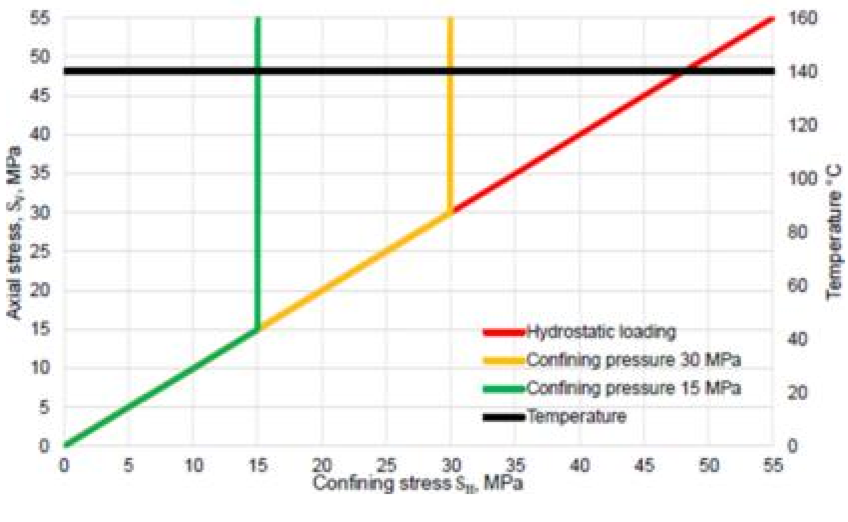


Figura 4.1: Schemat przebiegu badań ultradźwiękowych.

Dynamiczne parametry sprężystości: współczynnik Poissona $\nu_d$, moduł Younga $E_d$, moduł sprężystości postaciowej $G_d$ i moduł sprężystości objętościowej $K_d$ obliczono w oparciu o następujące równania:

$$\nu_d = \frac{1/2-(V_S/V_P)^2}{1-(V_S/V_P)^2} \tag{4.1}$$

$$E_d = \rho\frac{{V_P}^2(1+v)(1-v)}{(1-v)} \tag{4.2}$$

$$G_d = \rho {V_S}^2 \tag{4.3}$$

$$K_d = \rho({V_P}^2 - \frac{4}{3}{V_S}^2) \tag{4.4}$$

Określony w pracy skład mineralny próbek i wyznaczone na podstawie badań laboratoryjnych wartości modułu Younga oraz współczynnika Poissona pozwoliły ponadto na obliczenie wskaźnika kruchości analizowanych próbek, co opisano szerzej w rozdziale 4.5.

## 4.3 Parametry petrofizyczne i skład mineralny badanych skał

Badane próbki ze wszystkich trzech lokalizacji charakteryzowały się niskimi współczynnikami przepuszczalności absolutnej oraz porowatości efektywnej. Najniższą porowatością cechowały się granity karkonoskie oraz wulkanity z otworu Jeniniec-4, przy czym porowatość ta związana była głównie z naturalnymi mikroszczelinami. Porowatość międzyziarnowa w piaskowcach niecki mogileńsko-łódzkiej i riolitach z otworu Gorzów Wielkopolski-2 była słabo zróżnicowana. Średnia przepuszczalność we wszystkich analizowanych typach skał wynosiła znacznie poniżej 0,1 mD, a dla granitów i wulkanitów w większości przypadków nie przekraczała 0,001 mD. Wyznaczone parametry petrofizyczne pozwalają zaklasyfikować wszystkie analizowane skały do grupy petrotermalnych (figura 4.2).

Próbki skał karkonoskich reprezentują monzogranity, w których albit stanowi od 15 do 33,1%, ortoklaz i mikroklin odpowiednio 15 i 19%, a średnia zawartość kwarcu wynosi 23%. Wulkanity bloku Gorzowa są zbudowane głównie z kwarcu (średnio 22% i 38% odpowiednio dla otworów Jeniniec-4 i Gorzów Wielkopolski-2) i skalenia potasowego (ortoklazu i mikroklinu w ilości odpowiednio 41% i 24%). Pozwala to zaklasyfikować je jako riolity i riodacyty. Piaskowce rejonu niecki mogileńsko-łódzkiej zawierają głównie kwarc (średnio 52%) oraz plagioklazy. Charakteryzują się niską zawartością węglanów, a ilość minerałów ilastych nie przekracza 14%. Skały te mogą być zaklasyfikowane jako arenity lityczne.

## 4.4 Dynamiczne parametry sprężystości

W związku z tym, że podczas badań nie zaobserwowano korelacji pomiędzy prędkością fal P i S, a zastosowanym ciśnieniem efektywnym (15, 30 i 55 MPa), a ponadto próbki były pobrane ze stosunkowo szerokich interwałów głębokościowych, zdecydowano, że dla trzech powyżej wymienionych ciśnień efektywnych wyznaczone będą średnie prędkości fal. Próbki granitów pobrane z interwału od 155 do 184 m charakteryzowały się wyższymi prędkościami propagacji fal i wyższymi modułami sprężystości, co można wyjaśnić niższym stopniem ich przeobrażenia i mniejszą ilością naturalnych płaszczyzn nieciągłości (figura 4.3).

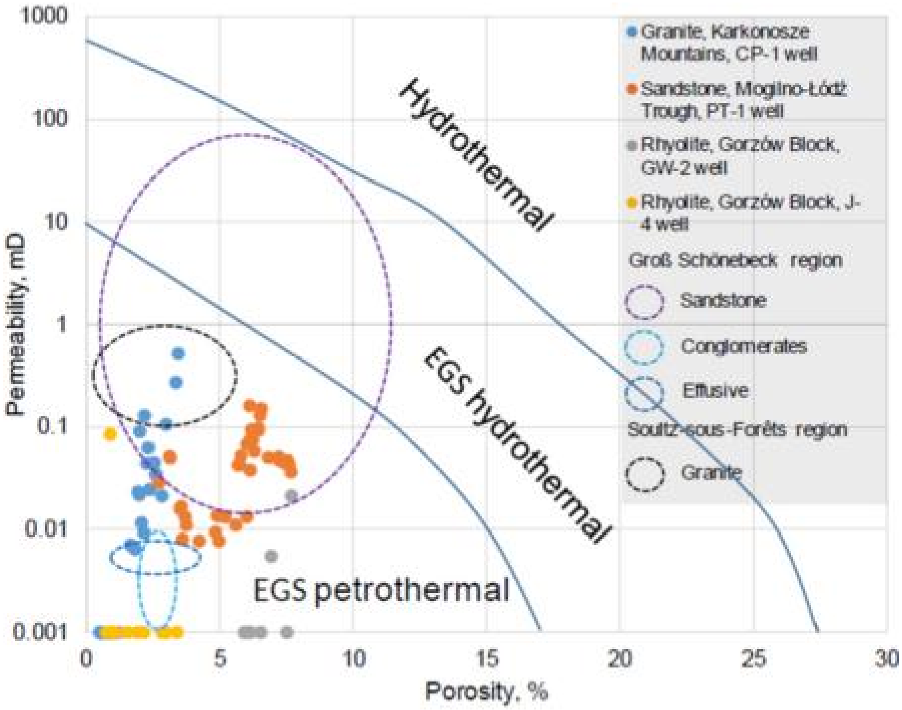


Figura 4.2: Klasyfikacja analizowanych skał na podstawie porowatości efektywnej i przepuszczalności, na tle wybranych formacji Europy Zachodniej.

Wzrost prędkości propagacji w reakcji na wzrost ciśnienia efektywnego był największy w niskich zakresach ciśnień, co odpowiadało zamykaniu się porów i naturalnych szczelin. W przypadku analizowanych piaskowców najwyższymi prędkościami fal charakteryzowały się próbki z najmniejszych głębokości, co było spowodowane podwyższoną zawartością kwarcu i obniżoną illitu. Niski współczynnik Poissona (poniżej 0,2) odzwierciedlał nasycenie przestrzeni porowej piaskowców powietrzem (pomiar na suchych próbkach) (figura 4.4). W wulkanitach z otworu Gorzów Wielkopolski-2, prawdopodobnie ze względu na ich większą porowatość, zmierzono niższe prędkości fal w porównaniu do skał z otworu Jeniniec-4. W części próbek z otworu Jeniniec-4 zanotowano spadek prędkości fal przy wyższych wartościach ciśnienia efektywnego, co najpewniej odzwierciedla początek procesu pękania próbek, prowadzącego do ich zniszczenia (figura 4.5). Na podstawie uzyskanych wyników obliczono korelacje pomiędzy prędkościami fal P, S, modułami sprężystości, a współczynnikami porowatości efektywnej. Najwyższe współczynniki determinacji uzyskano dla zależności liniowej pomiędzy współczynnikiem porowatości efektywnej i odpowiednio: prędkością fali P dla granitów - $R^2 = 0{,}91$ oraz modułem ścinania dla riolitów z otworu Gorzów Wielkopolski-2 - $R^2 = 0{,}87$.

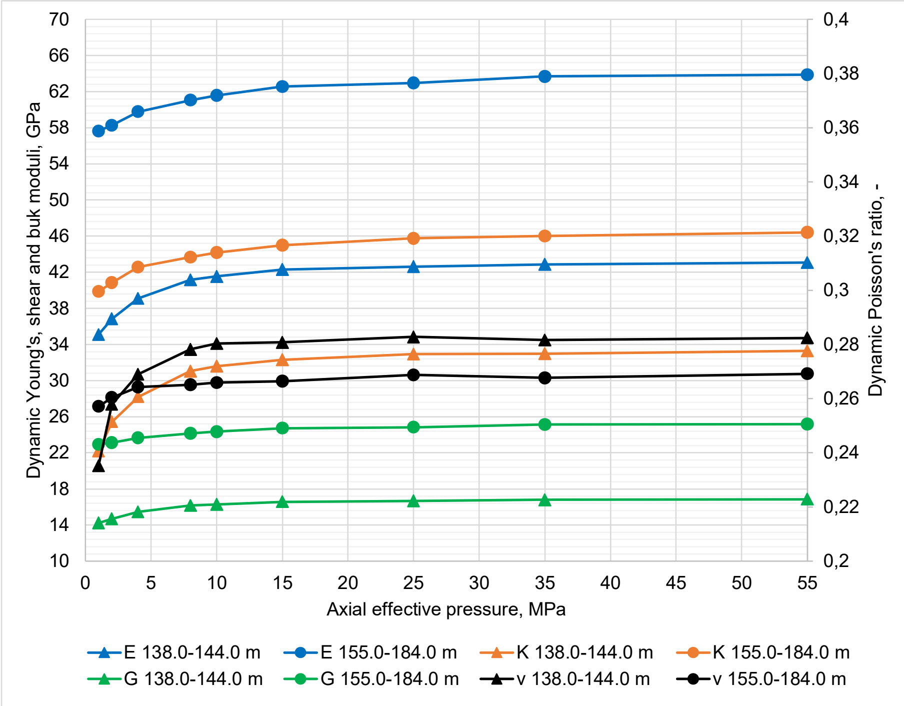


Figura 4.3: Średnie parametry sprężystości w funkcji osiowego ciśnienia efektywnego uzyskane podczas badań ultradźwiękowych próbek granitów karkonoskich: E – moduł Younga, G – moduł sprężystości postaci, K – moduł sprężystości objętościowej, v – współczynnik Poissona.

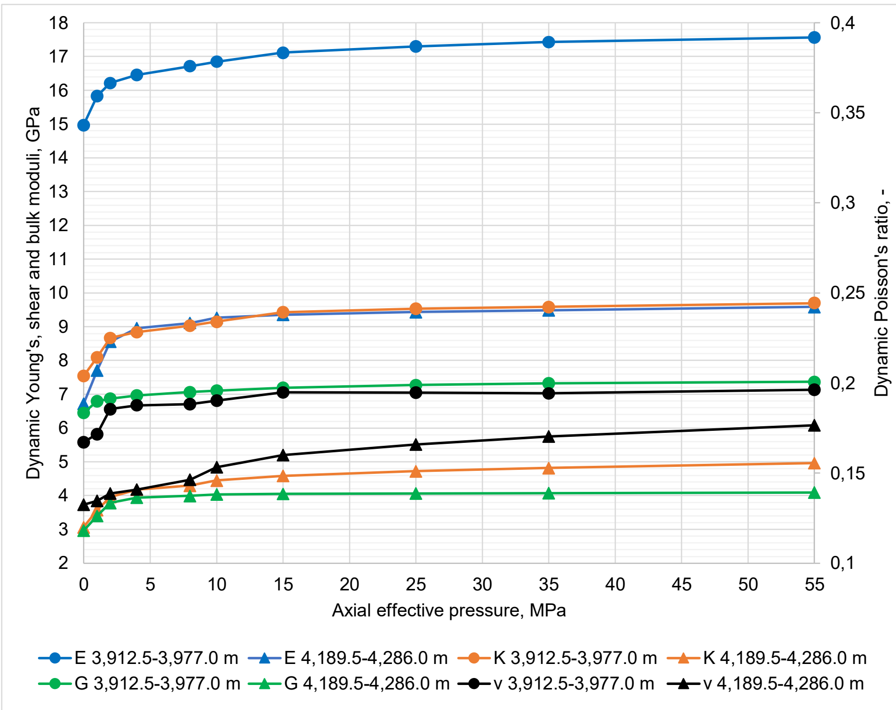


Figura 4.4: Średnie parametry sprężystości w funkcji osiowego ciśnienia efektywnego uzyskane podczas badań ultradźwiękowych piaskowców rejonu niecki mogileńsko-łódzkiej: E – moduł Younga, G – moduł sprężystości postaci, K – moduł sprężystości objętościowej, v – współczynnik Poissona.

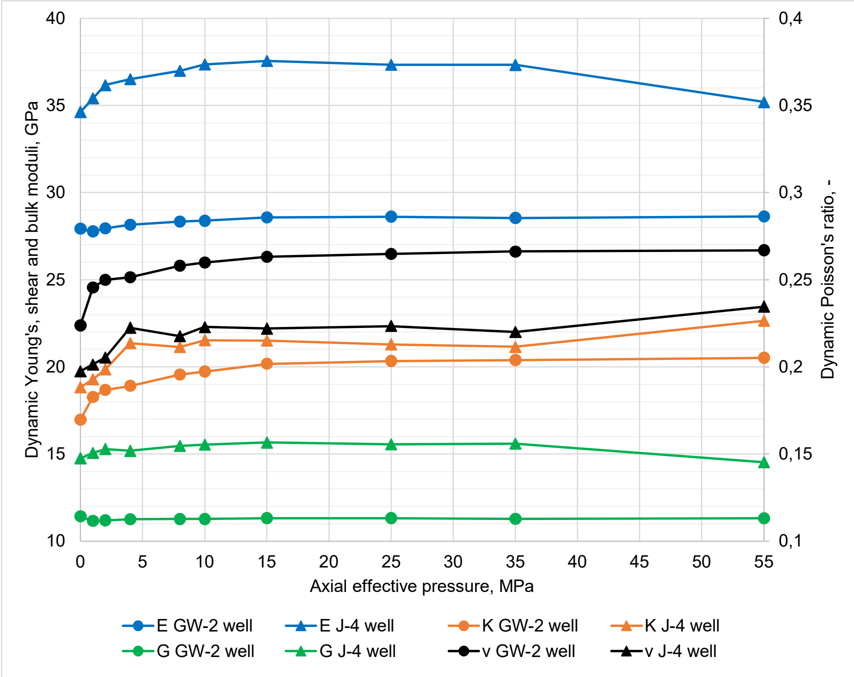


Figura 4.5: Średnie parametry sprężystości w funkcji osiowego ciśnienia efektywnego uzyskane podczas badań ultradźwiękowych wulkanitów bloku Gorzowa: E – moduł Younga, G – moduł sprężystości postaci, K – moduł sprężystości objętościowej, v – współczynnik Poissona.

## 4.5 Wskaźnik kruchości

Wskaźnik kruchości - *Brittleness index* (BI), jest parametrem powiązanym z zachowaniem się ośrodka skalnego podczas jego obciążania oraz ilością energii wymaganą do jego zniszczenia. W procesie stymulacji hydraulicznej niekonwencjonalnych złóż gazu ziemnego odzwierciedla on podatność danej części udostępnianego interwału, na tworzenie się rozbudowanej sieci szczelin, zwiększającej kontakt pomiędzy złożem i otworem. Wraz ze wzrostem wskaźnika BI wzrasta prawdopodobieństwo na tworzenie się pożądanej, rozbudowanej sieci szczelin, zwiększającej dopływ gazu do odwiertu. Z kolei przy niskich BI otwierające się szczeliny mają kształt prosty, dwuskrzydłowy, a objętość górotworu objęta procesem stymulacji jest mniejsza. W złożach geotermalnych BI może być używany jako wskaźnik stref potencjalnie korzystnych do stymulacji hydraulicznej. W niniejszej pracy BI obliczono w oparciu o określony wcześniej skład mineralny próbek (Jarvie i inni, 2007; Wang i Gale, 2009; Jin i inni, 2014a, 2014b) oraz wykorzystując zależności, wyznaczonych na podstawie badań laboratoryjnych, modułu Younga oraz współczynnika Poissona (Grieser and Bray, 2007).

Wskaźnik kruchości BI, określony na podstawie badań petrograficznych wykonanych na potrzeby tej pracy, niezależnie od zastosowanej metody obliczeniowej, jest wysoki dla wszystkich analizowanych formacji, za wyjątkiem wulkanitów z otworu Jeniniec-4, dla których wskaźnik ten osiąga średnie wartości. Wysokie wartości BI granitów, piaskowców i riolitów z otworu Gorzów Wielkopolski-2 (powyżej 74%) odzwierciedlają znaczny udział minerałów kruchych, tj. albitu, mikroklinu i kwarcu w granitach, kwarcu i skaleni potasowych oraz alkalicznych w piaskowcach, a także kwarcu i skalenia potasowego w riolitach. Najwyższą wartością wskaźnika BI, obliczoną na podstawie zależności pomiędzy dynamicznymi parametrami sprężystości, charakteryzują się granity karkonoskie, przy czym próbki pobrane z większej głębokości, o mniejszej liczbie spękań i szczelin, wykazują wyższą kruchość (68%) w porównaniu do pozostałych (50-53%). Wysokie wartości BI charakteryzują także riolity z otworu Jeniniec-4 - 53%, co wynika z wysokich modułów Younga tych próbek. Piaskowce z obydwu analizowanych interwałów charakteryzują się stosunkowo niskimi wartościami zarówno współczynnika Poissona, jak i modułu Younga, co przekłada się na niskie wartości BI (39-45%).

Ze względu na specyfikę granitowych skał typu HDR, w których głównym mechanizmem aktywacji szczelin jest hydrościnanie (indukowanie poślizgu i dylatacji ścian naturalnych szczelin poprzez działanie sił ścinających), wskaźnik kruchości BI w tego typu formacjach powinien być interpretowany w odmienny sposób niż w osadowych formacjach HDR, gdzie dominuje tworzenie się nowych szczelin lub otwieranie szczelin naturalnych pod wpływem działania sił tensyjnych. Strefy naturalnych spękań, stanowiące arterie przewodności w granitach, charakteryzują się znacznie niższymi modułami Younga oraz podwyższoną zawartością minerałów plastycznych, co przekłada się na niższe wartości wskaźnika kruchości. W zabiegach HF ulegają one stymulacji w pierwszej kolejności i przez to są najbardziej perspektywiczne. Zatem niskie wskaźniki BI w takich strefach świadczą o ich lepszej podatności do stymulacji hydraulicznej, w porównaniu do stref nieprzeobrażonych, o wyższych wartościach BI. Z drugiej jednak strony, najwyższe wartości BI, świadczą o wysokiej podatności na zabiegi HF w skałach osadowych typu HDR, o wysokich modułach Younga, niskich współczynnikach Poissona i z dominacją minerałów kruchych w składzie. Jest to zgodnie z tradycyjną interpretacją wskaźnika BI, gdyż skały te są bardziej zbliżone do formacji zbiornikowych dla węglowodorów, dla których pierwotnie przewidywano zastosowanie wskaźnika kruchości.

## 4.6 Podobieństwa i różnice analizowanych skał typu HDR w Polsce i Europie Zachodniej, w aspekcie ich podatności na hydrauliczne szczelinowanie

Nienaruszone granity karkonoskie charakteryzują się, podobnym do formacji udostępnionej w projekcie Soultz-Souz Forêts we Francji, składem mineralnym i podatnością na hydrauliczne szczelinowanie, wyrażoną przez wskaźnik BI. Przeobrażone granity karkonoskie, o podwyższonej ilości szczelin naturalnych i zwiększonej zawartości minerałów ilastych, wykazują znacznie niższe średnie moduły Younga w porównaniu do nienaruszonych skał w tej formacji. Podwyższona średnia zawartość minerałów ilastych w piaskowcach niecki mogileńsko-łódzkiej w porównaniu do analogicznych skał z rejonu Groß Schönebeck skutkuje niższymi wartościami wskaźnika BI obliczonego na podstawie składu mineralnego, co zwiększa prawdopodobieństwo tworzenia się szczelin dwuskrzydłowych. Dynamiczne moduły sprężystości piaskowców niecki mogileńsko-łódzkiej wykazują silną zmienność wraz z głębokością, ze względu na różnice w cementacji i rozwój naturalnych spękań. Niemniej jednak wartości BI oparte na zależności $E$ do $v$ dla tych skał, są znacznie niższe w porównaniu do piaskowców z rejonu Groß Schönebeck, co oznacza mniej korzystne warunki do rozwoju rozległej sieci szczelin podczas zabiegu. Mineralny wskaźnik BI dla ryolitów bloku Gorzowa jest silnie uzależniony od miejsca poboru próbek, ze względu na zmienność składu mineralnego i rozwój naturalnych pęknięć w tej formacji. Niższy geomechaniczny wskaźnik BI badanych ryolitów w porównaniu z odpowiadającą im formacją w basenie niemieckim wskazuje na większą podatność na szczelinowanie ze względu na lepiej rozwiniętą naturalną sieć spękań.

## 4.6 Podsumowanie

W artykule III zostały zaprezentowane wyniki badań laboratoryjnych skał typu HDR z wybranych, perspektywicznych dla EGS w Polsce lokalizacji. Wszystkie trzy przeanalizowane formacje, tj. karkonoskie granity, wulkanity bloku Gorzowa oraz piaskowce z niecki mogileńsko-łódzkiej, charakteryzowały się parametrami petrofizycznymi pozwalającym zaklasyfikować je jako skały typu petrotermalnego, odpowiedniego dla EGS. Próbki granitów cechowały się silnym zróżnicowaniem parametrów sprężystości, w zależności od stopnia przeobrażenia hydrotermalnego. Piaskowce posiadały znacznie niższe moduły Younga w porównaniu do analogicznych formacji HDR z obszaru Europy Zachodniej. Parametry mechaniczne badanych wulkanitów różniły się w zależności od struktury skały oraz formacji, z której zostały pobrane. Wskaźnik kruchości BI, niezależnie od zastosowanej metody obliczeniowej, jest wysoki dla wszystkich analizowanych formacji za wyjątkiem wulkanitów z otworu Jeniniec-4, dla których wskaźnik ten osiąga wartości średnie. W artykule zaproponowano nowy sposób interpretacji wskaźnika BI dla skał HDR magmowych. Jego obniżone wartości, powiązane w szczególności z obniżonym modułem Younga, mogą wskazywać strefy o obniżonej wytrzymałości w górotworze, charakterystyczne dla obszarów naruszonych tektonicznie i/lub zmienionych hydrotermalnie, które mogą służyć po stymulacji hydraulicznej jako arterie przewodności w systemie EGS. Obniżone wartości BI w skałach magmowych są zatem, w przeciwieństwie do skał osadowych, pożądane. Uzyskane w powyższych badaniach parametry petrofizyczne, petrograficzne oraz geomechaniczne stanowią wsad danych do oprogramowania FracPro, wykorzystanego do modelowania numerycznego geometrii szczeliny, opisanego w artykule V.

# 5. Potencjalne systemy geotermalne w zachodniej Polsce – zagadnienia petrotermalne i geochemiczne – artykuł IV

Parametry termiczne skał stanowią podstawowe dane wykorzystywane do wyznaczania strumienia cieplnego danego obszaru Ziemi, oceny reżimu termicznego i identyfikacji stref perspektywicznych dla geotermii. Ponadto interakcje ze skałą płynu roboczego, używanego w systemach wspomaganych, mogą prowadzić do rozpuszczenia lub wytrącania minerałów i w ten sposób modyfikować początkową porowatość i przepuszczalność szczelin wytworzonych hydraulicznie. Jest to jedno ze zjawisk, które determinuje wydajność systemów EGS. Badania prezentowane w publikacji IV wykonano na próbkach skalnych z opisanych wcześniej lokalizacji: rejonu Karkonoszy i bloku Gorzowa i na podstawie uzyskanych wyników dokonano oceny ich właściwości takich jak: przewodność termiczna, efuzyjność i dyfuzyjność. Artykuł zawiera także wyniki modelowania zmian temperatury skał i zasięgu ich schłodzenia podczas długotrwałej eksploatacji energii termalnej oraz wyniki modelowania geochemicznego interakcji geochemicznych, zachodzących na kontakcie ciecz robocza-skała, w trakcie eksploatacji ciepła z formacji HDR. Badania laboratoryjne oraz modelowania numeryczne były wykonane przez zespół naukowy, w którego skład wchodził doktorant. Miały one na celu poszerzenie zakresu dotychczasowego rozpoznania cech wybranych formacji, perspektywicznych dla rozwoju EGS w naszym kraju.

## 5.1 Parametry termiczne skał HDR

Własności cieplne skał opisywane przez ich parametry termiczne, takie jak np. efuzyjność, dyfuzyjność oraz przewodność cieplna, mają istotne znaczenie dla zapewnienia efektywnego transferu ciepła między formacją a cieczą roboczą w systemach HDR.

Na potrzeby dysertacji, pomiary termiczne zostały przeprowadzono przy użyciu analizatora TCi (C-Therm, Kanada), metodą przejściowego, płaskiego źródła ciepła (Di Sipio i inni, 2013; Labus i inni, 2023). Określono następujące parametry termiczne próbek skał:

- przewodność cieplną $k$ – zdolność materiału do przewodzenia ciepła,
- efuzyjność cieplną $e$ – właściwość materiału opisująca jak szybko zmienia się temperatura w materiale w odpowiedzi na zmianę temperatury na jego powierzchni,
- dyfuzyjność cieplną $\alpha$ – stosunek przewodności cieplnej do objętościowej pojemności cieplnej. Określa on szybkość zmiany temperatury w jednostce objętości materiału wywołaną transferem ciepła na jednostkę czasu.
- pojemność cieplną $c_{ps}$ – ilość ciepła niezbędną do zmiany temperatury materiału o jednostkę temperatury.

Do obliczenia wpływu parametrów termicznych na zasięg schłodzenia formacji podczas eksploatacji systemu EGS użyto modelu uproszczonego do pojedynczej domeny półnieskończonej (Labus i inni, 2023).

Dominujący wpływ na zróżnicowanie parametrów termicznych mają gęstość i porowatość skał. Na podstawie przeprowadzonych badań stwierdzono, że pojemność cieplna badanych skał jest ujemnie skorelowana z gęstością i dodatnio z porowatością, co wyjaśnia niska wartość ciepła właściwego kwarcu w porównaniu do powietrza, wypełniającego pory podczas badania. Efuzyjność, przewodność cieplna i dyfuzyjność są dodatnio skorelowane z porowatością. Przewodność termiczna ($k$) pozytywnie koreluje się z dyfuzyjnością, co pozwala wnioskować, że im wyższa wartość $k$ skały (oznaczająca, że można uzyskać więcej energii z danego źródła ciepła), tym szybciej energia ta jest uzupełniana z bardziej odległych części kolektora ze względu na wysoką dyfuzyjność. Optymalne wydajności systemów EGS osiągane są w skałach o równocześnie wysokiej efuzyjności, dyfuzyjności, pojemności i przewodności cieplnej. Skały z obydwu analizowanych formacji, biorąc pod uwagę temperaturę stref docelowych, charakteryzują się w tym kontekście korzystnymi wartościami omawianych parametrów. Obliczone parametry termiczne mieszczą się w zakresach podawanych w literaturze, przede wszystkim w odniesieniu do najczęściej wyznaczanej przewodności cieplnej. Najniższą średnią przewodność termiczną posiadają riolity z otworu J-4, 2,74 W/m·K, a najwyższą granity z rejonu Karkonoszy, 3,70 W/m·K. Podobne zależności występują w przypadku średniej efuzyjności, która wynosi dla tych skał odpowiednio 2338 i 2781 W·s$^{½}$/m$^2$/K (tabela 5.1). Granity karkonoskie charakteryzują się najwyższą dyfuzyjnością, co oznacza, że podczas potencjalnej eksploatacji geotermalnej skały te najszybciej osiągną równowagę termiczną. Powyższe cechy sprawiają, że jako lokalizacje EGS, granity karkonoskie są bardziej perspektywiczne od skał z bloku Gorzowa. Największą głębokość zasięgu schłodzenia (penetracji termicznej) obserwuje się w formacjach geologicznych o najwyższej średniej dyfuzyjności i przewodności cieplnej, takich jak granity z plutonu karkonoskiego, natomiast najmniejszą w ryolitach z bloku gorzowskiego (odwiert J-4). Po roku chłodzenia, głębokości penetracji wynoszą odpowiednio około 22 m i 21 m, a po 30 latach osiągają 160 m i 142 m (fig. 5.1). Spadek temperatury jest najmniej znaczący w plutonie karkonoskim, którego skały mają najwyższe wartości przewodności cieplnej i dyfuzyjności) (Fig. 5.1). Należy zauważyć, że skały bloku Gorzowa wykazują stosunkowo znaczący spadek temperatury, ze względu na niższe wartości obydwu tych parametrów. Jednakże, ze względu na wysoką temperaturę początkową tej formacji, spadek ten nie wyczerpuje zasobów geotermalnych, ani nie wpływa negatywnie na możliwość dalszej eksploatacji. Po 30 latach symulowanego poboru ciepła temperatura utrzymuje się na poziomie od 106°C do 108°C, co wskazuje na możliwość utrzymania długotrwałej eksploatacji.

Tabela 5.1: Wybrane średnie parametry termiczne testowanych skał

| Rodzaj skały, lokalizacja | Efuzyjność $e$, W·s$^{½}$/m$^2$/K | Dyfuzyjność $\alpha$, m$^2$/s | Przewodność termiczna $k$, W/m·K | Pojemność cieplna objętościowa $c_{ps}$, J/kg·K |
|---|---|---|---|---|
| Granit z rejonu Karkonoszy, otwór CP-1 | 2781,25 | 1,78 x 10$^{-6}$ | 3,70 | 809,82 |
| Riolit z bloku Gorzowa, otwór GW-2 | 2510,90 | 1,53 x 10$^{-6}$ | 3,10 | 831,00 |
| Riolit z bloku Gorzowa, otwór J-4 | 2338,39 | 1,37 x 10$^{-6}$ | 2,74 | 794,39 |

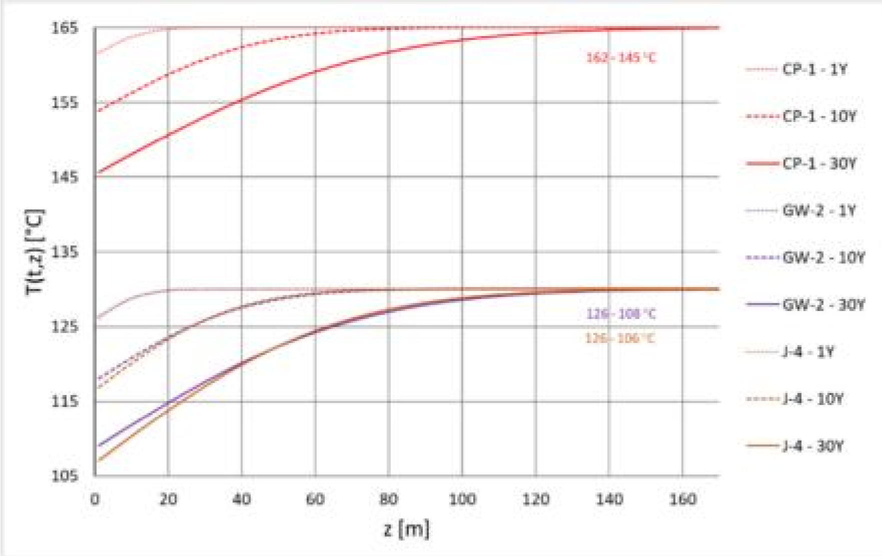


Figura 5.1. Zmiana temperatury T(t,z) w zależności od czasu i głębokości. Objaśnienia: CP-1, GW-2, J-4 –otwory wiertnicze; czas: 1Y – 1 rok, 10Y – 10 lat, 30Y – 30 lat.

## 5.2. Interakcje geochemiczne na kontakcie ciecz robocza-skała

Modelowanie geochemiczne przeprowadzono w programie React, będącym częścią symulatora Geochemist's Workbench 11. Założono zatłaczanie cieczy roboczej w postaci wody o niskiej mineralizacji w temperaturze 40°C. Dla każdego z kolektorów analizowano dwa przypadki: wodę o pH 7,5 oraz ciecz na bazie wody o tym samym składzie, energetyzowaną $CO_2$, do poziomu aktywności ciśnieniowej 100 bar, w celu uniknięcia skalingu. Przyjęto, że woda będzie reagowała ze skałą przez 20 dni, przepływając przez jej szczeliny i nagrzewając się do temperatury złożowej. Model miał objętość 12 500 $cm^3$, przy założonej porowatości szczelinowej 20%. W obliczeniach wykorzystano uproszczone równanie kinetyki rozpuszczania i krystalizacji równanie wg Lasaga (1984).

Modelowanie geochemiczne dowiodło, że potencjalne zmniejszenie porowatości spowodowane wytrącaniem się minerałów wtórnych jest mało prawdopodobne. Z drugiej strony, z powodu rozpuszczenia pierwotnych składników skały porowatość może wzrastać, powodować nadmiernie zwiększony przepływ cieczy roboczej i ostatecznie prowadzić do zmniejszenia wydajności kolektora (figura 5.2).

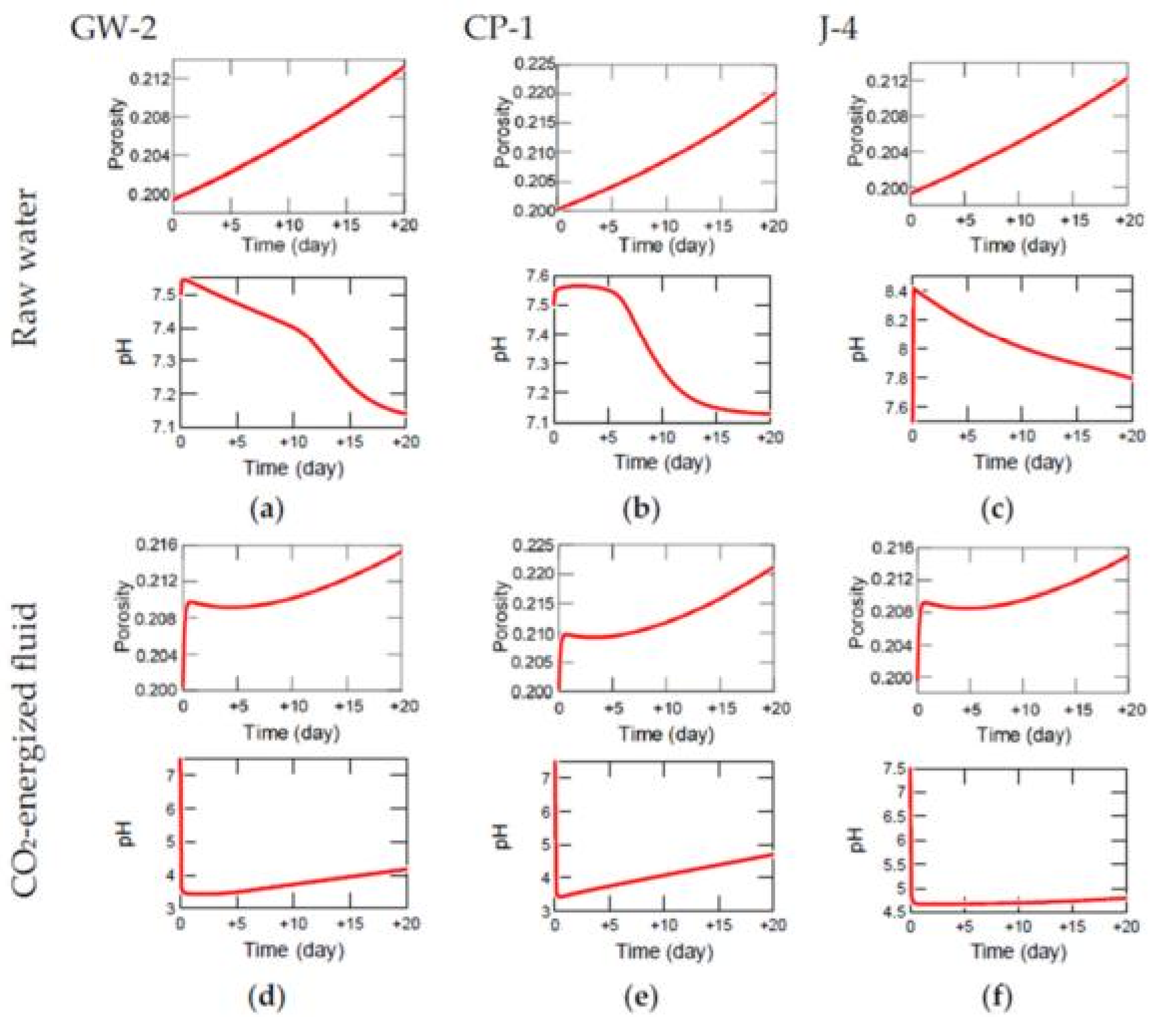


Figura 5.2: Zmiany w porowatości formacji oraz pH cieczy w wyniku kontaktu skały z czystą wodą: (a) – próbka GW-2, (b) – próbka CP-1, (c) – próbka J-4 i cieczą energetyzowaną $CO_2$: (d) – próbka GW-2, (e) – próbka CP-1, (f) – próbka J-4.

## 5.3. Podsumowanie

W artykule IV zaprezentowano wyniki laboratoryjnych badań parametrów termicznych skał z wybranych perspektywicznych dla EGS obszarów zachodniej Polski, rezultaty oszacowania zmian temperatury formacji i zasięgu ich schłodzenia oraz wyniki modelowania geochemicznego reakcji zachodzących w trakcie eksploatacji energii geotermalnej. Pomiary ujawniają, że granit Karkonoszy charakteryzuje się wysoką dyfuzyjnością i przewodnictwem cieplnym, co czyni go dobrym kandydatem do rozwoju systemów wspomaganych. Mimo, że ryolity bloku Gorzowa wykazują nieco niższe wartości tych parametrów, to ich wysokie temperatury początkowe są obiecujące z punktu widzenia długiej żywotności potencjalnych EGS. Wyniki symulacji geochemicznych wskazują, że wytrącanie się minerałów wtórnych, mogących spowodować uszkodzenie przepuszczalności, byłoby w analizowanych formacjach mało prawdopodobne. Przeciwnie, symulowany wzrost porowatości mógłby spowodować spadek oporu hydraulicznego, co spowodowałoby nadmierne zwiększenie prędkości przepływu i w konsekwencji negatywnie wpłynęło na wydajność EGS.

# 6. Wpływ parametrów sprężystości skał na geometrię szczeliny w wybranych, perspektywicznych dla EGS, lokalizacjach w Polsce – artykuł V

Geometria szczelin w HDR jest kontrolowana głównie przez naprężenia w górotworze, parametry geomechaniczne skał oraz występowanie płaszczyzn osłabienia, takich jak naturalne szczeliny i płaszczyzny warstwowania. Moduł Younga oraz współczynnik Poissona definiują zachowanie skały w aspekcie podatności na deformacje oraz zniszczenie pod wpływem przyłożonego naprężenia. Zgodnie z klasyczną koncepcją mechaniki pękania zakres odkształcenia spowodowanego naprężeniem w skale jest zdeterminowany przez ilość energii jaka została dostarczona do wywołania przemieszczenia. Oznacza to, że w praktyce parametry sprężystości skał wpływają bezpośrednio na geometrię szczelin hydraulicznych, a co za tym idzie na ich przewodność i w konsekwencji na istotne cechy wspomaganego systemu geotermalnego, takie jak odległości pomiędzy otworami wiertniczymi oraz uzyskiwane wydajności przepływu cieczy roboczej przez system szczelin.

W artykule V, na przykładzie dwóch odmiennych litologicznie, potencjalnych lokalizacji EGS z obszaru Polski, opisano rezultaty analizy wpływu parametrów sprężystości ośrodka skalnego typu HDR na geometrię szczelin wytworzonych w numerycznie symulowanych zabiegach HF. Podstawę do opracowania niniejszego artykułu stanowiły: zgromadzone wcześniej informacje i dane z artykułów przeglądowych (I i II), wyniki badań laboratoryjnych przeprowadzonych przez doktoranta (artykuł III), wyniki badań uzupełniających (artykuł IV), a także dodatkowe badania ultradźwiękowe wykonane przez doktoranta oraz testy wytrzymałościowe przeprowadzone pod jego nadzorem. Na bazie powyższych informacji, w oparciu o samodzielnie wykonane symulacje numeryczne, przeprowadzono analizę wrażliwości geometrii szczeliny oraz jej przewodności na zróżnicowanie modułu Younga oraz współczynnika Poissona dla dwóch perspektywicznych dla EGS obszarów w Polsce. Wykonane prace badawcze pozwoliły osiągnąć cele dysertacji, w tym wyznaczenie wpływu układów naprężeń na parametry sprężystości skał, wykonanie symulacji numerycznych geometrii szczelin w wybranych formacjach, określenie zależności parametrów geometrii szczeliny od parametrów sprężystości oraz sformułowanie rekomendacji technologicznych do zabiegów HF w HDR. Wyniki tego rodzaju analiz, podobnie jak opracowane na ich podstawie rekomendacje technologiczne, nie były dotychczas publikowane.

## 6.1 Wybór obszarów perspektywicznych i przygotowanie próbek do badań

Spośród trzech pierwotnie rozważanych perspektywicznych formacji typu HDR na terenie Polski wybrano dwie, reprezentujące typy litologiczne najczęściej wykorzystywane w systemach EGS: piaskowce czerwonego spągowca z obszaru niecki mogileńsko-łódzkiej (otwór Piotrków Trybunalski IG-1) oraz granity z rejonu Karkonoszy (otwór Czerwony Potok PIG-1). Zgodnie z metodyką opisaną w artykule III do badań petrofizycznych pobrano próbki w kierunku prostopadłym do płaszczyzn warstwowania skał.

## 6.2 Metodyka badań geomechanicznych dynamicznych i statycznych

Pomiary dynamiczne parametrów sprężystości próbek wykonano na urządzeniu Vinci AVS-700. Wyznaczono prędkości propagacji fali podłużnej oraz poprzecznej przy częstotliwości pracy przetworników 500 kHz. W odróżnieniu od badań opisanych w artykule III testy ultradźwiękowe były w tym przypadku prowadzone na próbkach w pełni nasyconych 2% roztworem chlorku potasu (zastosowanego w charakterze inhibitora pęcznienia minerałów ilastych). Celem tych badań było porównanie parametrów sprężystości próbek w pełni nasyconych cieczą oraz próbek suchych (artykuł III). Testy prowadzono w warunkach konwencjonalnego trójosiowego ściskania, przy wzroście ciśnienia hydrostatycznego od ciśnienia otoczenia do 55 MPa, według metodyki opracowanej przez doktoranta. Ciśnienie porowe utrzymywano na poziomie 2 MPa, tak aby wraz ze wzrostem ciśnienia uszczelnienia zwiększało się ciśnienie efektywne.

Testy wytrzymałościowe zostały wykonane na maszynie wytrzymałościowej MTS-810, w warunkach jednoosiowego oraz konwencjonalnego trójosiowego ściskania, zgodnie z rekomendacjami ISRM (Ulusay i Hudson, 2007). Celem tych badań było wyznaczenie statycznych parametrów sprężystości próbek, porównanie ich z parametrami dynamicznymi przedstawionymi w artykule III oraz wyznaczenie pomiędzy nimi korelacji. Testy wykonywano na próbkach nienasyconych, w temperaturze pokojowej i przy ciśnieniu uszczelnienia 15 i 30 MPa. Moduł Younga był wyznaczany na podstawie przedkrytycznej charakterystyki naprężeniowo-odkształceniowej, jako tangens kąta nachylenia prostej, będącej aproksymacją liniową krzywej zniszczenia. Ze względu na ograniczenia komory ciśnieniowej statyczne współczynniki Poissona zostały wyznaczone w warunkach jednoosiowego ściskania.

## 6.3 Metodyka symulacji numerycznych geometrii szczelin

Geometrię szczelin symulowano z wykorzystaniem oprogramowania Carboceramics FracPro, wykorzystując trójwymiarowy model domyślny o nazwie *3D shear-decoupled*. Jest to autorski model producenta oprogramowania opierający się na modelach PKN oraz KGD, jednakże oddzielający efekty naprężeń ścinających w mechanizmie otwierania się szczeliny. Model wykorzystuje efekt warstwowania kompozytowego, co oznacza, że traktuje złoże jako zespół wielu warstw o indywidualnych właściwościach geomechanicznych, w których rozchodzi się szczelina, ale również uwzględnia efekty propagacji szczeliny pomiędzy warstwami oraz występowanie barier w propagacji. W modelu tym nie została uwzględniona obecności szczelin naturalnych w skałach i dlatego zakłada on propagację nowo tworzonej szczeliny hydraulicznej w formacji nienaruszonej. Model ten został użyty ze względu na brak danych dotyczących występowania naturalnych płaszczyzn osłabienia skał w skali makro w analizowanych formacjach. W celu uproszczonego odzwierciedlenia charakterystycznych właściwości formacji granitowej zmienionej hydrotermalnie, w środkowej części modelowanej strefy docelowej zwiększono wartości współczynnika przepuszczalności oraz porowatości efektywnej do wartości maksymalnych uzyskanych dla tych skał w badaniach laboratoryjnych (artykuł III). Ze względu na powyższe uproszczenia modelu, zaprezentowane rezultaty powinny być traktowane jako wstępne informacje o charakterystyce geometrii indukowanej szczeliny, w funkcji parametrów sprężystości. Bardziej precyzyjne wyniki mogłyby być uzyskane podczas modelowania stymulacji naturalnego systemu szczelin w tej formacji oraz interakcji pomiędzy szczelinami naturalnymi oraz indukowanymi, co wymagałoby pozyskania przede wszystkim kompletu danych z profilowań geofizyki otworowej w istniejącym odwiercie, w tym pełnego profilu litologii, średnicy otworu, przepuszczalności, porowatości, zailenia, prędkości akustycznych, obrazowania ścianek otworu oraz analiz struktur zniszczeniowych ścian otworu typu wcięć (ang. *breakouts*) i szczelin z rozciągania (ang. *tensile fractures*).

Do modelowania zabiegów hydraulicznego szczelinowania w piaskowcach niecki mogileńsko-łódzkiej wykorzystany został uproszczony profil litologiczny otworu Piotrków Trybunalski IG-1. Dane konstrukcyjne modelowanego otworu zostały skompilowane na podstawie materiałów archiwalnych dotyczących innych odwiertów w formacji czerwonego spągowca w Polsce oraz literatury (Blocher i inni, 2016). Parametry petrofizyczne strefy docelowej przyjęto na podstawie własnych badań laboratoryjnych, zaprezentowanych w artykule III i IV. Analizowany zakres zmian modułu Younga wynosił od 14,5 do 50 GPa, a współczynnika Poissona od 0,1 do 0,35. Schemat pompowania opracowano na podstawie danych literaturowych (Zimmermann i inni, 2010; Zimmermann i Reinicke 2010; Blöcher i inni, 2016) oraz własnych doświadczeń zawodowych.

Podobnie jak w przypadku powyżej opisywanej formacji piaskowców, parametry petrofizyczne strefy docelowej w rejonie Karkonoszy przyjęto z wyników badań laboratoryjnych. Analizowany zakres zmian modułu Younga granitów wynosił od 16,75 do 80 GPa, a współczynnika Poissona od 0,07 do 0,37. Schemat pompowania opracowano na podstawie danych literaturowych (Schindler i inni, 2010; Meller i Ledesert, 2017) oraz własnego doświadczenia.

## 6.4 Zależności pomiędzy dynamicznymi i statycznymi parametrami sprężystości skał

Średni statyczny moduł Younga testowanych granitów $E_s$ (16-25 GPa) jest zgodny z publikowanymi wartościami dla granitu hydrotermalnie zmienionego (Lama i Vutukuri, 1978), przy czym granity pobrane z płytszego interwału, z makroskopowo większą liczbą spękań, posiadają niższe wartości $E_s$, co jest związane z podwyższoną zawartością minerałów ilastych. Piaskowce charakteryzują się niskimi $E_s$ (17,9-18,2 GPa) niezależnie od głębokości pobrania, co odpowiada danym literaturowym dla średnio wytrzymałych piaskowców (Lake, 2007). Granity wykazują bardzo silne zróżnicowanie parametrów sprężystości w zależności od metodyki ich wyznaczania. Średni moduł $E_d$ (43-61 GPa) jest ponad dwukrotnie wyższy od średniego $E_s$ w obu analizowanych interwałach, $v_d$ jest wyższy prawie dwukrotnie od $v_s$ w granitach bardziej płytko zalegających, a w głębiej zalegających prawie czterokrotnie (figura 6.1 A). Zróżnicowanie to jest najprawdopodobniej związane ze zmiennością hydrotermalną podobnie do rezultatów prezentowanych przez Lama i Vutukuri (1978), lub z obecnością mikropęknięć w próbkach (Shen i inni, 2024). Aby potwierdzić ten wniosek należałoby wykonać szczegółowe badania dystrybucji mikroszczelin, np. na podstawie wyników badań tomografii rentgenowskiej.

Analizowane piaskowce charakteryzują się zbliżonymi wartościami $E_s$ i $E_d$ (9-18 GPa), natomiast $v_d$ jest nieco wyższy od $v_s$ (odpowiednio 0,2 i 0,12-0,13). W przypadku obydwu analizowanych formacji zależność $E_s$ i $E_d$ jest dobrze opisywana modelem liniowym -

współczynniki determinacji $R^2$ wynoszą 0,84 dla piaskowców i 0,89 dla granitów (figura 6.1 B).

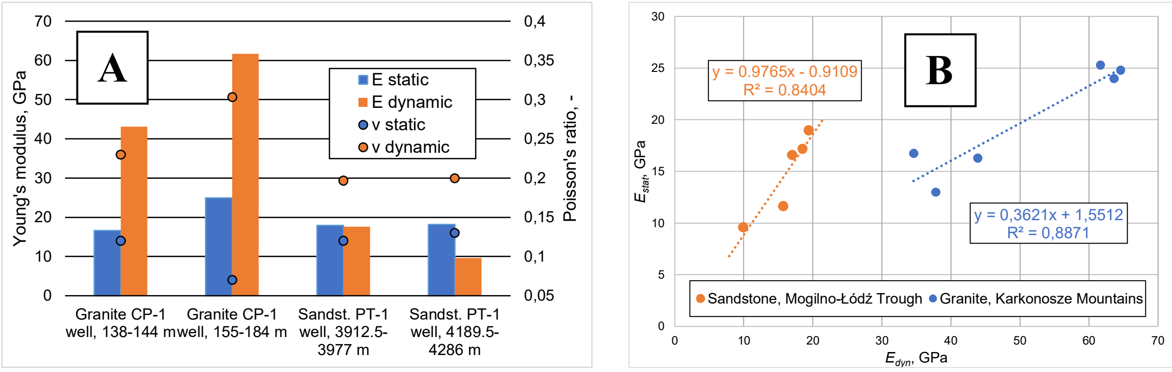


Figura 6.1: **A** – Porównanie średnich dynamicznych i statycznych modułów Younga oraz współczynników Poissona analizowanych granitów i piaskowców; **B** – Zależności pomiędzy dynamicznymi i statycznymi modułami Younga dla analizowanych formacji.

## 6.5. Wpływ nasycenia cieczą na dynamiczne parametry sprężystości

Obecność nieściśliwej cieczy usztywniającej przestrzeń porową analizowanych próbek w znaczący sposób wpływa na parametry sprężystości obydwu analizowanych formacji. Średni dynamiczny moduł Younga $E_d$ granitów, mierzony przy ciśnieniu osiowym 55 MPa, wynosił 43 GPa przed nasyceniem i 51 GPa po nasyceniu, a dla piaskowców, przy identycznym ciśnieniu, odpowiednio 9 i 31 GPa. W przypadku średniego dynamicznego współczynnika Poissona $v_d$ granitów zaobserwowano niewielkie zmiany (wzrost z 0,28 dla próbek suchych do 0,29 po nasyceniu), natomiast $v_d$ piaskowców zmienił się zasadniczo (wzrost z 0,17 do 0,31 po nasyceniu).

## 6.6 Wpływ parametrów sprężystości na geometrię wytworzonej szczeliny

Symulacja komputerowa szczelinowania hydraulicznego formacji piaskowców z niecki mogileńsko-łódzkiej, przy założeniu średnich wartości modułu $E$ i współczynnika $v$ wynoszących odpowiednio 19,2 GPa i 0,19, pozwoliła uzyskać szczelinę o następujących wymiarach: długość skrzydła - 61 m, wysokość - 81 m i rozwartość - 1,4 cm. Średnia przewodność szczeliny wynosiła 514 mD/m. Odnotowano też zjawisko embedmentu o wgłębieniu 0,027 cm. Wymiary te są zatem bardzo zbliżone do wymiarów szczeliny uzyskanej w jednym z przeprowadzonych zbiegów w projekcie Groß Schönebeck w Niemczech (Zimmermann i Reinicke, 2009). Średnia przewodność szczeliny jest nieco niższa niż w projekcie niemieckim (gdzie uzyskano około 800 mD/m), prawdopodobnie ze względu na zwiększoną koncentrację podsadzki w środkowej części szczeliny (figura 6.2). Wyższą przewodność można byłoby uzyskać poprawiając równomierność rozłożenia podsadzki w całej objętości szczeliny. Analiza wrażliwości dla modułu $E$ piaskowców tego rejonu wykazała, że wzrost modułu od 14,8 do 50,0 GPa spowodował wzrost wysokości szczeliny o 3,0 m, spadek długości skrzydła również o 3,0 m i spadek rozwartości o 0,09 cm (figura 6.3). Względne zmiany wartości tych parametrów wyniosły zatem odpowiednio: 3,7%, 4,9%, oraz 6,4%. Zaobserwowano także wzrost przewodności szczeliny o 12,7% i spadek intensywności embedmentu o 70%. Oznacza to, że w analizowanym przypadku piaskowców wpływ modułu

Younga formacji w strefie docelowej na geometrię szczeliny można uznać za niewielki i nie ma on istotnego znaczenia w kontekście odległości pomiędzy otworami w dublecie geotermalnym oraz objętości roboczej kolektora. Jednakże wpływ na przewodność szczeliny powyżej 12% może być istotny z punktu widzenia wydajności energetycznej systemu EGS. Aby to ocenić należałoby przeprowadzić dodatkowe symulacje wydajności systemu geotermalnego, w zależności od przewodności górotworu, czego nie obejmują cele niniejszej dysertacji. Stanowi to pole do dalszych badań nad efektywnością wspomaganych systemów geotermalnych na perspektywicznych obszarach w Polsce.

Analiza wrażliwości parametrów symulowanej szczeliny względem zmian wartości współczynnika $v$ omawianych piaskowców w zakresie od 0,1 do 0,35, nie wykazała jego wpływu na geometrię szczeliny niepodsadzonej oraz nie przekraczający 1,7% wpływ w przypadku szczeliny podsadzonej. Wpływ na przewodność szczeliny nie przekraczał 2,5%. Można zatem stwierdzić, że w omawianej formacji piaskowców współczynnik Poissona nie ma istotnego znaczenia dla geometrii szczeliny i jej przewodności.

Symulacja geometrii szczeliny w nienaruszonej tektonicznie formacji granitów karkonoskich, zakładając średnie wartości modułu $E$ i współczynnika $v$ wynoszące odpowiednio 62,9 GPa i 0,28, pozwoliła uzyskać długość skrzydła szczeliny na poziomie 337 m, wysokość szczeliny 160 m i rozwartość 0,58 cm. Średnia przewodność szczeliny wynosiła w tym przypadku 16 mD/m, a zjawiska embedmentu nie odnotowano. Relatywnie niska przewodność szczeliny jest w tym przypadku spowodowana niewielką jej rozwartością i przede wszystkim niską koncentracją podsadzki (figura 6.4). Aby zwiększyć przewodność szczeliny należałoby zwiększyć ilość podsadzki modyfikując schemat pompowania o dodatkowe etapy tłoczenia podsadzki po uformowaniu się kształtu szczeliny. Uzyskane długości skrzydła szczeliny odpowiadają w przybliżeniu odległościom pomiędzy otworami chłonnymi i produkcyjnymi we francuskim projekcie EGS Soultz-sous-Forêts.

Analiza wrażliwości względem modułu Younga wykazała, że wzrost modułu $E$ z 16,7 do 80,0 GPa nie wpłynął na wysokość szczeliny. Długość skrzydła niepodsadzonego spadła o 11 m, z 345 do 334 m, a rozwartość o 0,27 cm z 0,82 do 0,55 cm. Jednocześnie długość skrzydła podsadzonego wzrosła o 13 m z 307 do 320 m, a podsadzona wysokość o 11 m z 142 do 153 m (figura 6.5). Przewodność wzrosła z 14,3 do 16 mDm. Powyższe wyniki oznaczają, że przy omawianym wzroście modułu $E$ długość niepodsadzonego skrzydła szczeliny spadła o 11%, rozwartość spadła o 46,6%, długość podsadzonego skrzydła wzrosła o 4,1%, a podsadzona wysokość o 7,3%. Zatem wraz ze wzrostem modułu Younga, zmniejsza się niepodsadzona część szczeliny (figura 6.6). Spadek rozwartości szczeliny nie ma w tym przypadku istotnego wpływu na jej przewodność.

Analiza wrażliwości względem zmian współczynnika Poissona w zakresie od 0,1 do 0,35 wykazała spadek długości skrzydła szczeliny o 3 m i spadek jej rozwartości o 0,05 cm. Nie zaobserwowano wpływu na wysokość szczeliny i jej przewodność.

Można zatem stwierdzić, że wpływ modułu Younga nienaruszonej formacji granitów z rejonu Karkonoszy na długość i wysokość szczeliny jest stosunkowo niewielki, natomiast na jej rozwartość - znaczny, jednakże nie przekłada się to na istotne zmiany przewodności. Wpływ współczynnika Poissona na geometrię i przewodność można uznać za pomijalny. Należy jednak pamiętać, że w praktyce przemysłowej za najbardziej perspektywiczne dla EGS części formacji granitowych uważa się strefy szczelin naturalnych pełniących po stymulacji hydraulicznej funkcję przewodnych arterii w górotworze. Strefy takie w przeprowadzonych w pracy symulacjach nie zostały uwzględnione z powodu braku danych. Dlatego też skala wpływu modułów sprężystości na geometrię szczelin i ich przewodność w takich strefach może różnić się od wpływu jaki został wyznaczony w niniejszej pracy.

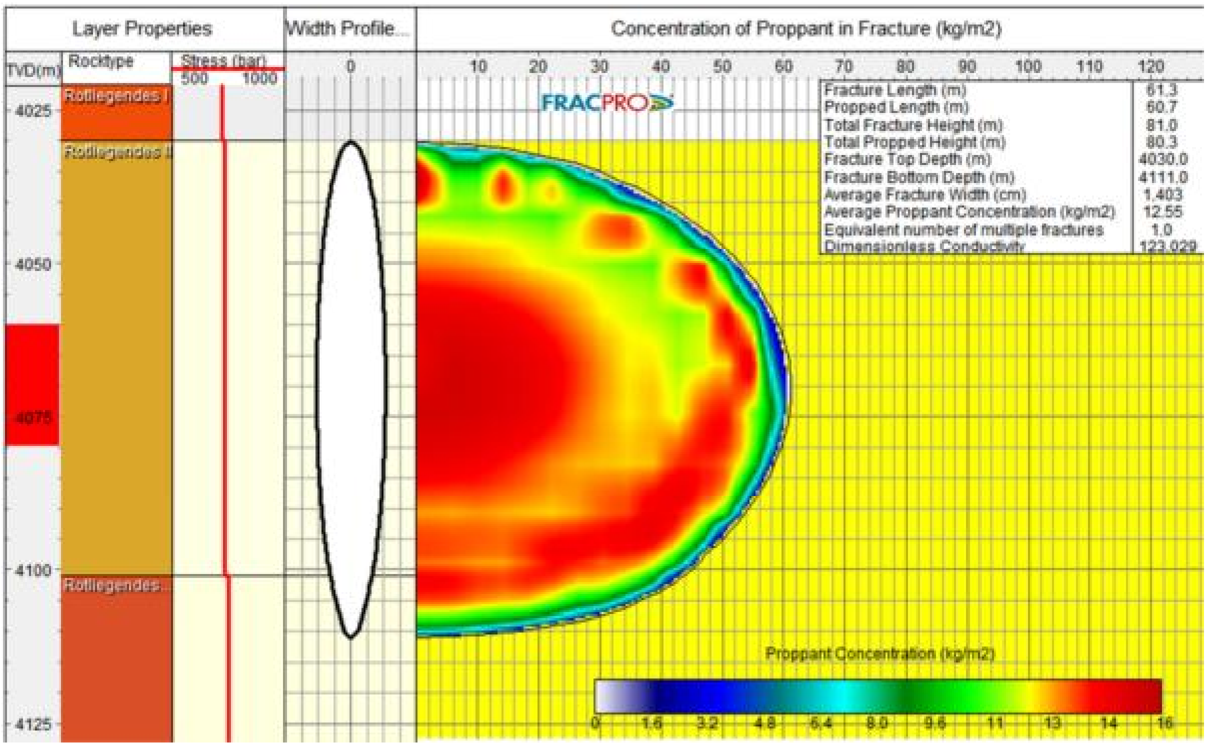


Figura 6.2: Koncentracja materiału podsadzkowego w formacji piaskowców z niecki mogileńsko-łódzkiej na tle profilu naprężenia σv, oznaczonego czerwoną linią w trzeciej kolumnie, od lewej strony.

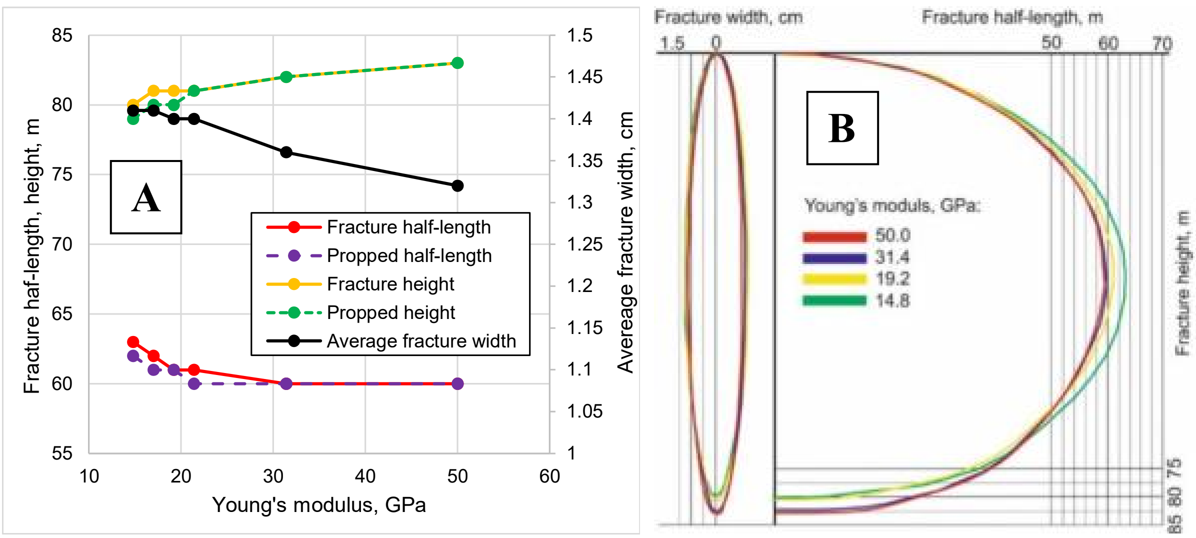


Figura 6.3: **A** – Zmiany geometrii szczeliny w funkcji modułu Younga w formacji piaskowców z niecki mogileńsko-łódzkiej. **B** – Zmiany kształtu szczeliny w funkcji modułu Younga. Objaśnienia: Fracture half-length – długość skrzydła szczeliny; Propped half-length – długość

podpartego skrzydła szczeliny; Fracture height, całkowita wysokość szczeliny; Propped height – wysokość podpartej szczeliny; Average fracture width – średnia rozwartość szczeliny.

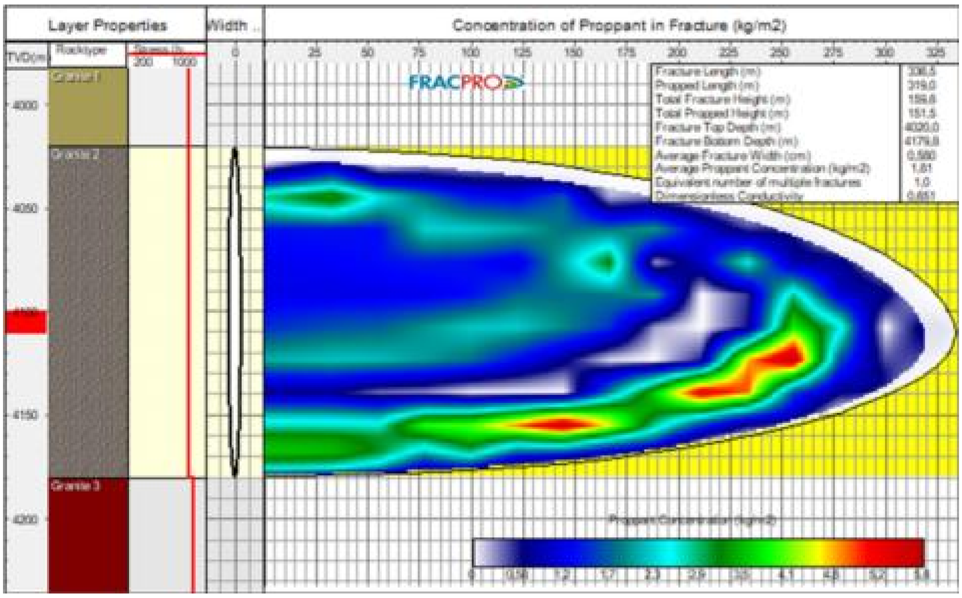


Figura 6.4: Koncentracja materiału podsadzkowego w granitach karkonoskich na tle profilu naprężenia σv oznaczonego czerwoną linią w trzeciej kolumnie, od lewej strony.

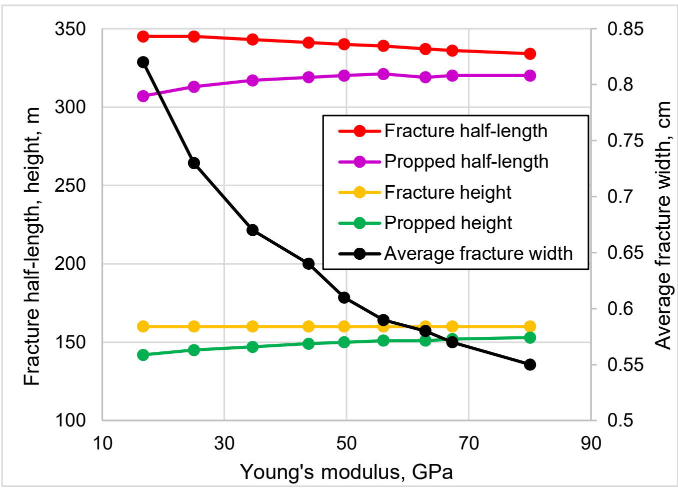


Figura 6.5: Zmiany geometrii szczeliny w funkcji modułu Younga w granitach karkonoskich. Objaśnienia: Fracture half-length – długość skrzydła szczeliny; Propped half-length – długość podpartego skrzydła szczeliny; Fracture height, całkowita wysokość szczeliny; Propped height – wysokość podpartej szczeliny; Average fracture width – średnia rozwartość szczeliny.

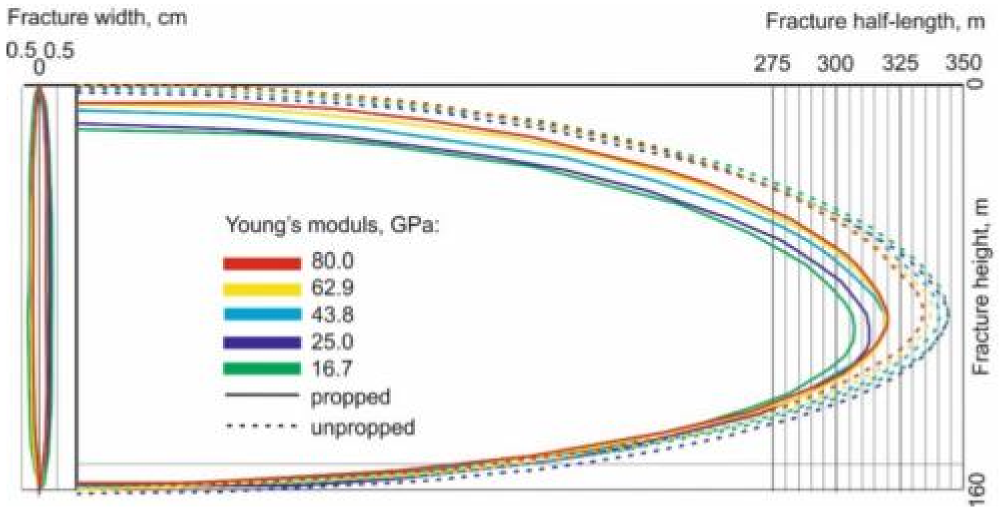


Figura 6.6: Zmiany kształtu szczeliny w funkcji modułu Younga w granitach karkonoskich.

## 6.7 Podsumowanie

W artykule V przedstawiono rezultaty badań wytrzymałościowych oraz uzupełniających badań ultradźwiękowych próbek skał HDR z perspektywicznych rejonów Polski. Na podstawie tych danych, a także wyników przeglądów literaturowych i badań opublikowanych w artykułach I, II i III wykonano symulacje numeryczne geometrii szczelin w HDR oraz wyznaczono wpływ parametrów sprężystości na geometrię szczeliny, co jest głównym celem naukowym dysertacji. Porównanie statycznych i dynamicznych modułów Younga analizowanych skał ujawniło duże różnice tych parametrów w formacji granitów, co prawdopodobnie związane jest ze zmiennością hydrotermalną tych skał. Testowane piaskowce charakteryzowały się natomiast bardzo zbliżonymi wartościami tych modułów. W przypadku obydwu formacji korelacja modułów dynamicznych do statycznych jest dobrze opisywana modelem liniowym - współczynniki determinacji $R^2$ wynoszą 0,84 dla piaskowców i 0,89 dla granitów. Wykazano też, że pełne nasycenie przestrzeni porowej próbek wodą prowadzi do znacznego wzrostu średniego dynamicznego modułu Younga, z 43 do 51 GPa dla granitów i z 9 do 31 GPa dla piaskowców. Istotny wzrost średniego współczynnika Poissona zaobserwowano jedynie w formacji piaskowców, tj. z 0,17 od 0,31. Symulacja szczelinowania hydraulicznego w formacji piaskowców pozwoliła uzyskać szczelinę o średnich wymiarach: długość skrzydła - 61 m, wysokość - 81 m i rozwartość - 1,4 cm, natomiast w formacji granitów: długość skrzydła szczeliny 337 m, wysokość szczeliny 160 m i rozwartość 0,58 cm. W obu analizowanych obszarach analiza wrażliwości wykazała, że wpływ modułu Younga na geometrię szczeliny nie przekracza kilku procent. Wpływ tego parametru na rozwartość szczeliny w piaskowcach również pozostaje na poziomie kilku procent, natomiast w granitach osiąga wartości rzędu kilkudziesięciu procent. Z kolei wpływ współczynnika Poissona na geometrię szczeliny oraz jej przewodność w obu formacjach jest marginalny. Istotne jest jednak to, że wzrost modułu Younga w formacji piaskowcowej prowadzi do znacznego ograniczenia zjawiska embedmentu oraz do zwiększenia przewodności szczeliny o kilkanaście procent. Może to mieć to istotny wpływ na efektywność systemu EGS zlokalizowanego w tego typu formacji. Z uwagi na brak danych dotyczących występowania oraz charakterystyki szczelin naturalnych w formacji granitowej – jak również interakcji między nimi a szczelinami indukowanymi – uzyskane wyniki należy traktować jako przybliżenie. Na podstawie wszystkich przeprowadzonych w ramach realizacji doktoratu prac sformułowano rekomendacje technologiczne do zabiegów szczelinowania hydraulicznego w wybranych perspektywicznych dla EGS formacjach w Polsce. Rekomendacje te zostały zaprezentowane w rozdziale 7 niniejszej dysertacji.

# 7. Rekomendacje technologiczne

Jak pokazuje światowe doświadczenie ostatnich kilkudziesięciu lat, zaprojektowanie opłacalnego ekonomicznie systemu geotermalnego, z zastosowaniem wspomagania przewodności w górotworze osiągniętego w zabiegu hydraulicznego szczelinowania, jest procesem złożonym i skomplikowanym. Pomimo tego, że gorące suche skały zalegają na pewnej głębokości niemalże w każdym miejscu na świecie, dostęp do energii w nich zgromadzonej wymaga pokonania wielu przeszkód specyficznych dla konkretnego obszaru, formacji czy nawet odwiertu. Poniżej przedstawiono spostrzeżenia sformułowane w efekcie realizacji pracy, które mogą być przydatne podczas projektowania zabiegów HF w HDR w Polsce.

**Formacje osadowe**

• W słabo zaangażowanych tektonicznie formacjach osadowych o niskiej przepuszczalności i nielicznych płaszczyznach nieciągłości, propagacja szczeliny jest determinowana głównie przez kierunek naprężeń głównych. Szczelina rozwiera się w kierunku prostopadłym do minimalnego naprężenia głównego, co w najczęściej spotykanym w Polsce, ekstensyjnym lub ekstensyjno-przesuwczym reżimie tektonicznym, oznacza propagację pionową. Przed wykonaniem zabiegu hydraulicznego szczelinowania istotne jest jednak zebranie pełnej informacji dotyczącej kierunków naprężeń poziomych w skali regionalnej oraz lokalnej w danym interwale perforacji. W formacjach osadowych tworzą się nowe szczeliny lub otwierają szczeliny istniejące – odpowiada za to mechanizm tensyjny, – relatywnie prosty do opisania modelami matematycznymi. Otwarcie szczeliny indukowanej wymaga przekroczenia ciśnienia szczelinowania formacji, przez co przebieg zabiegu w osadowych formacjach HDR jest w gruncie rzeczy podobny do stosowanego w niekonwencjonalnych złożach węglowodorów, a szczególnie w łupkach gazonośnych. Charakterystyczne dla tensyjnego mechanizmu otwierania szczeliny jest to, że po zmniejszeniu ciśnienia zabiegowego poniżej ciśnienia zamknięcia, szczelina ulega zaciśnięciu pod wpływem naprężeń panujących w górotworze.

• W celu podtrzymania przewodności szczeliny konieczne jest zastosowanie materiału podsadzkowego. Formacje HDR o entalpii odpowiedniej dla systemów EGS występują na terenie Polski na głębokościach poniżej 4000 metrów, zatem wykorzystywany materiał podsadzkowy musi charakteryzować się dużą wytrzymałością. Rekomendowany do tego celu może być ceramiczny materiał podsadzkowy, tzw. HSP (*high strength proppant*), o rozmiarze np. 20/40 mesh. Podsadzka taka ma wysoką gęstość, co determinuje użycie do jej transportu płynów sieciowanych lub liniowych na bazie polimerów naturalnych lub syntetycznych. Koncentracja polimeru musi pozwalać na wytworzenie płynu o lepkości umożliwiającej transport podsadzki. Płyn o koncentracji 30# (30 funtów polimeru na 1000 galonów wody) wydaje się być tutaj dobrym rozwiązaniem.

• Prognozowanie geometrii indukowanej szczeliny, jej objętości oraz przewodności, a na tej podstawie hydraulicznej wydajności systemu oraz dostarczanej przez niego w kolejnych latach energii jest możliwe ze stosunkowo dużą pewnością. Jednakże systemy w nienaruszonych skałach osadowych posiadają także kilka istotnych wad. Główną z nich jest relatywnie niewielka powierzchnia kontaktu górotworu z odwiertami, szczególnie w formacjach o podwyższonej plastyczności. W takim przypadku w kolektorze występować będzie jedna lub kilka szczelin, przez co powierzchnia styku cieczy roboczej ze skałą może być stosunkowo niewielka, co może znacząco obniżać wydajność systemu geotermalnego.

• Z punku widzenia analizowanych w niniejszej pracy właściwości mechanicznych skał na głębokości docelowej, można stwierdzić, że moduły sprężystości osadowych HDR mają niewielki wpływ na geometrię szczeliny. Relatywnie duże zmiany modułu Younga skał wywołują tylko kilkuprocentowe zmiany geometrii szczeliny. Uzyskane dane wykazały jednak, że pomimo niewielkich zmian w geometrii szczeliny, w tym jej rozwartości, wzrost modułu Younga pociąga za sobą zauważalny wzrost przewodności w analizowanym przypadku rzędu prawie 13%, co może mieć duże znaczenie dla ostatecznej wydajności systemu. Istotne znaczenie może mieć też, związane ze wzrostem modułu Younga, zmniejszanie się efektu embedmentu, co pomimo spadku rozwartości szczeliny, przyczynia się do zwiększenia jej przewodności.

• Współczynnik Poissona, drugi główny parametr geomechaniczny wykorzystywany podczas modelowań zabiegów hydraulicznego szczelinowania, w analizowanej formacji osadowej, nie wpływał w istotny sposób na geometrię szczeliny ani na jej przewodność. W rozpatrywanym zakresie jego zmian nie zanotowano wpływu na długość skrzydła, wysokość oraz rozwartość szczeliny. Wpływ na podsadzoną długość skrzydła i podsadzoną wysokość nie przekraczał 1,7%, co można uznać za wartość marginalną.

• Wyniki uzyskane w niniejszej pracy uzasadniają stwierdzenie, że w przypadku skał typu osadowych HDR bardziej perspektywiczne są formacje o wyższym module Younga i o wyższym wskaźniku kruchości BI. Wyższy moduł Younga, podobnie jak w przypadku formacji gazonośnych, zwiększa szansę na powstanie złożonego systemu szczelin, a więc w systemach HDR – większej powierzchni kontaktu cieczy roboczej ze skałą. W skałach tych prawdopodobieństwo wystąpienia efektu embedmentu jest mniejsze lub będzie on mniej intensywny, a przy tym wyższa będzie przewodność szczeliny, wpływająca bezpośrednio na wydajność systemu EGS.

**Formacje magmowe**

• Systemy EGS w skałach magmowych znacznie różnią się od systemów projektowanych w skałach osadowych. Doświadczenia światowe dowodzą, że w takich formacjach horyzonty perspektywiczne obejmują zmienione hydrotermalnie strefy występowania naturalnych nieciągłości, szczelin i spękań. Przewodność górotworu jest więc kontrolowana tam, w głównej mierze, przez przewodność szczelin naturalnych, reaktywowanych w procesie stymulacji hydraulicznej. Ponieważ strefy te mają znacznie niższą wytrzymałość mechaniczną niż okalające skały nienaruszone, a dominującym mechanizmem propagacji szczeliny jest hydrościnanie, zabiegi w tych strefach wymagają zastosowania ciśnień niższych od ciśnienia szczelinowania formacji. W rezultacie następuje reaktywacja szczelin naturalnych poprzez ich, rozwarcie, poślizg oraz w efekcie dylatację na powierzchniach czynnych. Natomiast nieliczne nowe szczeliny, o ile wystąpią, będą miały jedynie charakter połączeń pomiędzy szczelinami reaktywowanymi w trakcie hydrościnania.

• Przesunięcia ścian szczelin naturalnych, generowane w wyniku mechanizmu hydrościnania, skutkują trwałym zachowaniem przewodności tych szczelin po redukcji ciśnienia, dlatego w formacjach magmowych nie stosuje się materiałów podsadzkowych. To z kolei pozwala na zastosowanie cieczy zabiegowej o bardzo niskiej lepkości. W większości zabiegów opisywanych w literaturze, cieczą roboczą jest czysta woda. Jej objętości są zazwyczaj bardzo duże (ponad 1 000 $m^3$ na etap tłoczenia oraz ponad 10 000 $m^3$ na cały zabieg), co oznacza, że mają one charakter zabiegów typu *massive hydraulic fracturing*.

• Kolektor tworzony w zmienionych hydrotermalnie skałach magmowych charakteryzuje się złożoną geometrią. Długości reaktywowanych szczelin są znaczne, co pozwala zwiększyć odległość pomiędzy otworami chłonnymi i produkcyjnymi w systemie. Wzrost pojemności hydraulicznej całego systemu sprawia, że EGS w formacjach magmowych charakteryzują się zwiększoną wydajnością. Ponieważ głównymi kanałami przewodności w systemie są szczeliny reaktywowane, kluczowe znaczenie w jego projektowaniu ma szczegółowa charakterystyka układu szczelin naturalnych w skali regionalnej i lokalnej — w tym ich rozmieszczenia, orientacji oraz przewodności hydraulicznej. Równie istotne jest uwzględnienie w modelowaniach oddziaływań pomiędzy szczelinami naturalnymi a indukowanymi.

• W niniejszej pracy, ze względu na brak danych dotyczących występowania i charakterystyki szczelin naturalnych w formacji magmowej, potraktowano ją jako ośrodek nienaruszony, co miało istotny wpływ na uzyskane wyniki. W przeprowadzonych analizach przyjęto propagację szczelin nowo powstających w wyniku działania mechanizmu tensyjnego. Aby utrzymać ich przewodność, szczeliny te muszą zostać odpowiednio podsadzone. Pomimo ograniczeń zastosowanej metodyki, uzyskane wyniki pozwalają na sformułowanie wniosków istotnych z punktu widzenia hydraulicznej stymulacji formacji magmowych.

• Analiza wrażliwości geometrii szczeliny na zmiany modułu Younga w przedziale 16–80 GPa wykazała, że jego wzrost prowadzi do zmniejszenia długości skrzydeł szczeliny, przy jednoczesnym nieznacznym wzroście długości odcinka podsadzonego oraz wysokości szczeliny – łącznie o mniej niż 7,5%. Oznacza to, że wraz ze wzrostem modułu Younga skały zmniejsza się długość niepodsadzonego odcinka szczeliny. Najistotniejszy wpływ moduł Younga wywiera na rozwartość szczeliny – w analizowanym przypadku jej spadek wynosił aż 46%. Nie przekłada się to jednak na istotne zmiany w przewodności, ponieważ w rozpatrywanym modelu przewodność szczelin i tak pozostaje niska. Wynika to z faktu, że model nie uwzględnia efektu samopodsadzenia szczeliny – symulowane są nowe szczeliny, powstające w nienaruszonej formacji, na skutek działania sił tensyjnych (wywołanych ciśnieniem płynu szczelinującego), a nie szczeliny naturalne reaktywowane mechanizmem hydrościnania. W celu zwiększenia przewodności w takim układzie należałoby zwiększyć koncentrację materiału podsadzkowego w szczelinie, poprzez zwiększenie liczby etapów jego tłoczenia w końcowej fazie zabiegu stymulacyjnego.

• Podobnie jak w przypadku analizowanej w niniejszej pracy formacji osadowej, w rozpatrywanych skałach magmowych współczynnik Poissona wykazuje marginalny wpływ na geometrię szczeliny – z wyjątkiem rozwartości, która zmniejsza się, w zakresie poniżej 8%, wraz ze wzrostem tego parametru. Zmiana ta nie wpływa w istotny sposób na przewodność szczeliny.

• Ze względu na niewielką rozwartość pojedynczej szczeliny w modelowanym ośrodku nienaruszonym tektonicznie oraz jej niską przewodność, uzasadniona wydaje się być teza, że najbardziej perspektywicznymi strefami do stymulacji w skałach magmowych są strefy ze szczelinami naturalnymi. Potwierdzają to dane dostępne w literaturze światowej wskazujące, że aktywacja wielu drobnych naturalnych szczelin w procesie hydrościnania, przy ciśnieniach poniżej progu szczelinowania formacji, umożliwia uzyskanie wystarczającego kontaktu hydraulicznego pomiędzy odwiertami, w celu zapewnienia ekonomicznie opłacalnej eksploatacji systemu. Jednocześnie wiąże się to z mniejszym ryzykiem wystąpienia zjawisk sejsmiczności indukowanej w rejonie stymulacji. Potwierdzeniem mogą tu być obserwacje przeprowadzone w projektach EGS Soultz-sous-Forêts i Rittershoffen we Francji.

• Z uwagi na to, że hydrotermalnie zmienione strefy nieciągłości w górotworze wykazują istotnie obniżoną wytrzymałość mechaniczną w porównaniu z otaczającym je ośrodkiem, za bardziej perspektywiczne w kontekście stymulacji formacji magmowych uznać należy horyzonty charakteryzujące się niższym modułem Younga oraz wyższym współczynnikiem Poissona, a tym samym niższym wskaźnikiem kruchości (BI).

# 8. Podsumowanie i wnioski

Celem niniejszej pracy było określenie wpływu parametrów sprężystości wybranych perspektywicznych formacji gorących suchych skał (HDR) na geometrię kolektorów geotermalnych tworzonych w wyniku zabiegów hydraulicznego szczelinowania (HF) na potrzeby wspomaganych systemów geotermalnych (EGS) na terenie Polski. Praca została wykonana w programie Doktorat Wdrożeniowy edycja V we współpracy z Instytutem Nafty i Gazu – Państwowym Instytutem Badawczym. W pracy zrealizowano wszystkie założenia przedstawione w indywidualnym planie badawczym doktoranta. Na podstawie laboratoryjnie wyznaczonych parametrów petrofizycznych, petrograficznych oraz geomechanicznych, z wykorzystaniem symulacji numerycznych, określono geometrię szczelin powstających w procesie hydraulicznego szczelinowania dla dwóch geologicznych formacji o odmiennych cechach litologicznych, uznanych za perspektywiczne z punktu widzenia rozwoju systemów EGS.

Dokonano tego na drodze realizacji następujących celów szczegółowych:

- Wyznaczenie parametrów sprężystości próbek skalnych w warunkach ciśnienia i temperatury charakterystycznych dla rejonów potencjalnych systemów geotermalnych EGS na terenie Polski,
- Określenie zależności dynamicznych parametrów sprężystości w funkcji zmian naprężeń w górotworze oraz wyznaczenie korelacji pomiędzy dynamicznymi i statycznymi parametrami sprężystości,
- Opracowanie metodyki badań ultradźwiękowych skał w warunkach wysokich ciśnień i temperatur wraz z modyfikacją oprzyrządowania do badań ultradźwiękowych umożliwiającego prowadzenie badań w warunkach złożowych, typowych dla perspektywicznych obszarów EGS w Polsce,
- Wykonanie demonstratora technologicznego w postaci modeli geometrii szczelin w skałach HDR z wykorzystaniem oprogramowania komputerowego oraz sformułowanie rekomendacji technologicznych do zabiegów HF w skałach HDR w Polsce, z uwzględnieniem mechaniki ośrodka skalnego, w tym jego parametrów sprężystości.

Praca składa się z pięciu części, odpowiadających kolejnym etapom realizacji badań, z których każdy zakończony został przygotowaniem publikacji naukowej opisanej w niniejszej dysertacji.

Pierwszy etap obejmował przegląd literatury, skoncentrowany na analizie kluczowych projektów typu EGS prowadzonych na świecie, w których zastosowano technologię hydraulicznego szczelinowania oraz porównaniu tych doświadczeń z dostępnymi danymi dotyczącymi potencjalnych obszarów HDR na terenie Polski. Etap ten pozwolił na sformułowanie następujących wniosków:

1. W większości realizowanych na świecie projektów EGS główną metodą zwiększania przewodności górotworu i tworzenia kolektora geotermalnego było zastosowanie zabiegów hydraulicznego szczelinowania.

2. Systemy EGS były wdrażane zarówno w skałach magmowych, jak i osadowych. Formacje te różnią się istotnie pod względem mechanizmu stymulacji hydraulicznej, co wynika z odmiennych procesów generowania przewodnych szczelin.
3. Na obszarze Polski zidentyfikowano kilka regionów o podwyższonym potencjale geotermalnym, charakteryzujących się korzystnym gradientem geotermalnym. Do najbardziej perspektywicznych zalicza się m.in. rejon Karkonoszy, blok Gorzowa, nieckę szczecińską, nieckę mogileńsko-łódzką oraz blok Górnośląski.

Drugi etap prac obejmował uzupełniający przegląd literatury, poszerzający analizę obszarów perspektywicznych dla technologii EGS w Europie o kraje bałtyckie (Litwa, Łotwa, Estonia) oraz porównanie warunków geologicznych tych regionów z warunkami występującymi w Polsce. Etap ten pozwolił na sformułowanie następujących wniosków:

4. W krajach południowo-wschodniej części basenu bałtyckiego (Litwa, Łotwa, Estonia) rozkład gradientu geotermalnego oraz gęstości strumienia cieplnego nie odbiega istotnie od wartości rejestrowanych w Europie Zachodniej. Potencjał HDR w tych regionach związany jest głównie z obecnością podłoża krystalicznego.
5. Warunki geotermalne na Litwie są porównywalne z tymi występującymi w wybranych, perspektywicznych rejonach Polski. W pozostałych analizowanych krajach (Łotwa, Estonia) warunki te są nieco mniej korzystne.
6. Główną barierą rozwoju technologii HDR w państwach bałtyckich jest niewystarczające rozpoznanie lokalnych warunków tektonicznych, w szczególności rozwoju naturalnych stref szczelinowych i uskokowych, które mają istotny wpływ na kierunek propagacji szczelin podczas zabiegów HF w podłożu krystalicznym.

Trzeci etap prac obejmował laboratoryjną charakterystykę petrofizyczną i geomechaniczną próbek skalnych HDR, pochodzących z perspektywicznych obszarów na terenie Polski. Etap ten pozwolił na sformułowanie następujących wniosków:

7. Analizowane skały pochodzące z wybranych perspektywicznych obszarów dla EGS w Polsce – tj. bloku Gorzowa, rejonu Karkonoszy oraz niecki mogileńsko-łódzkiej – charakteryzują się niskimi współczynnikami przepuszczalności i porowatości efektywnej. Potwierdza to ich kwalifikację jako skał typu petrotermalnego, odpowiednich dla systemów EGS.
8. Testowane piaskowce wykazywały niższe wartości modułu Younga w porównaniu do analogicznych formacji z obszaru Europy Zachodniej. Próbki granitów cechowały się silnym zróżnicowaniem parametrów sprężystości, uzależnionym od stopnia przeobrażenia hydrotermalnego oraz obecności naturalnych szczelin i spękań. Parametry mechaniczne badanych wulkanitów różniły się w zależności od struktury skały oraz formacji, z której zostały pobrane.
9. Wskaźnik kruchości (*brittleness index*, BI), wyznaczany na podstawie relacji pomiędzy modułem Younga a współczynnikiem Poissona, może być użyteczny jako parametr oceny perspektywiczności danego interwału w obrębie formacji HDR. Należy jednak podkreślić, że jego interpretacja w skałach magmowych znacząco różni się od tej stosowanej dla skał osadowych.

Czwarty etap prac obejmował analizę parametrów termicznych magmowych skał typu HDR z obszaru zachodniej Polski, modelowanie zmian temperatury górotworu podczas eksploatacji ciepła oraz modelowanie procesów geochemicznych. Etap ten pozwolił na sformułowanie następujących wniosków:

10. Granity karkonoskie wykazują wyższe wartości efuzyjności, dyfuzyjności oraz przewodności cieplnej w porównaniu z riolitami z bloku Gorzowa, co czyni je bardziej perspektywicznymi pod względem efektywnej ekstrakcji ciepła w systemach typu EGS.
11. Wyniki modelowania geochemicznego wskazują, że zjawisko pogorszenia przepuszczalności w wyniku wytrącania się wtórnych minerałów jest mało prawdopodobne w obu analizowanych formacjach skalnych.
12. Rozpuszczanie niektórych składników mineralnych w trakcie długotrwałej eksploatacji może prowadzić do wzrostu porowatości skały, co może skutkować spadkiem oporu hydraulicznego i nadmiernym zwiększeniem prędkości przepływu, a w konsekwencji zmniejszeniem wydajności kolektora geotermalnego.

Etapem kończącym niniejszą dysertację było określenie wpływu parametrów sprężystości skał na geometrię kolektorów geotermalnych w wybranych, perspektywicznych lokalizacjach dla systemów EGS na terenie Polski. Analizy przeprowadzone w tym etapie pozwoliły na sformułowanie następujących wniosków:

13. W obu analizowanych obszarach – piaskowcach niecki mogileńsko-łódzkiej oraz granitach rejonu Karkonoszy – analiza wrażliwości wykazała, że wpływ modułu Younga na geometrię szczeliny, rozumianą jako długość skrzydeł i wysokość, nie przekracza kilku procent. Wpływ tego parametru na rozwartość szczeliny w piaskowcach również pozostaje na poziomie kilku procent, natomiast w granitach osiąga wartości rzędu kilkudziesięciu procent. Z kolei wpływ współczynnika Poissona na geometrię szczeliny oraz jej przewodność w obu formacjach jest marginalny.
14. Wzrost modułu Younga w formacji piaskowcowej prowadzi do istotnego ograniczenia zjawiska embedmentu oraz do zwiększenia przewodności szczeliny o kilkanaście procent. Może to mieć znaczący wpływ na efektywność systemu EGS zlokalizowanego w tego typu formacji.
15. Z uwagi na brak danych dotyczących występowania oraz charakterystyki szczelin naturalnych w formacji granitowej – jak również interakcji między nimi a szczelinami indukowanymi – uzyskane wyniki należy traktować jako przybliżenie. W przypadku skał magmowych, gdzie mechanizm tworzenia przewodnych struktur opiera się głównie na reaktywacji istniejących nieciągłości, dalsze badania powinny być prowadzone w oparciu o kompleksowe dane pochodzące z już wykonanych otworów. Dane te powinny obejmować m.in. pełny profil litologiczny, średnicę otworu, przepuszczalność, porowatość, stopień zailenia, prędkości fal akustycznych, obrazowanie ścian otworów oraz analizę struktur zniszczeniowych typu wcięć i szczelin z rozciągania.

# Bibliografia

Aliyu MD., Archer RA. Numerical simulation of multifracture HDR geothermal reservoirs. *Renewable Energy* **2021**, 164, 541–555. DOI:10.1016/j.renene.2020.09.085

Batchelor A.S. Reservoir behavior in a stimulated Hot Dry Rock system. Proceedings of the 11th Annual Workshop on Geothermal Reservoir Engineering, Stanford, CA, USA, 21–23 January 1986.

Batchelor A.S. Development of Hot-Dry-Rock geothermal systems in the UK. *IEE Proceedings* **1987**, 134, 5, 371–380

www.bestec-for-nature.com/index.php/projects-en (dostęp 19.03.2021)

Blöcher G., Reinsch T., Henninges J., Milsch H., Regenspurg S., Kummerow J., Francke H., Kranz S., Saadat A., Zimmermann G., Huenges E. Hydraulic history and current state of the deep geothermal reservoir Groß Schönebeck. *Geothermics* **2016,** 63, 27–43. DOI: 10.1016/j.geothermics.2015.07.008

Borodinecs A., Odineca T., Zajacs A., Migla L., Shutenkova O. Review of the Geothermal Energy Potential in the Europe and Latvia. 2020. https://ieei.rtu.lv/rtuaer/files/Review%20of%20the%20geothermal%20energy%20potential%20in%20the%20Europe%20and%20Latvia.pdf (dostęp: 24.02.2025).

Brotons V., Tomás R., Ivorra S., Grediaga A., Martínez-Martínez J., Benavente D., Gómez-Heras M. Improved correlation between the static and dynamic elastic modulus of different types of rocks. *Materials and Structures* **2016**, 49, 3021–3037. DOI:10.1617/s11527-015-0702-7

Bukowska M., Kasza P., Moska R., Jureczka J. The Young's modulus and Poisson's ratio of hard coals in laboratory tests. *Energies* **2022**, 15, 2477. DOI:10.3390/en15072477

Cheng Q., Wang X., Ghassemi A. Numerical simulation of reservoir stimulation with reference to the Newberry EGS. *Geothermics* **2019**, 77, 327–343. DOI:10.1016/j.geothermics.2018.09.011

Di Sipio E., Chiesa S., Destro E., Galgaro A., Giaretta A., Gola G., Manzella A. Rock thermal conductivity as key parameter for geothermal numerical models. *Energy Procedia* **2013**, 40, 87–94. DOI:10.1016/j.egypro.2013.08.011

Dixit NC., Hanks CL., Wallace WK., Ahmadi M., Awoleke O. In situ stress variations associated with regional changes in tectonic setting, northeastern Brooks Range and eastern North Slope of Alaska. *AAPG Bullletin* **2017**, 101, 343–360. DOI:10.1306/08051616013

Economides M., Martin T. Modern Fracturing Enhancing Natural Gas Production; ET Publishing: Houston, Tx, USA, 2007.

Eissa EA., Kazi A. Relation between static and dynamic Young's moduli of rocks. *International Journal of Rock Mechanics and Mining Sciences & Geomechanics Abstract* **1988**, 25, 479–482. DOI:10.1016/0148-9062(88)90987-4

Ellsworth WL., Giardini D., Townend J., Ge S., Shimamoto T. Triggering of the Pohang, Korea, earthquake (Mw 5.5) by enhanced geothermal system stimulation. *Seismological Research Letters* **2019**, 90(5), 1844–1858. DOI:10.1785/0220190102

www.energisers.agh.edu.pl (dostęp: 27.02.2025)

Grieser B., Bray J. Identification of production potential in unconventional reservoirs. Production and Operations Symposium, Oklahoma City, Oklahoma, 31 March-3 April, 2007. SPE 106623. DOI:10.2118/106623-MS

Guo T., Gong F., Wang X., Lin Q., Qu Z., Zhang W. Performance of enhanced geothermal system (EGS) in fractured geothermal reservoirs with $CO_2$ as working fluid. *Applied Thermal Engineering* **2019**, 152, 215–230 DOI:10.1016/j.applthermaleng.2019.02.024

Guo T., Tang S., Liu S., Liu X., Zhang W., Qu G. Numerical simulation of hydraulic fracturing of hot dry rock under thermal stress. *Engineering Fracture Mechanics* **2020**, 240,107350. DOI:10.1016/j.engfracmech.2020.107350

Held S., Genter A., Kohl T. et al. Economic evaluation of geothermal reservoir performance through modeling the complexity of the operating EGS in Soultz-sous-Forêts. *Geothermics* **2014**, 51, 270-280 10.1016/j.geothermics.2014.01.016

Jarvie D., Hill R., Ruble T. Pollastro R. Unconventional shale-gas systems: The Mississippian Barnett Shale of north-central Texas as one model for thermogenic shale-gas assessment. *AAPG Bulletin* **2007**, 91(4), 475-499. DOI:10.1306/12190606068

Jin X., Shah SN., Roegiers J., Zhang B. Fracability evaluation in shale reservoirs - An Integrated petrophysics and geomechanics approach. SPE Hydraulic Fracturing Technology Conference, The Woodlands, Texas, USA, 4-6 February, 2014a. SPE 168589. DOI:10.2118/168589-MS

Jin X., Shah SN., Truax J., Roegiers J. A practical petrophysical approach for brittleness prediction from porosity and sonic logging in shale reservoirs. SPE Annual Technical Conference and Exhibition, Amsterdam, The Netherlands, 27-29 October, 2014b. SPE 170972. DOI:10.2118/170972-MS

Joeleht A., Kukkonen IT. Thermal properties of granulite facies rocks in the Precambrian basement of Finland and Estonia. *Tectonophysics* **1998**, 291(1-4), 195–203. DOI:10.1016/S0040-1951(98)00040-7

Jung R. EGS – goodbye or back to the future 95. ISRM International Conference for Effective and Sustainable Hydraulic Fracturing. Brisbane, Australia, 2013. DOI:10.5772/56458

Kasza P. Zabiegi hydraulicznego szczelinowania i złóż niekonwencjonalnych i metody ich analizy. *Prace INiG-PIB* **2019**, 226. DOI:10.18668/PN2019.226

King G. Thirty Years of Gas Shale Fracturing: What Have We Learned? SPE Annual Technical Conference and Exhibition, Florence, Italy 19-22 September 210. DOI:10.2118/133456-MS

Kukkonen IT., Pentti M. St1 Deep Heat Project: Geothermal energy to the district heating network in Espoo. IOP Conference Series: Earth and Environmental Science vol. 703, 17$^{th}$ World Conference ACUUS 2020, Helsinki, Finland, 3–4 February 2021 DOI:10.1088/1755-1315/703/1/012035.

Labus K., Labus M., Leśniak, G. Thermal properties of rocks from deep boreholes in Poland in terms of obtaining geothermal energy from enhanced geothermal systems. *Advances in Geo-Energy Research* **2023**, 8(2) 76-88. DOI:10.46690/ager.2023.05.02

Ladner F., Häring M. Hydraulic characteristics of the Basel-1 enhanced geothermal system. Geothermal Resources Council Transactions **2009**, 33, 199–204.

Lake L. Petroleum Engineering Handbook. Society of Petroleum Engineers: Richardson, TX, USA, 2007.

Lama RD., Vutukuri VS. Handbook on mechanical properties of rocks, vol II. Trans Tech Publications, Clausthal, 1978.

Lasaga A.C. Chemical kinetics of water-rock interactions. *Journal of Geophysical Research* **1984**, 89, 4009–4025. DOI: 10.1029/JB089iB06p04009

Legarth B., Tischner T., Huenges E. Stimulation experiments in sedimentary, low-enthalpy reservoirs for geothermal power generation, Germany. *Geothermics* **2003**, 32, 487–495. DOI:10.1016/j.geothermics.2003.07.007

Legarth B., Huenges E., Zimmermann G. Hydraulic fracturing in a sedimentary geothermal reservoir: results and implications. *Intentional Journal of Rock Mechanics and Mining Sciences* **2005**, 42, 1028–1041. DOI:10.1016/j.ijrmms.2005.05.014

Lei Z., Zhang Y., Zhang S., Fu L., Hu Z., Yu Z., Li L., Zhou J. Electricity generation from a three-horizontal-well enhanced geothermal system in the Qiabuqia geothermal field, China: slickwater fracturing treatments for different reservoir scenarios. *Renewable Energy* **2020**, 145, 65–83. DOI:10.1016/j.renene.2019.06.024

Lei Z., Zhang Y., Zhang S., Shi Y. Numerical study of hydraulic fracturing treatments and geothermal energy extraction from a naturally fractured granitic formation. *Geothermics* **2023**, 111, 102692. DOI:10.1016/j.geothermics.2023.102692

Lu S-M. A global review of enhanced geothermal system (EGS). *Renewable and Sustainable Energy Reviews* **2018**, 81, 2 2902–2921. DOI:10.1016/j.rser.2017.06.097

Masłowski M., Kasza P., Czupski M., Wilk K., Moska R. Studies of fracture damage caused by the proppant embedment phenomenon in shale rock. *Applied Sciences* **2019**, 9(11), 2190. DOI:10.3390/app9112190.

Masłowski M., Labus M. Preliminary studies on the proppant embedment in Baltic Basin shale rock. *Rock Mechanics and Rock Engineering* **2021**, 54, 2233–2248. DOI:10.1007/s00603-021-02407-0

McClure M., Horne R. An investigations of stimulation mechanisms in enhanced geothermal systems. *International Journal of Rock Mechanics and Mining Sciences* **2014**, 72, 242–260. DOI:10.1016/j.ijrmms.2014.07.011

Meller C., Ledésert B. Is there a link between mineralogy, petrophysics, and the hydraulic and seismic behaviors of the Soultz-sous-Forêts granite during stimulation? A review and reinterpretation of petro-hydromechanical data toward a better understanding of induced seismicity and fluid flow. *Journal of Geophysical Research Solid Earth* **2017**, 122, 9755–9774. DOI:10.1002/2017JB014648

Motuza G., Sliaupa S., Stephenson R. Genesis of high intensity intracratonic heat flow anomalies: Case study of Western Lithuania. Proceedings of the EGS-AGU-EUG Joint Assembly, Nice, France, 6–11 April 2003.

Niezgoda T., Miedzińska D., Sławiński G. Energia z głębokich pokładów gorących suchych skał (HDR). *Inżynieria Bezpieczeństwa Obiektów Antropogenicznych* **2018**, 3–4, 65–69.

Nurmi P. Preliminary Evaluation of the Estonian Geoenergy Potential and Overview of Available Technologies, Expert Opinion for Using Those Technologies in the Estonian Geological Conditions, Suggestions for Possible Further Actions and Examples of Case Studies. Technical Report. Tallin. 2021. Available online: https://www.researchgate.net/publication/352197150 (accessed on 25 February 2025).

Olasolo P., Juárez MC., Morales MP., D´Amico S., Liarte IA. Enhanced geothermal systems (EGS): a review. *Renewable and Sustainable Energy Reviews* **2016**, 56, 133–144. DOI: 10.1016/j.rser.2015.11.031

Park S., Kim K-I., Xie L., Yoo H., Min K-B., Kim M., Yoon B., Kim K.Y., Zimmermann G., Guinot F., Meier, P. Observations and analyses of the first two hydraulic stimulations in the Pohang geothermal development site, South Korea. *Geothermics* **2020**, 88, 101905. DOI:10.1016/j.geothermics.2020.101905

Rickman R., Mullen M., Petre E., Grieser B., Kundert D. A Practical Use of Shale Petrophysics for Stimulation Design Optimization: All Shale Plays Are Not Clones of the Barnett Shale. SPE Annual Technical Conference and Exhibition, Denver, Colorado, USA, September 2008. DOI:10.2118/115258-MS

Sapińska-Śliwa A., Kowalski T., Knez D., Śliwa T., Gonet A., Bieda A. Geological and drilling aspects of construction and exploitation geothermal systems HDR/EGS. *AGH Drilling Oil Gas* **2015**, 31, 49–62. DOI:10.7494/drill.2015.32.1.49

Schill E., Genter A., Cuenot N., Kohl T. Hydraulic performance history at the Soultz EGS reservoirs from stimulation and long-term circulation tests. *Geothermics* **2017**, 70, 110-124. DOI:10.1016/j.geothermics.2017.06.003

Schindler M., Baumgärtner J., Gandy T., Hauffe P., Hettkamp T., Menzel H., Penzkofer, P., Teza, D., Tischner, T., Wahl G. Successful hydraulic stimulation techniques for electric power production in the Upper Rhine Graben, Central Europe. Proceedings of the World Geothermal Congress, Bali, Indonesia, 25–29 April 2010.

Sharmin T., Khan N., Akram Md. S.., Ehsan M. M. A State-of-the-Art Review on Geothermal Energy Extraction, Utilization, and Improvement Strategies: Conventional, Hybridized, and Enhanced Geothermal Systems. *International Journal of Thermofluids* **2023**, 18, 100323. DOI: 10.1016/j.ijft.2023.100323

Shen S., Gao Y., Jia L. A Comparison of the relationship between dynamic and static rock mechanical parameters. *Applied Sciences* **2024**, 14, 4487. DOI:doi.org/10.3390/app14114487

Sliaupa, S.; Motuza, G.; Korabliova, L.; Ciuraite, K.; Puronas, V. Geothermal Potential of Hot Granites of Lithuania. In Proceedings of the World Geothermal Congress 2010, Bali, Indonesia, 25–29 April 2010.

Szewczyk J., Gientka D. Mapa Gęstości Ziemskiego Strumienia Cieplnego Polski. Państwowy Instytut Geologiczny, Warszawa, 2009.

Szewczyk, J. Geophysical and hydrogeological aspects of utilization of thermal energy in Poland. *Przegląd Geologiczny* **2010**, *7*, 566–573

Tester J., Anderson B., Batchelor A., Blackwell D., DiPippo R., Drake M., Garnish J., Livesay B., Moore M., Nichols K. et al. The Future of Geothermal Energy—Impact of Enhanced Geothermal Systems (EGS) on the United States in the 21st Century; Massachusetts Institute of Technology, Cambridge, MA, USA; Idaho National Laboratory: Idaho Falls, ID, USA, 2006.

Ulusay R., Hudson J. The complete ISRM suggested methods for rock characterization, testing and monitoring: 1974-2006. Ankara, Turkey, ISRM Turkish National Group, 2007.

Wang F., Gale J. Screening criteria for shale gas systems. *Gulf Coast Association of Geological Societes Transactions* **2009**, 59: 779-793.

Wójcicki A., Sowiżdżał A., Bujakowski W. Ocena Potencjału Bilansu Cieplnego i Perspektywicznych Struktur Geologicznych dla Potrzeb Zamkniętych Systemów Geotermicznych (Hot Dry Rocks) w Polsce. Ministerstwo Środowiska, Warszawa, 2013.

Van Heerden W. General relations between static and dynamic moduli of rocks. *International Journal of Rock Mechanics and Mining Sciences & Geomechanics Abstracts* **1987**, 24 (6), 381-385. DOI: 10.1016/0148-9062(87)92262-5

Vidal J., Genter A. Overview of naturally permeable fractured reservoirs in the central and southern Upper Rhine Graben: Insights from geothermal wells. *Geothermics* **2018**, 74, 57–73. DOI:10.1016/j.geothermics.2018.02.003.

Villeneuve M., Heap M., Kushnir A., Quin T., Baud P., Zhou G., Xu T. Estimating in situ rock mass strength and elastic modulus of granite from the Soultz-sous-Forêts geothermal reservoir (France). *Geothermal Energy* **2018**, 6, 1–29. DOI:10.1186/s40517-018-0096-1

Xie L., Min K-B., Song Y. Observations of hydraulic stimulations in seven enhanced geothermal system projects. *Renewable Energy* **2015**, 79, 56-65. DOI:10.1016/j.renene.2014.07.044

Zimmermann G., Moeck I., Blöcher G. Cyclic waterfrac stimulation to develop an enhanced geothermal system (EGS)—conceptual design and experimental results. *Geothermics* **2010**, 39, 59–69. DOI:10.1016/j.geothermics.2009.10.003

Zimmermann G., Reinicke A. Hydraulic stimulation of a deep sandstone reservoir to develop an enhanced geothermal system: laboratory and field experiments. *Geothermics* **2010**, 39, 70–77. DOI:10.1016/j.geothermics.2009.12.003

Zoback M. Reservoir Geomechanics. Cambridge University Press. Cambridge, UK, 2007.

# Streszczenie

Wśród rozwijanych obecnie technologii niskoemisyjnych źródeł produkcji energii jednym z największych potencjałów charakteryzują się wspomagane systemy geotermalne ang. *Enhanced Geothermal Systems* (EGS). Tworzone są one w tzw. gorących suchych skałach ang. *hot dry rocks* (HDR) - formacjach zalegających zazwyczaj poniżej 4000 metrów, w warunkach wysokich ciśnień i temperatur. Charakteryzują się one bardzo niską przepuszczalnością, porowatością i najczęściej nie zawierają wody lub zawierają jej bardzo małe ilości. Z tego względu ich energia termiczna nie może być transportowana na powierzchnię w taki sposób, w jaki ma to miejsce w konwencjonalnych systemach geotermalnych. Odpowiedzią na problemy z dostępnością do energii skał typu HDR jest sztuczne wytworzenie lub zwiększenie w tych formacjach przewodności hydraulicznej, osiągane najczęściej dzięki wykorzystaniu technologii hydraulicznego szczelinowania (HF). W efekcie tworzony jest system geotermalny, w którym ciecz robocza krąży w obiegu zamkniętym: najpierw tłoczona jest otworem chłonnym do górotworu, nagrzewa się przepływając przez wytworzone lub reaktywowane w HDR szczeliny, a następnie po ogrzaniu jest wydobywana na powierzchnię gdzie jej ciepło jest wykorzystywane do produkcji energii cieplnej i/lub elektrycznej. Schłodzona ciecz jest powtórnie zatłaczana do złoża. Projekty EGS rozwijane są na świecie od lat 70 XX wieku, a komercyjne elektrownie wykorzystujące tą technologię funkcjonują obecnie m.in. we Francji i Niemczech. W Polsce od początku XXI wieku wzrasta zainteresowanie tą niekonwencjonalną gałęzią geotermii, co zaowocowało realizacją projektów naukowych i powstaniem szeregu publikacji. Pomimo szerokiego spektrum badawczego części z tych prac, ich efekty nie były ukierunkowane na opracowanie jakichkolwiek elementów technologicznych zabiegów HF w polskich formacjach HDR. Odpowiedzią na tą lukę badawczą jest niniejsza praca doktorska.

Działania badawcze zrealizowane w ramach rozprawy doktorskiej można podzielić na dwie części: (1) badania laboratoryjne na próbkach skalnych pobranych z perspektywicznych dla EGS obszarów na terenie Polski, poprzedzone rozszerzoną analizą literaturową w aspekcie kluczowych elementów technologii HF w systemach EGS oraz (2) symulacje komputerowe zabiegów HF wraz z oceną wpływu parametrów sprężystości skał na geometrię szczelin hydraulicznych.

W przeprowadzonym przeglądzie literaturowym przeanalizowano najważniejsze projekty EGS prowadzone dotychczas na świecie pod kątem parametrów geologicznych, petrofizycznych, tektonicznych oraz elementów technologii HF w nich wykorzystanych. Przegląd ten pozwolił określić cechy zabiegów HF charakterystyczne dla geotermii wspomaganej, geometrię szczelin w kolektorach oraz zakresy parametrów zabiegowych stosowane w realizowanych projektach. Uzyskane informacje odniesiono do warunków charakterystycznych dla perspektywicznych formacji w Polsce. Na podstawie przeprowadzonych prac wydany został artykuł w czasopiśmie *Energies* (Moska i inni. 2021).

Wykonano także uzupełniający przegląd literatury, rozbudowując zagadnienia dotyczące obszarów perspektywicznych dla technologii EGS w Europie o kraje bałtyckie (Litwę, Łotwę Estonię) oraz porównanie warunków geologicznych do warunków Polskich. Praca ta została opublikowana w czasopiśmie *Energies* (Moska i inni. 2023).

W kolejnym etapie prac wykonano badania laboratoryjne na próbkach rdzeniowych pobranych z trzech perspektywicznych dla EGS obszarów na terenie Polski: rejonu Karkonoszy, bloku Gorzowa oraz niecki mogileńsko-łódzkiej. Dokonano charakterystyki parametrów petrofizycznych oraz petrograficznych tych skał. Przedstawiono wyniki testów geomechanicznych przeprowadzonych metodą ultradźwiękową w warunkach złożowych, na zmodyfikowanym do tego celu przez doktoranta stanowisku badawczym. Wskazano także w jaki sposób wskaźnik kruchości skał wykorzystywany dotąd w przemyśle naftowo-gazowniczym może być używany do oceny podatności na hydrauliczne szczelinowanie w tych formacjach. Badania te zostały opublikowane w czasopiśmie *Advances in Geo-Energy Research* (Moska i inni, 2024).

Wykonano także uzupełniające badania termiczne pozyskanych próbek oraz symulacje numeryczne w dwóch obszarach: zmian temperatury formacji i zasięgu chłodzenia podczas długotrwałej eksploatacji energii termalnej oraz reakcji chemicznych zachodzących w trakcie pozyskiwania ciepła. Na tej podstawie dokonano analizy potencjału systemów EGS w zachodniej Polsce. Analiza ta została opublikowana w czasopiśmie *Energies* (Labus i inni, 2025).

Finalnym etapem prac było wykonanie przez doktoranta symulacji numerycznych zabiegów szczelinowania hydraulicznego w oparciu o pozyskane w poprzednich etapach dane i informacje. Na przykładzie dwóch odmiennych litologicznie potencjalnych lokalizacji EGS z obszaru Polski opisano rezultaty analizy wpływu parametrów sprężystości ośrodka skalnego typu HDR na geometrię szczelin w zabiegach HF. Zaprezentowano także analizy wrażliwości geometrii szczeliny oraz jej przewodności na zróżnicowanie modułu Younga oraz współczynnika Poissona w analizowanych formacjach. Wyniki tych prac zostały opublikowane w czasopiśmie *Energies* (Moska i inni, 2025).

Wyniki prac, badań i symulacji przeprowadzonych w całym okresie realizacji pracy pozwalają stwierdzić, że analizowane skały posiadają parametry petrofizyczne, charakterysyczne dla formacji EGS-petrotermalnych. Wpływ modułu Younga oraz współczynnika Poissona na geometrię szczeliny hydraulicznej w analizowanych formacjach można uznać za niewielki, natomiast wpływ na przewodność, może być istotny dla efektywności systemu geotermalnego w skałach osadowych. Interwały o wyższym module Younga i wyższym wskaźniku kruchości są bardziej perspektywiczne dla systemów EGS w skałach osadowych. W formacjach magmowych bardziej obiecujące wydają się być odcinki o niższym module Younga i wskaźniku kruchości, mogące odzwierciedlać strefy naturalnych nieciągłości lokalnych, które w takich skałach ulegają stymulacji w pierwszej kolejności.

# Abstract

Among the currently developing low-emission energy production technologies, Enhanced Geothermal Systems (EGS) exhibit some of the highest potential. These systems are created within so-called *hot dry rocks* (HDR) - a geological formations typically located at depths greater than 4000 meters, under conditions of high pressure and temperature. HDR are characterized by extremely low permeability and porosity and usually contain little to no water. As a result, their thermal energy cannot be transported to the surface in the same manner as in conventional geothermal systems. To address the limited natural fluid conductivity in HDR, artificial stimulation is employed to enhance their hydraulic conductivity, most commonly through hydraulic fracturing (HF) technology. This process creates a geothermal system in which a working fluid circulates in a closed loop: it is first injected into the reservoir through an injection well, heated as it flows through artificially created or reactivated fractures within HDR, and then extracted to the surface where its heat is utilized for thermal and/or electrical energy production. The cooled fluid is then reinjected into the reservoir, completing the cycle. EGS projects have been developed worldwide since the 1970s, with commercial power plants currently operating in countries such as France and Germany. In Poland interest in this unconventional branch of geothermal energy has been increasing since the early 21st century, leading to the implementation of scientific projects and the publication of numerous studies. Despite the wide research scope of some of these efforts, their outcomes have not been directed toward the development of HF-related technological elements tailored to Polish hot dry formations. This doctoral dissertation aims to address that specific research gap.

The research activities undertaken in this dissertation can be divided into two main parts: (1) laboratory investigations on rock samples collected from prospective EGS regions in Poland, preceded by an extensive literature review focused on key elements of HF technology in EGS, and (2) numerical simulations of HF treatments, combined with the assessment of the impact of rock elasticity parameters on hydraulic fracture geometry.

The conducted literature review examined the most significant EGS projects carried out worldwide, with particular attention paid to their geological, petrophysical, and tectonic parameters, as well as the HF technologies employed. This analysis enabled the identification of HF treatment features typical of EGS, fracture geometries within reservoirs, and the operational parameter ranges used in those projects. These findings were compared to the conditions characteristic of promising formations in Poland. The results of this study were published in *Energies* (Moska et al., 2021).

A complementary review was also conducted, expanding the analysis of prospective EGS areas in Europe to include the Baltic counties (Lithuania, Latvia, Estonia) and comparing their geological conditions with those in Poland. This work was published in *Energies* (Moska et al., 2023).

The next part of the work involved laboratory testing of core samples obtained from three geologically prospective EGS areas in Poland: the Karkonosze region, the Gorzów Block, and the Mogilno-Łódź Trough. Collected samples were characterized in terms of petrophysical and petrographic properties. Results of geomechanical testing, performed using ultrasonic methods under reservoir conditions on a research setup modified by the doctoral candidate,

were also presented. Additionally, it was demonstrated how the brittleness index, traditionally used in the oil and gas industry, can be applied to assess the susceptibility of these formations to hydraulic fracturing. These studies were published in *Advances in Geo-Energy Research* (Moska et al., 2024).

Supplementary studies of the samples thermal parameters were also performed, along with numerical simulations in two areas: (1) the temperature distribution and cooling extent during long-term heat extraction, and (2) the chemical reactions occurring during thermal energy production. These simulations provided the basis for evaluating the EGS potential in western Poland. This analysis was published in *Energies* (Labus et al., 2025).

The final stage of the dissertation involved numerical simulations of hydraulic fracturing treatments, based on data acquired during the earlier research phases. Using two geologically distinct potential EGS locations in Poland, the influence of rock elasticity parameters (specifically Young's modulus and Poisson's ratio) on fracture geometry was analyzed. Sensitivity analyses of fracture geometry and conductivity in response to variations in these parameters were also performed. The results of this work were published in *Energies* (Moska et al., 2025).

The findings from the entire body of research, including testing and simulation, indicate that the analyzed rocks exhibit petrophysical properties characteristic of petrothermal EGS formations. The impact of Young's modulus and Poisson's ratio on hydraulic fracture geometry in these formations is generally limited, however, their influence on fracture conductivity may significantly affect the performance of geothermal systems in sedimentary rocks. Intervals with higher Young's modulus and brittleness index are more promising for EGS development in sedimentary formations. In contrast, in magmatic formations, sections with lower Young's modulus and brittleness index, possibly representing natural zones of weakness, are more likely to be preferentially stimulated during HF treatments.

# Załączniki

W tym rozdziale zaprezentowane są pełne teksty artykułów naukowych opisanych skrótowo w rozdziałach 2 - 6. Artykuły są wymienione w następującej kolejności:

Artykuł I: **Rafał Moska,** K. Labus, P. Kasza, *Hydraulic Fracturing in Enhanced Geothermal Systems – Field, Tectonic and Rock Mechanics Conditions – A Review,* Energies, Volume 14, 5725, 2021. DOI:10.3390/en14185725

Artykuł II: **Rafał Moska,** K. Labus, P. Kasza, A. Moska, *Geothermal Potential of Hot Dry Rock in South-East Baltic Basin Counties – A Review,* Energies, Volume 16, 1662, 2023. DOI: 10.3390/en16041662

Artykuł III: **Rafał Moska,** K. Labus, P. Kasza, *Dynamic Elastic Properties, Petrophysical Parameters and Brittleness of Hot Dry Rocks from Prospective Areas of Central Europe,* Advances in Geo-Energy Research, Volume 14, 2, 90-105, 2024. DOI: 10.46690/ager.2024.11.03

Artykuł IV: K. Labus, **Rafał Moska,** M. Labus, *Potential Enhanced Geothermal System in Western Poland – Petrothermal and Geochemical Issues*, Energies, Volume 18, 876, 2025. DOI: 10.3390/en18040876

Artykuł V: **Rafał Moska,** K. Labus, P. Kasza, *Impact of Rock Elastic Properties on Fracture Geometry in Potential Enhanced Geothermal Systems in Poland,* Energies, Volume 18, 2869, 2025. DOI: 10.3390/en18112869

**Artykuł I: Hydrauliczne szczelinowanie we wspomaganych systemach geotermalnych – przegląd uwarunkowań tektonicznych, geomechanicznych i powiązanych z nimi aspektów technologicznych.**

energies

MDPI

*Review*

# Hydraulic Fracturing in Enhanced Geothermal Systems—Field, Tectonic and Rock Mechanics Conditions—A Review

Rafał Moska [1,*], Krzysztof Labus [2] and Piotr Kasza [1]

[1] Oil and Gas Institute—National Research Institute, 25A Lubicz Str., 31-503 Krakow, Poland; kasza@inig.pl
[2] Faculty of Mining, Safety Engineering and Industrial Automation, Silesian University of Technology, 2 Akademicka Str., 44-100 Gliwice, Poland; krzysztof.labus@polsl.pl
* Correspondence: moska@inig.pl

**Abstract:** Hydraulic fracturing (HF) is a well-known stimulation method used to increase production from conventional and unconventional hydrocarbon reservoirs. In recent years, HF has been widely used in Enhanced Geothermal Systems (EGS). HF in EGS is used to create a geothermal collector in impermeable or poor-permeable hot rocks (HDR) at a depth formation. Artificially created fracture network in the collector allows for force the flow of technological fluid in a loop between at least two wells (injector and producer). Fluid heats up in the collector, then is pumped to the surface. Thermal energy is used to drive turbines generating electricity. This paper is a compilation of selected data from 10 major world's EGS projects and provides an overview of the basic elements needed to design HF. Authors were focused on two types of data: geological, i.e., stratigraphy, lithology, target zone deposition depth and temperature; geophysical, i.e., the tectonic regime at the site, magnitudes of the principal stresses, elastic parameters of rocks and the seismic velocities. For each of the EGS areas, the scope of work related to HF processes was briefly presented. The most important HF parameters are cited, i.e., fracturing pressure, pumping rate and used fracking fluids and proppants. In a few cases, the dimensions of the modeled or created hydraulic fractures are also provided. Additionally, the current state of the conceptual work of EGS projects in Poland is also briefly presented.

**Keywords:** enhanced geothermal systems; EGS; hot dry rock; HDR; hydraulic fracturing; rock mechanics

check for updates

**Citation:** Moska, R.; Labus, K.; Kasza, P. Hydraulic Fracturing in Enhanced Geothermal Systems—Field, Tectonic and Rock Mechanics Conditions—A Review. *Energies* **2021**, *14*, 5725. https://doi.org/10.3390/en14185725

Academic Editors: Dalia Štreimikienė and Tomas Balezentis

Received: 10 August 2021
Accepted: 8 September 2021
Published: 11 September 2021



## 1. Introduction

The XXI century is a time of global change in the approach in the field of energy acquisition. The current existing methods of energy production, based on conventional resources such as coal, natural gas and radioactive materials, are gradually being replaced by environmental-friendly, low-emission technologies, such as hydrogen, wind and sun farms, biomass combustion and geothermal systems. Among these modern green technologies, great potential is exhibited by so-called enhanced geothermal systems (EGS) [1]. EGS allows to extract an earth's thermal energy from impermeable (or very low permeable) hot dry rocks (HDR), which in natural conditions do not contain water, or contain a small amount [1–3]. The idea of the EGS system thermal collector is to use thermal energy of the HDR formation to heat up the process fluid in situ, extract it to the surface and use it to drive a turbine generating electricity on a commercial scale. The HDR formations are usually accessed by at least two 3–6 km deep wells, connected in a perspective layer by a network of induced fractures. The process fluid circulates in a loop between the injection and the production wells, is heated up underground in a conduction process and then releases energy at the surface (Figure 1). The main feature dividing the EGS system from the conventional geothermal system is that EGS requires creating an artificial conductivity in the reservoir, which allows gaining hydraulic connections between wells [4]. Such conductivity is obtained on EGS sites by the reservoir stimulation, which can be divided into three types, as follows: thermal, chemical and hydraulic. In thermal stimulation, cold water injection causes micro-cracking of the grains, matrix and fracture filling. Thermoelastic effects reduce the normal stress on fractures and thus promote fracture opening. The chemical stimulation consists of injecting an acid fluid to dissolve materials around the wellbore, such as cuttings from drilling and hydrothermal minerals plugging the fracture zones. For this purpose, carbonate-dissolving acids can be used. On the other hand, biodegradable chelating agents do not dissolve clay minerals and quartz. This technology was developed and used in the oil and gas industry and was adapted to deep geothermal wells to enhance the fracture network, particularly in EGS projects [5]. In hydraulic stimulation (hydraulic fracturing (HF)), an artificial fracture in the reservoir is created, or a pre-existing fracture is reopened by injecting process fluid at high pressure [6]. In the intrusive HDR strata, fresh water is most commonly used as a process fluid. In some cases, especially fracturing in tight sediments, water with some chemical additives to prevent undesirable liquid–rock interactions is also used. The polymer-based fluids, due to their increased viscosity, are characterized by better carrier properties. It allows the addition of the proppant materials, which prevent fracture closure after the operation.

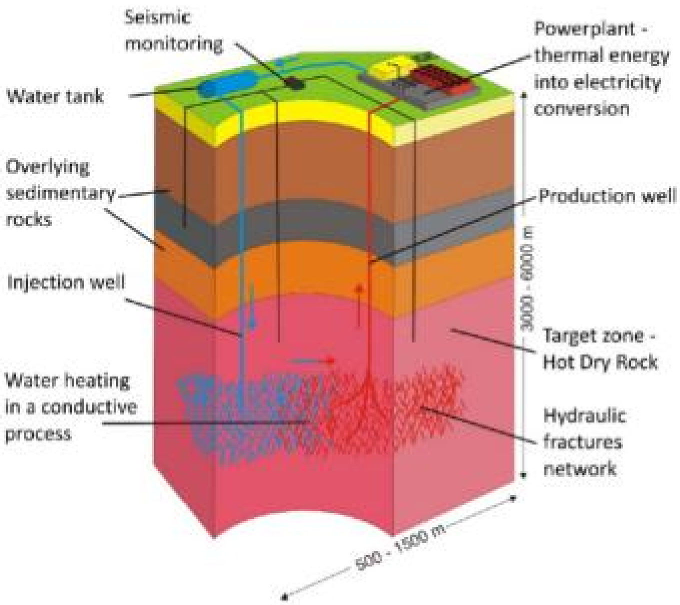


**Figure 1.** Principle of operation of a doublet enhanced geothermal system.

Designing the stimulation operations, in particular HF, requires a detailed analysis of the number of parameters such as petrophysics, petrographic and mechanic properties of the rock, as well as hydrogeologic and tectonic conditions in the field. The development of EGS technology has been ongoing since the 1970s [7]. Over the following years, a couple of research projects were carried out in order to understand the hot, deep reservoir parameters better and to improve the efficiency of heat extraction [8–10]. Some of these projects did not go beyond the research stage; however, several of them were converted into independent systems supplying energy to the power grid. With a high estimated probability, by 2050, the power of all EGS plants in the world will equal the power of hydrothermal systems and will reach the performance of about 70 GWe [1].

The aim of this paper is to collect, show and compare the major geological, tectonic and mechanical parameters of the world's EGS systems, as well as present at a glance the course and results of the hydraulic stimulation in these systems. The paper deals only with hydraulic HDR stimulation and other types of stimulation activities are not considered here. While collecting the materials, we focused on the tectonic stress regime and its influence on the fracture dimensions and propagation, as well as rock mechanic properties, such as Young's Modulus and Poisson's ratio, having a significant influence on the shape of the fracture and fracking pressure parameters.

**2. Hydraulic Method of Stimulation Low-Permeable Reservoir**

The HF operations, as one of the production stimulation methods of conventional and unconventional hydrocarbon deposits, have been known for many years (e.g., [11,12]). HF in the unconventional reservoir consists of creating or reopening the fractures in the low permeable rock and filling them with a proppant to avoid fracture closure and improve the conductivity between the reservoir and wellbore. Propagation of fracture is obtained by the hydraulic action of the fracturing fluid on the deposit. Fluid pumped from the surface through the wellbore causes stresses in the rock. If the pumping rate and pressure are large enough, inducted stresses exceed the critical stresses, which causes rock failure and fracture propagation [6,13]. Further pumping leads to fracture propagation in the vertical and horizontal directions deeper in the reservoir [14]. The fracking fluid transports the proppant grains, which fills the fractures. The process of fracturing ends when pumping with adequate capacity and pressure is stopped; after the flow stops, the fluid filtrates through the pore space of the rock, which causes a slow pressure drop. The formation stresses begin to outweigh the inducted pressure, which leads to the closure of the fracture. The proppant grains left in the fracture prevent it from fully closing and losing the hydraulic conductivity. As a result, the propped fractures constitute highly permeable arteries communicating the well and the reservoir [15]. The HDR formations are characterized by no permeability or very low permeability; therefore, reservoir stimulation, including HF, is the only method of accessing such kinds of deposits [4]. The deep wells in EGS are similar to oil and natural gas wells and in completion drilling technology. The differences concern the greater depth, a larger magnitude of stresses, higher temperatures and the presence of crystalline, igneous rocks, which are usually heat exchangers [16]. The assumptions of EGS require drilling at least two (doublets) or more (e.g., a triplet) of wells connected to each other by fracture systems in situ. The HF design process in the EGS site is similar to this kind of operation in the natural gas site. The greatest technological goal that must be met during this procedure is the prediction of the geometry of the fractures and estimation of the propagation direction between wells, so as on the one hand, gain hydraulic conductivity and on the other hand, to avoid thermal short-circuiting, leading to a decrease in temperature of the received liquid [4].

Most of the EGS fields are located in the extensional or strike-slip faulting regime; thus, in the case of vertical or subvertical wells, fractures propagate vertically with the direction more or less parallel to the wellbore. The geometry of the vertical fracture is described by basic mathematical models: KGD (Kristianowich-Zheltov, Geertsma-deKlerk) and PKN (Perkins, Kern). The models differ in the mathematical assumptions regarding the direction of deformation at the opening of the slot (vertical or horizontal). Simplifying, the models assume an elliptical fracture shape in the side view (Figure 2). The result of the model is the equation of the fracture, which binds fracture height, length, width (Figure 3) and the influence of additional parameters, such as rheology of the fracturing fluid, pumping pressure and elastic parameters of the rock [6]. Since their development, the fracture geometry models have been modified and refined many times and are offered as a key element of commercial software for oil and gas service companies.

The fracture propagation is also the subject of numerical modeling. There are three conceptual models that explain the increase in permeability during hydraulic stimulation [4,17]: (1) hydraulic fracturing (or pure opening mode)—creating new fractures in the tensile mode; (2) hydraulic jacking—reopening pre-existing fractures in tensile mode, (3): hydraulic shearing (or pure shear stimulation)—inducting slip and dilatation of natural fractures in a shear mode. Generally, hydraulic shearing is regarded as the primary mechanism of permeability enhancement in a fractured reservoir, and it is consistent with the observations of induced seismicity when the injection pressure is lower than the minimum principal stress for most EGS projects [17]. There is also a suggested mixed stimulation mechanism (MMS). The idea of MMS is that continuous pathways for flow involve both new and pre-existing fractures. The key idea is that propagating new fractures may terminate against pre-existing fractures [4].

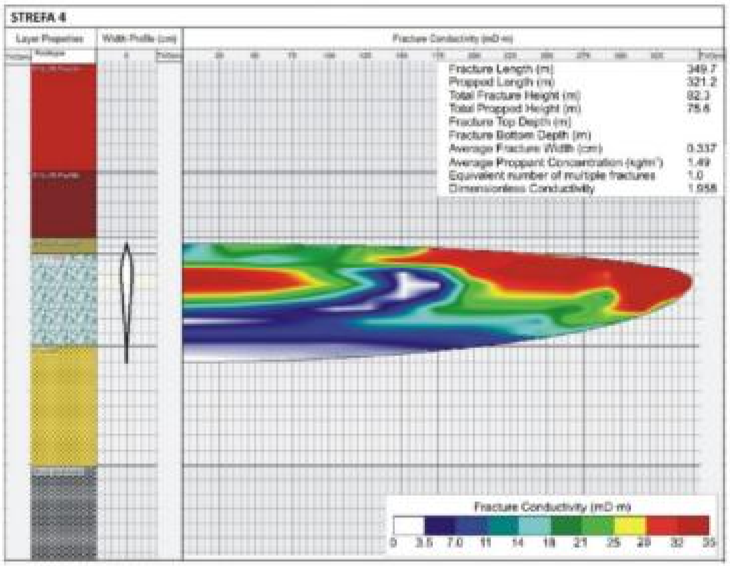


**Figure 2.** An exemplary model of a wing of the fracture. Color filling means fracture conductivity [15].

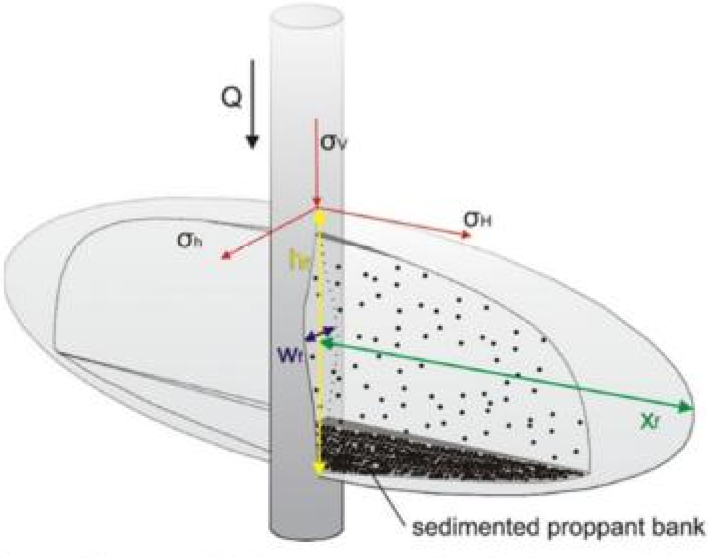


**Figure 3.** Dimensions of the fracture: $x_f$—length, $h_f$—height, $w_f$—width. Q—flow, $\sigma_V$—vertical stress, $\sigma_H$, $\sigma_h$—horizontal stresses. Based on [18].

*Rock Mechanics in the Design of Hydraulic Fracturing Operation*

Good recognition of the tectonic conditions of a field and the petrophysical parameters of productive strata, as well as top and bottom layers, is the key to design an effective HF operation in a reservoir (both geothermal and hydrocarbons). Fractures always propagate in the direction perpendicular to the minimum stress; thus, the information about the direction and magnitude of principal stresses (vertical ($\sigma_V$) and horizontal minimum and maximum ($\sigma_H$ and $\sigma_h$, respectively)) is critically important. In the normal faulting regime (extension), where vertical stress dominates ($\sigma_V > \sigma_H > \sigma_h$), vertical fractures will be created. In a strike-slip faulting regime, where the magnitude of vertical stress is less than the magnitude of one of the horizontal stresses ($\sigma_H > \sigma_V > \sigma_h$), vertical fractures propagate as well. In the reverse faulting regime (compressive), where the magnitudes of both horizontal stresses dominate ($\sigma_H > \sigma_h > \sigma_V$), a horizontal fracture propagates [19–21] (Figure 4).

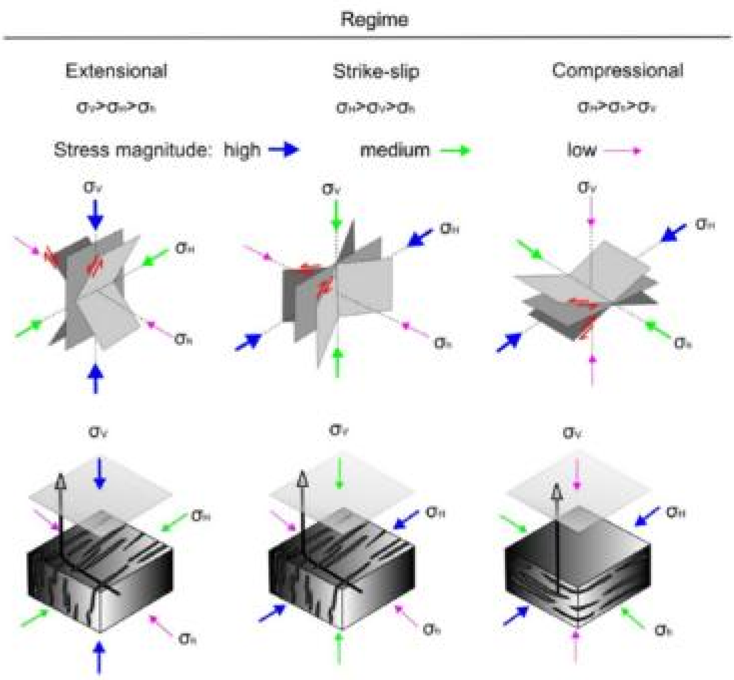


**Figure 4.** Tectonic regimes and stresses activity. Based on [20].

The stress directions in the field could be in line with the regional stress map; however, the local fluctuations of the stress state caused by local geological/tectonic conditions often occur. Directions of the $\sigma_H$ and $\sigma_h$ are determined based on focal mechanism calculation, as well as in the wells, in the way of breakout and tensile fracture analysis. The magnitude and elastic parameters of the reservoir determine the dimensions of the fracture [15]. Young's modulus ($E$) defines how much energy is required to accomplish the displacement, which is a classic linear elastic fracture mechanics concept. When increasing $E$, the height and length of the fracture increases, while width decreases. The net pressure (fracturing and closure differential pressure) also increases. Rocks with a large Young's modulus require more energy to displace. In these formations, fractures tend to be relatively narrow, and the rock is referred to as "hard" [6]. Poisson's ratio ($\upsilon$), reflecting rock deformation, occurs perpendicular to the deformation induced by the stress. In the reservoir, $\upsilon$ determines rocks' ability to fail under stress [22]. In formations of low $\upsilon$, the embedment phenomenon rises, which leads to a decrease in the conductivity of the fracture (e.g., [23–25]). Both $E$ and $\upsilon$ parameters allow determining susceptibility for fracking, defined by the brittleness index [22,26–30].

## 3. Literature Review

The selected most important global EGS projects are shown in Figure 5. The authors focused on presenting the data sets and information required to design a hydraulic fracturing treatment at an EGS site, as well as the information of already performed hydraulic fracturing operations and their effects. Data include the geological information from lithology, depth of deposit, target zone temperature and method of thermal energy transport, as well as geophysical data, i.e., stress regime and magnitudes, rock mechanics parameters and ultrasonic velocities. Fracturing data include pressure, pumping rate, fracking fluids, chemical additives and proppants. Based on these data, a summary table (Table 1) was prepared. Clearly, the presented data are selective, and many elements were omitted. The described EGS projects are only part of the projects that have been conducted and implemented around the world. Projects such as Hijiori and Ogahi in Japan, Rosmanowes and Fjällbacka in Europe, Paralana in Australia and other projects in the USA are not considered in this paper. At the end of the paper, the state of current work and prospects for the EGS installation in Poland were briefly described.

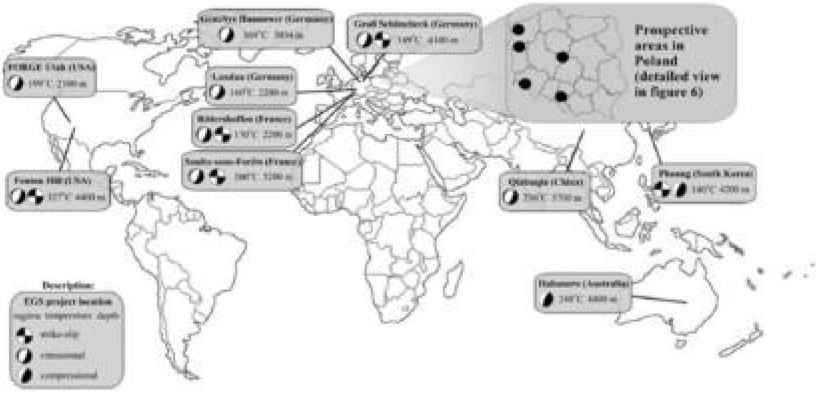


**Figure 5.** EGS projects reviewed in this paper. Beach balls represent the tectonic regime.

### *3.1. Fenton Hill (USA)*

The Fenton Hill project, located in Valles Caldera in northern New Mexico, was the world's first EGS pilot project. The aim was to develop methods of energy extracting from the granite and metamorphic HDR horizons. The target horizon consisted of biotite granodiorite and gneiss [31]. Static 3-axial tests allowed to designate the elastic parameters of the granodiorite from 4102 m depth amounted to 33 GPa and 0.12–0.22 (-) for Young's modulus and Poisson's ratio, respectively. Stress gradients of this area were estimated as $\sigma_V = \sigma_H$—25 MPa/km, $\sigma_h$—13–19 MPa/km [32].

The first phase of the project (1974–1980) involved drilling the GT-2 well to a depth of about 2930 m, where the temperature amounted to about 180 °C. The second phase, from 1979, included drilling the EE-1 production well to a depth of 3064 m and performing a fracturing treatment. Due to insufficient results, the horizontal sections GT-2A and GT-2B were drilled, where a sufficient hydraulic connection was obtained at a depth of about 2700 m. In the following years, a number of circulation tests were carried out at this site, during which a thermal power of 3–5 MWt and energy production in a binary cycle with 60 kW was achieved. In 1979, the drilling of two-directional production wells, EE-2 and EE-3, to a depth of 4390 m, where the temperature reached 327 °C. The HF treatments carried out in this well did not meet the expected results due to an unforeseen change in the stress state in the deeper parts of the stimulated horizon [16].

Re-drilling the EE-3 borehole and routing it in the area of the fractures created during the earlier HF (EE-3A) allowed for sufficient hydraulic connection. In 1986, tests of the flow in a closed loop were carried out using 37,000 $m^3$ of water, of which more than 80% was recovered. The pumping rate was between 0.64 and 1.10 $m^3$/min, whereas the wellhead pressure was between 26.9 and 30.3 MPa. The liquid temperature on the surface reached 192 °C. The formation fracturing pressure was below 19 MPa, and below this pressure, the volume of the stimulated reservoir did not increase. Long-term flow tests have been carried out since 1992, whereas water was injected at a rate of 0.75–0.90 $m^3$/min, while the temperature of the received water was over 180 °C [16].

Fenton Hill was the first site to confirm that energy production from HDR rocks on a commercial scale is possible. The experiences gained from this project were widely used in further EGS activities.

### 3.2. Habanero (Cooper Basin, Australia)

The Cooper Basin is located in the north-eastern part of South Australia, near the Queensland border. This area is very well recognized due to activities connected to oil and gas extraction. The crystalline basement (Big Lake Suite granite batholith) is located at a depth of 3400–3500 m (the area known as the Nappamerri Trough), where an increased geothermal gradient occurs (55–60 °C/km) [33]. Increased content of radioactive elements (e.g., uranium) causes, in this formation, local, relatively shallow zones of elevated temperature [1]. It is estimated that the batholith granites have a thickness of about 10 km. They are medium- to coarse-grained, light grey granites with aplitic and alaskite dykes and veins. Biotite is almost completely altered into chlorite, especially in shallower regions. Much of the feldspar is also altered. Their yellowish alteration is related to the oxidation process associated with the presence of permeable fractures. Granites are potassium-rich, with a silica content of 75% [33]. One of the most significant features of the Habanero area is that the stress regime of the crystalline basement is compressive (reverse faulting), i.e., the vertical stress is less than the horizontal stress. Granites remain under overpressure conditions (5000 psi above hydrostatic pressure). Among the areas of EGS projects, only Habanero and Fjällbacka (Sweden) are characterized by such kind of stress regime [4].

In 2003, the first wellbore dedicated to EGS systems—Habanero-1, with a depth of 4421 m—was drilled and completed. The investor was the private company Geodynamics Limited. The well tests have shown that the overpressure in the granite batholith is close to the fracture pressure [33]. The first hydraulic stimulation at the Habanero-1 well took place in 2003. Firstly, a series of temperature logs were recorded, the last of which showed 248.5 °C at a depth of 4390 m, with a slight upward trend in temperature over time.

In the initial stage—the fracture initiation phase, a significant part of the flow was recorded at a depth of 4254 m, whilst the lower part of the well was filled with salt to divert the flow to the above levels. After the injection of 1600 $m^3$ of water, based on the recorded microseismic events and the PTS tool, it was noted that a sufficient vertical extension of the area was achieved and that further expansion of the zone would probably occur naturally. In the main stage, water was pumped for two days at a rate of 0.79 $m^3$/min, and then the rate was increased over several days up to 1.11 and 1.43 $m^3$/min, reaching 16,350 $m^3$ total volume of water. Based on the microseismic, the SRV indicator (Stimulated Reservoir Volume) was estimated at 0.7 $km^3$, assuming the parallelogram geometry. It was a significantly higher value than the primary assumptions and higher than required for the adopted economic model of heat generation over a period of 25 years. At that time (the beginning of the 21st century), it was the largest geothermal system in HDR rocks in the world [33].

The seismic network, consisting of geophones located in eight surrounding boreholes, at depths from 100 to 850 m, up to 5 km far from the main well, was used. A total amount of approximately 11,700 events were recorded in the seismic cloud. The velocity of the P-wave in the granite at a depth below 3673 m, amounting to 5525 m/s, was recorded [33]. The elastic parameters of the granitic batholith used for modeling the breakout and tensile fractures were estimated at $E$—65 GPa, $\upsilon$—0.25 (-) [34].

The significant success of the operations conducted at the Habanero-1 well resulted in the further development of EGS projects in this area. In the following years, three more wellbores were drilled in this area: Habanero-2 (2004), 3 (2008) and 4 (2012), and two wells west of Habanero: Jolokia-1 (2010) and Savina-1 (2009) [35]. HF treatments were performed in all Habanero wells and in the Jolokia-1 well. Most treatments were performed using pure water without additives. Only in the above-described stimulation of the Habanero-1 well, NaCL-based brine was used, and in the Jolokia-1 well, high-density NaBr-based brine was used. In the years 2003–2012, 7 HFs were performed in total. From 556 to 34,023 $m^3$ of water was pumped into the reservoir, depending on the procedure. A detailed description of the performed activities was presented by Holl and Barton [35].

Barton et al. [36] presented a geomechanical model of the Big Lake Suite granite from the Habanero area. Stress magnitudes obtained from the geophysical logs and data collected during drilling clearly show the strike-slip regime in the sedimentary layers of the overlying strata, undergoing the reverse and over-thrust regime at the target zone. Therefore, at the crystalline zone, the maximum horizontal stress is the maximum principal stress. $\sigma_H$ may even amount to 150 MPa at the reservoir depth. The minimum horizontal stress $\sigma_h$ is intermediate between $\sigma_H$ and $\sigma_V$. The $\sigma_H/\sigma_h/\sigma_V$ ratio is estimated at about 1.35–1.45/1.10–1.25/1.0 at the reservoir depth. In the reverse stress regime of the Habanero region, the original N-S strike structures with a slight dip are stimulated first. Since these structures are in critical stress, stimulation occurs at pressures much less than the overburden pressure (in this case, the minimum principal stress). The fracturing process more easily induces shear in primary fault zones (sensitive to stress changes), which are optimally oriented to the stress field, than creates new hydraulic tension fractures [34–36].

Hogarth and Holl [37] formulated a few conclusions from over a dozen years of operations on wells in the Habanero EGS project. They pointed out that the fracture system in the EGS target is likely to be complex and related to brittle failure in a complex deformation history. Furthermore, the major flow path in an EGS reservoir is likely to be through pre-existing, high slip likelihood faults; thus, the in situ stress regime must be well understood so that wells can be oriented to maximize the chance of intersecting fractures with high "slip likelihood".

At the Habanero site, a 1MWe power plant was commissioned in 2013, and then by 2015, its capacity was increased to 40 MWe [1]. In the following years, the Geodynamics company closed the project due to insufficient economic viability and change in company policy [38].

### 3.3. Rhine Graben EGS Projects

The Rhine Graben, a part of the European Cenozoic rift system, is located in Western Europe, within the borders of northern Switzeland (Basel), eastern France and southwestern Germany (Frankfurt am Main). This area is characterized by specific temperature conditions favorable for obtaining geothermal energy.

The temperature anomalies are the result of large-scale convection in the fracture system associated with nearly vertical faults crossing Cenozoic, Jurassic and Triassic sediments, as well as the Hertzian crystalline basement [39]. The tectonic regime of this area is normal to a more or less pronounced strike-slip component. Quasi-pure strike-slip events also occur, especially in the deeper part of the reservoir [40].

#### 3.3.1. Soultz-sous-Forêts (France)

The first EGS project in the Rhine Graben area was the Soultz-sous-Forêts, which was established in the 1990s, and at present includes four wells. The system is based on a triplet, consisting of one injector and two producers. The wellbores reach a crystalline basement, composed in the shallower parts of MFK porphyry granites and in the deeper parts of two-mica granite (containing biotite and muscovite) [41]. In each of the wells, there is at least one permeable naturally fractured zone in the productive horizon.

The first borehole accessing the Carboniferous granite basement at the temperature of about 160 °C at a depth of 3590 m was the GPK-1 vertical well completed in 1992. In this well, the first HF treatment in this area was conducted. In the next years (1994–2003), further wells were completed in the triplet system, which reached the granite basement at a depth of 5060–5270 m, where the temperature amounted to about 200 °C (GPK-2, 3 and 4) [39]. The distance between the wells in the productive zone is about 600 m. The directional sections of the wells are located along the N-S axis, parallel to the direction of the maximum horizontal stress [41].

The hydraulic stimulation of each of the boreholes was started by pumping tens of thousands of liters of fresh water, then brine of a density of 1.2 kg/L, in the total amount of about 800 $m^3$, initiating the fracture propagation. Then, MHF (massive hydraulic fracturing) was performed. The HF in the GPK-2 well was carried out for 6 days with a pumping rate of about 3 $m^3$/min. The wellhead and bottom pressure showed a slight but constant upward trend during pumping as a result of the shear stress-induced fracking. The maximum overpressure of 150 bar was lower than expected and indicated that the reservoir was close to the critical condition. An increase in productivity from 0.02 to 0.4 L/(s·bar) were observed [42]. In the GPK-2 and GPK-3 wells, a simultaneous stimulation was carried out to concentrate the fracturing process in the part of the reservoir between these wells. A total of 34,000 $m^3$ of water was pumped in. The wellhead and bottom pressure charts show the dependence of the pressure on the pumping efficiency, which suggested filling the pore space rather than its effective stimulation. However, the productivity factor of the GPK-3 borehole was increased from 0.2 to 0.3 L/(s·bar), while the hydraulic connection between the two boreholes was significantly improved. The GPK-4 well was of marginal production importance before stimulation. Two HFs were performed in this well. Water was pumped with a rate of 1.8–2.7 $m^3$/min, whereas a total of 9300 $m^3$ of liquid was pumped in at the first and 12,300 $m^3$ at the second frac. A high overpressure (170 bar) at the beginning of the first frac, as well as its slight decrease, may indicate an artificial fracture creation. The well productivity increased from 0.01 to 0.2 L/(s·bar); however, the hydraulic connection between GPK-3 and GPK-4 was still poor [42].

Currently, a 1.5 MW power plant is installed at the EGS Soultz site. It is planned to be developed to 3 MW [43].

#### 3.3.2. Rittershoffen (France)

The success of the Soultz project in France resulted in the commencement of another EGS in the town of Rittershoffen, about 6 km southeast of Soultz. The geological and tectonic conditions of this area do not significantly differ from Soultz; however, the 150 °C isotherm lies slightly shallower there. The tectonic regime is, like in the case of Soultz, extensional and strike-slip [44]. The project was initiated in 2004, and the first GRT-1 well was drilled after obtaining permission in 2013. The second GRT-2 (directional) well complementing the doublet system was completed in 2014 [45]. Both wells access the Rittershoffen fault zone and a crystalline target zone at a depth of about 2200 m. The temperature recorded at the bottom of the GRT-1 well (2526 m TVD) was 163 °C, while in the GRT-2 well, at a depth of TVD 2693 m, the temperature of 177 °C was measured [44]. The GRT-1 well was stimulated in three ways: thermal, chemical and hydraulic.

The hydraulic stimulation was carried out in 2013 when 3250 $m^3$ of water without proppant was pumped at a rate from 0.6 to 4.8 $m^3$/min [5]. Several hundred seismic events of the highest magnitude in the range of 1.4–1.6 were recorded [46]. The P-wave modeling of the granite target zone, based on the focal mechanisms, allowed to determine the velocity of 5600 m/s at a depth of 2550 m [47]. The magnitudes of the principal stresses, calculated based on the formulas cited from [47], for a depth of 2200 m are $\sigma_V$—54.8 MPa, $\sigma_h$—29.6 MPa, while the pore pressure is 22.5 MPa.

Since 2016, the Rittershoffen doublet EGS was integrated into the local power grid and currently generates 25 MWth of nominal thermal power [48].

#### 3.3.3. Landau (Germany)

The first German geothermal project—Landau, led by GeoX GmbH, aims to obtain geothermal energy from a fault system in the Permian sedimentary rocks and a granitic basement of the Rhine Graben. The doublet system was drilled in 2005–2006, reaching the depth of the open holes between 2100 and 2200 m and the distance between the wells of approximately 1200 m. Because of the thermal convection in the fault zone, the geothermal gradient of this area is elevated; thus, the temperature measured in the relatively shallow productive horizon amounted to about 160 °C [42].

The Gt La-1 borehole, after initial testing and cleaning, turned out to have sufficient productivity, whereas the Gt La-2 required MHF stimulation. The stimulation was carried out gradually. In the first stage, a preliminary test was performed with the wellhead pressure reaching 100 bar in peak and the pumping rate in the step-up system reaching 5.16 $m^3$/min (a total of 4600 $m^3$ of liquid). Afterward, the main HF was carried out with a wellhead pressure exceeding 110 bar and a flow rate of up to 9.0–11.4 $m^3$/min. A total of 6600 $m^3$ of liquid was pumped in [42]. In the Gt La-2 well, an acidizing treatment was also performed of 95 $m^3$ of 33% HCl, pumped at a rate of 0.6 $m^3$/min by coiled tubing, while fresh water was pumped through the annulus. The temperature logs before and after acidizing and showed that the outlet had shifted from sedimentary rocks to granite. After HF and acidizing activities, the production capacity of the Gt La-2 well increased five-fold [42]. Currently, the Landau geothermal power plant supplies 2.9 MW of electricity to the German power grid and 3MW of thermal energy [43].

#### 3.3.4. Basel (Switzerland)

Another EGS project in the Rhine Graben area was the Swiss project Deep Heat Mining in Basel. The BS-1 well in the city of Basel was completed in 2006, accessing the granite target zone. In the same year, the MHF was performed, injecting 12,000 $m^3$ of water at a wellhead pressure of 300 bar. The data analysis confirmed a consistent improvement in rock permeability of two orders of magnitude as a result of several high conductivity fracture activations. During the treatment, local seismic events of magnitude up to 2.7 were noted. A few hours later, an event of magnitude 3.4 occurred, which resulted in the wellbore pressure drop to a hydrostatic level within a few days [49]. As a result of this event, the Basel EGS project was suspended and finally terminated.

### *3.4. GeneSys Hanower (Germany)*

The GeneSys project was carried out in Hanover in 2009 and was a continuation of the GeneSys Horstberg test project. The purpose was to demonstrate the operation of the EGS installation in a single well, accessing low-permeable sedimentary formation. Two concepts of operating installation were considered. The first one assumed that cold water, pumped through the lower perforation zone, is heated up during the flow through the inducted vertical fracture and returns to the borehole in the upper perforation zone, where it is transported to the surface in the annular space. The second concept, so-called "huff-puff", was a cyclic one assumed cold water injected into a large fracture and produced back as hot water defined residence time [50,51].

The target zone was the Middle Buntsandstein sediments consisting of clay–mud–sandstone sequences, accessed by the Groß Buchholz Gt1 borehole, of 3834 m TVD. The temperature at the bottom of the well was 169 °C. From a depth of 3160 m, the well was deviated at an angle of 30°, whereas the deviation corresponded to the direction of the minimum horizontal stress. Elastic parameters of the target interval rocks varied depending on the rock type. The $E$ modulus of the sandstone ranged from 45 to 65 MPa, while $v$ ratio ranged from 0.19 to 0.22 (-). The $E$ modulus measured for clay deposits was very high for this type of rock and amounted to 49 GPa, while $v$ was 0.23 (-). For the salt layer, a limiting the horizon at the top, $E$ modulus of 33 GPa and the $v$ ratio of 0.25 (-) were assumed. $\sigma_h$ in the target interval was 72–83 MPa, which corresponded to 90% of the $\sigma_V$. The tectonic regime of this area is described as extensional; however, slight differences in the magnitude of $\sigma_V$ and $\sigma_h$ stresses indicate almost isotropic conditions. Numerical simulations of the fracture dimensions and propagation, based on the assumed pumping rate of 4.8 $m^3$/min and the total water volume of 20,000 $m^3$ of water, allowed obtaining a profile of a vertical fracture 1320 m in length, 430 m in height and 2.1 cm width [52].

The conducted minifrac tests showed a fracking pressure of 37.0 MPa when pumping with a rate of 0.1 $m^3$/min and a total liquid volume of 2.5 $m^3$. In a step-rate test, the maximum wellhead pressure of 42.0 MPa with a rate of 0.72 $m^3$/min was achieved. After the pumping, the wellhead pressure remained at a constant level, which confirms the very low permeability of the formation. The main frac was performed in 2011. Pure water without chemical additives was used. The planned 20,000 $m^3$ of water was pumped in for 5 days with a capacity of 5.4 $m^3$/min. The pumping was carried out in several stages. In each of them, the pumping rate was quickly increased to the assumed values and then held for some time at a more or less constant level, and fluctuations in pressure were observed. The wellhead pressure reached a maximum of 46.0 MPa. The observed pressure curves indicated good conductivity and negligible friction loss. Seismic monitoring did not reveal any events related to the conducted activities. Low-efficiency injection tests were conducted several months after the main frac confirmed the conductivity of the fracture system in an area of approximately 1 $km^2$. Because of the high salinity of the water, there was a salt plug trend in the wellbore; however, it was assessed as a local problem in Hanover. Finally, the GeneSys project was successful, and the experiences were used in other EGS sites [52].

### 3.5. *Groß Schönebeck (Germany)*

The Groß Schönebeck area is located in Germany, north of Berlin, in the north-eastern part of the North German Basin. The basin formation occurred between the Late Carboniferous and Early Permian, when the deposited volcanic rocks were covered by a Rotliegend siliciclastic sequence of alluvial fans, ephemeral streams, playa deposits and aeolian sands. Then, cyclic evaporitic sediments were deposited during the Upper Permian Zechstein. Sediments are covered by Mesozoic and Cenozoic strata [53].

Groß Schönebeck is a research area of the German Research Centre for Geosciences (GFZ Potsdam). The purpose of the GFZ EGS geothermal project was to develop technologies to increase the permeability of deep aquifers using hydraulic fracturing methods. The goal was to learn how to control the stimulation of a variety of rocks so that geothermal energy can be exploited from any kind of reservoir where it is needed [54]. The target zone consists of two types of Rotliegend deposits: low-permeable clastics at the top and volcanic (rhyolite, andesite) at the bottom [2]. These rocks, lying at a depth of 3850–4258 m, were accessed by an old hydrocarbon exploration well (GrSk 3/90), completed in 1990, and deepened in the purpose of EGS in 2000 to a depth of 4309 m [54]. In 2006, a second well (GrSk 4/05) was directionally drilled and completed in the production strata [55]. The older well was adapted as an injection well, while the other directional one as a production well. The distance between the wells at the reservoir depth was 241–470 m [56]. The temperature of 149 °C, at a depth of 4285 m and the formation pressure of about 44.9 MPa at a depth of 4220 m was recorded in the injection well [54]. Investigations of the stress state in the Rotliegend formation, based on 3D modeling and confirmed by data from HF, show the dependence of $\sigma_h \geq 0.55\ \sigma_V$ and $\sigma_H \leq 0.78–1.00\ \sigma_V$ in the normal to strike-slip tectonic regime. The magnitudes at a depth of about 4100 m were estimated at $\sigma_V$—100 MPa, $\sigma_h$—55 MPa and $\sigma_H$—78–100 MPa [57].

Blöcher et al. [55] compiled the parameters of the number of HF treatments performed at both wells in the Groß Schönebeck project. In 2002, in the GrSk 3/90 well, four HF treatments were performed at two depth intervals of the open hole section. HTU linear gel (cationic, hydrophilic, polymer-based) and brine were used as a fracturing fluid. Total weight of approximately 8500–8700 kg, 20/40 mesh Carbo-Lt proppant was also used in the two treatments. The pumping rate was 2.0–2.6 $m^3$/min, and the total volume of the pumped fluid was 103–129 $m^3$. The originally created vertical fractures were characterized by a half-length of 32 m, height of 72 m and width of 0.16 cm. In the same well, in 2003, two large MHF (massive hydraulic fracturing) treatments were carried out using water without proppant. One in the open hole section and the other in the slotted liner section.

About 4300 and 7300 $m^3$ of water were pumped in, with a rate of 1.44 and 2.4 $m^3$/min, respectively, which allowed to create the fracture of dimensions: 160 m half-length, 96 m height and 0.5 cm width. The GrSK 4/05 production well was stimulated three times in 2017. During the first treatment, 13,170 $m^3$ of water with 20/40 mesh quartz sand with a maximum rate of 9.0 $m^3$/min was pumped. The dimensions of the fracture were: half-length—190 m, height—135 m and width—0.8 cm. The next two HF treatments were performed using a crosslinked gel with a high-strength 20/40 mesh proppant, at intervals protected by a perforated liner; 280–310 $m^3$ of fracking fluid and 95–113 t of proppant were pumped in, with a rate of 3.0–4.0 $m^3$/min. The resulting fracture dimensions were about 60 m in half-length, 95–115 m in height and 0.53 cm in width [55].

### 3.6. Pohang (South Korea)

The first EGS project in South Korea was the Pohang project, named after a city in the southeastern part of the Korean peninsula. The main objective of this project, which started in 2010, was to obtain a 1MW power plant in a doublet system. The drilling location was selected due to one of the highest geothermal gradients in Korea, i.e., 30 °C/km [58]. Before the EGS activities in this area, several low-temperature geothermal wells were drilled [59], as well as EXP-1 wellbore for stress field measurement in the reservoir [17]. The target zone for the Pohang EGS wells was a crystalline basement consisting mainly of Permian laminated granodiorites at a depth of approximately 2400 m to more than 4500 m. The crystalline formations are covered by andesites and crystal tuffs. These deposits are covered by the sedimentary formation of about 1 km thickness, consisting of Cretaceous mudstones and sandstones interlayered by volcanic intrusions and eruptions. The Tertiary cover is semi-consolidated siltstone of 200–400 m thick [17]. Stress models of this area, at a depth of 4.2 km, indicate two possible tectonic regimes: (1) strike-slip, where the ratio of $\sigma_H$ to $\sigma_V$ is 1.2, $\sigma_h$ to $\sigma_V$ ratio is 0.8 and the maximum horizontal stress acts in the azimuth line of 114°; the compression regime (2) (reverse faulting), where the ratio of $\sigma_H$ to $\sigma_V$ is 2.29 and the ratio of $\sigma_h$ to $\sigma_V$ is from 0.8 to 1.08–1.15 [17]. In order to obtain access to the granodiorite basement, two wells were drilled: PX-2 vertical well in 2015, of 4341 m depth, and PX-1, originally vertical, deepened directionally in 2016 to the depth of 4215 m. Both wells in the bottom sections were open holes and separated by a distance of about 600 m. The stable temperature recorded in the PX-2 well, at a depth of 4209 m (MD), amounted to 140 °C [17].

Core samples of granodiorite were collected during drilling the PX-2 well [60]. Granodiorite was consisted mainly of albite (43.1%), quartz (28.6%), microcline (13.7%) and muscovite (10.1%) and was characterized by a volumetric density of 2.63 g/$cm^3$ and a porosity of 0.48%. The performed uniaxial compressive strength tests allowed estimation of the average UCS at 106.7 MPa, and the average $E$ modulus and $v$ ratio of 33.5 GPa and 0.21, respectively. Triaxial tests were also performed in several steps of confining pressure. The average measured cohesion factor was 15.2 MPa, whereas the angle of internal friction was 60.2°. The average measured velocities of the ultrasonic P- and S-waves amounted to 4336 and 2676 m/s, respectively, which resulted in the dynamic $Ed$ modulus of 44.9 GPa [60]. However, these tests were not being performed at the reservoir conditions. Ultrasonic velocities measured during acoustics in this interval were 5920 and 3290 m/s, respectively, for the P- and S-waves, which means that the values measured in situ are higher by 36.4 and 22.7%, respectively. The observed increases are consistent with the literature data cited by Kwon et al. [60]. For Troy granite, increases of 40% and 20% for P- and S-wave, respectively, occurred, while the pressure was increased from atmospheric to 40 MPa. These value compilations allow easy assessment of how much the mapping of reservoir conditions during laboratory tests has an influence on the wave velocities.

Several HF activities were performed on the Pohang site [58]. The first treatment occurred in 2016 in the PX-2 well, where 1970 $m^3$ of water was pumped. The maximum wellhead pressure was 89.2 MPa, while the maximum pumping capacity reached 2.8 $m^3$/min. The stimulation mechanism was interpreted as a combination of tensile fracture extension and hydraulic jacking. The second HF was performed in 2016 in the PX-1 well, where 3907 $m^3$ of water was pumped in a period of 14 days, with a maximum reservoir pressure of 27.7 MPa and a pumping rate of 1.1 $m^3$/min. As a result of the conducted work, the transmissivity of the rock surrounding the PX-1 well increased approximately 6.4 times. The stimulation mechanism was interpreted as hydraulic shearing with hydraulic jacking. The seismic monitoring recorded the maximum magnitude of the events of 1.7 and 2.2, after the shut-in stage, in the PX-2 and PX-1 wells, respectively. A good correlation between the amount of the injected liquid and the magnitude of the seismic event in both wells was observed. The observed seismic maxima occurred during periods of the large total volume of liquid injection [17]. In 2017, the second HF on the PX-2 well was carried out at a wellhead pressure of 90 MPa, during which the maximum magnitude of the recorded seismic events amounted to 3.1. Another treatment in the PX-1 well was performed in the same year in the form of a Cyclic Soft Stimulation (CSS), consisting of pumping the liquid alternately with low and high rates to reduce the risk of induced seismicity. Recorded seismic events during these works did not exceed a magnitude of 2.0 [61].

On 15 November 2017, an earthquake of a relatively large magnitude of 5.5 occurred in the Pohang area, which resulted in the discontinuation of the EGS Pohang program. Ellsworth et al. [62], based on modeling the pore pressure variability in rocks, suggest that the increase in the pressure may initiate local seismic events in fault zones, which may accumulate into larger seismic events. A number of aftershocks were recorded, while the largest one was on 11 February 2018 (4.8) [63].

### 3.7. FORGE Utah (USA)

The EGS project, led by the U.S. Department of Energy's Frontier Observatory for Geothermal Energy (FORGE), is located about 300 km southwest of Salt Lake City, Utah. In earlier years in this area, conventional geothermal energy was obtained (Blundell Thermal Power Station, UT, USA). The aim of the project, established in 2016, was to demonstrate that the EGS installation can be commercially used for large-scale energy production. The geothermal collectors of this area are Tertiary plutonic Mineral Mountain rocks, consisting of diorite, granodiorite, quartz monzonite, syenite and granite. The main minerals are plagioclase, K-feldspar and quartz, with a low content of biotite, hornblende and clay minerals [64]. The stress regime of this area is normal [65].

In 2017, a vertical borehole was completed (58–32), reaching 2290 m deep, where the temperature of 199 °C was recorded. In the interval of the crystalline rocks (1329 m in total), granite and quartz monzonite with low permeability mostly occurred. Microscanner images and televiewer logs confirmed that the $\sigma_H$ in this wellbore tends NNE-SSW. The $\sigma_h$ gradient is defined as 16.7–17.6 kPa/m and allows calculation of the magnitude of about 38–40 MPa in the productive interval. In the case of the $\sigma_V$, the gradient is defined as 25.6 kPa/m, which determines the magnitude of about 59 MPa at a depth of 2300 m [65]. In 2017 (directly after completion) and in 2019, an open hole interval was stimulated. Minifrac tests, DFIT, and step rate tests were carried out with a pumping rate of 1.43 $m^3$/min and pressure of about 27.6 MPa. Calcium carbonate (200 mesh) was also pumped to slightly prop the fractures taking fluid and enhancing the differentiation between fractures identified in pre- and post-FMI logs.

In 2019, a number of HFs were carried out in the open-hole part at the bottom of the well and in the two above perforated intervals. Tests were designed to determine the viability of stimulating fractures with different orientations behind the casing. The lower perforated zone was located in the region of critically stressed fractures, trending NNE parallel to $\sigma_H$, which means that these fractures would be the easiest to shear, dilate and propagate. The uppermost zone contained fractures oriented at a high angle to $\sigma_H$ (noncritically stressed). This zone was represented with the upper limits of the pressures required to stimulate the granitoid [65,66]. In the open hole section, the results were similar but slightly lower than those of the 2017 tests, suggesting the fracture system had developed some degree of permanence. The formation readily took fluid at modest injection rates of 2.38 $m^3$/min, which allows concluding that the hydraulic connection between the 58–32 well and the planned boreholes will be possible. The lower perforated zone was also successfully treaded. The fracturing pressure in the critically stressed area was 29 MPa, with a pumping rate of 0.8 $m^3$/min. The shallow, noncritically stressed zone was treated at the pressure of 45 MPa. During the treatments, a number of fracture closure pressure interpretations using various methods were also conducted.

The closure pressure increased with the pumping rate and the volume of the pumped water, which indicates the poroelastic effect and the presence of pre-existing natural fractures [66].

Project FORGE Utah is currently underway. Drilling a production borehole, accessed to the fracture network created in well 58–32 is planned, then loop test and build a power plant [67].

### 3.8. Qiabuqia (China)

The Qiabuqia geothermal site is located in the north-eastern part of the Qinghai–Tibetan Plateau. In the geological past, this area was uplifted several times, and igneous intrusion caused a local thermal anomaly to spread along the deep fault zones. The target HDR zone, below 3000 m, is built mainly from the Mid-Late Triassic Indonesian granite characterized by low porosity (2–5%) and very low permeability (0.2–0.7 mD). The overlying rocks are Neogene mudstones and Quaternary sandstones [68]. The Qinghai–Tibetan Plateau is under the tectonic influence of the Indian Ocean Plate and the Eurasian Plate. The focal mechanisms recorded in this area indicate that $\sigma_H$ in an NE 50–60° direction dominates (which is approximate to the direction of plate extrusion), whereas $\sigma_h$ is in an NW direction consistent with the expansion of the Gonghe basin. The stress regime in this area is strike-slip, turning into compressional in the southern part. The magnitude of $\sigma_V$ is based on computer modeling at 95–100 MPa and $\sigma_H$ at 85–92 MPa, while the magnitude of $\sigma_h$ at 68–72 MPa, at a depth of about 3700 m, was estimated [69]. The elastic parameters of the Qiabuqia granite were estimated as $E$—40–56 GPa and $\upsilon$—0.25–0.33 (-) [68].

The EGS project currently underway in this area involves a triplet system, including one injector and two producers. The target zone is drilled through four wells: GR1, GR2, DR3 and DR4. At the bottom of the deepest one (GR1, completed in 2017), a temperature of 236 °C at a depth of 3705 m was recorded.

The numerical simulations of fracturing operations in the GR1 well have been performed so far. Above the described stress magnitude, the mechanical properties of the rock as well as using of 50# crosslinked gel with HSP 20/40 mesh proppant were assumed. By increasing the fracture length, the width and fracture extension were observed during the increase in the pumping rate. The length of the fracture wing reached 600 m, whereas the height of about 100 m. The width, assuming the pumping rate of 6 $m^3$/min, exceeded 5 mm. An increase in the length of the wing and height was noted during pumping of up to 12,000 $m^3$ of fluid. Continuation pumping resulted in a further increase in the length, but at the same time, a significant decrease in the height. The highest proppant concentration and conductivity was achieved at the bottom of the fracture.

About 100 m in length of the fracture wing, at the farthest distance from the wellbore, has not been propped [68].

The modeling indicated that the tensile strength of the rock, as well as Young's modulus, had a significant effect on the fracture geometry, while porosity, permeability and Poisson's ratio had little effect. In the case of the slickwater-based stimulation scenario, low pumping rates of 0.5–3 $m^3$/min were proposed to avoid the use of high-power fracturing equipment, and total liquid volumes of 12,000 to 20,000 $m^3$ of slick to obtain the desired fracture network [69].

Based on the numerical simulations, a triplet system located at the line of the maximum horizontal stress (NE-SW) azimuth and separated from each other by about 300–500 m was designed. Forecasts of the thermal and energy efficiency for this system were also prepared [69].

Table 1. Selected geological, tectonic and fracturing data compilation from EGS sites.

| EGS Site, Activities Duration | Productive Layer Depth (m) | Temp. (°C) | Lithology, Stratigraphy | Stress Regime | Stress Magnitudes: $\sigma_V$, $\sigma_H$, $\sigma_h$ (MPa), Pore Pressure: $P_p$ (MPa) | Ultrasonic Velocities $V_P$, $V_S$ (Compressional, Shear Wave) (m/s), Elastic Parameters: Young's Modulus $E$ (GPa), Poisson's Ratio $\nu$ (-) | Fracturing Fluid | Estimated Fracture Dimensions: l—Half Length (m), h—Height (m), w—Width (mm) |
|---|---|---|---|---|---|---|---|---|
| Fenton Hill (USA) 1974–1995 | About 4400 [EE-2 well] [16] | 327 at 4390 m [16] | Core samples from EE-2 well: granodiorite, gneiss [31] | Strike-slip/normal [32] | Estimated gradients: $\sigma_V = \sigma_H$—25 MPa/km, $\sigma_h$—13–19 MPa/km, $P_P$—10 MPa/km [32] | 3-axial lab test, confining: 20 MPa EE-2 core, 3916 m depth: $E$—15–22, $\nu$—0.12–0.17. 4102 m depth: $E$—33, $\nu$—0.12–0.22 [31] | MHF—fresh water [32] | |
| Habanero Cooper Basin (Australia) 2003–2016 | About 4400 [33] | 248.5 [33] | Syenogranite, medium and coarse-grained [34] | Strike-slip (overlay); reverse, over-thrust (batholith target zone) [35] | At 4267 m $\sigma_V$—97.9 $\sigma_H$—150.9 $\sigma_h$—124.4 $P_P$—73.1 [35] | From modeling at 3657 m TVD: $E$—65, $\nu$—0.25 [36]. From logging at 3674 m (granite) $V_P$—5525 [44] | Mostly fresh water [33], water, NaCl- and NaBr-based brine [34] | |
| Rhine Graben EGS projects (Western Europe): Soultz-sous-Forêts, 90-present Landau, 2005/6-present Rittershoffen, 2013-present | Soultz 5200 [39] Landau 2200 [42] Ritters. 2200 [44] | Soultz about 200 [39] Landau about 160 [42] Ritters. about 170 [44] | Porphyric granites MFK, two-mica granites. Carboniferous [41] | Mixed, normal and strike-slip [44] | At 2200 m: $\sigma_V$—54.8 $\sigma_V$ > or < $\sigma_H$ $\sigma_h$—29.6 $P_P$—22.5; calculated, based on equations from [47] | Estimated E for pure granite at the target zone—up to 80 GPa, at the zones of increased hydraulic conductivity, and clay content may be significantly lower. [70] | Soultz—frac initiation: brine, then MHF—fresh water [42] Rittershoffen—MHF: water without proppant [5] | |
| GeneSys Hannower (Germany) 2005–2013 | 3834 [52] | 169 [52] | Low permeable Buntsandstein sediments, Permian [50,52] | Normal [52] | $\sigma_h$—72–83, $\sigma_h$ = 0.9 $S_V$ [52] | From lab tests and log, sandstones: $E$—45–65, $\nu$—0.19–0.22; clays: $E$—49, $\nu$—0.23 [52] | Fresh water [52] | l—1320 h—430 w—21 [52] |
| Groß Schönebeck (Germany), 2006-present | About 4100 [57] | 149 at 4285 m [54] | Clastic and volcanic rock (rhyolite, andesite) Rotliegend, Permian [2] | Normal—strike-slip $\sigma_s \geq 0.55\ \sigma_V$, $\sigma_H \leq 0.78$–$1.00\ \sigma_V$ [57]] | $\sigma_V$—100, $\sigma_H$—78–100, $\sigma_h$—55 [57] $P_P$—44.9 at 4220 m [54] | Volcanic rocks: $E$—55 $\nu$—0.20 Sediments: $E$—55 $\nu$—0.18 [20] | HTU linear gel, brine, Carbo-Lt 20/40; MHF—fresh water or with quartz sand 20/40 mesh, crosslinked gel with high strength 20/40 mesh [55] | l—32 h—72 w—1.6; MHF: l—160, h—96, w—5 [55] |

**Table 1.** *Cont.*

| EGS Site, Activities Duration | Productive Layer Depth (m) | Temp. (°C) | Lithology, Stratigraphy | Stress Regime | Stress Magnitudes: $\sigma_V$, $\sigma_H$, $\sigma_h$ (MPa), Pore Pressure: $P_p$ (MPa) | Ultrasonic Velocities $V_P$, $V_S$ (Compressional, Shear Wave) (m/s), Elastic Parameters: Young's Modulus $E$ (GPa), Poisson's Ratio $\nu$ (-) | Fracturing Fluid | Estimated Fracture Dimensions: l—Half Length (m), h—Height (m), w—Width (mm) |
|---|---|---|---|---|---|---|---|---|
| Pohang (South Korea) 2010–2017 | About 4200 [17] | 140 at 4209 m [17] | Laminated Granodiorite, Permian [17] | Strike-slip / reverse [58] Strike-slip [71] | $\sigma_V$—107, $\sigma_H$—133–153, $\sigma_h$—98–119 [58] $\sigma_V$—110, $\sigma_H$—115–138, $\sigma_h$—81–105 [71] | $V_P$—4336, $V_S$—2676 $E_d$—44.9 (laboratory tests, atmospheric conditions); $V_P$—5920, $V_S$—3290 (sonic logging) [60] | Fresh water [17] | |
| FORGE Utah (USA) 2016–present | about 2300 [65] | 199 [65] | Tertiary granites, quartz monzonites, monzonites [65,66] | Normal [65] | Based on gradients [65], at a depth of 2290 m: $\sigma_h$—38–40, $\sigma_V$ -59. | Granite sample from 52-21 well, 3-axial test, confining pressure 55 MPa: E -73.7, $\nu$—0.22 [72] | | |
| Qiabuqia (China) 2016/17-present | about 3700 [68] | 236 [68,73] | Middle triassic granite, Anisian [73] | Normal [69] | Based on modeling at 3700 m $\sigma_V$—95–100 $\sigma_H$—85–92, $\sigma_h$—68–72 [69] | $E$—40–56 $\nu$—0.25–0.33 [68] $E$—42 $\nu$—0.23 [69] | For modeling was assumed: #50 crosslinked gel with HSP 20/40 proppant [68] | l—up to 600 h—about 100 w—5 [68] |
| Poland (prospective EGS areas): Karkonosze Mountains, Gorzów Block, Mogilno-Łódź Trough, Szczecin Trough Upper Silesian Block | about 4000 about 4300 about 5700 [2] about 5000 [74] about 5000 [74] | 165 153 175 [2] above 150 [74] 170 [74] | Upper Carboniferous granite, Lower Permian volcanic rocks Low-permeable Triassic sediments [2] Permian or Carboniferous sediments [74] Carboniferous sediments [74] | Western Poland—normal with strike-slip component [75,76] Upper Silesian Block—strike-slip [77] | $\sigma_V$: Karkonosze Mount.—96; Gorzów Block—103; Mogilno-Łódź Trough—120–153; Szczecin Trough—120; Upper Silesian Block—120. Based on assumed average rock density from [78] | | Fracturing operations at this site have not been performed yet | Fracturing operations at this site have not been performed yet |

## 4. EGS Prospects in Poland

In recent years, the interest in obtaining energy from EGS collectors in Poland has increased. The restrictive EU regulations on greenhouse gas emissions and the desire to reduce the share of fossil fuels in the national energy balance encourage the search for new ways of obtaining green energy, including energy from deep geothermal sources. The success of Western European EGS projects sparked a discussion on the profitability of EGS installations in Polish conditions [74,79–81].

Thus far, a preliminary research project was carried out to assess the thermal balance potential of prospective geological structures for the needs of EGS systems in HDR rocks in Poland [2]. The project involved the study of Polish rock structures under three different geological conditions: massifs of crystalline rocks, volcanic rocks under the sedimentary cover and sedimentary basins. The key element of the location selection was the analysis of the Earth's crust temperature on the basis of maps of the Earth's heat flux density distribution in Poland. A series of field geological and geophysical surveys, laboratory tests of rock samples and numerical simulations allow for the determination of several perspective areas [2,82].

Relatively extensive massifs of igneous rocks, useful for EGS technology, are found in the south of Poland (Sudetes and the Fore-Sudetic Block). The most promising area is the granitoid pluton of the Karkonosze Mountains (part of the Sudetes), which is characterized by a geothermal gradient of about 4 °C/100 m, with a temperature of up to 16 °C at a depth of 4.0 km below the ground level (Figure 6). The target zone for stimulation is set up there at a depth of less than 4000 m and a temperature of about 165 °C. $\sigma_V$ in this zone, assuming an average rock density of 2.4 g/cm$^3$ [78], is about 96 MPa in the presumably normal stress regime [75,76].

The Gorzów block is a structure particularly significant in the context of the use of unconventional geothermal resources of volcanic rock. The Permian trachyandesites of the Gorzów Block, located at a depth of below 4300 m, are characterized by large thickness, increased temperatures on a regional scale and contain gas bubbles, which provides good prospects for fracturing. This location shows a significant analogy to the Groß Schönebeck reservoir near Berlin, where the geothermal gradient is 3.5–4.0 °C/100 m, and the temperature reaches approximately 150 °C at a depth of 4.3 km [2,81]. The deposition depth allows to calculate $\sigma_V$ of about 103 MPa.

The largest thicknesses of sedimentary rocks are typical for the central part of the Polish Basin (9–12 km) and the Carpathians (up to approx. 20 km). Due to the complicated geological structure and strong tectonic involvement of the Carpathians [83], this area does not have much potential for the EGS. However, within the Carpathian Foredeep, in the central part of the Upper Silesian Block, an area with increased values of the Earth's heat flux was identified.

The intense heat flux is typical for the Variscan fold belt and in the northern zone of the Lower Silesian internodes, where the heat flow values exceeded 107 mW/m$^2$. The Upper Paleozoic, Devonian and Carboniferous formations lie on the Precambrian and Lower Paleozoic sediments in the form of a continuous cover. The lower part of the Carboniferous profile includes carbonates and clastic, flysch and molasse sediments, forming the Upper Silesian Coal Basin. The thickness of carbonates ranges from 200 to 1500 m, while the thickness of the clastic deposits of Carboniferous, which are a potential petrogeothermal reservoir rock, reaches over 5000 m [84]. At considerable depths, the hydraulic conductivity of Carboniferous sandstones is less than 10–8 m/s [85].

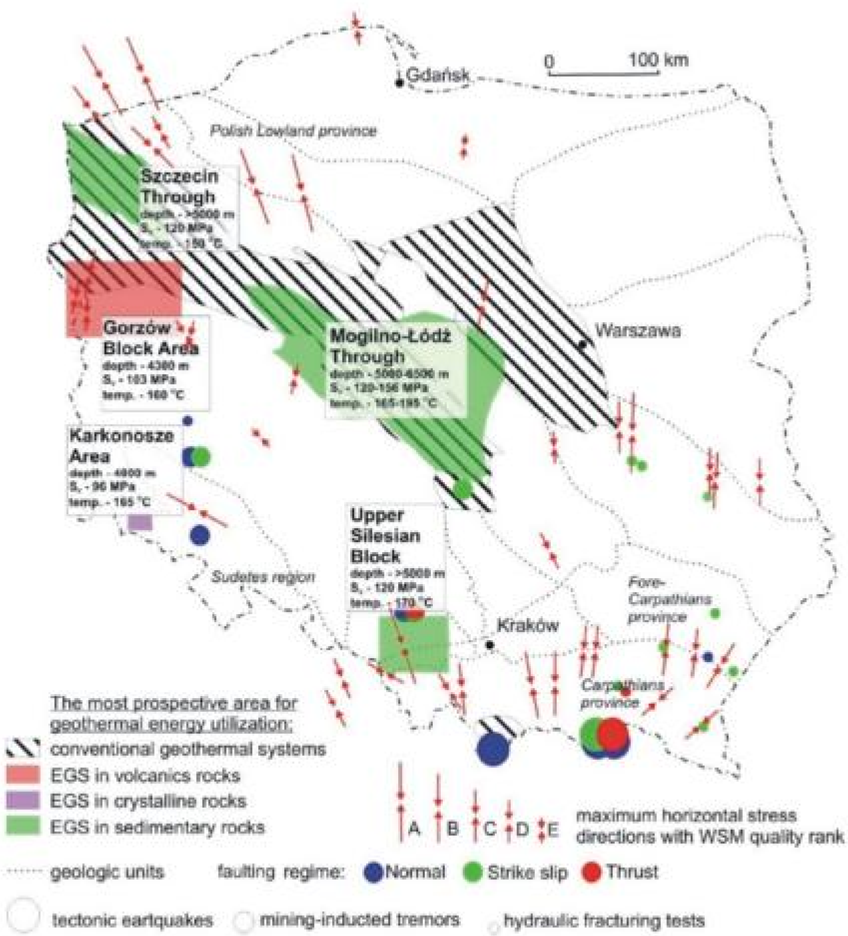


**Figure 6.** Prospective areas for geothermal energy utilization in enhanced geothermal systems in Poland. Explanation: $\sigma_V$ was calculated for given depth, based on average density of overlying rocks—2.4 g/cm$^3$ from [78]. Prospective areas were marked based on data from [74]. Horizontal stress directions and faulting regime were compiled from [75–77,86].

Two areas with potential for EGS were identified in the Polish Lowlands: the Szczecin Trough and the Mogilno-Łódź Trough. The Szczecin Trough is a strongly elongated fold element covering the Zechstein–Mesozoic complex, with a general direction along the NW-SE axis. This form was influenced by the block tectonics of the older basement and the salt tectonics, mobilizing Zechstein salts [87]. Along this structure, a zone of intense halokinetic phenomena occurs. In the area of the Szczecin Trough, which is relatively poorly geologically recognized, the EGS prospects relate to the Permian or Carboniferous sediments at depths above 5000 m below sea level, with temperatures above 150 °C. The deposition depth allows the calculation of vertical principal stress of about 120 MPa. The Mogilno-Łódź Trough is a fragment of a higher-order structure—the Szczecin–Mogilno–Łódź–Miechów Trough, stretching from the northwest to the southeast of Poland.

Potential petrogeothermal reservoirs in this area are Lower Triassic rocks, represented by Buntsandstein sediments deposited at a depth of about 5700 m and developed as a complex of claystone and siltstones with limestone and sandstone beds. The compact sandstones of the Lower Buntsandstein are considered potential deposits for the EGS, especially since their thickness locally exceeds 1500 m. The Middle Triassic (Muschelkalk) formations, formed as limestones and marls, are characterized by a much lower thickness, up to 300 m. The Upper Triassic, with a thickness of up to 2400 m, is represented by clastic and evaporative sediments of Keuper and clayey sandstone deposits of the Rhaetian. The most promising structure for EGS in Poland is the Mogilno–Łódź Trough, while the Upper Silesian Block seems to be a promising location for the future [74].

The legal issues related to the HF implementation in Poland are regulated at European Union and national level. Minimum principles for the exploration and production using HF technology were established in UE Commission recommendations from 22 January 2014 [88]. However, these recommendations concern only hydrocarbons extraction, in terms of high-volume HF (injecting 1000 $m^3$ or more of water per fracturing stage or 10,000 $m^3$ or more of water during the entire fracturing process into a well), whereas fracturing regulations in terms of geothermal resources have not been developed so far. In Poland, there are no internal prohibitions for HF operations; thus, EU Commission recommendations are valid. Assuming that high-volume fracking in HDR would be treated the same as fracking for hydrocarbon extraction, a strategic environmental assessment may be required before granting licenses for exploration or production to prevent, manage and reduce the impacts on and risks for human health and the environment.

Stimulation of HDR horizons and the design of fracturing operations to create a geothermal collector have not been carried out in Poland so far. Nevertheless, the extensive experience was gained in hydraulic and chemical stimulation operations, based on fracturing in unconventional deposits and matrix acidizing [15,89]. Research works were also carried out in the field of the design, environmental impact and performance of energized fluids for fracturing [90]; the embedment phenomena [24,25]; and the dynamic elastic parameters of the various types of rocks [27,30]. Their results may be useful in the implementation of a prospective Polish HDR geothermal collector program.

## 5. Conclusions

In this paper, 10 hydraulically stimulated world's enhanced geothermal systems (EGS) were reviewed. The focus of the review concerned geological, geophysical as well as stimulation parameters.

The target zones in most EGS sites are usually crystalline rocks, i.e., granite or granodiorites, characterized by low permeability and porosity (e.g., Habanero, Pohang, Forge Utah EGS projects). However, in some projects, a geothermal collector is created in mixed, crystalline and low permeable clastic rock, e.g., Groß Schönebeck and GeneSys Hannover EGS projects. These rocks are generally deposited at a depth of 2000–5000 m, whereas the localizations are chosen mostly due to the high geothermal gradient caused by local temperature anomalies near-vertical faults and fractures, connecting the sedimentary cover and crystalline basement, constituting heat-conductive areas. Target zone temperatures are typically between 150 to over 300 °C, which determines the flow rate directly in the heat exchanger and the efficiency of the powerplant. Tectonic field conditions are not the main criterion for selecting an EGS location.

Many of the locations are characterized by normal or strike-slip faulting regimes, while several projects were located in the areas of reverse/overthrust faulting regime (e.g., Habanero, Australia, Fjällbacka, Sweden). The faulting regime directly affects the direction of fracture propagation. It seems that the best conditions for fracturing in EGS are in the reverse regime due to the preferred horizontal fractures capable of connecting vertical boreholes in this area. However, European EGS projects in normal strike-slip faulting regime areas (preferred vertical fracture propagation) were also successful (e.g., Soultz, France, Landau, Germany). The P-wave velocities in crystalline rocks are usually in the range of about 4400–5500 m/s; thus, they are higher than the velocities in typical clastic rocks. Elastic parameters of the crystal base rocks reported in the literature are varied depending on the measurement method. It can be stated that Young's modulus and Poisson's ratio of crystalline rocks from measurements in reservoir conditions are in the range of about 45–75 GPa and 0.12–0.25 (-), respectively.

The range of pressure and pumping rates in hydraulic fracturing (HF) treatments are varied depending on the needs. The amount of water injected into the well is varied from a few thousand up to more than 10,000 $m^3$ (Massive Hydraulic Fracturing operation) during the entire fracturing process. Fresh water without chemical additives in the main fracking stages is commonly used; however, linear as well as crosslinked gels are also applied (i.e., Groß Schönebeck project). In some cases, a 20/40 mesh quartz sand or high-strength proppant is also used. The obtained fracture dimensions depend on the pumping rate, pressure and total pumped liquid volume. The half-length and height of the fracture may reach more than several hundred meters, whereas width may exceed several centimeters, which determines the distance between bottoms of the boreholes.

HF operations usually cause seismic events recorded by installed seismic monitoring. The most common are low-magnitude events, imperceptible to people; however, there are also large ones, i.e., in Pohang, Korea, in 2017. The liquid pumped under pressure during the HF operation may facilitate skidding on the stressed local fault surfaces, which in unfavorable conditions may generate seismic events; however, shocks with a relatively high magnitude are rare.

The success of the Western European EGS projects caused a discussion on the profitability of the EGS-type installation in Polish conditions. The preliminary research project has been carried out so far to assess the thermal balance potential of prospective geological structures for the needs of EGS systems in HDR rocks in Poland. Based on the set of the Earth's heat flux density distribution data in Poland, several main prospective areas were finally selected. The most promising formations are the crystalline basement of Karkonosze Mountains, volcanic rocks of Gorzów Block and sedimentary deposits of the Szczecin Trough, the Mogilno-Łódź Trough and the Upper Silesian Block.

**Author Contributions:** Conceptualization, literature review, investigation, manuscript writing, visualization, R.M.; supervision, literature review, investigation, manuscript editing, manuscript review, K.L.; supervision, manuscript editing, manuscript review, founding acquisition, P.K. All authors have read and agreed to the published version of the manuscript.

**Funding:** This paper is based on the research carried out in the Oil and Gas Institute - National Research Institute (Poland), financed by Ministry of Education and Science of Poland. DK-4100-18/21.

**Institutional Review Board Statement:** Not applicable.

**Informed Consent Statement:** Not applicable.

**Data Availability Statement:** The data presented in this study are available on request from the corresponding author.

**Conflicts of Interest:** The authors declare no conflict of interest.

## Nomenclature

| | |
|---|---|
| HF | Hydraulic fracturing |
| MHF | Massive hydraulic fracturing |
| EGS | Enhanced geothermal systems |
| HDR | Hot dry rock |
| $\sigma_V$ | Principal vertical stress (MPa) |
| $\sigma_H$ | Maximum horizontal stress (MPa) |
| $\sigma_h$ | Minimum horizontal stress (MPa) |
| $P_p$ | Pore pressure (MPa) |
| $V_P$ | Compressional wave velocity (m/s) |
| $V_S$ | Shear wave velocity (m/s) |
| $E$ | Young's modulus (GPa) |
| $v$ | Poisson's ratio (dimensionless) |

## References

1. Lu, S.-M. A global review of enhanced geothermal system (EGS). *Renew. Sustain. Energy Rev.* **2018**, *81*, 2902–2921. [CrossRef]
2. Wójcicki, A.; Sowiżdżał, A.; Bujakowski, W. *Ocena Potencjału Bilansu Cieplnego i Perspektywicznych Struktur Geologicznych dla Potrzeb Zamkniętych Systemów Geotermicznych (Hot Dry Rocks) w Polsce*; Ministerstwo Środowiska: Warsaw, Poland, 2013. (In Polish)
3. Zhang, H.; Wan, Z.; Elsworth, D. Failure behavior of hot-dry-rock (HDR) in enhanced geothermal systems: Macro to micro scale effects. *Geofluids* **2020**, *2020*, 8878179. [CrossRef]
4. McClure, M.; Horne, R. An investigations of stimulation mechanisms in enhanced geothermal systems. *Int. J. Rock Mech. Min. Sci.* **2014**, *72*, 242–260. [CrossRef]
5. Vidal, J.; Genter, A.; Schmittbuhl, J. Pre- and post-stimulation characterization of geothermal well GRT-1, Rittershoffen, France: Insights from acoustic image logs of hard fractured rock. *Geophys. J. Int.* **2007**, *206*, 845–860. [CrossRef]
6. Economides, M.; Martin, T. *Modern Fracturing Enhancing Natural Gas Production*; ET Publishing: Houston, TX, USA, 2007.
7. Brown, D.; Duchane, D.; Heiken, G.; Hriscu, V. *Mining the Earth's Heat: Hot Dry Rock Geothermal Energy*; Springer: Berlin/Heidelberg, Germany, 2012.
8. Hills, R.; Hand, M.; Mildren, S.; Morton, J.; Reid, P.; Reynolds, S. Hot dry rock geothermal exploration in Australia, application of the in situ stress field to hot dry rock geothermal energy in the Cooper Basin. In Proceedings of the PESA Eastern Australian Basins Symposium II, Adelaide, Australia, 19–22 September 2004.
9. Schellschmidt, R.; Schultz, R.; Pester, S. Geothermal energy in Germany. In Proceedings of the World Geothermal Congress, Bali, Indonesia, 25–29 April 2010.
10. Huenges, E. *Geothermal Energy Systems: Exploration, Development and Utilization*; Wiley-VCH: Weinheim, Germany, 2010.
11. King, G. Thirty years of gas shale fracturing: What we have learned? In Proceedings of the SPE Annual Technical Conference and Exhibition, Florence, Italy, 20–22 September 2010. [CrossRef]
12. Gandossi, L. *An Overview of Hydraulic Fracturing and Other Formation Stimulation Technologies for Shale Gas Production*; JRC Technical Reports; Publications Office of the European Union: Luxembourg, 2013. [CrossRef]
13. Yildizdag, K.; Weber, F.; Konietzky, H. Hydraulic Fracturing. Available online: https://tu-freiberg.de/sites/default/files/media/professur-felsmechanik-32204/E-book/15_hydraulic_fracturing_0.pdf (accessed on 2 February 2021).
14. Rafiee, M.; Soliman, M.; Pirayesh, E.; Meybodi, H. Geomechanical considerations in hydraulic fracturing designs. In Proceedings of the SPE Canadian Unconventional Resources Conference, Calgary, AB, Canada, 30 October–1 November 2012. [CrossRef]
15. Kasza, P. Hydraulic fracturing in unconventional reservoirs and methods of their analysis. *Prace INiG-PIB* **2019**, *226*. (In Polish with English Abstract). [CrossRef]
16. Tester, J.; Anderson, B.; Batchelor, A.; Blackwell, D.; DiPippo, R.; Drake, M.; Garnish, J.; Livesay, B.; Moore, M.; Nichols, K.; et al. *The Future of Geothermal Energy—Impact of Enhanced Geothermal Systems (EGS) on the United States in the 21st Century*; Massachusetts Institute of Technology: Cambridge, MA, USA; Idaho National Laboratory: Idaho Falls, ID, USA, 2006.
17. Park, S.; Kim, K.-I.; Xie, L.; Yoo, H.; Min, K.-B.; Kim, M.; Yoon, B.; Kim, K.Y.; Zimmermann, G.; Guinot, F.; et al. Observations and analyses of the first two hydraulic stimulations in the Pohang geothermal development site, South Korea. *Geothermics* **2020**, *88*, 101905. [CrossRef]
18. Legarth, B.; Huenges, E.; Zimmermann, G. Hydraulic fracturing in a sedimentary geothermal reservoir: Results and implications. *Int. J. Rock Mech. Min. Sci.* **2005**, *42*, 1028–1041. [CrossRef]
19. Zoback, M. *Reservoir Geomechanics*; Cambrige University Press: Cambrige, UK, 2007. [CrossRef]
20. Zimmermann, G.; Moeck, I.; Blöcher, G. Cyclic waterfrac stimulation to develop an enhanced geothermal system (EGS): Conceptual design and experimental results. *Geothermics* **2010**, *39*, 59–69. [CrossRef]
21. Zimmermann, G.; Blöcher, G.; Reinicke, A.; Brandt, W. Rock specific hydraulic fracturing and matrix acidizing to enhance a geothermal system—Concepts and field results. *Tectonophysics* **2011**, *503*, 146–154. [CrossRef]
22. Rickman, R.; Mullen, M.; Petre, E.; Grieser, B.; Kundert, D. A Practical use of shale petrophysics for stimulation designing optimalization: All shale plays are not clones of the Barnett Shale. In Proceedings of the SPE Annual Technical Conference and Exhibition, Denver, CO, USA, 21–24 September 2008. [CrossRef]
23. Masłowski, M.; Biały, E. Studies of the embedment phenomenon in stimulation treatments. *Nafta-Gaz* **2016**, *12*, 1101–1106. [CrossRef]
24. Masłowski, M.; Kasza, P.; Czupski, M.; Wilk, K.; Moska, R. Studies of fracture damage caused by the proppant embedment phenomenon in shale rock. *Appl. Sci.* **2019**, *9*, 2190. [CrossRef]
25. Masłowski, M.; Labus, M. Preliminary studies on the proppant embedment in Baltic Basin shale rock. *Rock Mech. Rock Eng.* **2021**, *54*, 2233–2248. [CrossRef]
26. Grieser, W.; Bray, J. Identification of production potential in unconventional reservoirs. In Proceedings of the Production and Operations Symposium, Oklahoma City, OK, USA, 1–3 April 2007. [CrossRef]
27. Moska, R.; Kasza, P.; Masłowski, M. Rock anisotropy and brittleness from laboratory ultrasonic measurements in the service of hydraulic fracturing. *Acta Geodyn. Geomater.* **2018**, *15*, 1. [CrossRef]
28. Moska, R.; Masłowski, M. Attempts to determine the geomechanical and Thomsen's anisotropy parameters of coal from Upper Silesian Coal Basin area. *Nafta-Gaz* **2019**, *11*, 700–707. [CrossRef]
29. Wu, H.; Zhang, P.; Dong, S.; Huang, Y.; Zhang, M. Brittleness index analysis of coal samples. *Acta Geophys.* **2019**, *67*, 789–797. [CrossRef]

30. Moska, R. Brittleness index of coal from the Upper Silesian Coal Basin. *Acta Geodyn. Geomater.* **2021**, *18*, 91–101. [CrossRef]
31. Duffield, R.; Nunz, G.; Smith, M.; Wilson, M. *Hot Dry Rock Geothermal Energy Development Program Annual Report, Fiscal Year 1980*; Los Alamos National Lab: Santa Fe, NM, USA, 1980.
32. Norbeck, J.; McClure, M.; Horne, R. Field observations at the Fenton Hill enhanced geothermal system test site support mixed-mechanism stimulation. *Geothermics* **2018**, *74*, 135–149. [CrossRef]
33. Wyborn, D.; da Graaf, L.; Davidson, S.; Hann, S. Development of Australia's first hot fractured rock (HFR) underground heat exchanger, Cooper Basin, South Australia. In Proceedings of the World Geothermal Congress, Antalya, Turkey, 24–29 April 2005.
34. Holl, H.-G. *What Did We Learn about EGS in the Cooper Basin?* Geodynamics Limited Technical Report; Geodynamics Limited: Milton, Australia, 2015. [CrossRef]
35. Holl, H.-G.; Barton, C. Habanero Field—Structure and state of stress. In Proceedings of the World Geothermal Congress, Melbourne, Australia, 19–25 April 2015.
36. Barton, C.; Moos, D.; Hartley, L.; Baxter, S.; Foulquier, L.; Holl, H.; Hogarth, R. Geomechanically coupled simulation of flow in fractured reservoirs. In Proceedings of the 38th Workshop on Geothermal Reservoir Engineering, Stanford, CA, USA, 11–13 February 2013.
37. Hogarth, R.; Holl, H.-G. Lessons learned from the habanero EGS project. In Proceedings of the Transactions—Geothermal Resources Council, Salt Lake City, UT, USA, 2–4 October 2017.
38. Australian Broadcast Corporation News. Available online: https://www.abc.net.au/news/2016-08-30/geothermal-power-plant-closes-deemed-not-financially-viable/7798962 (accessed on 4 May 2021).
39. Vidal, J.; Genter, A. Overview of naturally permeable fractured reservoirs in the central and southern Upper Rhine Graben: Insights from geothermal wells. *Geothermics* **2018**, *74*, 57–73. [CrossRef]
40. Cuenot, N.; Charlety, J.; Dorbath, L.; Hasser, H. Faulting mechanisms and stress tensor at the European HDR site of Soultz-Sous-Forêts. In Proceedings of the Thirtieth Workshop on Geothermal Reservoir Engineering, Stanford, CA, USA, 31 January–2 February 2005.
41. Schindler, M.; Nami, P.; Schellschmidt, R.; Teza, D.; Tischner, T. Summary of hydraulic stimulation operations in the 5 km deep crystalline HDR/EGS reservoir at Soults-sous-Forets. In Proceedings of the 33th Workshop on Geothermal Reservoir Engineering, Stanford, CA, USA, 28–30 January 2008.
42. Schindler, M.; Baumgärtner, J.; Gandy, T.; Hauffe, P.; Hettkamp, T.; Menzel, H.; Penzkofer, P.; Teza, D.; Tischner, T.; Wahl, G. Successful hydraulic stimulation techniques for electric power production in the Upper Rhine Graben, Central Europe. In Proceedings of the World Geothermal Congress, Bali, Indonesia, 25–29 April 2010.
43. BESTEC GmbH. Available online: https://www.bestec-for-nature.com/index.php/projects-en (accessed on 19 March 2021).
44. Baujard, C.; Genter, A.; Dalmais, E.; Maurer, V.; Hehn, R.; Rosillette, R.; Vidal, J.; Schmittbuhl, J. Hydrothermal characterization of wells GRT-1 and GRT-2 in Rittershoffen, France: Implications on the understanding of natural flow systems in the Rhine graben. *Geothermics* **2017**, *65*, 255–268. [CrossRef]
45. Baujard, C.; Genter, A.; Maurer, V.; Dalmais, E.; Graff, J.-J.; Schmittbuhl, J. The ECOGI EGS Project in Rittershoffen, France. *GRC Transactions* **2014**, *38*, 267–270.
46. Maurer, V.; Baujard, C.; Gaucher, E.; Grunberg, M.; Wodling, H.; Lehujeur, M.; Vergne, J.; Lengline, O.; Schmittbuhl, J. Seismic monitoring of the Rittershoffen project (Alsace, France). In Proceedings of the 2nd European Geothermal Workshop, Strasbourg, France, 24–25 October 2013.
47. Lengline, O.; Boubacar, M.; Schmittbuhl, J. Seismicity related to the hydraulic stimulation of GRT1, Rittershoffen, France. *Geophys. J. Int.* **2017**, *208*, 1704–1715. [CrossRef]
48. ES Geotermie. Available online: https://geothermie.es.fr/en/ (accessed on 13 July 2021).
49. Ladner, F.; Häring, M. Hydraulic characteristics of the Basel-1 enhanced geothermal system. *GRC Trans.* **2009**, *33*, 199–204.
50. Orzol, J.; Jung, R.; Jatho, R.; Tischner, T.; Kehrer, P. The GeneSys-Project: Extraction of geothermal heat from tight sediments. In Proceedings of the World Geothermal Congress, Antalya, Turkey, 24–29 April 2005.
51. Tischner, T.; Evers, H.; Hauswirth, H.; Jatho, R.; Kosinowski, M.; Sulzbacher, H. New concepts for extracting geothermal energy from one well: The GeneSys project. In Proceedings of the World Geothermal Congress, Bali, Indonesia, 25–29 April 2010.
52. Tischner, T.; Krug, S.; Pechan, E.; Hesshaus, A.; Jatho, R.; Bischoff, M.; Wonik, T. Massive hydraulic fracturing in low permable sedimentary rock in the Genesys project. In Proceedings of the 38th Workshop on Geothermal Reservoir Engineering, Stanford, CA, USA, 11–13 February 2013.
53. Holl, H.-G.; Moeck, I.; Schandelmeier, H. Characterisation of the tectono-sedimentary evolution of a geothermal reservoir—Implications for exploitation (southern permian basin, NE Germany). In Proceedings of the Word Geothermal Congress 2005, Antalya, Turkey, 24–29 April 2005.
54. Huenges, E.; Holl, H.-G.; Bruhn, D.; Brandt, W.; Saadat, A.; Moeck, I.; Zimmermann, G. Current state of the EGS project Groß Schönebeck—Drilling into the deep sedimentary geothermal reservoir. In Proceedings of the European Geothermal Congress 2007, Unterhaching, Germany, 30 May–1 June 2007.
55. Blöcher, G.; Reinsch, T.; Henninges, J.; Milsch, H.; Regensprug, S.; Kummerow, J.; Francke, H.; Kranz, S.; Saadat, A.; Zimmermann, G.; et al. Hydraulic history and current state of the deep geothermal reservoir Groß Schönebeck. *Geothermics* **2015**, *63*, 27–43. [CrossRef]

56. Hassanzadegan, A.; Blöcher, G.; Zimmermann, G.; Milsch, H.; Moeck, I. Induced stress in a geothermal doublet system. In Proceedings of the Thirty-Sixth Workshop on Geothermal Reservoir Engineering, Stanford, CA, USA, 31 January–2 February 2011.
57. Moeck, I.; Holl, H.-G. The stress regime in Rotliegend reservoir of the Northeast German Basin. *Int. J. Earth Sci.* **2009**, *98*, 1643–1657. [CrossRef]
58. Farkas, M.P.; Hofman, H.; Zimmermann, G.; Zang, A.; Bethmann, F.; Cottrell, M.; Josephson, N. Hydromechanical analysis of the second hydraulic stimulation in well PX-1. *Geothermics* **2021**, *89*, 101990. [CrossRef]
59. Lee, T.J.; Song, Y. Lesson learned from low-temperature geothermal development in Pohang, Korea. In Proceedings of the 8th Asian Geothermal Symposium, Hanoi, Vietnam, 9–10 December 2008.
60. Kwon, S.; Xie, L.; Park, S.; Kim, K.-I.; Min, K.-B.; Kim, K.Y.; Zhuang, L.; Choi, J.; Kim, H.; Lee, T.J. Characterization of 4.2-km-deep fractured granodiorite cores from Pohang geothermal reservoir, Korea. *Rock Mech. Rock Eng.* **2019**, *52*, 771–782. [CrossRef]
61. Hofmann, H.; Zimmermann, G.; Farkas, M.; Huegenes, E.; Zang, A.; Leonhardt, M.; Kwiatek, G.; Martinez-Garzon, P.; Bonhoff, M.; Min, K.-B.; et al. First field application of cyclic soft stimulation at the Pohang Enhanced Geothermal System site in Korea. *Geophys. J. Int.* **2019**, *217*, 926–949. [CrossRef]
62. Ellsworth, W.L.; Giardini, D.; Townend, J.; Ge, S.; Shimamoto, T. Triggering of the Pohang, Korea, earthquake (Mw 5.5) by enhanced geothermal system stimulation. *Seismol. Res. Lett.* **2019**, *90*, 1844–1858. [CrossRef]
63. Ree, J.-H.; Kim, K.-H.; Lim, H.; Seo, W.; Kim, S.; An, X.; Kim, Y. Fault reactivation and propagation during the 2017 Pohang earthquake sequence. *Geothermics* **2021**, *92*, 102048. [CrossRef]
64. Jones, C.; Moore, J.; Simmons, S. Lithology and Mineralogy of the Utah FORGE EGS Reservoir: Beaver County, Utah. *GRC Trans.* **2018**, *42*. Available online: https://publications.mygeoenergynow.org/grc/1034039.pdf (accessed on 1 September 2021).
65. Moore, J.; McLennan, J.; Pankow, K.; Simmons, S.; Podgorney, R.; Wannamaker, P.; Jones, C.; Rickard, W.; Xing, P. The Utah Frontier Observatory for Research in Geothermal Energy (FORGE): A Laboratory for characterizing, creating and sustaining enhanced geothermal systems. In Proceedings of the 45th Workshop on Geothermal Reservoir Engineering, Stanford, CA, USA, 10–12 February 2020.
66. Xing, P.; McLennan, J.; Moore, J. In-situ stress measurements at the Utah Frontier Observatory for Research in Geothermal Energy (FORGE) site. *Energies* **2020**, *13*, 5842. [CrossRef]
67. US Departament of Energy. Available online: https://www.energy.gov/eere/forge/enhanced-geothermal-systems (accessed on 23 March 2021).
68. Lei, Z.; Zhang, Y.; Yu, Z.; Hu, Z.; Li, L.; Zhang, S.; Fu, L.; Zhou, L.; Xie, Y. Exploratory research into the enhanced geothermal system power generation project: The Qiabuqia geothermal field, Northwest China. *Renew. Energy* **2019**, *139*, 52–70. [CrossRef]
69. Lei, Z.; Zhang, Y.; Zhang, S.; Fu, L.; Hu, Z.; Yu, Z.; Li, L.; Zhou, J. Electricity generation from a three-horizontal-well enhanced geothermal system in the Qiabuqia geothermal field, China: Slickwater fracturing treatments for different reservoir scenarios. *Renew. Energy* **2020**, *145*, 65–83. [CrossRef]
70. Meller, C.; Ledesert, B. Is there a link between mineralogy, petrophysics, and the hydraulic and seismic behaviors of the Soultz-sous-Forêts granite during stimulation? A review and reinterpretation of petro-hydromechanical data toward a better understanding of induced seismicity and fluid flow. *J. Geophys. Res. Solid Earth* **2017**, *112*, 9755–9774. [CrossRef]
71. Park, S.; Xie, L.; Kim, K.-I.; Kwon, S.; Min, K.-B.; Choi, J.; Yoon, W.-S.; Song, Y. First hydraulic stimulation in fractured geothermal reservoir in Pohang PX-2 well. *Procedia Eng.* **2017**, *191*, 829–837. [CrossRef]
72. US Departament of Energy. Enhanced Geothermal System Testing and Development at the Milford, Utah FORGE Site. 2016. Available online: https://www.energy.gov/sites/prod/files/2016/09/f33/Conceptual_Geologic_Model_FORGE_Milford_UT.pdf (accessed on 23 March 2021).
73. Feng, J.; Zhang, Y.; Luo, J. Geology of hot dry rocks in Gonghe Basin of Qinghai-Tibet Plateau. In Proceedings of the 54th U.S. Rock Mechanics/Geomechanics Symposium, Golden, CO, USA, 28 June–1 July 2020. ARMA-2020-0011.
74. Sowiżdżał, A.; Gładysz, P.; Pająk, L. Sustainable use of petrothermal resources—A review of the geological conditions in Poland. *Resources* **2021**, *10*, 8. [CrossRef]
75. Jarosiński, M. Recent tectonic stress field investigations in Poland: A state of the art. *Geol. Quaterly* **2005**, *50*, 303–321.
76. Zuchiewicz, W.; Badura, J.; Jarosiński, M. Neotectonics of Poland: Selected examples. *Biul. Państwowego Inst. Geol.* **2007**, *425*, 105–128, (In Polish with English Abstract).
77. Jarosiński, M. Rozwarstwienie współczesnego pola naprężeń w zachodniej części polskich Karpat Zewnętrznych. *Przegląd Geol.* **1997**, *45*, 768–776. (In Polish)
78. Jarosiński, M. Współczesny reżim tektoniczny w Polsce na podstawie analizy testów szczelinowania hydraulicznego ścian otworów wiertniczych. *Przegląd Geol.* **2005**, *53*, 863–872. (In Polish)
79. Sapińska-Śliwa, A.; Kowalski, T.; Knez, D.; Śliwa, T.; Gonet, A.; Bieda, A. Geological and drilling aspects of construction and exploitation geothermal systems HDR/EGS. *AHG Drill. Oil Gas* **2015**, *31*, 49–62. [CrossRef]
80. Niezgoda, T.; Miedzińska, D.; Sławiński, G. Energia z głębokich pokładów gorących suchych skał (HDR). *Inżynieria Bezpieczeństwa Obiektów Antropog.* **2018**, *3–4*, 65–69. (In Polish)
81. Sowiżdżał, A. Geothermal energy resources in Poland—Overview of the current state of knowledge. *Renew. Sustain. Energy Rev.* **2018**, *82*, 4020–4027. [CrossRef]

82. Sowiżdżał, A.; Górecki, W.; Hajto, M. Geological conditions of geothermal resource occurrences in Poland. *Geol. Q.* **2020**, *64*, 185–196. [CrossRef]
83. Górecki, W. (Ed.) *Atlas of Geothermal Waters and Energy Resources in the Western Carpathians*; Ministry of Environment of Poland, ZSE AGH: Krakow, Poland, 2011.
84. Buła, Z.; Żaba, J. Pozycja tektoniczna Górnośląskiego Zagłębia Węglowego na tle prekambryjskiego i dolnopaleozoicznego podłoża. In *Geologia i Zagadnienia Ochrony Środowiska w Regionie Górnośląskim*; Jureczka, J., Buła, Z., Żaba, J., Eds.; Polish Geological Institute, Polish Geological Society: Warsaw, Poland, 2005. (In Polish)
85. Różkowski, A. (Ed.) *Środowisko Hydrogeochemiczne Karbonu Produktywnego Górnośląskiego Zagłębia Węglowego*; Prace Naukowe Uniwersytetu Śląskiego w Katowicach; University of Silesia: Katowice, Poland, 2004. (In Polish)
86. Heidbach, O.; Rajabi, M.; Cui, X.; Fuchs, K.; Muller, B.; Reinecker, J.; Reiter, K.; Tingay, M.; Wenzel, F.; Xie, F.; et al. The world stress map database release 2016: Crustal stress pattern across scales. *Tectonophysics* **2018**, *744*, 484–498. [CrossRef]
87. Miecznik, M.; Sowiżdżał, A.; Tomaszewska, B.; Pająk, L. Modelling geothermal conditions in part of the Szczecin Trough—The Chociwel Area. *Geologos* **2015**, *21*, 187–196. [CrossRef]
88. *European Union Commission Recommendation of 22 January 2014 on Minimum Principles for the Exploration and Production of Hydrocarbons (Such as Shale Gas) Using High-Volume Hydraulic Fracturing (2014/70/EU)*; European Union Commission: Brussels, Belgium, 2014.
89. Czupski, M.; Kasza, P.; Leśniak, Ł. Development of selective acidizing technology for an oil field in the Zechstein main dolomite. *Energies* **2020**, *13*, 5940. [CrossRef]
90. Wilk, K.; Kasza, P.; Labus, K. Impact of Nitrogen Foamed Stimulation Fluids Stabilized by Nanoadditives on Reservoir Rocks of Hydrocarbon Deposits. *Nanomaterials* **2019**, *9*, 766. [CrossRef]

**Artykuł II: Potencjał geotermalny gorących suchych skał w krajach południowo-wschodniej części basenu bałtyckiego.**

*energies*

MDPI

*Review*

# Geothermal Potential of Hot Dry Rock in South-East Baltic Basin Countries—A Review

**Rafał Moska [1,*], Krzysztof Labus [2,*], Piotr Kasza [1] and Agnieszka Moska [1]**

[1] Oil and Gas Institute—National Research Institute, 25A Lubicz Str., 31-503 Krakow, Poland
[2] Faculty of Mining, Safety Engineering and Industrial Automation, Silesian University of Technology, 2 Akademicka Str., 44-100 Gliwice, Poland
* Correspondence: moska@inig.pl (R.M.); krzysztof.labus@polsl.pl (K.L.)

**Abstract:** The beginning of 2022 was a time of major changes in the perception of energy availability and security in European countries. The aggression of Russia against Ukraine destabilizing the European energy economy, combined with the withdrawal from fossil fuels which has been going on for a dozen years, has strengthened activities to introduce new energy technologies based on renewable energy sources. One of the most promising and stable sources of renewable energy is geothermal energy, in particular enhanced geothermal systems (EGS) in hot dry rocks (HDR). These deposits occur at a great depth in almost every place on Earth, but due to their low permeability, they require hydraulic fracturing, which results in high investment costs. This technology has been developed for several decades. The current situation in Europe seems to confirm that its rapid development to a level that guarantees stable and profitable operation is crucial. This is of particular importance in the case of former member states of the economic zone of the Council for Mutual Economic Assistance, which until recently were heavily dependent on Russian energy. This review, based on the latest available data, covers potential HDR prospective areas in the countries of the south-eastern Baltic basin, including Lithuania, Latvia, Estonia and Poland. It is specific to this region that the original heat flux density is lower as a result of the paleoclimatic effect associated with the youngest ice age; however, thermal conditions do not deviate too much compared to western Europe, especially Rhine Graben, and significantly exceed the conditions of Finland, where an EGS project is currently being operated. In Lithuania, the most prospective area is the ZNI intrusion (south of Klaipeda), characterized by a geothermal gradient of up to 40 °C/1000 m. In addition, the Precambrian batholith south of Liepāja (Latvia) and the Rapakivi granites in the north and center of Estonia are promising EGS sites. Poland has relatively the most explored EGS potential, in both volcanic, crystalline and sedimentary rocks, especially in the area of the Szczecin Trough, Gorzów Block, Moglino-Łódź Trough and Karkonosze Mountains. Unfortunately, local tectonic conditions, in particular the development of faults and natural fracture zones that affect the directions of fracture propagation during hydraulic fracturing, have not been sufficiently recognized, which is one of the main barriers to the expansion of EGS pilot projects in these countries. These issues present challenges for the researchers, especially in terms of petrophysical analyses of rocks in target zones and local stress conditions, which have a key impact on fracturing operations and profitability of the systems. Despite high investment costs on the one hand and a significant slowdown in the global economy in 2022 on the other, it remains hopeful that the authorities of individual countries will decide to accelerate research work, leading to the implementation of pilot projects of EGS installations, and that this technology will be further improved to ensure a stable clean energy supply.

**Keywords:** geothermal energy; geothermal potential; hot dry rock (HDR); enhanced geothermal systems (EGS); Baltic countries

check for updates

**Citation:** Moska, R.; Labus, K.; Kasza, P.; Moska, A. Geothermal Potential of Hot Dry Rock in South-East Baltic Basin Countries—A Review. *Energies* **2023**, *16*, 1662. https://doi.org/10.3390/en16041662

Academic Editor: Marco Fossa

Received: 11 December 2022
Revised: 29 January 2023
Accepted: 3 February 2023
Published: 7 February 2023

## 1. Introduction

The beginning of the 2022 year was a time when the geopolitical and energy supply situation in Europe changed significantly. The aggression of Russia against Ukraine made the European countries aware that the directions of energy supply need to be immediately diversified, especially regarding natural gas, oil and steam coal. These mineral resources have become a strong economic weapon in the hands of Russia and are used to effectively blackmail energy-dependent European countries, expecting them to accept military activities near their borders. It seems clear that now is the last moment to intensify the trend away from fossil fuels towards renewable energy in the European energy market. The leaders of the energy transformation process are highly developed, "old European Union" countries such as Germany, the Benelux Union and France, which are gradually abandoning not only the use of fossil fuels, but also nuclear energy. This trend is also observed in Central and Eastern Europe; however, the lower level of energy industry development, resulting from the Soviet influence until the 1990s, resulted in a much less developed renewable energy sector in these countries. In this light, it seems natural to quickly search for and develop new energy solutions that, on the one hand, will be emission-free and stable over time and, on the other, will increase the energy independence of countries.

One of the most promising clean energy technologies is enhanced or engineered geothermal systems (EGS), which use the petrothermal energy of hot dry rocks (HDR), accessible at great depths, almost everywhere on Earth [1–3]. These technologies have been developed for years in many countries around the world and are still being improved, breaking technical barriers and increasing profitability [4]. This review presents the current state and prospects for the development of EGS in countries of the south-east Baltic Basin, including Lithuania, Latvia, Estonia and Poland. The focus was primarily on the analysis of areas where geothermal collectors could potentially be developed in HDR rock, and the conditions that should be met, similar to the installations operating in western Europe. This study was based on a wide set of data from the latest, currently available literature, which have not been compiled in this way so far. New general maps and summary tables of data were developed, in which potential prospective areas for EGS-type installations are indicated.

## 2. Current State of Energy Production and Consumption in the Baltic States

Until recently, the energy systems of the Baltic states were very different. The Estonian system was purely thermal; the Latvian system was based on water and thermal technologies; and the Lithuanian system was dominated by nuclear energy [5]. The changes and modernizations carried out in the energy industry in the last decade, as well as the abandonment of nuclear energy, have led to major changes in the production structure. According to Eurostat data for 2020, primary energy consumption in the Baltic states is not very high compared to other countries in the Euro area. Renewable sources have a higher share in energy production than the Euro area average, with the highest value in Latvia, which also has the highest participation of renewables in electricity production. The share of renewable energy for cooling and heating in the Baltic countries is more than twice the EU average, and the Baltic countries have a lower dependence on fossil fuels. Estonia, due to the extensive use of oil shale (phasing out by 2040 at the latest) and increasingly renewable fuels, has the lowest dependence on energy imports, with a share of only 10.5% (Figure 1).

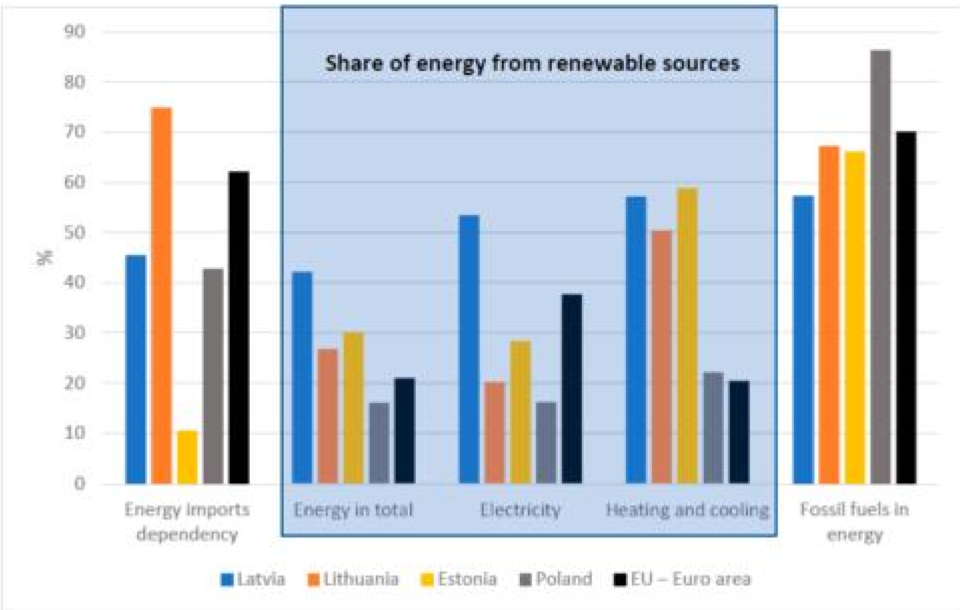


**Figure 1.** Dependence on energy imports and share of energy from renewable sources and fossil fuels in Baltic countries, Poland and the Euro area in 2020 (after: [6]). (The presented data also include Poland, which, like the Baltic countries, joined the EU in 2004, but previously belonged to the Eastern Bloc and thus to the economic zone of the Council for Mutual Economic Assistance).

## 3. Development of Enhanced Geothermal Systems in the World

The first HDR/EGS pilot project was launched in Fenton Hill, New Mexico, USA in 1979. It served as a testing ground for many years when significant discoveries were made, and the principles of engineered geothermal systems, including hydraulic stimulation, and operation methods were described, both from the point of view of geology, tectonics, field engineering and surface thermal energy recovery installations [4]. Although the EGS technology was very underdeveloped at this time, Fenton Hill became the first site to confirm that energy production from HDR on a commercial scale is possible and could be profitable in the future. This project resulted in increased interest in this technology and the launch of research projects around the world. In the 1970s and 1980s, research work on hydraulic fracturing technology in HDR continued in Rosemanowes, UK [7,8]. In the underground geothermal collector target zone, an unfavorable phenomenon of thermal short circuiting was observed, consisting of creating a preferred flow path in the rock, which resulted in cooling the formation and reducing the temperature of the liquid produced. The unfavorable effect of the proppant used to support fractures formed in the hydroshearing mechanism was also observed [4,9]. In the 2000s, a large commercial project was implemented in Habanero (Cooper Basin, Australia), where specific, favorable geological and tectonic conditions prevailed in the HDR target zone: temperature reaching 250 °C at a depth of less than 4000 m, a compressive stress regime causing the formation of horizontal fractures, and the presence of horizontal natural fractures facilitating fluid flow between vertical wells [10–12]. The operation of a 1 MW power plant was demonstrated there, but despite wide-ranging plans to launch a 40 MW power plant, the work was finally abandoned in 2016.

Most of the EGS installations function in intrusive igneous rock, i.e., granite, granodiorite; however, projects were also carried out in low-porosity, tight sedimentary and mixed rocks, e.g., Genesys, Groß Schönebeck in Germany [13,14] (Table 1). The working fluid that transports thermal energy to the surface was usually fresh water; however, liquids based on linear and cross-linked polymers were also used in sedimentary formations e.g., Groß Schönebeck [14]. They also experimented with the use of supercritical $CO_2$ for these purposes [15]. In single cases, work was carried out on the functioning of EGS technology in rocks made available through a single well [16]. Currently, work on the development of EGS technology is being carried out in China and the United States, among others [17–19]. In Europe, research work continues on projects such as Soultz-sous-Forêts (France), Landau, Groß Schönebeck and ST1 Deep Heat (Finland) (Table 1) [14,20,21]. The opening of pre-existing or newly formed fractures as a result of pumping the treatment liquid into HDR is associated with the risk of seismic events caused by the activation of fault surfaces subjected to stresses in the formation. These low-magnitude local events were commonly reported in all ongoing projects: however, in two cases (Basel, Switzerland and Phoang, Republic of Korea) relatively high-magnitude events that caused damage to the surface were a reason to stop the projects [22–26]. The best example how the EGS can provide energy for local needs for a long period of time are projects carried out on the Rhine Graben (France, Germany). Small-scale power plants or geothermal heating plants, operating in Soultz-sous-Forêts, Landau and Rittershoffen, provide several MWe and several dozen MWth power [2].

**Table 1.** Selected geological and technological data on European EGS sites.

| Country (EGS Site), Activities, Duration | Depth, m | Temperature, °C (Geothermal Gradient, °C/km) | Geological Conditions | Target Zone Stimulation Mechanism | References |
|---|---|---|---|---|---|
| United Kingdom (Rosemanowes) 1977–1985 | about 2000 | below 100 | Granite Carnmenellis batolith, Permian. Strike-slip tectonic regime | hydraulic, hydroshearing | [4] |
| France (Soultz-sous-Forêts) 1990-present | 5200 | about 200 (about 38) | Porphyric granites MFK, two-mica granites, Carboniferous, Normal with strike-slip component tectonic regime | hydraulic, hydroshearing | [20,27,28] |
| Germany (Groß Schönebeck) 2006-present | about 4100 | 149 (about 36) | Clastic and volcanic rocks (rhyolite, andeside) Rotliegend, Permian. Normal-strike-slip tectonic regime | hydraulic | [29–31] |
| Germany (Landau) 2005-present | 2200 | about 160 (about 72) | Porphyric granites MFK, two-mica granites, Carboniferous, Normal with strike-slip component tectonic regime | hydraulic, hydroshearing | [27,28,32] |
| Finland (ST1 Espoo) 2014-present | 6400 | 100–110 (15–17) | Low porosity, natural fractured granite, pegmatite, gneiss and amphibolite. Precambrian Reverse faulting regime. | hydraulic | [21,33] |

## 4. Technical Aspects of Geothermal Collectors in Hot Dry Rocks

Extracting a large amount of thermal energy, which can be used not only in heating but also in the production of electricity, requires access to rocks deposited at great depths, where high temperature prevails. The high crustal stresses in these zones cause rocks to have different petrophysical properties, compared to the generally highly porous and permeable rocks in shallower conventional geothermal reservoirs. Due to the fact that hot dry rocks have very low porosity and permeability, it is necessary to create an artificially hydraulic connection between drilled wells, to allow the working fluid to circulate in a loop between two or more wells and transfer heat energy into surface. For this purpose, a hydraulic fracturing technology, which originated in the oil industry, is mainly used. It involves injecting a fracturing fluid at high pressure through the well into the low permeability rocks. Recalling principles of fracking in unconventional gas deposits, the pressure of the fluid creates new fractures in the rock or opens pre-existing ones, thus creating highly permeable arteries through which gas can enter into the well. The composition of the fracking fluid depends on the type of rock. In ductile formations, characterized by a low Young's modulus and a high Poisson's ratio, crosslinked or linear gel fluids are usually used, while for brittle ones (high Young's modulus, and low Poisson's ratio), slickwater or two-phase fluids (foams) are applied. Fracturing fluid usually contains a small amount of environmentally safe chemical additives depending on the specific needs. Proppant material is often added to the fluid, to keep the fractures open after pumping pressure ceases [34]. More viscous fluids are capable of transporting higher-weight proppants, while slickwater and foams are characterized by significantly lower transport properties.

Since the 1970s, hydraulic fracturing technology has also been used to create underground heat exchangers in EGS. The design and development of both HDR and gas wells are very similar, except for the higher depths of the EGS and therefore the stresses in the reservoir, the higher temperature and the presence of crystalline or igneous rocks at the target depth with high density and mechanical strength. The objective of fracturing, in HDR, is to hydraulically connect two or more wells in such a way that the flow of working fluid guarantees the economically optimal operation of the system, i.e., the temperature and volume of the fluid obtained from the production well are stabilized at an appropriate level. Excess flow may cause unfavorable short circuiting, which causes cooling of the formation, and consequently, lowering the temperature of the obtained fluid. The main types of underground heat exchanger systems are presented in Figure 2. The most commonly used are type A and B—EGS doublet or triplet—where cool water is pumped into the injection well and the heated water is received from production wells. On the other hand, the less expensive single-well circulation concepts (C, D) are rarely used because of lower efficiency.

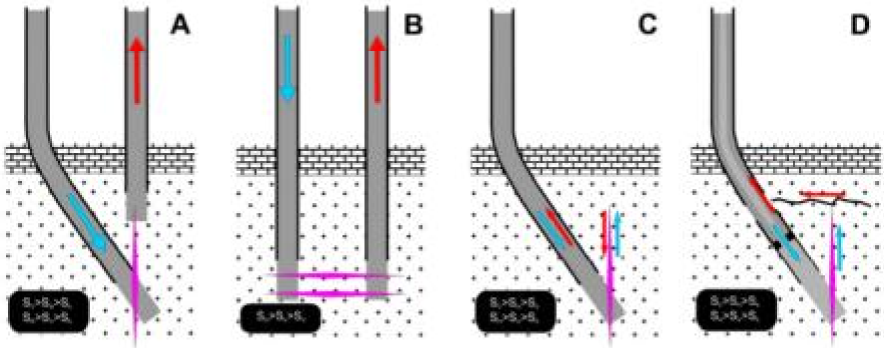


Figure 2. The most common types of underground heat exchanger systems. $S_V$—principal vertical stress; $S_H$, $S_h$—maximum and minimum horizontal stress, respectively. (A)—doublet in extensional stress regime, (B)—doublet in lateral compressive regime, (C)—single directional well for injection and production cycling in extensional stress regime, (D)—single directional well for continuous injection and production in extensional stress regime.

In HDR-type formations, the dominant role in hydraulic conductivity of rocks is played by natural fractures, activated by shear forces acting in their planes (hydroshearing stimulation mechanism), whereas inducted fractures, opening in a direction perpendicular to the minimum horizontal stress (pure opening mechanism), are in the minority. Open fractures in hydroshearing are formed at relatively low pressures because their strength is lower than that of the surrounding rock. Pumping pressure that is too high can "overstimulate" HDR formation, causing irreversible rock movements and leading to a short circuit (e.g., Rosemanowes, Fjalbacka) [4]. The walls of the shear-activated fractures move relative to each other during treatment and shift slightly when pumping stops. This results in desired natural fracture conductivity and consequently no need for expensive proppants and more viscous fluids with higher transport capacities during operations (Figure 3). In most cases, when there are no water-sensitive clay minerals in the formation, fresh water without any additives is used. If clay minerals are presented, i.e., in sedimentary formations, clay control additives are recommended. If proppants are used (especially in tight sedimentary HDR formations), there is generally a small risk of the embedment phenomena (pressing the grains of proppant into the fracture surface) due to the high strength of the rocks [3]. Fracking operations in HDR formations are usually massive type, using large volumes of fresh water (more than 1000 $m^3$ per stage or more than 10,000 $m^3$ per entire operation). At the design of the fracturing procedure in HDR formations, it is important to know the preferred orientation of natural fractures, because even if new fractures develop, they will only reach a few meters in length and then intersect the natural ones. Henceforth, the conductivity will occur through the natural fractures. Therefore, the correct sequence of work during the development of an EGS reservoir is to drill a well, then perform hydraulic fracturing and record microseismic events that inform about the direction and intensity of energy propagation in the reservoir, and finally drill a second well passing through the seismic cloud in a suitable location [3].

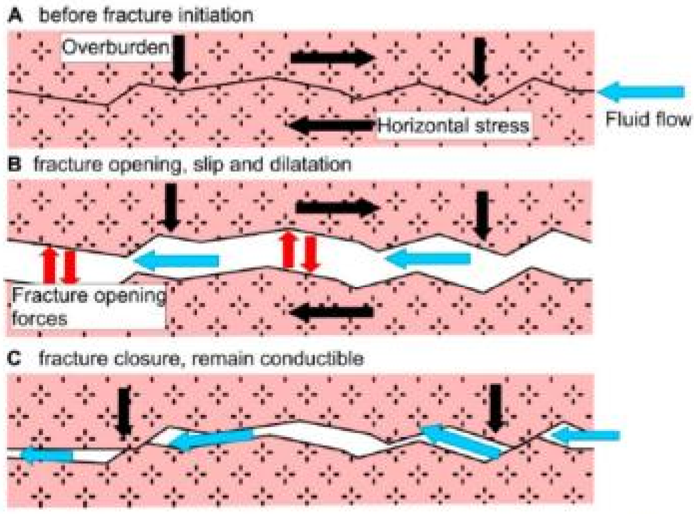


Figure 3. Basic principles of hydroshearing. Blue arrows depict fluid flow, black—principal stress directions, red—fracture opening forces.

## 5. Potential of Hot Dry Rock in Countries of the South-East Baltic Basin

### 5.1. Lithuania

Lithuania is located in the central-eastern part of the Baltic sedimentary basin in central-eastern Europe. Although the country does not have volcanic activity or hot springs, it does have several of geothermal reservoirs that have been explored for years [35]. The only geothermal heating plant in Lithuania, Klaipeda Geothermal Demonstration Plant, was built in 2000 with capacity 13.6 MW [36,37]. The plant uses a Devonian aquifer in the western part of the country, which supplies geothermal water from 1100 m at 38 °C. The plant operated intermittently over the years 2001–2017, due to financial and technical problems, and has been stopped now. There are also small-scale shallow geothermal pump systems in the country used not only for heating but also balneology and fish and shrimp farming [38,39]. The geothermal gradient in Lithuania varies from 12 °C/km in the east to 42 °C/km in the west [40]. In Lithuania, there are several prospective areas to obtain petrothermal energy from hot dry rocks. The crystalline basement of the country is a part of the East European Craton of the Early Precambrian consolidation. The basement, overlain by sedimentary cover with a thickness of several hundred meters to more than 2 km, is composed of two lithotectonic zones. The eastern part of the country is attributed to the East Lithuanian Domain composed mainly of mafic metavolcanic and felsic metasedimentary rocks, metamorphosed in amphibolite to granulite facies conditions and strongly migmatised [41]. A characteristic feature of this area is the occurrence of lenticular belts, interpreted as fold and thrust sheet structures. The western part of the country comprises the West Lithuanian Granulite, with felsic, and metapelitic gneisses, originating from psammites, pelites, felsic and intermediate volcanics. Intrusive Saxony-type charnockites, as well as garnet- and cordierite-bearing granitoids, form a major part of this zone. In the Mesoproterozoic, the Riga pluton intruded on the northern part of the West Lithuanian Granulite domain, forming a batholith up to 250 km in diameter, and creating the most prospective zone in terms of geothermal potential of Lithuania. This area is generally characterized by high heat flow and high heat production by the granitoids, due to the presence of radiogenic heat-producing elements: Th, U, and K. The most prospective geological formation is the Zemaiciu Naumiestis intrusion (ZNI) in southwest of the country (Figure 4). This pluton consists mainly of massive, biotite, medium- to coarse-grained monzogranites, along with a minority of biotite syenogranites and porphyric quartz monzodiorites, with fracture populations at a density of several to several dozen per 10 m. Exploration boreholes and modeled profiles of this structure revealed an intrusion thickness of about 4 km and its bottom at a depth of 6 km. The ZNI heat flow anomaly ranges from 83 to 100 $mW/m^2$, while the geothermal gradient measured in deep wells averages between 35–40 °C depending on the area, which gives a modelling temperature of 150 °C at the target depth (4.5–5.0 km). According to preliminary assumptions [41], the geothermal potential of ZNI would probably be sufficient for a power plant of up to 5 MW, assuming single injection and two producing wells at a 500 m offset, an injection rate of approximately 150 L/s and a production rate of 75 L/s per well.

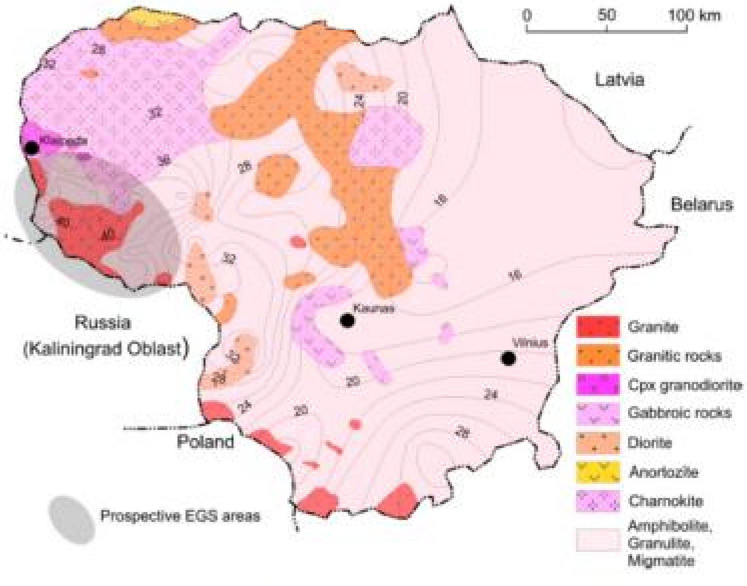


Figure 4. Generalized map of the Lithuanian crystalline basement in the background of geothermal gradient distribution (based on [40,42]).

## 5.2. *Latvia*

Latvia, similar to Lithuania, is located in the south-eastern part of the Baltic sedimentary basin in central-eastern Europe. It borders Lithuania to the south, and geologically, lies in the Precambrian East European Craton. The Cambrian strata covering the crystalline bedrock are characterized by an anomalously high average temperature, ranging from 38 °C in the northwest to more than 120 °C in the southwest, which has been explained in terms of mantle processes and high heat generation of crustal lithologies [43]. The average geothermal gradient varies within the interval of 8 °C/1000 m–19 °C/1000 m in the northern and eastern part of the country, but the average geothermal gradient reaches 35 °C/1000 m in the central and southwestern parts. In the geological cross section of Latvia, three lithological structures of different geothermal gradients can be distinguished: 1. Terrigeneous Devonian and Carboniferous rocks, 2. Silurian and Ordovician Carboniferous clay deposits, and 3. Cambrian and Venda terrigeneous rocks [44]. In the Cambrian and Venda area, the gradients vary from 6 °C to 31 °C/1000 m, whereas the maximum is reached in the southwest of Latvia. The temperature reaches 38–62 °C at the depth of 1281–1714 m in the southwest of Liepaja city, and 33–55 °C at the depth of 1100–1436 m, near the Lithuanian border (Figure 5). The bedrock of the Cambrian and Venda area is Precambrian crystalline basement, similar to the Lithuanian area. Despite the lack of literature data on temperature at depths over 2000 m in this area, taking into account the thermal gradients, it can be assumed that the potential drilled borehole should be at least 4000 m deep, to reach temperature of not less than 140 °C at the target HDR zone. This temperature can meet the expected values for small-scale enhanced geothermal systems (about one to several MW power), such as projects like Groß Schönebeck (Germany) and Phoang (South Korea) [25,29]. However, EGS projects are also known where the target zone was characterized by lower temperature conditions, which in this case would allow the drilling of a shallower well [21,33].

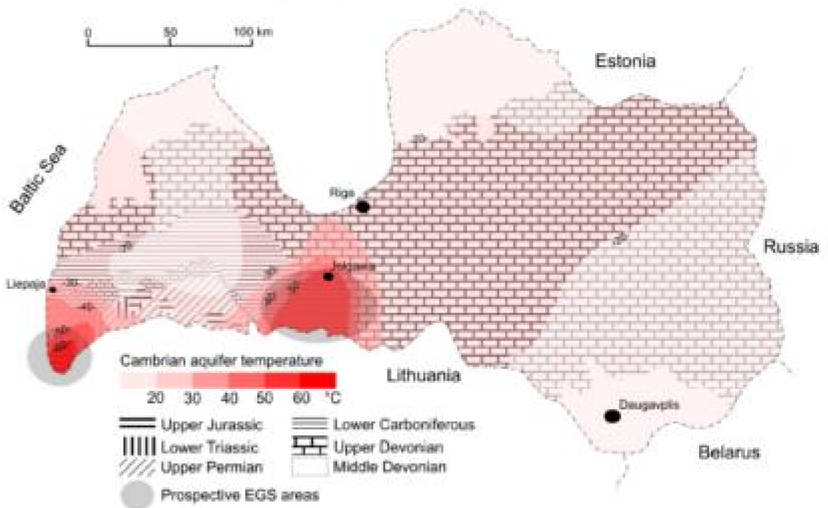


**Figure 5.** Average temperature in Cambrian underground water horizon, on the background of the geological setting of Latvia (based on [44,45]).

### 5.3. Estonia

Estonia is the northernmost among the countries of the south-east Baltic basin. The Precambrian crystalline basement here is a continuation of the north-eastern Latvian basement, and a part of the Baltic-Belorussian granulite belt. The crystalline bedrock is overlain by sedimentary rocks (sandstones, dolomites, limestones, silts and clays) of the Ediacaran to Paleozoic age. The sedimentary cover is about 100 m thick in the north and more than 780 m thick in southern Estonia [46]. Granulites are deposited in most of the country area and are represented by intermediate and mafic metavolcanic rocks with minor felsic bodies. High-grade is usually well preserved, but particularly in western Estonia strong retrograde and metamorphism have occurred [47,48]. In the western part of Saaremaa island and in the Naissaar and Mariamaa zones (Figure 6) the gneissic rocks are intersected by several generations of intrusive rocks, of which the most important ones are the rapakivi plutons: Naissaar, Neeme, Märjamaa, Ereda and Riga [49,50]. This formation can be correlated with those in southern Finland [49,51]. Approximate temperatures in the bedrock at a depth of 500 m range between 11 °C and 16 °C, with the highest values in the north and north-east of the country [52], and are similar to the temperatures in southern Finland [53]. According to Jõeleht [54], the heat flow density, adjusted for paleoclimatic effects, varies between 28–68 $mWm^{-2}$. In the upper basement of northern Estonia, the temperatures are somewhat higher, due to the thermal shielding effect of Cambrian clays, with low thermal conductivity. The highest values of heat flow density (68 $mWm^{-2}$) were calculated for the Meriküla well, in north-east Estonia, and the Saviranna well located about 25 km NEE from Tallinn (48 $mWm^{-2}$). This is attributed to the high heat production of the Neeme rapakivi granite, compared to gneiss, which is generally dominant in the area [55]. Granulites are characterized by a heat production of 0.94 $\mu W \cdot m^{-3}$, which is slightly higher compared to regions analyzed in Finland [56].

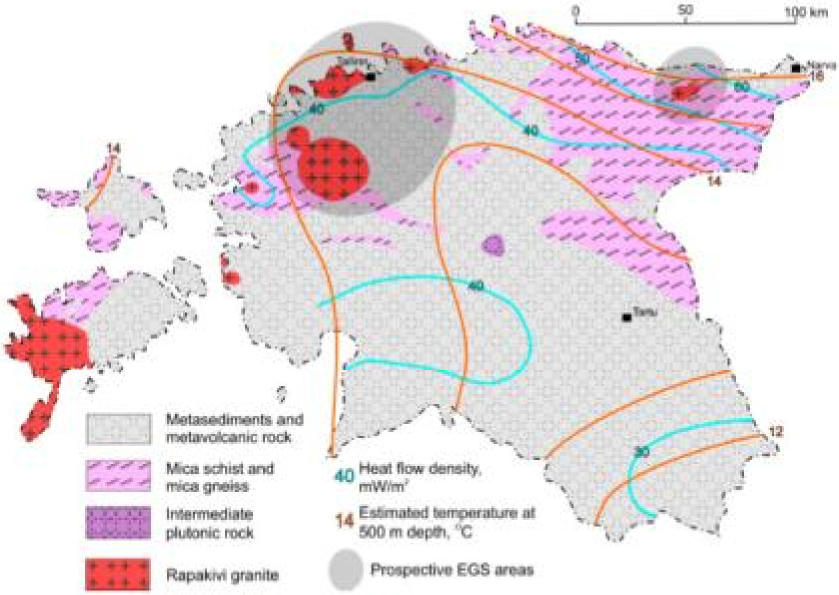


**Figure 6.** Elements of the Estonian crystalline basement, heat flow density and estimated temperature (based on [49,57]).

The ST1 Deep Heat geothermal project in Espoo, southern Finland, could serve as a reference point for potential EGS locations. The typical geothermal gradient in this area is relatively low (15–17 °C/km), which corresponds to a heat flow of 52 $mW/m^2$ [58], therefore, the goal was to achieve 40 MW in a combined heat and power plant, fed with 115 °C water from hot dry rock at a depth of 6000 m, making this the deepest EGS in the world. By 2020, two wells were drilled, the main (OTN-3) and the observation well (OTN-2), of depths 6400 and 3300 m, respectively. The target zone is a Precambrian crystalline basement consisting of granite, pegmatite, gneiss as well as amphibolite-rocks of similar origin to the potential sites in Estonia. Due to a very low porosity of 0.5%, total flow is realized there through structures subjected to brittle deformation, that is, induced and natural fractures [21], similar to typical natural fractures in HDR granitic rocks in the world. Drill bit seismics and vertical seismic profiling in OTN-2 revealed a fissured structure with a dip of 44° ENE. The final trajectory of OTN-3 was continued into this structure at a distance of 1 km. In June and July 2018, hydraulic stimulation was performed in the interval of 5800–6100 m. During a 49-day period, fresh water was pumped with a capacity of 400–800 $m^3$/min, allowing wellhead pressure to fluctuate in the range of 60–90 MPa [59]. In 2020 another stimulation was performed, pumping about 7000 $m^3$ of fresh water through the 1300 m open hole. The stimulation zone is characterized by a reverse faulting regime (unlike the regional strike-slip regime in this area) [33], resulting in a preferred vertical direction of the propagation of the new induced fractures. Information about the mechanism of stimulation in OTN-2 well is not available in the literature; however, the world experiences in granitoids stimulation suggest that the mechanism could be hydroshearing-slip and dilatation in the plane of natural fractures. The discrepancy between the regional state of stress and the local actual state in the area of the OTN boreholes may be an important hint for the designers of the potential HDR stimulation technology in Estonia, drawing attention to the fracture propagation directions in the rock mass and thus the quality of connections between injector and producer wells. At the same time, it appears that the local reverse faulting regime could impede the use of a single well EGS arrangement as in the GeneSys Hannower project [13,16]. The horizontal propagation of the inducted fractures could restrict the flow between the stimulated rock horizons in the vertical well. It is worth mentioning that in the ST1 project, a system of so-called "Road Lights" was implemented, consisting in special procedures for responding to the revealed seismic events. Reaching an event magnitude above 2.1 means that the operation is aborted. More than 50,000 microevents below magnitude 1.9 have been recorded so far. Lessons learned from the failure of "cyclic soft stimulation" in Phoang [24,60] and events in the BS-1 well in Basel [22], as well as carrying out works at a great depth, could significantly reduce the risk of relatively strong seismic events felt on the surface of the earth, as a result of hydraulic stimulation operations. The ST1 project is currently being continued.

### 5.4. *Poland*

Poland is not included among the Baltic states in the political sense of the word; however, in terms of considerations on EGS, it seems to be a good comparison area, first due to its geographical location, second as the former member of Eastern Block belonged to the economic zone of the Council for Mutual Economic Assistance, which determined the slower energy development compared to the countries of western Europe, and finally due to the current rapid economic development, enabling the allocation of significant funds to renewable energy sources. Despite significant changes in the Polish energy sector in recent years, fossil fuels still occupy the largest percentage share in the energy balance, covering over 85% of the total demand (Figure 1). Due to the restrictive regulations of the European Union in the field of greenhouse gas emissions, the desire to reduce the consumption of fossil fuels in the overall energy balance and thus to reduce high emission fees, a significant increase in interest in renewable energy sources, including geothermal and especially unconventional EGS-type systems, is currently observed in Poland. The first steps in this direction were made in the first decade of the 21st century, when a preliminary scientific project was carried out to assess the thermal potential of geological structures for the purposes of EGS in Poland [31]. Three types of structures were considered: crystalline bedrock, volcanic rocks under the sedimentary cover and sedimentary basins. This project was based on analyses of the Earth's crust temperature and heat flux density maps. Additionally, a series of field geophysical studies, laboratory tests and numerical simulations were carried out, which allowed several prospective areas to be identified [3,31].

The highest heat flux density of earth in Poland is observed in the western and central parts of the country [61]. The values correlate well with the crustal temperature at a depth of 2 km [62]. Geothermal gradients and heat flow anomalies are higher than the corresponding values in the most promising areas of Lithuania, Latvia and Estonia. In this area, the Permian trachyandesites of the Gorzów Block were deposited (Figure 7, Table 2). This formation is located at a depth below 4300 m, is characterized by large thickness, and contains gas bubbles, which ensures good prospects for fracturing. The location described shows a meaningful analogy to the Groß Schönebeck reservoir near Berlin, where the geothermal gradient is 3.5–4.0 °C/100 m, and the temperature at a depth of 4.3 km reaches approximately 150 °C [31,63].


**Figure 7.** Prospective areas for conventional and unconventional geothermal energy utilization and Earth's heat flow density in Poland against the background of simplified geologic setting (based on [31,61,64]).

**Table 2.** Selected parameters of the potential EGS sites in the countries of the south-east Baltic basin.

| | Potential EGS Site | Geothermal Gradient, °C/1000 m | Heat Flow Anomaly, mW/m² | Target Depth, m, Temperature, °C | Lithology, Stratigraphy | References |
|---|---|---|---|---|---|---|
| Lithuania | Zemaiciu Naumiestis intrusion (ZNI), south of Klaipeda | 35–40 | 83–100 | 4500–5000, 150 | syenogranite, porphyric quartz monzodiorite | [41,65] |
| Latvia | Precambrian batholith, south of Liepalia | up to 35 | No data | below 1740, 140 at 4000 * | intrusive igneous rocks | [44,66] |
| Latvia | Precambrian batolith, center and south of the country | up to 35 | No data | below 1500, 140 at 4000 * | intrusive igneous rocks | [44] |
| Estonia | Nothern and center of the country, Precambrian basement | 26–28 in sedimentary cover; 14 in the Precambrian | 40–50 42 | 4000, 58–73 ** depending on the site | rapakivi granites | [49,67,68] |
| Poland | Karkonosze Mountains, SW of the country | 44 | 65 | 4000, 165 | intrusive igneous rocks, Carboniferous | [31,61] |
| Poland | Gorzów Block NW of the country | 35–40 | 105 | 4300, 160 | trachyandesites, Permian | [31,61] |
| Poland | Mogilno-Łódź Trough country center | up to 34 in the best target area | 75–90 | 5000–6500, 165–195 | sandstones, buntsandstein, lower Triassic | [31,61,63] |
| Poland | Szczecin Trough NW of the country | up to 27 | 85–100 | >5000, above 150 | sediments, Carboniferous, Permian | [61,63,69] |
| Poland | Upper Silesian Block S of the country | up to 45 | 80–95 | >5000, 170 | clastic deposits of Carboniferous | [61,63,70] |

* Calculated taking into account the given thermal gradient, ** Calculated based on data from [49].

Two potential EGS areas were identified in the Polish Lowlands: the Szczecin and the Mogilno-Łódź Troughs. The first one forms a fold element elongated along the NW–SE axis, covering the Zechstein–Mesozoic complex. This structure was influenced by the block tectonics of the basement as well as by halokinetic movements, which mobilized Zechstein salts [71]. In the Szczecin Trough, the EGS prospects concern the Permian or Carboniferous strata, located more than 5000 m below sea level, with temperatures exceeding 150 °C [3]. Potential petrogeothermal reservoirs in the Mogilno-Łódź Trough area comprise Lower Triassic, such as the Buntsandstein formation of claystone and siltstones with limestone and sandstone beds located about 5700 m. The compact sandstones of Lower Buntsandstein can be considered as having the EGS potential, due to their thicknesses locally exceeding 1500 m. The Middle Triassic limestones and marls (Muschelkalk), are significantly less thick, up to 300 m. Upper Triassic clastic sediments and evaporates (Keuper) and clayey sandstones (Rhaetian) form a complex of 2400 m thickness [63]. In addition, extensive massifs of igneous rocks situated in southern Poland are considered suitable for EGS technology. The most promising is the Karkonosze granitoid pluton in the Sudeten Mountains, with a geothermal gradient of approximately 40 °C/1000 m, and temperatures reaching 160 °C at 4.0 km below ground level [31]. An intense heat flux is typical for the Variscan fold belt and in the northern zone of the Lower Silesian internides. The Upper Paleozoic, Devonian and Carboniferous sediments form a continuous cover on the Precambrian and Lower Paleozoic complexes. In the Upper Silesian Coal Basin, the deeper part of the Carboniferous profile consists of carbonates and clastic, flysch, and molasse sediments. Carbonates are 200 to 1500 m thick, while Carboniferous clastic sediments, which form a potential petrogeothermal reservoir, reach more than 5000 m in thickness [72].

## 6. Discussion

For the analyzed region of Europe, the lowered primary heat flux density is specific as a result of the paleoclimatic effect associated with the youngest ice age, when the ice cover cooled the surficial layers of the earth's crust for tens of thousands of years. This effect is observed at least to a depth of 1000 m [53]. However, the distribution of the geothermal gradient and the heat flow density in this region do not differ significantly from the values measured in Western Europe, especially in the Rhine Graben, and significantly exceed the thermal conditions parameters for Finland, where the EGS project is currently being developed (Tables 1 and 2). HDR-type rocks, characterized by low porosity and permeability, are found in each of the countries analyzed. Prospective areas in Poland, i.e., the Gorzów Block, the Szczecin and Mogilno-Łódź Troughs and the Upper Silesian Block, are located in the eastern margin of the Western European Paleozoic Platform, where prospective EGS rocks are tight sedimentary rocks, volcanites and granitoids in the Karkonosze region. In the Baltic countries (Lithuania, Latvia and Estonia), the potential of HDR lies in the crystalline basement. The thickness of the overlying sedimentary formations decreases eastward, from just over 2000 m in the western part of Lithuania to less than 500 m in the Estonian Laeva (Figure 8).

Prospective hot dry granites and volcanites in Poland are deposited at a depth of about 4000 to 4300 m, which is a similar depth range as EGS installations in Groß Schönebeck and shallower than in Soultz-sous-Forêts. The temperature of the target zone, calculated from the geothermal gradient (35–40 °C/km), is comparable to the eastern Germany EGS sites (about 150 °C), and significantly exceeds the temperature in Espoo (Finland) (Tables 1 and 2). The tight sedimentary formations of Poland in Mogilno-Łódź and Szczecin Troughs are located deeper (5000 m to over 6500 m) comparable to the crystalline basement target zone in Espoo and porphyric granites in Rhine Graben; however, they are warmer than the rock of Finland (much above 150 °C), and at the deepest parts reach predicted temperatures similar to those in Soultz-sous-Forêts (up to 195 °C).

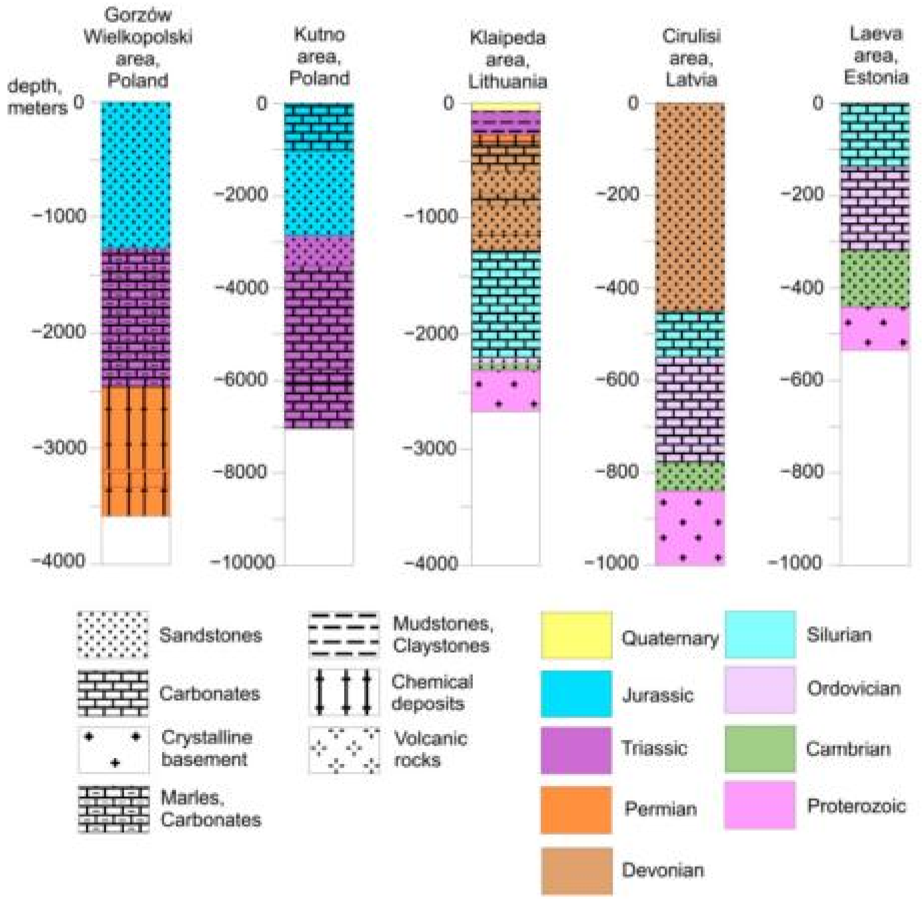


**Figure 8.** Simplified lithostratigraphic profiles of selected areas in Baltic countries. Based on [31,63,73–75].

The top of the intrusive igneous rocks, which are prospective formations in Lithuania, Latvia and Estonia, are deposited relatively shallow (from about 2500 m in Latvia, to about 500 m in Estonia, Figure 8); however, looking at the geothermal gradient and thermal heat flow data at these depths, temperature there is too low for the implementation of profitable collectors. Higher temperatures are reached at a depth of 4000–5000 m, where predicted values are comparable to temperatures in western Poland and eastern Germany (150 °C). This does not apply to Estonia, where a geothermal gradient in the range of less than 26–28 °C/km, determines a temperature in the range of 58–73 °C at a depth of 4000 m, which means conditions similar to those in Finland.

The predicted regional tectonic regime in prospective Polish locations is normal with a strike-slip component [3,76,77], which in general corresponds to the regime in western Europe. A separate issue is the local tectonic conditions, in particular the development of faults and natural fracture zones, affecting the directions of fracture propagation during the fracking operation. These conditions in the discussed countries, especially in Lithuania, Latvia and Estonia, have not been sufficiently recognized, creating one of the main barriers to the development of EGS pilot projects in these countries. Detailed recognition of local geological and tectonic conditions is possible after drilling the well to the appropriate expected target depth and performing well logging, as well as a set of laboratory measurements including rock mechanics tests on the core samples. So far, such deep exploratory wells have not been drilled. The analyses can be and usually are based on data from hydrocarbon or geothermal wells; however, they usually do not reach the target depths for EGS technology, and the extrapolations may be fraught with significant errors.

For Poland, a recent tectonic stress regime was designated, based on analyses of hydraulic fracturing of borehole walls [76,77]. However, these studies concern only selected areas that do not correspond well with the potential areas for EGS in this country. Furthermore, the methodology of this research was undermined by other authors [78], who pointed out that the results obtained do not justify drawing conclusions for the entire country, or even on a regional scale.

In order to deepen the knowledge about the geothermal conditions of south-east Baltic basin countries, closely related to regional and local geological/ thermal conditions, laboratory tests should be performed including measurements of core samples from the target zones. In particular, thermal and petrophysical parameters should be assessed, including thermal conductivity, rock fracture conductivity, rock strength (UCS, Young's modulus, Poisson's ratio in the reservoir conditions), and field testing should be conducted, i.e., minifracs to determine instantaneous shut-in pressure, corresponding to minimum principal stress. and analysis of tensile fractures to designate the rock anisotropy.

In the context of the development of EGS, the legal aspects of hydraulic fracturing operations in geothermal wells are also of key importance. In the individual analyzed countries, the legislation is very diverse: while in Poland and Estonia HF operations are allowed by law, in Lithuania there are heavy restrictions, and in Latvia the situation is not clearly standardized. Despite the uncertainties mentioned above, including technical difficulties, lack of research data and cost intensity, the development of EGS technology seems inevitable. Currently, Eastern European countries cannot afford to increase their dependence on energy from any other country, hence the development of unconventional technologies, including EGS, can greatly help in the pursuit of full energy independence.

## 7. Conclusions

The south-east Baltic Basin countries (Lithuania, Latvia, Estonia and Poland), as former members of the Eastern Bloc, are not as well developed in terms of power engineering as the countries of western Europe. In 2022, the conflict in Ukraine made it necessary to significantly intensify the diversification of energy sources and increase the use of renewable energy, including EGS in these countries. In this paper, a wide set of the latest available literature data on potential areas for EGS technology in these countries were compiled and compared with the respective data from western European EGS sites.

As a result of the paleoclimatic effect associated with the youngest ice age, the south-east Baltic basin area is characterized by a lowered heat flux density, the highest values of which were recorded in Poland and Lithuania (65–105 mW/m$^2$). Heat flux density decreases towards the north-east, to 40–50 mW/m$^2$ in Estonia. The distribution of the geothermal gradient shows a similar trend, from 35–45 °C/km in Poland and the western part of Lithuania (which is comparable to the values in the western European EGS sites-Groß Schönebeck and Soultz-sous-Forêts), to below 30 °C/km in Estonia. In Poland, the prospective HDR-type formations of the Gorzów and Silesia Blocks, Karkonosze Mountains, Mogilno-Łódź and Szczecin Troughs are associated to volcanic, intrusive and tight sedimentary rocks, petrophysically similar to HDR in western Europe.

In Lithuania, Latvia and Estonia, HDR potential is shown by the crystalline basement, located in the west and south of each of these countries. Local tectonic conditions, in particular the development of fault and natural fracture zones in relation to the necessary hydraulic fracturing operations have not been sufficiently recognized, creating significant barriers in the development of EGS pilot projects in these countries. In addition, deep wells reaching potential target zones have not yet been drilled, especially in Lithuania, Latvia and Estonia, hence the detailed analyses require extrapolation of data from shallower zones. These issues present challenges for the researchers, especially in terms of detailed thermal and petrophysical analyses of target zone rocks and local stress state conditions, having a key impact on fracturing operations and the profitability of the system.

Fracking operations in the Baltic states are not completely banned as in western Europe. It seems that the main factor holding back the pilot projects is the relatively high costs of this type of investment, which must be covered by the investor, which in most cases is the State Treasury. We remain hopeful that, in light of the political and economic situation of Europe in 2022, the authorities of individual countries will decide to start pilot work in this type of installation and EGS will be able to be further refined to ensure stable supplies of clean energy for future years.

**Author Contributions:** Conceptualization, literature review, investigation, manuscript writing, visualization, overall supervision, R.M.; investigation, manuscript writing, manuscript review, K.L.; supervision, manuscript review, P.K.; manuscript writing, visualization, A.M. All authors have read and agreed to the published version of the manuscript.

**Funding:** This paper is based on research carried out at the Oil and Gas Institute-National Research Institute (Poland), and the Silesian University of Technology, as part of the implementation doctorate program RJO/SDW/005-33, founded by Ministry of Education and Science of Poland.

**Data Availability Statement:** The data presented in this study are available on request from the corresponding author.

**Conflicts of Interest:** The authors declare no conflict of interest.

## References

1. Olasolo, P.; Juares, M.C.; Morales, M.P.; D'Amico, S.; Liarte, I.A. Enhanced geothermal systems (EGS): A review. Renew. *Sustain. Energy Rev.* **2016**, *56*, 133–144. [CrossRef]
2. Lu, S.M. A global review of enhanced geothermal system (EGS). *Renew. Sustain. Energy Rev.* **2018**, *81*, 2902–2921. [CrossRef]
3. Moska, R.; Labus, K.; Kasza, P. Hydraulic Fracturing in Enhanced Geothermal Systems—Field, Tectonic and Rock Mechanics Conditions—A Review. *Energies* **2021**, *14*, 5725. [CrossRef]
4. Tester, J.; Anderson, B.; Batchelor, A.; Blackwell, D.; DiPippo, R.; Drake, M.; Garnish, J.; Livesay, B.; Moore, M.; Nichols, K. *The Future of Geothermal Energy—Impact of Enhanced Geothermal Systems (EGS) on the United States in the 21st Century*; Massachusetts Institute of Technology: Cambridge, MA, USA, 2006.
5. Krishans, Z.; Mutule, A.; Oleinikova, I.; Kutjuns, A. Application of Risk Assessment Method for Baltic States Power System Development Optimization. In Proceedings of the International Conference on Probabilistic Methods Applied to Power Systems, Stockholm, Sweden, 11–15 June 2006. [CrossRef]
6. ec.europa.eu/Eurostat. Available online: https://ec.europa.eu/eurostat/cache/infographs/energy_dashboard/endash.html?geo=LV&year=2020&language=EN&detail=1&nrg_bal=&unit=MTOE&chart=chart_seven,chart_six,chart_two,chart_five,chart_one,chart_four&modal=0 (accessed on 21 November 2022).
7. Batchelor, A.S. Reservoir behavior in a stimulated Hot Dry Rock system. In Proceedings of the 11th Annual Workshop on Geothermal Reservoir Engineering, Stanford, CA, USA, 21–23 January 1986.
8. Batchelor, A.S. Development of Hot-Dry-Rock geothermal systems in the UK. *Thermal Power IEE Proc.* **1987**, *134A*, 371–380. [CrossRef]
9. Richards, H.; Parker, R.; Green, A.; Jones, R.; Nicholls, J.; Nicol, D.; Randall, M.; Richards, S.; Stewart, R.; Willis-Richards, J. The performance and characteristics of the experimental hot dry rock geothermal reservoir at Rosemanowes, Cornwall (1985–1988). *Geothermics* **1994**, *23*, 73–109. [CrossRef]
10. Wyborn, D.; da Graaf, L.; Davidson, S.; Hann, S. Development of Australia's first hot fractured rock (HFR) underground heat exchanger, Cooper Basin, South Australia. In Proceedings of the World Geothermal Congress, Antalya, Turkey, 24–29 April 2005.
11. Holl, H.G. *What Did We Learn about EGS in the Cooper Basin? Geodynamics Limited Technical Report*; Geodynamics Limited: Milton, Australia, 2015.
12. Holl, H.G.; Barton, C. Habanero Field—Structure and state of stress. In Proceedings of the World Geothermal Congress, Melbourne, Australia, 19–25 April 2015.
13. Orzol, J.; Jung, R.; Jatho, R.; Tischner, T.; Kehrer, P. The GeneSys-Project: Extraction of geothermal heat from tight sediments. In Proceedings of the World Geothermal Congress, Antalya, Turkey, 24–29 April 2005.
14. Blöcher, G.; Reinsch, T.; Henninges, J.; Milsch, H.; Regenspurg, S.; Kummerow, J.; Francke, H.; Kranz, S.; Saadat, A.; Zimmermann, G. Hydraulic history and current state of the deep geothermal reservoir Groß Schönebeck. *Geothermics* **2015**, *63*, 27–43. [CrossRef]
15. Wakahama, H.; Mito, S.; Ohsumi, T.; Ueda, A.; Yajima, T.; Satoh, H.; Sugyima, K.; Ozawa, A.; Todaka, N.; Sato, T.; et al. A concept of $CO_2$ Georeactor sequestration at the Ogachi HDR site. *Energy Procedia* **2009**, *1*, 3683–3689. [CrossRef]
16. Tischner, T.; Evers, H.; Hauswirth, H.; Jatho, R.; Kosinowski, M.; Sulzbacher, H. New concepts for extracting geothermal energy from one well: The GeneSys project. In Proceedings of the World Geothermal Congress, Bali, Indonesia, 25–29 April 2010.
17. Lei, Z.; Zhang, Y.; Yu, Z.; Hu, Z.; Li, L.; Zhang, S.; Fu, L.; Zhou, L.; Xie, Y. Exploratory research into the enhanced geothermal system power generation project: The Qiabuqia geothermal field, Northwest China. *Renew. Energy* **2019**, *139*, 52–70. [CrossRef]

18. Lei, Z.; Zhang, Y.; Zhang, S.; Fu, L.; Hu, Z.; Yu, Z.; Li, L.; Zhou, J. Electricity generation from a three-horizontal-well enhanced geothermal system in the Qiabuqia geothermal field, China: Slickwater fracturing treatments for different reservoir scenarios. *Renew. Energy* **2020**, *145*, 65–83. [CrossRef]
19. Moore, J.; McLennan, J.; Pankow, K.; Simmons, S.; Podgorney, R.; Wannamaker, P.; Jones, C.; Rickard, W.; Xing, P. The Utah Frontier Observatory for Research in Geothermal Energy (FORGE): A Laboratory for characterizing, creating and sustaining enhanced geothermal systems. In Proceedings of the 45th Workshop on Geothermal Reservoir Engineering, Stanford, CA, USA, 10–12 February 2020.
20. Vidal, J.; Genter, A. Overview of naturally permeable fractured reservoirs in the central and southern Upper Rhine Graben: Insights from geothermal wells. *Geothermics* **2018**, *74*, 57–73. [CrossRef]
21. Kukkonen, I.T.; Pentti, M. St1 Deep Heat Project: Geothermal energy to the district heating network in Espoo. In Proceedings of the 17th World Conference ACUUS 2020, Helsinki, Finland, 3–4 February 2021; IOP Conference Series: Earth and Environmental Science. IOP Publishing: Bristol, UK, 2021; Volume 703, p. 012035. [CrossRef]
22. Ladner, F.; Häring, M. Hydraulic characteristics of the Basel-1 enhanced geothermal system. *GRC Trans.* **2009**, *33*, 199–204.
23. Ellsworth, W.L.; Giardini, D.; Townend, J.; Ge, S.; Shimamoto, T. Triggering of the Pohang, Korea, earthquake (Mw 5.5) by enhanced geothermal system stimulation. *Seismol. Res. Lett.* **2019**, *90*, 1844–1858. [CrossRef]
24. Hofmann, H.; Zimmermann, G.; Farkas, M.; Huegenes, E.; Zang, A.; Leonhardt, M.; Kwiatek, G.; Martinez-Garzon, P.; Bonhoff, M.; Min, K.-B. First field application of cyclic soft stimulation at the Pohang Enhanced Geothermal System site in Korea. *Geophys. J. Int.* **2019**, *217*, 926–949. [CrossRef]
25. Park, S.; Kim, K.I.; Xie, L.; Yoo, H.; Min, K.B.; Kim, M.; Yoon, B.; Kim, K.Y.; Zimmermann, G.; Guinot, F. Observations and analyses of the first two hydraulic stimulations in the Pohang geothermal development site, South Korea. *Geothermics* **2020**, *88*, 101905. [CrossRef]
26. Ree, J.H.; Kim, K.H.; Lim, H.; Seo, W.; Kim, S.; An, X.; Kim, Y. Fault reactivation and propagation during the 2017 Pohang earthquake sequence. *Geothermics* **2021**, *92*, 102048. [CrossRef]
27. Schindler, M.; Nami, P.; Schellschmidt, R.; Teza, D.; Tischner, T. Summary of hydraulic stimulation operations in the 5 km deep crystalline HDR/EGS reservoir at Soults-sous-Forets. In Proceedings of the 33th Workshop on Geothermal Reservoir Engineering, Stanford, CA, USA, 28–30 January 2008.
28. Baujard, C.; Genter, A.; Dalmais, E.; Maurer, V.; Hehn, R.; Rosillette, R.; Vidal, J.; Schmittbuhl, J. Hydrothermal characterization of wells GRT-1 and GRT-2 in Rittershoffen, France: Implications on the understanding of natural flow systems in the Rhine graben. *Geothermics* **2017**, *65*, 255–268. [CrossRef]
29. Huenges, E.; Holl, H.-G.; Bruhn, D.; Brandt, W.; Saadat, A.; Moeck, I.; Zimmermann, G. Current state of the EGS project Groß Schönebeck—Drilling into the deep sedimentary geothermal reservoir. In Proceedings of the European Geothermal Congress 2007, Unterhaching, Germany, 30 May–1 June 2007.
30. Moeck, I.; Holl, H.G. The stress regime in Rotliegend reservoir of the Northeast German Basin. *Int. J. Earth Sci.* **2009**, *98*, 1643–1657. [CrossRef]
31. Wójcicki, A.; Sowizdżał, A.; Bujakowski, W. *Ocena Potencjału Bilansu Cieplnego i Perspektywicznych Struktur Geologicznych dla Potrzeb Zamkniętych Systemów Geotermicznych (Hot Dry Rocks) w Polsce*; Ministerstwo Środowiska: Warsaw, Poland, 2013. (In Polish)
32. Schindler, M.; Baumgärtner, J.; Gandy, T.; Hauffe, P.; Hettkamp, T.; Menzel, H.; Penzkofer, P.; Teza, D.; Tischner, T.; Wahl, G. Successful hydraulic stimulation techniques for electric power production in the Upper Rhine Graben, Central Europe. In Proceedings of the World Geothermal Congress, Bali, Indonesia, 25–29 April 2010.
33. Leonhardt, M.; Kwiatek, G.; Martinez-Garzon, P.; Bonhoff, M.; Heikkinen, P.; Dresen, G. Seismicity during and after stimulation of a 6.1 km deep enhanced geothermal system in Helsinki, Finland. *Solid Earth* **2021**, *12*, 581–594. [CrossRef]
34. Kasza, P. Hydraulic fracturing in unconventional reservoirs and methods of their analysis. *Prace INiG-PIB* **2019**, *226*, 1–147. (In Polish)
35. Povilas, S.; Rasteniene, V.; Zinevicius, F. Geothermal Potential of Lithuania and Outlook for its Utilization. In Proceedings of the World Geothermal Congress 2000, Kyushu-Tohoku, Japan, 28 May–10 June 2000.
36. Zinevicius, F.; Sliaupa, S. Lithuania–Geothermal Energy Country Update. In Proceedings of the World Geothermal Congress 2010, Bali, Indonesia, 25–29 April 2010.
37. Zinevicius, F.; Sliaupa, S.; Mazintas, A.; Dagilis, V. Geothermal Energy Use in Lithuania. In Proceedings of the World Geothermal Congress 2015, Melbourne, Australia, 19–25 April 2015.
38. Zinevicius, F.; Sliaupa, S.; Mazintas, A.; Dagilis, V. Geothermal Energy Use, Country Update for Lithuania. In Proceedings of the European Geothermal Congress 2016, Strasbourg, France, 19–24 September 2016.
39. Zinevicius, F.; Sliaupa, S.; Mazintas, A.; Nika, N. Geothermal Energy Update–Lithuania. In Proceedings of the World Geothermal Congress 2021, Reykjavik, Iceland, 24–27 October 2021.
40. Rasteniene, V.; Puronas, V. Geothermal Atlas of Lithuania. In Proceedings of the World Geothermal Congress 2005, Antalya, Turkey, 24–29 April 2005.
41. Sliaupa, S.; Motuza, G.; Korabliova, L.; Ciuraite, K.; Puronas, V. Geothermal Potential of Hot Granites of Lithuania. In Proceedings of the World Geothermal Congress 2010, Bali, Indonesia, 25–29 April 2010.
42. Motuza, G.; Motuza, V.; Salnikova, E.; Kotov, A. Extensive charnockitic-granitic magmatism in the crystalline crust of West Lithuania. *Geologija* **2008**, *61*, 1–16. [CrossRef]

43. Povilanskas, R.; Satkunas, J.; Jurkus, E. Conditions for deep geothermal energy utilisation in southwest Latvia: Nica case study. *Baltica* **2013**, *26*, 193–200. [CrossRef]
44. Borodinecs, A.; Odineca, T.; Zajacs, A.; Migla, L.; Shutenkova, O. Review of the Geothermal Energy Potential in the Europe and Latvia. 2020. Available online: https://ieei.rtu.lv/rtuaer/files/Review%20of%20the%20geothermal%20energy%20potential%20in%20the%20Europe%20and%20Latvia.pdf (accessed on 10 December 2022).
45. Dreimanis, A.; Kārklin, O.L. Latvia. In *Encyclopedia of European and Asian Regional Geology*; Encyclopedia of Earth Science; Springer: Dordrecht, The Netherlands, 1997. [CrossRef]
46. Soesoo, A.; Nirgi, S.; Plado, J. The evolution of the Estonian Precambrian basement: Geological, geophysical and geochronological constraints. *Proc. Karelian Res. Cent. Russ. Acad. Sci.* **2020**, *10*, 18–33. [CrossRef]
47. Koppelmaa, H.; Klein, V.; Puura, V. Metamorfitsheskije kompleksii kristallitsheskogo fundamenta Estonii. In *Metamorfitsheskije kompleksii fundamenta russkoi plitii*; Dagelaiskii, V., Bondarenko, L., Eds.; Nauka: Leningrad, Russia, 1978; pp. 43–76. (In Russian)
48. Puura, V.; Vaher, R.; Klein, V.; Koppelmaa, H.; Niin, M.; Vanamb, V.; Kirs, J. *The Crystalline Basement of Estonian Territory*; Nauka: Leningrad, Russia, 1983; p. 208. (In Russian)
49. Nurmi, P.A. Preliminary Evaluation of the Estonian Geoenergy Potential and Overview of Available Technologies, Expert Opinion for Using Those Technologies in the Estonian Geological Conditions, Suggestions for Possible Further Actions and Examples of Case Studies. Technical Report. Tallin. 2021. Available online: https://www.researchgate.net/publication/352197150_Preliminary_evaluation_of_the_Estonian_geoenergy_potential_and_overview_of_available_technologies_expert_opinion_for_using_those_technologies_in_the_Estonian_geological_conditions_suggestions_for_possiblefurtheractionsandexamplesofcasestudies (accessed on 11 October 2022).
50. Eklund, O.; Soesoo, A.; Linna, A. *The Precambrian Rocks of Southern Finland and Estonia*; Institute of Geology at Tallinn University of Technology and University of Turku, Department of Geology: Tallin, Estonia, 2007.
51. Rämö, O.T.; Huhma, H.; Kirs, J. Radiogenic isotopes of the Estonian and Latvian rapakivi granite suites: New data from the concealed Precambrian of the East European Craton. *Precambrian Res.* **1996**, *79*, 209–226. [CrossRef]
52. Soesoo, A. *Geothermal Potential of Estonia*; Estonian Geothermal Association, Institute of Geology at TUT: Tallin, Estonia, 2012.
53. Kukkonen, I.; Jõleleht, A. Weichselian temperatures from geothermal heat flow data. *J. Geophys. Res. Atmos.* **2003**, *108*, 2163. [CrossRef]
54. Jõeleht, A. Estonia. In *Atlas of Geothermal Resources in Europe*; Hurter, S., Haenel, R., Eds.; Publication EUR 17811; European Commission: Brussels, Belgium, 2002; pp. 28–29.
55. Jõeleht, A. *Geothermal Heat Flow and Radiogenic Heat Production of Estonian Precambrian Basement*; Geological Survey of Estonia, Department of Marine Geology and Geophysics: Talinn, Estonia, 1994.
56. Joeleht, A.; Kukkonen, I.T. Thermal properties of granulite facies rocks in the Precambrian basement of Finland and Estonia. *Tectonophysics* **1998**, *291*, 195–203. [CrossRef]
57. Hurter, S.; Haenel, R. *Atlas of Geothermal Resources in Europe*; Leibniz Institute for Applied Geosciences, European Communities: Brussels, Belgium, 2002.
58. Kukkonen, I.T.; Pentti, M.; Heikkinen, P.J. St1 Deep Heat Project: Hydraulic stimulation at 5–6 km depth in crystalline rock. In Proceedings of the LITHOSPHERE Symposium, Virtual, 19–20 January 2021.
59. Kwiatek, G.; Saarno, T.; Ader, T.; Blueme, F.; Bohnhoff, M.; Chendorian, M.; Dresen, G.; Keikkinen, P.; Kukkonen, I.; Leary, P.; et al. Controlling fluid-induced seismicity during a 6.1-km-deep geothermal stimulation in Finland. *Sci. Adv.* **2019**, *5*, 7224. [CrossRef]
60. Farkas, M.P.; Hofman, H.; Zimmermann, G.; Zang, A.; Bethmann, F.; Cottrell, M.; Josephson, N. Hydromechanical analysis of the second hydraulic stimulation in well PX-1. *Geothermics* **2021**, *89*, 101990. [CrossRef]
61. Szewczyk, J.; Gientka, D. *Mapa Gęstości Ziemskiego Strumienia Cieplnego Polski*; Polish Geological Institute: Warsaw, Poland, 2009. (In Polish)
62. Szewczyk, J. Geophysical and hydrogeological aspects of utilization of thermal energy in Poland. *Przegl. Geol.* **2010**, *7*, 566–573. (In Polish)
63. Sowiżdżał, A.; Gładysz, P.; Pająk, L. Sustainable use of petrothermal resources—A review of the geological conditions in Poland. *Resources* **2021**, *10*, 8. [CrossRef]
64. Available online: http://geoportal.pgi.gov.pl/css/zrozum_z/images/podrecznik/gs/Rys_GS_wstep2.jpg (accessed on 30 December 2022).
65. Motuza, G.; Sliaupa, S.; Stephenson, R. Genesis of high intensity intracratonic heat flow anomalies: Case study of Western Lithuania. In Proceedings of the EGS-AGU-EUG Joint Assembly, Nice, France, 6–11 April 2003.
66. Eihmanis, E. Incorporation of Geothermal Heat Sources in Latvian heat Supply Systems. In Proceedings of the World Geothermal Congress 2000, Kyushu-Tohoku, Japan, 28 May–10 June 2000.
67. Chomać-Pierzecka, E.; Sobczak, A.; Soboń, D. The Potential and Development of the Geothermal Energy Market in Poland and the Baltic States—Selected Aspects. *Energies* **2022**, *15*, 4142. [CrossRef]
68. Joeleht, A.; Kukkonen, I. Physical properties of Vendian to Devonian sedimentary rocks in Estonia. *GFF* **2002**, *124*, 65–72. [CrossRef]
69. Górecki, W. (Ed.) *Atlas of Geothermal Resources in the Polish Lowlands*; AGH University of Science and Technology: Cracow, Poland, 2006.
70. Karwasiecka, M. The comparison of geothermal environment in the Upper Silesian Coal Basin and Lublin Coal Basin. *Geologia* **2008**, *34*, 335–357.

71. Miecznik, M.; Sowiżdżał, A.; Tomaszewska, B.; Pająk, L. Modelling geothermal conditions in part of the Szczecin Trough—The Chociwel Area. *Geologos* **2015**, *21*, 187–196. [CrossRef]
72. Buła, Z.; Żaba, J. Pozycja tektoniczna Górnośląskiego Zagłębia Węglowego na tle prekambryjskiego i dolnopaleozoicznego podłoża. In *Geologia i Zagadnienia Ochrony Środowiska w Regionie Górnośląskim*; Jureczka, J., Buła, Z., Żaba, J., Eds.; Polish Geological Institute, Polish Geological Society: Warsaw, Poland, 2005. (In Polish)
73. Tuuling, I. The Leba Ridge-Riga-Pskov Fault Zone—A major East European Craton interior dislocation zone and its role in the early Palaeozoic development of the platform cover. *Est. J. Earth Sci.* **2019**, *68*, 161–189. [CrossRef]
74. Brehme, M.; Nowak, K.; Banks, D.; Petrauskas, S.; Valickas, R.; Bauer, K.; Burnside, N.; Boyce, A. A Review of the Hydrochemistry of a Deep Sedimentary Aquifer and Its Consequences for Geothermal Operation: Klaipeda, Lithuania. *Geofluids* **2019**, *2019*, 4363592. [CrossRef]
75. Available online: https://otworywiertnicze.pgi.gov.pl/ (accessed on 30 December 2022).
76. Jarosiński, M. Współczesny reżim tektoniczny w Polsce na podstawie analizy testów szczelinowania hydraulicznego ścian otworów wiertniczych. *Przegląd Geol.* **2005**, *53*, 863–872. (In Polish)
77. Jarosiński, M. Recent tectonic stress field investigations in Poland: A state of the art. *Geol. Q.* **2006**, *50*, 303–321.
78. Śmigielski, M.; Koprianiuk, M. Współczesny reżim tektoniczny w Polsce na podstawie analizy testów szczelinowania hydraulicznego ścian otworów wiertniczych w Polsce–dyskusja. *Przegląd Geol.* **2006**, *54*, 126–128. (In Polish)

**Artykuł III: Charakterystyka petrofizyczno-geomechaniczna gorących suchych skał z perspektywicznych obszarów w Polsce.**

Advances in Geo-Energy Research

Vol. 14, No. 2, p. 90-105, 2024

Original article

# Dynamic elastic properties, petrophysical parameters and brittleness of hot dry rocks from prospective areas of Central Europe

Rafał Moska[1]*, Krzysztof Labus[2], Piotr Kasza[1]

[1] *Oil and Gas Institute-National Research Institute, Kraków 31-503, Poland*

[2] *Institute for Applied Geology, Silesian University of Technology, Gliwice 44-100, Poland*

**Keywords:**
Enhanced geothermal systems
hot dry rock
petrophysical parameters
mineral composition
hydraulic fracturing

**Cited as:**
Moska, R., Labus, K., Kasza, P. Dynamic elastic properties, petrophysical parameters and brittleness of hot dry rocks from prospective areas of Central Europe. Advances in Geo-Energy Research, 2024, 14(2): 90-105.
https://doi.org/10.46690/ager.2024.11.03

**Abstract:**
Enhanced geothermal systems in hot dry rocks are among the most promising sources of green renewable energy, with increasing interest in Central and Eastern Europe. The effective implementation of enhanced geothermal systems in new areas is based on the use of insights from ongoing projects, particularly in the study of petrophysical properties and reservoir stimulation technologies. This study aimed to characterize hot dry rocks in Central Europe by analyzing permeability, porosity, mineral composition, elastic properties, and brittleness index to assess their susceptibility to hydraulic fracturing. Drill core samples were collected from three formations: granites from the Karkonosze Mountains, volcanic rocks from the Gorzów Block, and tight sandstones from the Mogilno-Łódź Trough. The results indicated that the petrophysical properties and mineral compositions of these rocks are comparable to the corresponding Western European formations. Altered granites and some volcanic rocks showed significant decreases in wave velocities compared to intact samples, while sedimentary formation exhibited lower elastic moduli, indicating less favorable conditions for the development of the fracture network. Dynamic elastic tests suggested that brittleness index interpretation should differ between sedimentary and igneous hot dry rocks. In sedimentary formations, high brittleness index values indicate zones with elevated potential for complex fracture networks, aligning with the classic brittleness index concept. On the contrary, in igneous formations, low brittleness index values indicate zones of alteration and well-developed natural fractures, which are beneficial for hydroshearing stimulation.

## 1. Introduction

Ambitious EU climate neutrality plans have changed the European approach to energy production. The development of emission-free energy solutions including solar and wind power plants, biomass and geothermal power plants related to these ever tightening commitments was additionally accelerated by the emergence of the conflict in Ukraine, when European states leaders realized that even a temporary return to energy import from the east, in the near future, will be difficult to achieve. This complicated political and energy situation in Europe has resulted in strengthening the diversification of imports and energy production. One of the renewable energy branches that is currently accelerating is the obtaining energy from petrothermal resources, i.e., from deep impermeable or low permeable rocks, more commonly known as hot dry rocks (HDR) in geothermal systems of artificially increased permeability, known as enhanced geothermal systems (EGS). EGS have been known and developed throughout the world

*Corresponding author.
*E-mail address*: moska@inig.pl (R. Moska); krzysztof.labus@polsl.pl (K. Labus); kasza@inig.pl (P. Kasza).

Yandy Scientific Press

2207-9963 
Received July 10, 2024; revised August 5, 2024; accepted August 26, 2024; available online September 1, 2024.

since the 1970s (Tester et al., 2006; Moska et al., 2021). In Western Europe, primarily in France and Germany (Huenges et al., 2007; Blöcher et al., 2016; Vidal and Genter, 2018), petrothermal power plants supplied electricity and heat to the local grid for several years (BESTEC GmbH, 2024a, 2024b). In Central Europe, one of the first research projects on EGS were launched after 2010 in Poland, when the thermal balance potential of prospective geological structures for the needs of EGS was assessed (Wójcicki et al., 2013). In the next years, the state of knowledge was updated, and other prospective areas were considered (Sowiżdżał et al., 2021; Labus et al., 2023), as well as, preparation of the fracturing technology elements for selected areas is currently underway (Moska et al., 2021, 2023).

Extracting petrothermal energy from EGS, unlike conventional hydrothermal systems, requires hydraulic fracturing (HF) in the reservoir to create conductive fractures connecting injection and production wells. HF operations, as the reservoir stimulation methods have been widely known for over 70 years, however, since the 1970s they have also been used to create underground heat exchangers in HDR. The aim of HF in unconventional reservoir, e.g., shales, is to obtain the best possible connection between reservoir and wellbore, i.e., obtaining a high stimulation reservoir volume (King, 2010), to allow the gas to migrate from high volume of reservoir rock into well. In EGS, the purpose is to hydraulically connect two or more wells, to ensure economic and stable production, without causing premature cooling of the formation due to thermal short-circuiting (McClure and Horne, 2014). Unlike shale gas reservoirs, the main conductivity in HDR igneous formations is mainly provided by originally closed natural fractures (Tester et al., 2006; Baujard et al., 2017; Vidal and Genter, 2018). Naturally fractured rocks are characterized by a lower strength compared to the corresponding solid ones, resulting in lower breakdown pressure during stimulation treatment. Natural fractures are activated by shear forces in the hydroshearing mechanism, whereas other fracturing mechanisms are in minority and support the connecting of natural fractures by artificial ones (mixed stimulation mechanism) (McClure and Horne, 2014). The thermal contrast of the cold water pumped into the HDR reservoir causes the rock to contract, opening natural fractures. The vertical principal stress temporally decreases, which facilitates slippage on the fracture surface under the influence of horizontal stress. The fracture surfaces remain displaced and conductive without the use of proppant after pumping has stopped. There is also no risk of embedment phenomena, which can significantly reduce the conductivity of propped fractures in ductile rocks (Masłowski and Labus, 2021).

The design of HF is unique to the specific reservoir and well. The basic data necessary to complete the HF project include (Kasza, 2019):

1) Borehole data: Depth, well construction (wellhead parameters, pipe and cementing durability, drilling mud type), types of works, operations and measurements performed in the well.
2) Reservoir data: Rock porosity, permeability, thickness, temperature, pressure, saturation, rock mechanics properties, mineral composition, skin effect, and principal stresses.

Information about the mechanical properties of the reservoir rock, together with the state of stresses, allows to determine the energy needed to create or reopen the fracture, as well as its length and width. The Poisson's ratio ($v$) reflects the rocks' ability to fail under stress (Rickman et al., 2008). As the $v$ increases, the breakdown pressure and fracture closure pressure increase, thus the low $v$ rocks are easier to fracking. On the other hand, Young's modulus ($E$) describes the rocks' ability to maintain the fracture. As $E$ increases, the fracturing pressure and fracture length increase, whereas its width decrease. $E$ is used to calculate fracturing pressure and fracture height profile.

Susceptibility for HF in the reservoir can be described by brittleness index (BI) (Zhang et al., 2016). In oil and gas industry, BI is used to select the sweet spots-most promising intervals for perforation, mainly in the unconventional reservoirs (e.g., shales). A rock with a high BI, in general is characterized by properties that allow to create the relatively widespread network of fractures, defined by high stimulated reservoir volume parameter. Reservoir volume parameter is the volume of the hydraulically stimulated rock, calculated based on microseismic events recorded in monitoring wells (King, 2010).

The aim of this paper is to characterize HDRs in new prospective areas in Central Europe on the example of Poland, in terms of their petrophysical and mechanical properties in relation to HF operations, that could be performed in promising EGS projects in the future. Such a characterization, including petrophysical, petrographic parameters and HDR brittleness indices of Central Europe, has not been published before. The area of Poland is characterized by a high geothermal gradient compared the other countries of the south east Baltic basin, as well as relatively high heat flow anomaly (Moska et al., 2023). The geology of the country is also relatively well explored in terms of conventional geothermal energy, whereas preliminary research work on EGS has been carried out for several years (Górecki et al., 2013; Wójcicki et al., 2013; Moska et al., 2021; Labus et al., 2023). The work was prepared based on a review of the literature on research on EGS in Poland and Western Europe. HDR characterization based on laboratory measurement included main reservoir data needed for HF design, i.e., rock permeability and porosity, mineral composition, and rock elastic parameters determined using ultrasonic method in simulated reservoir conditions. Such a set of dynamic elastic data, supported by petrophysical and petrographic characteristics of new prospective areas, can constitute the basis for modeling the geometry of hydraulic fractures. Finally, a comparison between Western European and prospective Polish HDR parameters and indications concerning laboratory ultrasonic-based rock mechanics testing of HDR were formulated.

## 2. Materials and methods

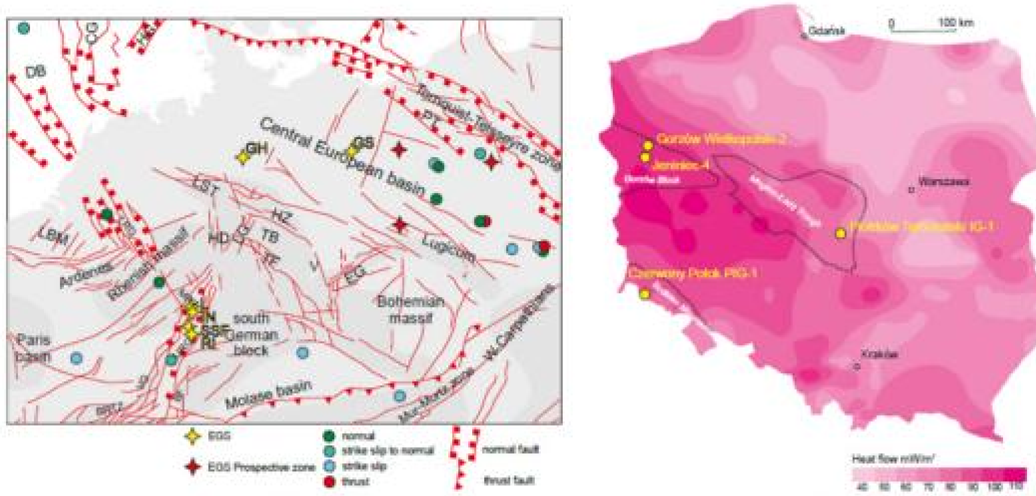


(a) (b)

**Fig. 1**. (a) Tectonic sketch map of Central Europe with recent tectonic regime in principal structural units and location of current and prospective EGS. Modified after (Grünthal et al., 2018). BF-black forest, BRTZ-Bresse-Rhine transitional zone, BF-Black Forest, BRTZ-Bresse-Rhine transitional zone, CG-Central Graben, DB-Doggerbank, EG-Eger Graben, HD-Hessian depression, HG-Horn Graben, HZ-Harz mountains, LBM-London-Brabant massif, LG-Leine Graben, LRG-Lower Rhine Graben, LST-Lower Saxonian tectogene, LU-Lugicum, MRZ-Middle Rhine zone, PT-Polish trough, TB-Thuringian basin, TF-Thuringian Forest, URG-Upper Rhine Graben, V-Vogtland, VG-Vosges, EGS: GH-GeneSys Hannover, GS- Groß Schönebeck, IN-Insheim, L-Landau, RI-Rittershoffen, SSF-Soultz-sous-Forêts and (b) location of the sampled boreholes in the background of the heat flow map of Poland. Yellow dots/description-boreholes; white dashed lines-boundaries of geological regions considered. Based on (Szewczyk and Gientka, 2009; Karnkowski, 2010).

## 2.1 Research area

Based on the literature, three prospective HDR were selected for this study: Karkonosze granitoid pluton of Pennsylvanian age, located in the Sudeten Mountains (Czech-Polish border), Permian volcanic rocks of the Gorzow Block German-Polish border, and Lower Triassic sedimentary formation of the Mogilno-Łódź Trough area (Central Poland) (Szewczyk and Gientka, 2009; Karnkowski, 2010; Wójcicki et al., 2013; Moska et al., 2021, 2023 Sowiżdżał et al., 2021; Labus et al., 2023) (Fig. 1). These sites are well documented geologically and are characterized by elevated Earth's heat flux, which results in elevated temperatures in target zones. The structures considered are situated at the depth of more than 4,000.0 m and characterized by typical HDR petrophysical parameters, including low porosity and permeability. Since the potential target zones in these structures were not previously accessible by deep drilling, it was decided to collect samples from shallower depths in existing wells. The Karkonosze granitoid, sampled in the Czerwony Potok PIG-1 (CP-1) borehole is represented by gray-pink, medium to coarse-crystalline granite, moderately fractured, with pegmatite veins. The volcanic rocks from the Gorzów Wielkopolski-2 (GW-2) and Jeniniec-4 (J-4) wells are red-pink and brownish rhyolites with white calcite veins. Sedimentary rocks from Piotrków Trybunalski IG-1 borehole (PT-1) are represented by fine to medium-grained, red and gray sandstones with subhorizontal lamination. The recent tectonic regime in the main structural units in Central Europe and the locations of the boreholes are presented in Fig. 1. Basic data regarding the samples are presented in Table 1, and the appearance of the rocks is shown in Fig. S1 in Supplementary file.

## 2.2 Sample preparation and characteristics

Cylindrical samples with a diameter of 2.54 cm (1 inch) and a length of 5.08 cm (2 inches) were cut from the drill cores in the vertical direction (along the borehole axis) to reflect the variation of vertical and horizontal stresses in triaxial rock mechanics tests (Fig. 2). Samples were cut out according to ISRM suggested method (Ulusay and Hudson, 2007).

## 2.3 The research cycle

The research was divided into the following stages (Fig. 3): Core sampling, basic petrophysical and petrological measurements, and ultrasonic core testing. The results can be used in HF projects in the areas considered, and they also provide the possibility of comparison with data from other EGS around the world.

### 2.3.1 Mineral composition

The mineral composition of the samples was determined based on the X-ray diffraction method using the D2 Phaser apparatus by Bruker (Germany)-(CuK$\alpha$ lamp, voltage 30 kV,

**Table 1**. Summary of data on the samples analyzed.

| No. | Location/Borehole | Depth intervals (m) | Number of samples | Stratigraphy | Litology |
|---|---|---|---|---|---|
| 1 | Karkonosze Mountains/Czerwony Potok PIG-1 | 137.80-183.86 | 38 | Pensylvanian | Granite |
| 2 | Gorzów Block/Gorzów Wielkolpolski-2, Jeniniec-4 | 3,348.0-3,356.0 | 8 | Rotliegend | Rhyolite |
| | | 3,264.0-3,277.0 | 11 | Rotliegend | Rhyolite |
| 3 | Mogilno-Łódź Trough/Piotrków Trybunalski IG-1 | 3,912.5-4,286.0 | 39 | Lower Triassic | Sandstone |

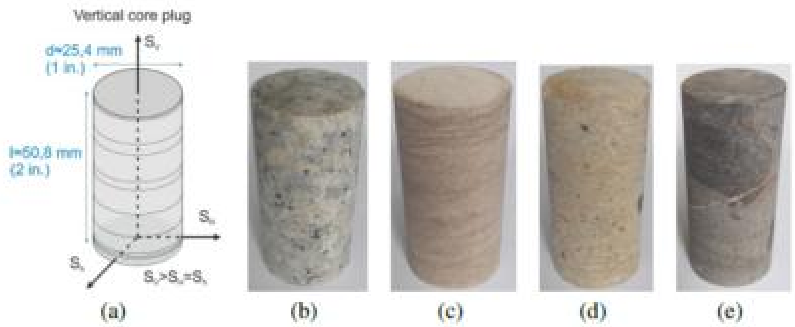


**Fig. 2**. (a) Dimensions of the sample. Samples were cut perpendicular to the lamination (along the borehole trajectory). $S_V$ is vertical principal stress, $S_H$ is maximum horizontal stress, $S_h$ is minimum horizontal stress. $S_V > S_H = S_h$ is extensional tectonic regime, conventional triaxial stress state. Samples prepared for laboratory tests: (b) granite, (c) sandstone, (d) and (e) rhyolite.

current 10 mA, 2Θ°-62°, step 0.020°. Quantitative analysis conducted using the Rietveld method was supported from HighScore Plus software by Malvern Panalytical (UK).

### 2.3.2 Effective porosity and density

Effective porosity is defined as the ratio of the pore volume of the rock to the total volume of the rock. The method used to measure the porosity coefficient does not take into account the morphology of the pore space and the separated pore space. The values presented in the paper were obtained by the HPG-100 helium porosimeter, from EPS (UK). The measurement consists of registering the pressure drop of a known volume of helium after it is injected into the chamber with the core sample. The grain density and the bulk density were calculated based on the effective porosity results.

### 2.3.3 Permeability

For each sample, the absolute nitrogen permeability was determined as the arithmetic mean of at least seven measurements of permeability at different inlet pressures (from lowest to the highest), with the input nitrogen pressure ranging from 1 to 7 bar. The determination coefficient $R^2$ for the set of at least 7 measurements was assumed to be at least 0.99. The permeability coefficient was determined using DGP-100, using the EPS (Aberdeen, UK) digital gas permeameter and calculated based on Eq. (1):

$$k = \frac{\mu_g Q_b P_b}{A} \frac{2l}{P_w^2 - P_b^2} \tag{1}$$

where $k$ is absolute permeability, mD; $\mu_g$ is nitrogen dynamic viscosity in test temperature, cP; $Q_b$ is nitrogen flow, ml/s; $P_w$ is inlet nitrogen pressure, atm; $P_b$ is outlet pressure, atm; $A$ is face area of the sample, cm$^2$; $l$ is length of the sample, cm.

### 2.3.4 Rock mechanics

Laboratory ultrasonic methods of the rock elastic parameter measurements has been known and used for several decades. Unlike classical methods of static stress and strain relations, elastic wave propagation is nondestructive and performed in reservoir conditions relatively well reflects the wireline acoustic logging. The differences are mainly in the frequency and in scale effect. Moduli from static tests can be converted into dynamic ones and vice versa. Correlations between these moduli have been developed and updated for years, according to the rock type and range of values (Davarpanah et al., 2020).

Ultrasonic velocities in the rock are influenced by numerous factors including: stresses, temperature, fluid saturation, anisotropy, wave frequency, and their combinations. In general, the velocity increases with confining pressure and differential pressure, where cracks and fractures play an essential role in this increase. Water saturation makes it difficult to compress the rock, which increases the velocity of the P-wave. Saturation does not affect the S-wave velocity, and the observed effect is due to the density of the rock. The velocity increases

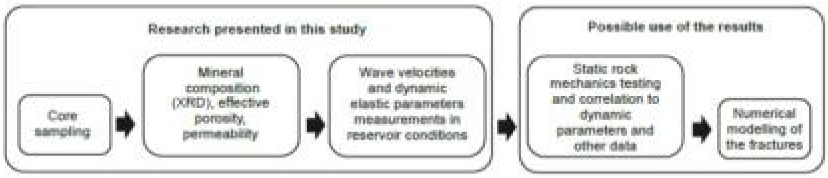


**Fig. 3**. Scheme of the research cycle.

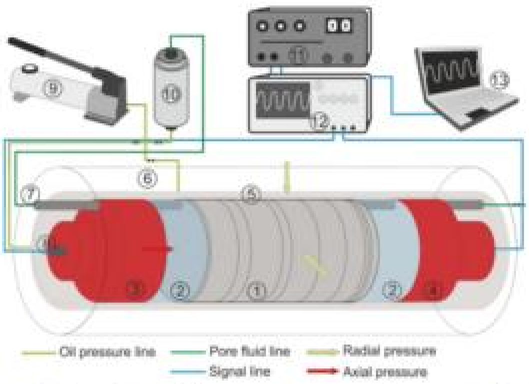


**Fig. 4**. Acoustic velocity system setup. 1-core sample, 2-titanium spreader, 3-piston/transmitter, 4-receiver, 5-rubber sleeve, 6-core holder, 7-pore pressure inlet, 8-wireline inlet, 9-hand pump, 10-pressure accumulator, 11-pulser, 12-oscilloscope, 13-data acquisition.

with the viscosity of the pore fluid. Anisotropic grain arrangement, lamination or preferred cracks and fractures orientation cause velocities to vary depending on direction. An increase in temperature by 100 °C causes a decrease in velocity by only a few percent. The velocity depends on frequency in an attenuating medium and thus increases slightly with it (Bourbié et al., 1987).

Rock mechanics experiments were carried out on the Acoustic Velocity System AVS-700 by Vinci (France), a device for determining the velocities of elastic waves in reservoir conditions (Fig. 4). The device is equipped with piezoelectric transducers, operating at a frequency of 500 kHz, generating and receiving longitudinal (P) and shear (S) waves. Core samples were tested under conventional triaxial conditions, at temperatures up to 140 °C and pore pressures up to 55 MPa.

Based on waves velocities, the dynamic elastic parameters are calculated using:

$$\nu = \frac{\frac{1}{2} - (\frac{V_S}{V_P})^2}{1 - (\frac{V_S}{V_P})^2} \tag{2}$$

$$E = \rho \frac{V_P{}^2(1+\nu)(1-\nu)}{(1-\nu)} \tag{3}$$

$$G = \rho V_S{}^2 \tag{4}$$

$$K = \rho \left(V_P{}^2 - \frac{4}{3} V_S{}^2\right) \tag{5}$$

where $V_P$ is P-wave velocity, m/s; $V_S$ is S-wave velocity, m/s; $\nu$ is Poisson's rato; $E$ is Young's modulus, GPa; $\rho$ is bulk density, g/cm$^3$; $G$ is shear modulus, GPa; $K$ is bulk modulus, GPa.

For the purpose of this paper, based on the data presented by Wójcicki et al. (2013), the following depths of HDR target zones were assumed: granite of Karkonosze Mountains-4,000 m, rhyolite from Gorzów Block-4,300 m and sandstone from Mogilno-Łódź Trough area-5,000-6,500 m. The tectonic regime in Poland, according to literature (Jarosiński, 2005; Zuchiewicz et al., 2007; Moska et al., 2021) can be assumed as normal with strike-slip component or strike slip, which means that in the first case the principal vertical stress $S_V$, exceeds the maximum horizontal stress $S_H$, where the difference between $S_H$, and $S_H$, could be relatively small, and in second case, maximum horizontal stress $S_H$ exceeds vertical stress $S_V$. Due to the fact, that rocks at these depths have not been drilled so far, and reservoir or tectonic data are not available, it was assumed that the average rock density is 2.4 g/cm$^3$ (Jarosiński, 2005). Therefore, the vertical principal stress $S_V$ is equal to: 96 MPa, 103 MPa and 120-156 MPa for the Karkonosze Mountains, Gorzów Block and Mogilno-Łódź Trough areas, respectively. Temperatures at the target zone depths, based on heat flux density in Poland (Wójcicki et al., 2013), were assumed to be 165, 160 and 165-195 °C for the respective areas mentioned above. Since the assumed pressure and temperature exceeds the maximum measuring ranges of the laboratory rock mechanics setup used in our experiments, it was decided that the ultrasonic tests would be performed to the maximum capabilities of the device.

The testing methodology was adopted to enable comparison with the static stress-strain tests. Since the deposition depth and tectonic conditions of tested HDR were determined based on the assumptions, ultrasonic tests were performed under a wide range of pressure conditions, from ambient to reservoir conditions. Samples were tested under dry conditions, therefore, confining pressure equaled effective pressure. The methodology was adopted from the proposed methods to determine the strength of rock materials in triaxial compression (Ulusay and Hudson, 2007). At first, axial and radial stresses of 15 and 30 MPa were applied under hydrostatic conditions, then axial stresses, were increased. In hydrostatic conditions, axial and radial pressures were applied simultaneously, from ambient pressure to 55 MPa (Fig. 5). For each radial pressure condition, i.e., 15, 30 and 55 MPa, measurements of at least four samples were performed. Each core sample was used for testing and compressed only once (first load test). A total of 64 samples were tested.

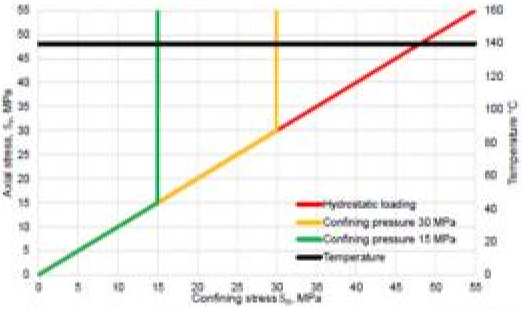


**Fig. 5**. Scheme of pressure-temperature conditions in ultrasonic measurements.

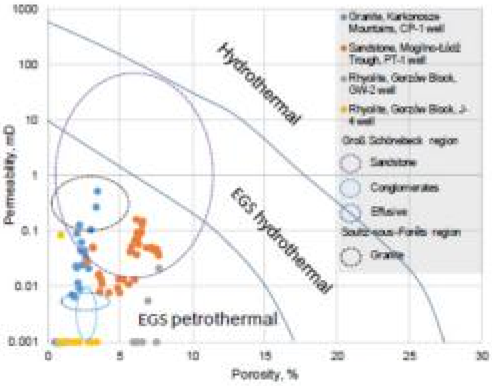


**Fig. 6**. Permeability-porosity-based classification of the geothermal rocks analyzed, compared to other European formations. Based on Surma and Geraud (2003); Sausse et al. (2005); Moeck (2014); Sowiżdżał et al. (2022).

### *2.3.5 Brittleness calculation*

Rock brittleness is an important rock property related to the behavior of rocks during fragmentation and the energy consumption in this process. The definition of BI, an important parameter for characterizing the fragility of a rock mass has changed over the years. The concepts were based on stress-strain (Andreev, 1995), energy balance analyzes (Tarasov and Potvin, 2013), Lame's parameter $\lambda\rho$-$\mu\rho$ crossplot studies (Goodway et al., 2010) and the composite method (Mullen and Roundtree, 2007). However, currently the most popular BI definitions are based on: relationship of brittle and ductile minerals in mineral composition (Jarvie et al., 2007; Wang and Gale, 2009; Jin et al., 2014a, 2014b), and relationship of Young's modulus to Poisson's ratio of the rock (Grieser and Bray, 2007; Rickman et al., 2008; Wu et al., 2019; Moska et al., 2021). The mineral composition BI concept is based on distinction between brittle (the most frequent quartz and dolomite) and ductile minerals content (clay minerals, calcite and total organic carbon). Mineral BI may vary significantly for the same rock depending on the adopted BI definition:

$$\mathrm{BI}_{\mathrm{Jarvie}} = \frac{Q}{Q+D+C+C_l} \tag{6}$$

$$\mathrm{BI}_{\mathrm{Wang}} = \frac{Q+D}{Q+D+C+C_l} \tag{7}$$

$$\mathrm{BI}_{\mathrm{Jin}} = \frac{Q+P_l+K_f+M+C+D}{T} \tag{8}$$

where BI is brittleness index; the symbols correspond weight fraction of: $Q$ is quartz, $D$ is dolomite, $C$ is calcite, $C_l$ is clay minerals, $P_l$ is plagioclase, $K_f$ is potassium feldspar, $M$ is brittle mica, $T$ is weight fraction of total minerals.

The mineral BI is in range between 0 and 100, where values near 0 correspond to purely ductile rock, and near 100 mean purely brittle.

The clearer result is provided by BI based on $E$ and $\nu$ parameters. In this case, the key to determine reference minimum and maximum $E$ and $\nu$ values in relation to all rocks found in nature:

$$\mathrm{BI}_{\mathrm{Grieser}} = \frac{\mathrm{YM}_{\mathrm{BI}}+\mathrm{PR}_{\mathrm{BI}}}{2} \tag{9}$$

where

$$\mathrm{YM}_{\mathrm{BI}} = \frac{\mathrm{YM}-\mathrm{YM}_{\mathrm{min}}}{\mathrm{YM}_{\mathrm{max}}-\mathrm{YM}_{\mathrm{min}}} \times 100\% \tag{10}$$

$$\mathrm{PR}_{\mathrm{BI}} = \frac{\mathrm{PR}-\mathrm{PR}_{\mathrm{max}}}{\mathrm{PR}_{\mathrm{min}}-\mathrm{PR}_{\mathrm{max}}} \times 100\% \tag{11}$$

where $\mathrm{YM}_{\mathrm{BI}}$ is BI from $E$, $\mathrm{PR}_{\mathrm{BI}}$ is BI from $\nu$, YM is measured $E$, PR is measured $\nu$. $\mathrm{YM}_{\mathrm{min}}$, $\mathrm{YM}_{\mathrm{max}} \in [0,10]$ and $\mathrm{PR}_{\mathrm{min}}$, $\mathrm{PR}_{\mathrm{max}} \in [0,0.5]$.

$\mathrm{YM}_{\mathrm{min}}$, $\mathrm{YM}_{\mathrm{max}}$, $\mathrm{PR}_{\mathrm{min}}$, and $\mathrm{PR}_{\mathrm{max}}$ are constants, defining minimum and maximum values of obtained results, which corresponds to values from 0 to 10 Mpsi (0-68.95 GPa) for $E$ and from 0 to 0.5 dimensionless for $\nu$. $\mathrm{BI}_{\mathrm{Grieser}}$ is in the range between 0 and 70, where values near zero means fully ductile rock, whereas near 70 fully brittle rock. The key factor for a proper estimation of BI is to adopt the minimum and maximum values of $E$ and $\nu$ to compare the rocks witch each other. Some authors suggest using other reference point values (Rickman et al., 2008): $\mathrm{YM}_{\mathrm{min}}$, $\mathrm{YM}_{\mathrm{max}} \in [1,8]$ (Mpsi) (6.895, 55.16 GPa) and $\mathrm{PR}_{\mathrm{min}}$, $\mathrm{PR}_{\mathrm{max}} \in [0.15, 0.4]$:

$$\mathrm{BI}_{\mathrm{Rickman}} = \frac{50}{7}(E-28\nu+10.2) \tag{12}$$

Wu et al. (2019) proposed narrower values, however they analyzed BI of the steam coal samples, which can be considered as a special case. Regardless of the method of BI definition, brittle rocks typically exhibit a unique set of features including low elongation upon load application, higher ratio of compressive strength to tensile strength, and higher internal friction angles, which favors the formation of extensive fracture networks in such rocks (Zhang et al., 2016). Therefore, BI can be used to compare rocks of the same type from different locations, in terms of their elastic features connected with susceptibility to fracking. This group also includes HDR, both igneous, and sedimentary formations similar to tight gas sandstones.

Despite the confirmed usefulness of BI in shale gas deposits, some authors noted that this parameter may not be appropriate for characterizing the brittleness of other rocks in certain circumstances, and its definition is imprecise (Her-

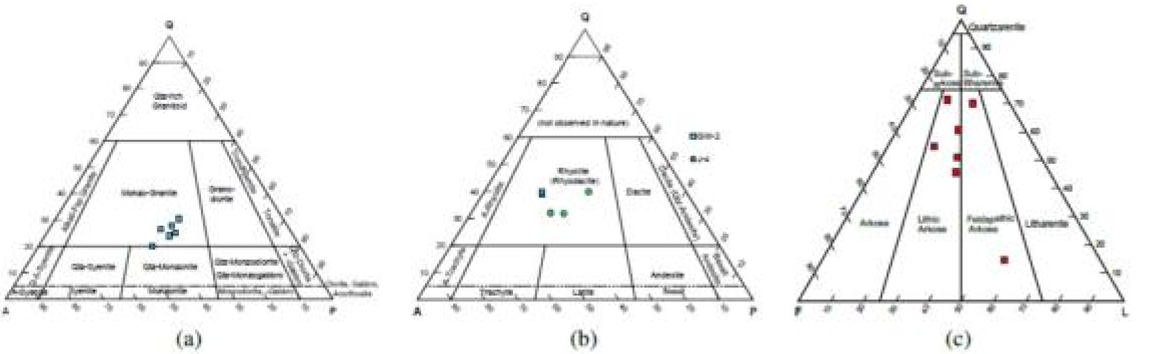

**Fig. 7**. Samples from: (a) The Karkonosze Mountains (CP-well) in the background of the QAP classification diagram, (b) the Gorzów Block (GW-2 and J-4 wells) in the background of the QAPF volcanic classification diagram and (c) the Mogilno-Łódź Trough area (PT-well) in the background of the QFL classification diagram.

wanger et al., 2015; Holt et al., 2015). Bai (2016) points out that brittle formations do not equate to formations that are easier to fracture, since the brittle rocks may have greater strength under higher confinement, i.e., are more difficult to fracture, and vice versa. The brittleness and ductility of the formation also cannot be related to the $E$ and $v$ parameters, since uniaxial compressive strength or fracture toughness gives better relation.

HDR differs significantly from unconventional shale or tight gas deposits. In HDR, especially granite, the major role in conductivity between wells is played by natural fracture zones, which can be stimulated (artificially widened and enlarged) in the hydroshearing mechanism. The strength of these zones, measured as uniaxial compressive strength, can be critically lower than that of the surrounding unfractured rocks. BI based on the $E$ to $v$ ratio can account for natural fracture zones, if the data used are from a sonic log performed in fractured and unfractured interval. If the data come from a laboratory small-scale sample rock mechanics testing, the influence of natural fracture zones can be harder to determine due to difficulties in collecting samples with fractures, as well as in the testing itself.

This article presents selected methods for calculating the BI index based on minerals and the $E$ to $v$ ratio, developed by various authors. In order to compare the obtained results with each other and compare with the presented literature data, methods suggested by Grieser and Bray (2007); Jarvie et al. (2007); Rickman et al. (2008); Wang and Gale (2009); Jin et al. (2014a, 2014b) were used.

## 3. Results and discussion

### 3.1 Permeability, porosity and density measurements

Rocks tested at all locations are characterized by low effective porosity and permeability. Granite from Karkonosze Mts., as well as rhyolite from J-4 well in Gorzów Block area have the lowest porosity. The calculated average porosity in this case is mainly natural cracks and fractures, and to a much lesser extent the porosity of the skeleton. The intergranular porosity in the sandstones of the Mogilno-Łódź Trough and rhyolite from GW-2 well in the Gorzów Block translates into relatively small differences between the minimum and maximum values obtained (Table S1, in Supplementary file). The average permeability values of all the rocks tested are significantly below 0.1 mD, and in the case of intrusive and volcanic rocks most of the samples showed permeability below the lower measurement range (0.001 mD). Bulk densities correspond to the literature values for relevant rock formations (Bourbié et al., 1987; Pława and Plewa, 1992). The petrophysical parameters allow to classify all investigated rocks to petrothermal formations (Fig. 6). Granite from Karkonosze Mts. have slightly lower permeability compared to the average corresponding values of Soultz-sous-Forêts Carboniferous granite basement. Sandstones from Mogilno-Łódź Trough are characterized by relatively narrow distribution of parameters, compared to sandstones from Groß Schönebeck, where the permeability falls in the wide range of 0.01 to 100 mD (Fig. 6).

### 3.2 Mineral composition measurements

Fig. 7 describes the location of granite, rhyolite and trachyandesite samples on the QAP diagram, as well as sandstone samples on the QFL diagram. Statistical parameters of the mineral composition can be seen in the Table S2 in Supplementary file.

The Karkonosze granitoid pluton in the Sudeten Mountains was formed in the Variscian orogeny 300-350 million years ago. Samples collected from depth from 138.0 to 184.0 m, represent a K-feldspar granite (Fig. 7(a)), where the dominant role in mineral composition is played by albite (average 33.1%) together with orthoclase and microcline (average 15%-19%, respectively). The average quartz content is 23% biotite, illite, kaolinite and chlorite are in the minority. Volcanic rocks from Gorzów Block are mainly built of quartz (average from 22% to 38% for J-4 and GW-2 wells respectively) and K-

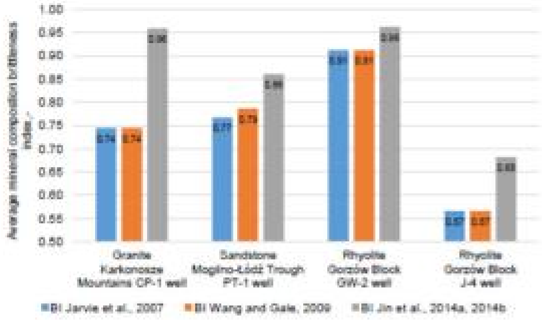


**Fig. 8**. Average mineral brittleness (BI) of the samples.

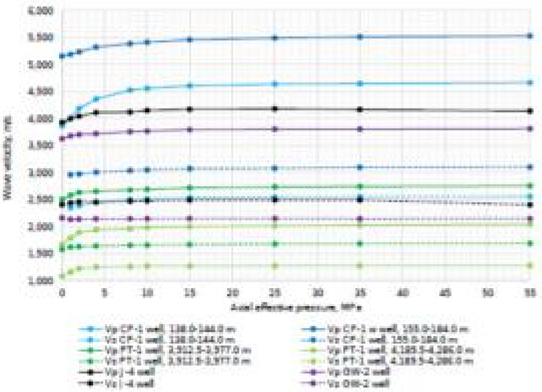


**Fig. 9**. Average compressional ($V_P$) and shear ($V_S$) wave velocities versus axial effective pressure for Karkonosze Mountains granite (CP-1 well), Mogilno-Łódź Trough sandstones (PT-1 well), and Gorzów Block rhyolite (GW-2 and J-4 wells), measured in triaxial conditions. 138.0-144.0 m; 155.0-158.0 m–depth intervals of granite samples collected. 3,912.5-3,977.0 m; 4,189.5-4,286.0 m–depth intervals sandstone samples collected.

feldspar (orthoclase for GW-2 well and microcline for J-4 well, 41% and 24% in average respectively), which allows them to be classified in the QAPF volcanic diagram as rhyolite and rhyodacite (Fig. 7(b)). They also contain plagioclase (albite), clay minerals and others (Table S2, in Supplementary file). Lower Triassic sandstones from Mogilno-Łódź Trough contain mainly quartz (52% in average) and plagioclase (albite, 14% in average). They are characterized by a small amount of carbonates, while clay minerals content (especially illite) reaches a dozen percent (14% in average). These sandstones can be classified as lithic arkose and feldspathic litharenite in QFL diagram (Fig. 7(c)).

Fig. 8 shows a high mineral BI for all types of the considered rocks, except for rhyolite from J-4 well, for which BI can be described as average. Regardless of the calculation method used, the BI for granites and sandstones exceeds 0.7, reflecting the high content of brittle minerals, especially albite, microcline and quartz in granites, quartz, potassium and alkali

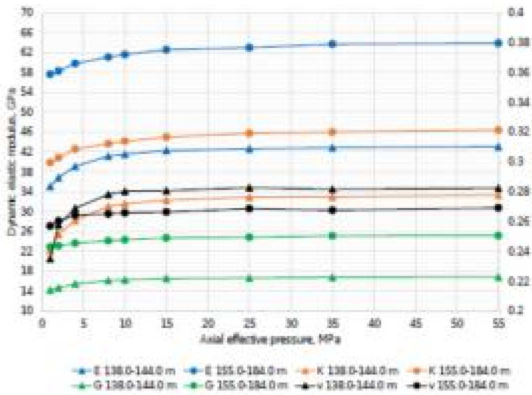


**Fig. 10**. Average dynamic elastic parameters versus axial effective pressure for the Karkonosze Mountains granite (CP-1 well), measured under triaxial conditions. 138.0-144.0 m; 155.0-158.0 m-depth intervals of the samples collected. *E*, *K*, *G*-dynamic Young's, bulk, shear modulus respectively, $\nu$-dynamic Poisson's ratio.

feldspar in sandstones, and quartz and alkali feldspar in rhyolite from GW-2 well. It can be seen that method presented by Jarvie et al. (2007) and the computational methods showed by Wang and Gale (2009) give very similar results for the rocks considered. Noticeably higher BI values were obtained using the equation of Jin et al. (2014a, 2014b), which results from the highest content of minerals defined as brittle. However, it should be remembered that all applied computational methods were originally developed for sedimentary rocks, and therefore may not fully reflect the variability of the mineral BI of the considered formations. Mineral BI in HDR should rather be used to compare the susceptibility for fracking in the fracture initiation phase, of similar formations types from different depths or wells.

### 3.3 Ultrasonic measurements

Figs. 9-12 show average propagation velocities of compressional and shear waves and the average dynamic elastic parameters versus axial effective pressure for all samples tested under triaxial conditions. The granite and sandstone samples were taken from a relatively wide depth interval, resulting in significant variability in the ultrasonic properties of these rocks. For this reason, no correlation of the P- and S-wave velocities with the applied radial pressure from 15 to 55 MPa was observed. Such relationships could be observed if individual samples were very similar in terms of structure and mineral composition. Therefore, it can generally be expected that an increase in radial confining pressure causes an increase in the P- and S-wave velocities (Bourbié et al., 1987). Due to the observations described above and the small number of the samples, it was decided to determine average velocity curves and dynamic elastic parameters for all samples of a given rock, tested in triaxial conditions, i.e., for 15, 30 and 55 MPa radial confining pressure. Therefore, each curve of velocity and elastic parameters for granite (Figs. 9 and 10) and sandstone (Figs. 9 and 11) represents the average of the corresponding parameters

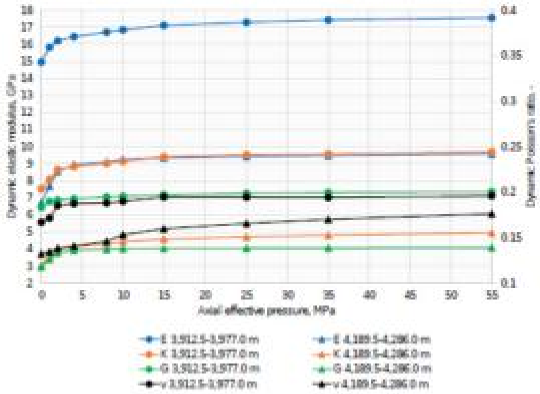


**Fig. 11.** Average dynamic elastic parameters versus axial effective pressure for Mogilno-Łódź Trough sandstones (PT-1 well), measured under triaxial conditions. 3,912.5-3,977.0 m; 4,189.5-4,286.0 m-depth intervals of samples collected. *E*, *K*, *G*-dynamic Young's, bulk, shear modulus respectively, *v*-dynamic Poisson's ratio.

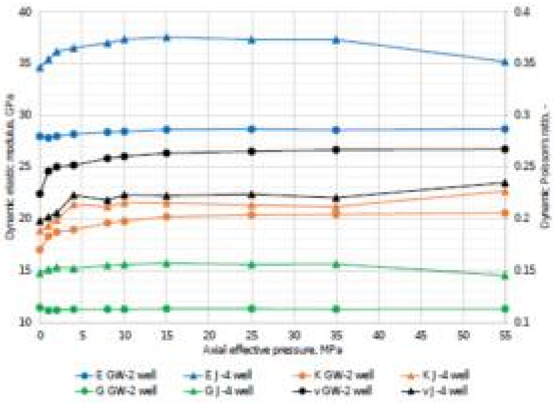


**Fig. 12.** Average dynamic elastic parameters versus effective axial pressure for Gorzów Block rhyolite (GW-2 and J-4 wells), measured under triaxial conditions. *E*, *K*, *G*-dynamic Young's, bulk, shear modulus respectively, *v*-dynamic Poisson's ratio.

of at least five samples, measured at the three mentioned three values of radial confining pressure. In the case of rhyolite from the GW-2 and J-4 wells (Figs. 9 and 12), each curve is the average of relevant parameters from at least two samples. Additionally, granite and sandstone samples were divided into two groups in terms of sampling depth and related P-wave velocities.

The variability of wave velocities depending on the sampling depth is shown in Fig. 9. Granite samples collected from the 155.0-184.0 m interval are characterized by higher P- and S-wave velocity and dynamic elastic moduli. This can be explained by a lower alteration and a lower number of natural cracks and fractures in the deeper interval. The highest increases in velocities and moduli are observed at low values of effective pressure as a result of the gradual closing of the pore space in rock samples. Above an effective pressure of 15 MPa, the velocity increase slows down and eventually flattens out, due to the higher bulk modulus of the grain skeleton with a closed pore space. Also, the sandstones show strong variability with depth. In this case, the higher waves velocities and elastic moduli for the shallower samples are probably due to variability in mineral composition. Samples from the 3,912.5 to 3,997.0 m interval are characterized by an elevated amount of quartz and a lower content of illite. The relatively low value of *v* (below 0.2) is probably related to minimal saturation of the samples (measured under dry conditions). The rhyolite of the GW-2 well, consisting of 95% quartz and feldspar, exhibits lower velocities compared to the rhyolite of the J-4 well, probably due to its higher porosity (6%-8%). In the rhyolite of the J-4 well, a decrease in velocity is clearly visible, after exceeding the axial pressure of 25 MPa for the P wave and 35 MPa for the S-wave. This behavior can be associated with microcracking of the matrix (groundmass), which is the beginning of sample disintegration. The decrease in velocities reflects lowered *E* and *G* moduli, which for the maximum axial pressure reach values similar to those for ambient pressure. At the same time, an increase in *v* is recorded, which reflects an increase in radial deformation compared to the axial deformation. A summary of data from ultrasonic tests, including minimum, maximum, and average wave velocities and elastic parameters of measured samples is presented in Table S3 in Supplementary file.

Fig. 13 presents a cross plot of *E* and *v* of measured samples. A relatively low *v* of sandstones from both intervals of the PT-1 well is visible, corresponding to their low *E*. This is reflected in the lowest BI value compared to the other rock types studied-Fig. 14. Granites are characterized by high BI due to the relatively high level of *E*, while in the rhyolite group the variability depends on the drill hole considered. The relatively low ductility, low matrix permeability and presence of natural fractures in granite, and rhyolite from J-4 well allow to consider slickwater or fresh water with shale inhibitor as a fracturing fluid, which would be consistent with the common trend of fracking in plutonic and volcanic rocks (Tester et al., 2006; Blöcher et al., 2016; Moska et al., 2021). Open fractures in these types of rocks exhibit self-propping capacity due to the hydroshearing mechanism. Fracking such rocks may not require the use of any type of proppant material or any fluids to transport it. The selection of fracturing fluid for the tested sandstones requires taking into account the proppant material, which involves considering the main fracturing fluid as a polymer-based, linear, or cross-linked gel, similar to the fluids used in the sedimentary intervals of the Groß Schönebeck project (Blöcher et al., 2016).

The correlation plots for the parameters of the tested rocks are shown in the Fig. 15. As the effective porosity decreases, the wave velocities increase, which corresponds to the increase of elastic moduli. Granites and rhyolites from the GW-2 well show the highest coefficient of determination (0.90 and 0.78, respectively, for the P-wave linear regression model; 0.68 and 0.81, respectively, for the S-wave). An increase in the effective

Załącznik: Artykuł III



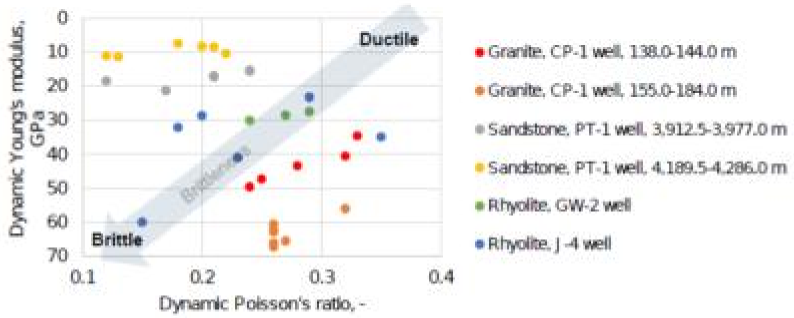


**Fig. 13**. Cross plot of dynamic Young's modulus and dynamic Poisson's ratio of measured samples, showing brittleness increasing towards the southeast corner of the plot.

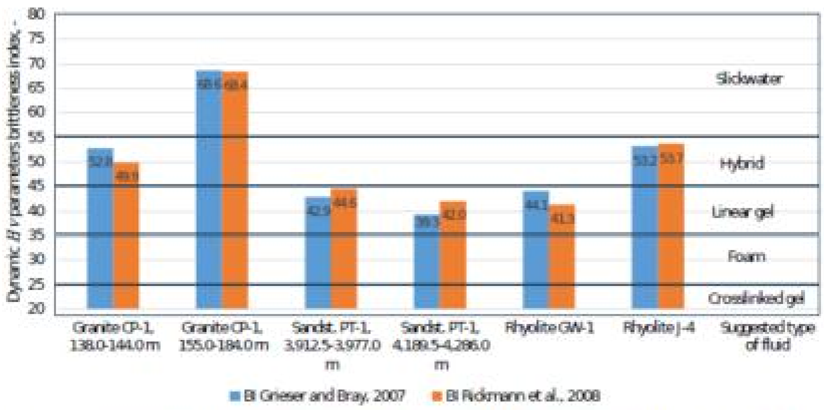


**Fig. 14**. Dynamic $E$ to dynamic $\nu$-based BI of measured samples, based on methods by Rickman et al. (2008) and Grieser and Bray (2007). In the method by (Rickman et al., 2008) the following values $YM_{max} = 10$ Mpsi (68.95 GPa) and $PR_{min} = 0.12$ were used to fit to parameters of measured samples. Suggested types of fracturing fluid correspond only to the results calculated according to Rickman et al. (2008).

porosity of dry rock leads to a decrease in the dynamic elastic moduli and strength of the rock. A reduction in $E$ in the igneous HDR is usually the indicator of altered or naturally fractured zone, which may be desirable for hydroshearing stimulation. Reduced E in sedimentary HDR is rather undesirable as it leads to a reduction the fracture lengths and overall tendency to produce less-developed fracture networks.

For over 30 years, several EGS projects have been developed in Western Europe (Batchelor, 1987; Wallroth et al., 1999; Blöcher et al., 2016; Kukkonen and Pentti, 2021). Most of them started as research projects, but only a few have reached the stage of application in the energy sector. Due to their research purpose, these projects are usually well described in the literature. The published data generally concern the results of stimulation and well tests, seismic monitoring, and to a lesser extent, information from laboratory core measurements, including petrophysical and geomechanical studies. In most projects, laboratory geomechanical ultrasonic tests were not performed at all or their results were not published. Therefore, in this paper, we compared our new results with published data, being aware, that differences in methodology may generate difficulties in the comparisons.

All lithological types examined in this study can be classified as petrothermal formations (Fig. 6). The Karkonosze Mts. granites are characterized by lower permeability than the Soultz granite, for which the average permeability obtained from modeling, based on well logging, ranges from 0.1 to 1.0 mD. In both cases, depth variability is visible, depending on the mineral composition and the development of natural fractures. The sandstones of the Mogilno-Łódź Trough are characterized by permeability in the range of approx. 0.01-0.1 mD and an average porosity of 0.055, which corresponds to the lower limit of the permeability range and average porosity of sandstones of the German Basin, presented in literature (Moeck, 2014; Sowiżdżał et al., 2022). Rhyolite samples, regardless of their porosity show permeability below 0.001 mD which is slightly lower than effusive the rocks from the Groß Schönebeck area (Sowiżdżał et al., 2022).

Comparing the Karkonosze granites in terms of mineral composition with their Western European counterparts is difficult due to the large variation in mineral composition within a single formation. Although the main granite body

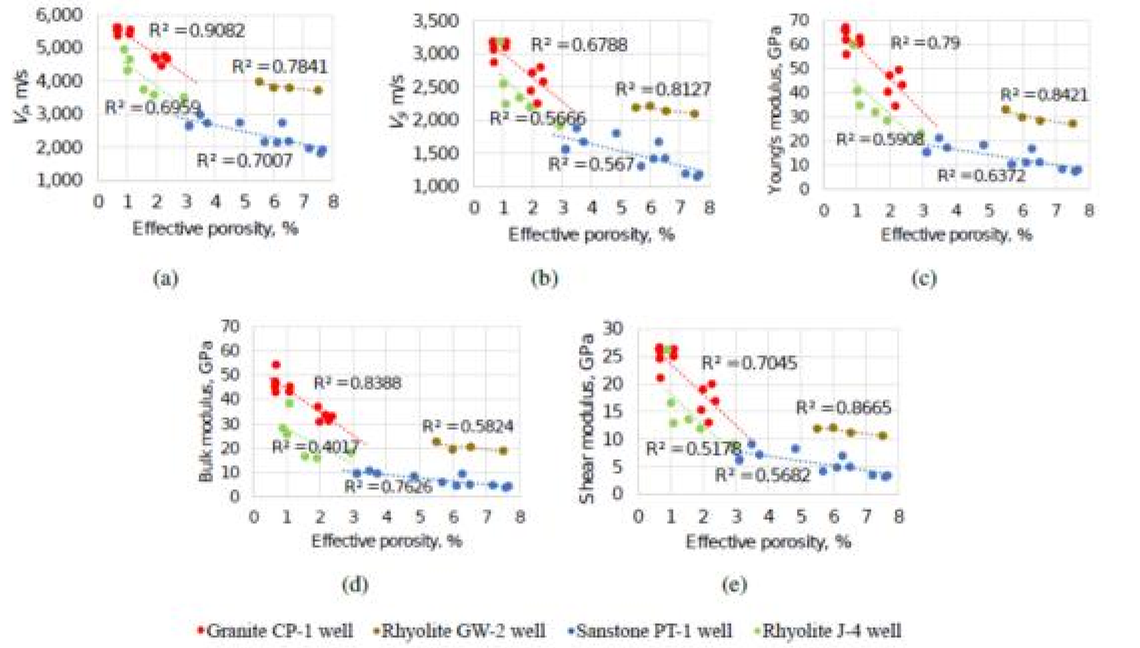


**Fig. 15**. Linear regression models for P-(a), S-(b) wave velocity, (c), (d), (e) dynamic elastic moduli and effective porosity of measured samples.

in Soultz is characterized by a low clay content (Table S4, in Suppementary file), some of its zones are highly modified. For example, in the GPK1 well in Soultz, several zones of anomalous mineral composition were identified, i.e., clay-rich fractured and altered zones of increased potassium, or leucogranitic dikes with elevated uranium and potassium content (Sausse, 2002; Sausse et al., 2006). Zones of increased clay mineral content corresponding to fractured zones can be prospective for conductivity in EGS. In the conditions of the Karkonosze Mountains, it can be assumed that zones of a similar nature may be promising. Samples taken from a depth of 138.0-144.0 m, in which a greater number of fractures and greater alteration were found, contained an increased amount of clay minerals, especially kaolinite, illite, and chlorite. These samples are characterized also by significantly lower wave velocities-reflecting lower mechanical strength. Such zones, which can occur at greater depths with higher temperatures, may form conducting arteries after hydraulic stimulation.

Similarly to granites from Karkonosze Mts., examined sandstones from Mogilno-Łódź Trough and rhyolite from Gorzów Block are difficult to compare directly. EGS's in sedimentary and volcanic rocks are a minority, and the only projects in Europe in this type of formations are Genesys in Hannover and Groß Schönebeck near Berlin (Tischner et al., 2013; Blöcher et al., 2016). While in Genesys the target formation was Middle Buntsandstein (Volpriehausen sequence), in the Groß Schönebeck project, the target is Upper/Lower Rotliegend (Dethlingen formation). The formation in Groß Schönebeck can be treated analogously to the Rotliegend in the Gorzów Block. Data on the mineral composition of volcanites from the GT GrSK well in the Groß Schönebeck area are limited, but they are generally referred to as andesites in which permeability is mainly related to natural fractures (Zimmermann et al., 2010). They consist mainly of quartz and plagioclase, with small amounts of mica, carbonates, and chlorite (Table S4, in Suppementary file).

The sedimentary cover in Dethlingen is represented by well-sorted, medium- to fine-grained, poorly cemented sandstones (Zimmermann et al., 2010). Regional data for this formation characterize it as having a medium-high quartz content and significant carbonate content, while K-feldspar and plagioclase are in the minority (McCann, 1998) (Table S4, in Supplementary file). No information was found on the average content of clay minerals. Compared to these rocks, the examined sandstones from Mogilno-Łódź Trough contain lower amounts of quartz and carbonates, but an increased content of feldspar. The content of clay minerals does not exceed several percent.

The mineral content of considered formations allows the determination of BI values of 0.96, 0.86 and 0.68-0.96 for granites, sandstones and rhyolites respectively. BI of comparable Western European formations, calculated on the basis on data available in literature (Table S4, in Supplementary file) and using the method proposed by Jin et al. (2014a, 2014b) are 0.99, 0.94 and 0.94 for Soultz granites, Groß Schönebeck sandstones and volcanites, respectively. This means that all examined rocks are characterized by slightly lower susceptibility for HF operations (less development of the inducted fractures network and greater tendency to create double wing fractures) especially in the fracture initiation stage.

The mechanical parameters of target zones in EGS, as one of the most important information required for designing hydraulic stimulation, are reported in many works including (Zimmermann et al., 2010; Meller and Ledésert, 2017; Villeneuve et al., 2018). Typically, these data come from dipole sonic logging (Mullen and Roundtree, 2007) or less often from laboratory stress-strain core testing. On the other hand, wave velocity data, especially from laboratory core measurements under reservoir conditions, are often unavailable. Although this type of information is not necessary if logging data are available, such tests provide precise data at smaller scales, but when combined with petrophysics, petrography, and other data from large data set, can provide reliable and useful information.

Ultrasonic testing of granite from the Karkonosze Mts. revealed a significant difference in velocities between samples from the shallower and deeper intervals. While samples taken from the 138.0-144.0 m interval, significantly altered, fractured and with an elevated clay minerals content, show velocities on average of 4,700 and 2,600 m/s for the P- and S-wave respectively, the samples taken from the deeper, less altered and fractured interval, i.e., 155.0-184.0 m, show velocities of 5,500 and 3,100 m/s, respectively. The velocities of the deeper samples correspond to their higher dynamic moduli ($E$ up to 67 GPa) (Table S3, in Suppementary file). This interval is probably characterized by higher strength, and therefore the fracturing pressure could be higher there. The $E$ values for Soultz granite are in the range of 40-80 GPa for fresh intact rock, but in the fractured zones they can be much lower (Meller and Ledésert, 2017; Villeneuve et al., 2018). Hot dry granites from other EGS are characterized by very diverse $E$ and $v$ e.g., from 15-33 GPa and 0.12-0.22 in Fenton Hill; by 65 GPa and 0.25 in Habanero, 40-56 GPa and 0.23-0.33 in Qiabuqia, to 73.7 GPa and 0.22 in FORGE Utah (Moska et al., 2021).

Data presented for granite not related to HDR areas are variable. Domede et al. (2019) in comparison of mechanical properties for several dozen types of granites showed, that the range of P-wave velocity is from 2,260 to 6,690 m/s, while the range of $E$ and $v$ is 12.9-85.0 GPa and 0.14-0.36, with a mean value of 47 GPa and 0.25, respectively. Bourbié et al. (1987) suggested, that P- and S-wave velocities for granite are in the range of 4,500-6,000 and 2,500-3,300 m/s, respectively, with a density of 2.5-2.7 g/cm$^3$, and $v$ between 0.18 and 0.33. Plewa and Plewa (1992) reported dynamic $E$ and $v$ parameters of 54.5 GPa and 0.20, respectively, for dry biotite granite. Domonik (2011) showed a relatively low variability of the static $E$ for granite from the Strzegom massif (Poland), depending on the depth and the associated pressure. While in surface conditions, the average static $E$ modulus was calculated to be approximately 65 GPa, at a depth of about 3,500.0 m, this average modulus was close to 75 GPa. In these studies, static $v$ was found to range from 0.15 to 0.35, regardless of depth and pressure.

The wave velocities for the sandstones from the Mogilno-Łódź Trough showed strong variability with depth, probably due to the mineral composition, while the relatively low $v$ is related to the measurement under unsaturated conditions. Despite significant discrepancies in moduli between sampling intervals, the average $E$ (11-18 GPa) of these sandstones is much lower compared to the data presented for the Groß Schönebeck site (55 GPa), while $v$ reaches similar values (0.18-0.20) (Tables S3 and S5, in Supplementary file). The sandstones of the Genesys Hannower project also had significantly higher $E$ (45-65 GPa) and similar $v$ (0.18-0.22) (Tischner et al., 2013). This results in lower fracturing pressure, increased fracture width and reduced length, in the case of rocks of the Mogilno-Łódź Trough, compared to sandstones from the above-mentioned sites under similar stress conditions.

The examined rhyolites from the Gorzów Block are characterized by variable velocities depending on the sampling well. Samples from the GW-2 well showed lower velocities (on average 3,800 and 2,200 m/s for the P- and S-waves respectively), while samples from the J-4 well had velocities on average 4,100 and 2,400 m/s for respected waves, with high variability between individual samples. The average values obtained for $E$ (29-35 GPa for GW-2 and J-1, respectively), are lower than those presented for the Groß Schönebeck site (55 GPa), while the $v$ (0.23-0.27) is elevated (Tables S3 and S5, in Supplementary file). The dynamic elastic data presented for the rhyolite from the FORGE site (Utah, USA) show high variability of the $E$ and $v$ parameters (21-67 GPa and 0.19-0.39, respectively) (Bauer et al., 2017).

The BI range based on the $E$ to $v$ ratio is 49.9-68.4 for granites, 42.0-44.6 for sandstones and 41.3-53.7 for rhyolites, depending on the wellbore and sampling depth. However, the average values for comparable sedimentary and volcanic formations, based on the data presented in the literature (Table S5, in Supplementary file), concerning Groß Schönebeck formations and calculated using the method proposed by Rickman et al. (2008) are 78.0 and 74.5, respectively. It should be noted that the mentioned literature probably reports $E$ to $v$ values obtained from static testing or well logging, The BI values obtained for all formations considered in this study, using both mineral-based and $E$-$v$ ratio methods, are in the middle or upper limits of the ranges which means that these rocks may generally be susceptible to fracture propagation. The mineral-based BI calculation method proposed by Jin et al. (2014a, 2014b) gives the highest BI results due to inclusion of a large number of brittle minerals versus ductile minerals. However, the remaining tested methods (Jarvie et al., 2007; Wang and Gale, 2009) give very similar results. In the case of methods based on the $E$ to $v$ ratio, the differences in results depending on the method used are insignificant. It should be noted, however, that the reference values in the method proposed by (Rickman et al., 2008) were modified due to match the parameters of measured samples. It is important to note that the calculated BI should rather be treated as the BI for the intact rock body, despite the presence of natural fractures and alteration in some samples.

In light of the above, in the case of HDR formations, the method of BI interpretation may be useful but also controversial. Since BI's were originally intended for evaluation of sedimentary rocks, especially shale gas deposits, in the case of

HDR, its application without interpretive modifications seems inappropriate. In shale rocks, the increase of permeability during hydraulic stimulation occurs through the process of hydraulic fracturing (pure opening mode-creating new fractures in the tensile mode) or hydraulic jacking (reopening preexisting fractures in tensile mode). Generally, in these models, a high content of brittle minerals (e.g., quartz) and low content of plastic minerals (clays), favor the formation of an extensive fracture network, increasing the stimulated reservoir volume and, consequently, the volume of the reservoir hydraulically connected to the well.

Therefore, in simple terms, the greater the BI (calculated based on mineral content or elastic parameters) the greater the likelihood of obtaining an extensive fracture network and greater gas flowback. In EGS the goal is to create a connection between two or more wells, however, too extensive fracture network, or more precisely too high conductivity, may lead to undesirable thermal short circuiting, which leads to a decrease of temperature in the production well. In typical HDR formations (granites, volcanites), the main role in stimulation is played by the hydroshearing mechanism (inducing slip and dilatation of natural fractures in shear mode). Naturally fractured intervals are stimulated first, and new fractures are even created, which act as connectors between other natural fractures. Naturally fractured, altered intervals are generally characterized by a lower uniaxial compressive strength and a significantly lower $E$ (Table S5, in Supplementary file). These properties can significantly reduce mineral and geomechanical BI as a result of the elevated clay content and reduced $E$, respectively.

Therefore, it should be considered whether BI should be interpreted differently in HDR formations stimulated by the hydroshearing mechanism than in the rocks to which it was originally adapted and applied. In granites, rhyolites, or andesites, the lowest values of the $E$ and the increased content of plastic minerals (and thus the lowest BI compared to rest of considered interval) may indicate prospective zones for hydroshearing stimulation. On the other hand, in less naturally fractured sedimentary HDR, much more similar to the formation for which BI was originally intended and applied, the highest values may be considered more favorable.

Laboratory ultrasonic measurements can provide useful, complementary data for well logging or, in the absence of logging data and a large number of tested samples over wide depth interval, can be used as input to HF operation design software. The tests showed that elastic parameters of granites and sandstones were quasi-stabilized above the effective axial pressure of 25 MPa in triaxial tests. Although the tests were performed up to a confining pressure of 55 MPa it can be assumed, based on the literature (Bourbié et al., 1987), that a further increase in confining pressure should result in moduli changes, which could be insignificant in HF design. In the case of the tested rhyolites from J-4 well, a decrease in the P-wave velocity above 35 MPa axial pressure was observed, which can be associated with the previously mentioned microcracking of the matrix, which may be equivalent to the beginning of sample disintegration.

Testing under dry conditions seems appropriate for low-porous and permeable HDR, however, it can be mentioned that even in the case of low porosity and stress-resistant rock skeleton of the sample, saturation may lead to some increase in the moduli, due to the increase in P-wave velocity. In turn, a change in temperature by 100 °C causes a change in the P-wave velocity by less than 5% (Bourbié et al., 1987), which makes it possible to consider performing tests at lower temperatures, without a significant impact on the moduli.

So far no EGS project has been initiated in this part of Europe. Therefore, the results obtained of the dynamic elastic moduli in relation to the petrophysical and petrographic parameters, especially for the granite from the Karkonosze Mts. and the sandstone from the Mogilno-Łódź Trough, due to large the number of samples examined, could be used to a preliminary design an HF operation under expected conditions in these areas. Such a study, combined with the simulation of flow between wells, depending on the assumed rock features, stresses, and parameters of fracking operation, as well as evaluation of the potential for thermal energy extraction from these areas, would be an important step towards the development of enhanced geothermal systems, following the example of Western European countries.

## 4. Conclusions

1) Newly obtained data indicate that petrophysical parameters determining the HF operations in three prospective HDR formations in Central Europe: granites from the Karkonosze Mts., sandstones of the Mogilno-Łódź Trough and rhyolites from the Gorzów Block, have similar values to those in rocks in active HDR sites: Soultz granites, sandstones of the German Basin and effusive rocks from the Groß Schönebeck area, respectively.
2) The intact granites Karkonosze Mts. are similar in terms of mineral composition and susceptibility to fracturing to the corresponding Soultz formation. The elevated average clay content of the Mogilno-Łódź Trough compared to the Groß Schönebeck area leads to a decrease in mineral-BI, which facilitates the formation of double wing fractures. The BI of the Gorzów Block rhyolites is strongly dependent on the sampling location due variability of the mineral composition and development of natural fractures.
3) The altered granites, with well-developed natural fractures, and increased clay content, show a significantly lower mean $E$ compared to less altered ones. The dynamic elastic moduli of the sandstones show strong variability with depth, due to the differential cementation and development of natural fractures. Nevertheless, the BI values based on the $E$ to $v$ ratio are much lower compared to the sedimentary rocks of the Groß Schönebeck, which means less favorable conditions for the development of a multi-fracture network. On the other hand, lower BI of the tested rhyolites compared to the corresponding formation in German Basin suggests a higher susceptibility to fracking due to a better developed natural fracture network.
4) Mineral, and elastic moduli-based BI are useful in interpreting susceptibility to HF. In sedimentary rocks with

intergranular porosity, higher BI indicates greater susceptibility to HF, but in igneous rocks with fracture porosity, low BI indicates zones of alteration and fractures that are desirable for hydroshearing stimulation.

## Acknowledgements

The authors would like to thank Jacek Nowak PhD and Zdzisław Adamczyk DSc from the Silesian University of Technology for their help in work related to XRD research. This paper is based on research carried out at Silesian University of Technology and Oil and Gas Institute - National Research Institute (Poland), as a part of the implementation doctorate program RJO/SDW/005-33, founded by Ministry of Science and Higher Education of Poland.

## Supplementary file

http://doi.org/1046690/ager.2024.11.03

## Conflict of interest

The authors declare no competing interest.



## References

Andreev, G. Brittle Failure of Rock Materials: Tests Results and Constitutive Models. Rotterdam, Netherlands, A. A. Balkema, 1995.

Bai, M. Why are brittleness and fracability not equivalent in designing hydraulic fracturing in tight shale gas reservoirs. Petroleum, 2016, 2(1): 1-19.

Batchelor, A. Development of Hot-Dry-Rock geothermal systems in the UK. IEE Proceedings A, 1987, 134(5): 371-380.

Bauer, S., Barrow, P., Robbins, A., et al. Mechanical and fluid flow properties of basaltic andesite and rhyolite analogue rocks. Paper Presented at the 42nd Workshop on Geothermal Reservoir Engineering 2017, Stanford, California, 13-15 February, 2017.

Baujard, C., Genter, A., Dalmais, E., et al. Hydrothermal characterization of wells GRT-1 and GRT-2 in Rittershoffen, France: Implications on the understanding of natural flow systems in the rhine graben. Geothermics, 2017, 65: 255-268.

BESTEC GmbH, 2024a.

BESTEC GmbH, 2024b.

Blöcher, G., Reinsch, T., Henninges, J., et al. Hydraulic history and current state of the deep geothermal reservoir Groß Schönebeck. Geothermics, 2016, 63: 27-43.

Bourbié, T., Coussy, O., Zinszner, B. Acoustics of porous media. Paris, France, Editions Technip, 1987.

Davarpanah, S., Ván, P., Vásárhelyi, B. Investigation of the relationship between dynamic and static deformation moduli of rocks. Geomechanics and Geophysics for Geo-Energy and Geo-Resources, 2020, 6: 29.

Domede, N., Parent, T., Sellier, A. Mechanical behavior of granite: A compilation, analysis and correlation of data from around the world. European Journal of Environmental and Civil Engineering, 2019, 23(2): 193-211.

Domonik, A. Influence of high pressure and temperature on young modulus and poisson ratio values for selected rock types. Biuletyn Państwego Instytutu Geologicznego, 2011, 446: 117-122. (in Polish)

Goodway, B., Perez, M., Varsek, J., et al. Seismic petrophysics and isotropic-anisotropic AVO methods for unconventional gas exploration. The Leading Edge, 2010, 29(12): 1500-1508.

Górecki, W., Hajto, M., Jasnos, J., et al. Geothermal atlas of the Eastern Carpathians. Kraków, Poland, AGH University of Science and Technology in Krakow. Ministry of Science and Higher Education Republic of Poland, the National Science Centre, 2013. (in Polish)

Grieser, B., Bray, J. Identification of production potential in unconventional reservoirs. Paper SPE 106623 Presented at the Production and Operations Symposium, Oklahoma City, Oklahoma, 31 March-3 April, 2007.

Grünthal, G., Stromeyer, D., Bosse, C., et al. The probabilistic seismic hazard assessment of Germany-version 2016, considering the range of epistemic uncertainties and aleatory variability. Bulletin of Earthquake Engineering, 2018, 16: 4339-4395.

Herwanger, J. V., Bottrill, A., Mildren, S. Uses and abuses of the brittleness index with application to hydraulic stimulation. Proceedings of the 3rd Unconventional Resources Technology Conference, San Antonio, Texas, 20-22 July, 2015.

Holt, R., Fjær, E., Stenebråten, J., et al. Brittleness of shales: Relevance to borehole collapse and hydraulic fracturing. Journal of Petroleum Science and Engineering, 2015, 131: 200-209.

Huenges, E., Holl, H., Bruhn, D., et al. Current state of the EGS project Groß Schönebeck-drilling into the deep sedimentary geothermal reservoir. Paper Presented at Proceedings European Geothermal Congress, Unterhaching, Germany, 30 May-1 June, 2007.

Jarosiński, M. Recent tectonic stress field investigations in Poland: A state of the art. Geological Quarterly, 2005, 50: 303-321.

Jarvie, D., Hill, R., Ruble, T., et al. Unconventional shale-gas systems: The Mississippian Barnett Shale of north-central Texas as one model for thermogenic shale-gas assessment. AAPG Bulletin, 2007, 91(4): 475-499.

Jin, X., Shah, S. N., Roegiers, J., et al. Fracability evaluation in shale reservoirs-an Integrated petrophysics and geomechanics approach. Paper SPE 168589 Presented at SPE Hydraulic Fracturing Technology Conference, The Woodlands, Texas, USA, 4-6 February, 2014a.

Jin, X., Shah, S. N., Truax, J., et al. A practical petrophysical approach for brittleness prediction from porosity and sonic logging in shale reservoirs. Paper SPE 170972 Presented at SPE Annual Technical Conference and Exhibition, Amsterdam, The Netherlands, 27-29 October, 2014b.

Karnkowski, P. Budowa geologiczna oraz geneza i ewolucja bloku Gorzowa. Przegląd Geologiczny, 2010, 58(8): 680-688. (in Polish)

Kasza, P. Hydraulic fracturing in unconventional reservoirs, and methods of their analysis. Kraków, Polska, Prace Naukowe INiG-PIB (226), 2019.

King, G. Thirty years of gas shale fracturing: what have we learned? Paper SPE 133456 Presented at SPE Annual Technical Conference and Exhibition, Florence, Italy, 19-22 September, 2010.

Kukkonen, I., Pentti, M. St1 Deep Heat Project: Geothermal energy to the district heating network in Espoo. IOP Conference Series: Earth and Environmental Science, 2021, 703: 012035.

Labus, K., Labus, M., Leśniak, G. Thermal properties of rocks from deep boreholes in Poland in terms of obtaining geothermal energy from enhanced geothermal systems. Advances in Geo-Energy Research, 2023, 8(2): 76-88.

Masłowski, M., Labus, M. Preliminary studies on the proppant embedment in Baltic Basin shale rock. Rock Mechanics and Rock Engineering, 2021, 54(5): 2233-2248.

McCann, T. Sandstone composition and provenance of the Rotliegend of the NE German Basin. Sedimentary Geology, 1998, 116(3-4): 177-198.

McClure, M., Horne, R. An investigation of stimulation mechanisms in enhanced geothermal systems. International Journal of Rock Mechanics and Mining Sciences, 2014, 72: 242-260.

Meller, C., Ledésert, B. Is there a link between mineralogy, petrophysics, and the hydraulic and seismic behaviors of the Soultz-sous-Forêts granite during stimulation? A review and reinterpretation of petro-hydromechanical data toward a better understanding of induced seismicity and fluid flow. Journal of Geophysical Research: Solid Earth, 2017, 122(12): 9755-9774.

Moeck, I. Catalog of geothermal play types based on geologic controls. Renewable and Sustainable Energy Reviews, 2014, 37: 867-882.

Moska, R., Labus, K., Kasza, P. Hydraulic fracturing in enhanced geothermal systems-field, tectonic and rock mechanics conditions-a review. Energies, 2021, 14(18): 5725.

Moska, R., Labus, K., Kasza, P., et al. Geothermal potential of hot dry rock in South-East Baltic Basin countries-a review. Energies, 2023, 16(4): 1662.

Mullen, M., Roundtree, R. A Composite determination of mechanical rock properties for stimulation design (What to do when you don't have a sonic log). Paper SPE 108139 Presented at SPE Rocky Mountain Oil and Gas Technology Symposium, Denver, Colorado, 16-18 April, 2007.

Plewa, M., Plewa, S. Petrofizyka. Warsaw, Poland, Wydawnictwa Geologiczne, 1992. (in Polish)

Rickman, R., Mullen, M., Petre, E., et al. A practical use of shale petrophysics for stimulation design optimization: All shale plays are not clones of the Barnett Shale. Paper SPE 115258 Presented at SPE Annual Technical Conference and Exhibition, Denver, Colorado, 21-24 September, 2008.

Sausse J. Hydromechanical properties and alteration of natural fracture surfaces in the Soultz granite (Bas-Rhin, France). Tectonophysics, 2002, 348(1-3): 169-185.

Sausse, J., Fourar, M., Genter, A. Petrophysics and permeability in the Soultz granite. Paper Presented at World Geothermal Congress, Antalya, Turkey, 24-29 April, 2005.

Sausse, J., Fourar, M., Genter, A. Permeability and alteration within the Soultz granite inferred from geophysical and flow log analysis. Geothermics, 2006, 35(5-6): 544-560.

Schindler, M., Nami, P., Schellschmidt, R., et al. Summary of hydraulic stimulation operations in the 5 km deep crystalline HDR/EGS reservoir at Soults-sous-Forets. Paper SGP-TR-185 Presented at the 33$^{th}$ Workshop on Geothermal Reservoir Engineering, Stanford, California, 28-30 January, 2008.

Sowiżdżał, A., Gładysz, P., Pająk, L. Sustainable use of petrothermal resources-a review of the geological conditions in Poland. Resources, 2021, 10(1): 8.

Sowiżdżał, A., Machowski, G., Krzyżak, A., et al. Petrophysical evaluation of the Lower Permian formation as a potential reservoir for $CO_2$-EGS-Case study from NW Poland. Journal of Cleaner Production, 2022, 379: 134768.

Surma, F., Geraud, Y. Porosity and thermal conductivity of the Soultz-sous-Forêts granite. Pure and Applied Geophysics, 2003, 160(5-6): 1125-1136.

Szewczyk, J., Gientka, D. Mapa gęstości ziemskiego strumienia cieplnego Polski. Warsaw, Poland, Polish Geological Institute, 2009. (in Polish)

Tarasov, B., Potvin, Y. Universal criteria for rock brittleness estimation under triaxial compression. International Journal of Rock Mechanics and Mining Sciences, 2013, 59: 57-69.

Tester, J., Anderson, B., Batchelor, A., et al. The Future of Geothermal Energy-Impact of enhanced geothermal systems (EGS) on the United States in the 21$^{st}$ Century. Massachusett, USA, Massachusetts Institute of Technology, 2006.

Tischner, T., Krug, S., Pechan, E., et al. Massive hydraulic fracturing in low permeable sedimentary rock in the GeneSys Project. Proceedings 38th Workshop on Geothermal Reservoir Engineering Stanford University, Stanford, California, 11-13 February, 2013.

Ulusay, R., Hudson, J. The complete ISRM suggested methods for rock characterization, testing and monitoring: 1974-2006. Ankara, Turkey, ISRM Turkish National Group, 2007.

Vidal, J., Genter, A. Overview of naturally permeable fractured reservoirs in the central and southern Upper Rhine Graben: Insights from geothermal wells. Geothermics, 2018, 74: 57-73.

Villeneuve, M., Heap, M., Kushnir, A., et al. Estimating in situ rock mass strength and elastic modulus of granite from the Soultz-sous-Forêts geothermal reservoir (France). Geothermal Energy, 2018, 6: 11.

Wallroth, T., Eliasson, T., Sundquist, U. Hot dry rock research experiments at Fjällbacka, Sweden. Geothermics, 1999,

28(4-5): 617-625.
Wang, F., Gale, J. Screening criteria for shale gas systems. Gulf Coast Association of Geological Societes Transactions, 2009, 59: 779-793.
Wójcicki, A., Sowiżdżał, A., Bujakowski, W. Ocena potencjału, bilansu cieplnego i perspektywicznych struktur geologicznych dla potrzeb zamkniętych systemów geotermicznych (hot dry rocks) w Polsce. Warsaw/Kraków, Poland, Ministerstwo Środowiska, 2013. (in Polish)
Wu, H., Zhang, P., Dong, S., et al. Brittleness index analysis of coal samples. Acta Geophysica, 2019, 67(3): 789-797.
Zhang, D., Ranjith, P., Perera, M. The brittleness indices used in rock mechanics and their application in shale hydraulic fracturing: A review. Journal of Petroleum Sciences and Engineering, 2016, 143: 158-170.
Zimmermann, G., Moeck, I., Blöcher, G. Cyclic waterfrac stimulation to develop an enhanced geothermal system (EGS)-conceptual design and experimental results. Geothermics, 2010, 39(1): 59-69.
Zuchiewicz, W., Badura, J., Jarosiński, M. Uwagi o neotektonice Polski: Wybrane przykłady. Biuletyn Państwowego Instytutu Geologicznego, 2007, 425: 105-128. (in Polish)

## Supplementary file

# Dynamic elastic properties, petrophysical parameters and brittleness of hot dry rocks from prospective areas of Central Europe

Rafał Moska[1,*], Krzysztof Labus[2], Piotr Kasza[1]

[1] *Oil and Gas Institute-National Research Institute, Kraków 31-503, Poland*

[2] *Institute for Applied Geology, Silesian University of Technology, Gliwice 44-100, Poland*

E-mail address: moska@inig.pl (R. Moska); krzysztof.labus@polsl.pl (K. Labus); kasza@inig.pl (P. Kasza).

[*] Corresponding author (ORCID: 0000-0002-6353-9287)

***Moska, R., Labus, K., Kasza, P. Dynamic elastic properties, petrophysical parameters and brittleness of Hot Dry Rocks from prospective areas of Central Europe. Advances in Geo-Energy Research, 2024, 14(2): 90-105.***

**The link to this file is:** https://doi.org/10.46690/ager.2024.11.03

(a) (b) (c) (d)

**Fig. S1**. Rock samples: (a) Sandstone from Mogilno-Łódź Trough area, (b) granite from Karkonosze Mountains, (c) and (d) rhyolite from Gorzów Block ((c) is GW-2 well and (d) is J-4 well). Scale in centimeters.

**Table S1**. Permeability, porosity and density of the samples.

| Type of the rock/number of samples | Location | Statistical parameters | Permeability (mD) | Grain density (g/cm$^3$) | Bulk density (g/cm$^3$) | Effective porosity (%) |
|---|---|---|---|---|---|---|
| Granite/38 | Karkonosze Mountains CP-1 well | Minimum | < 0.001 | 2.607 | 2.527 | 0.503 |
| | | Maximum | 0.518 | 2.643 | 2.621 | 3.436 |
| | | Average/Standard deviation | 0.038/0.094 | 2.622/0.009 | 2.582/0.029 | 1.529/0.862 |
| Sandstone/36 | Mogilno-Łódź Trough PT-1 well | Minimum | 0.008 | 2.640 | 2.460 | 2.720 |
| | | Maximum | 0.160 | 2.710 | 2.592 | 7.669 |
| | | Average/Standard deviation | 0.049/0.039 | 2.673/0.015 | 2.525/0.043 | 5.563/1.409 |
| Rhyolite/8 | Gorzów Block GW-2 well | Minimum | < 0.001 | 2.595 | 2.415 | 5.923 |
| | | Maximum | 0.021 | 2.635 | 2.467 | 7.673 |
| | | Average/Standard deviation | 0.004/0.007 | 2.621/0.011 | 2.443/0.018 | 6.772/0.678 |
| Rhyolite/11 | Gorzów Block J-4 well | Minimum | < 0.001 | 2.520 | 2.454 | 0.770 |
| | | Maximum | 0.085 | 2.606 | 2.570 | 3.393 |
| | | Average/Standard deviation | 0.009/0.024 | 2.557/0.033 | 2.507/0.046 | 1.959/0.914 |

**Table S2**. Mineral composition of the measured samples.

| Mineral | Statistical parameters | Granite, Karkonosze Mountains, CP-1 well (%) | Sandstone, Mogilno-Łódź Trough, PT-1 well (%) | Rhyolite, Gorzów, Block, GW-2 well (%) | Rhyolite, Gorzów Block, J-4 well (%) |
|---|---|---|---|---|---|
| Quartz | Minimum | 18.3 | 14.5 | 37.1 | 18.5 |
| | Maximum | 28.6 | 71.4 | 37.8 | 29.2 |
| | Average | 23.1 | 52.4 | 37.5 | 22.4 |
| Calcite/Dolomite | Minimum | -/- | 0.5/0.1 | -/- | -/- |
| | Maximum | -/- | 13.0/5.4 | -/- | -/- |
| | Average | -/- | 3.8/2.2 | -/- | -/- |
| Orthoclase/Microcline | Minimum | 8.5/15.5 | 0.8/- | 41.1/- | -/21.3 |
| | Maximum | 21.1/24.5 | 16.8/- | 41.2/- | -/27.2 |
| | Average | 14.9/19.0 | 9.7/- | 41.2/- | -/24.0 |
| Albite | Minimum | 28.6 | 10.2 | 16.5 | 14.5 |
| | Maximum | 35.4 | 18.3 | 16.8 | 22.9 |
| | Average | 33.1 | 14.0 | 16.7 | 17.9 |
| Biotite | Minimum | 0.7 | 0.1 | 0.8 | 1.9 |
| | Maximum | 2.8 | 0.3 | 1.0 | 4.3 |
| | Average | 1.7 | 0.2 | 0.9 | 2.8 |
| Kaolinite/Illite/Chlorite | Minimum | 0.7/3.8/2.9 | 0.5/1.3/0.6 | -/2.7/0.7 | 3.8/-/4.6 |
| | Maximum | 1.6/4.3/10.7 | 9.7/33.2/12.7 | -/3.0/0.8 | 3.8/-/33.0 |
| | Average | 1.1/4.1/5.6 | 2.5/14.0/3.4 | -/2.9/0.8 | 3.8/-/16.7 |
| Magnetite/Hematite | Minimum | -/- | -/- | 0.2/- | -/0.1 |
| | Maximum | -/- | -/- | 0.3/- | -/1.7 |
| | Average | -/- | -/- | 0.3/- | -/0.9 |
| Clinopyrokscne/Pyrope/ Antigorite/Lawsonite | Minimum | -/-/-/- | -/-/-/- | -/-/-/- | 1.1/0.8/1.3/2.4 |
| | Maximum | -/-/-/- | -/-/-/- | -/-/-/- | 2.6/0.8/26.1/2.4 |
| | Average | -/-/-/- | -/-/-/- | -/-/-/- | 1.7/0.8/10.5/2.4 |

**Table S3**. Summary of the dynamic elastic parameters of the measured samples. Minimum, maximum, and average values are presented for 55 MPa axial pressure in triaxial condition tests, where radial pressure is within the range 15-55 MPa.

| Area, rock type | Sampling depth (m) | Statistical parameter | Velocity (m/s) | | $V_P/V_S$ | $v$ | $E$ (GPa) | $K$(GPa) | $G$(GPa) | N |
|---|---|---|---|---|---|---|---|---|---|---|
| | | | P-wave | S-wave | | | | | | |
| Karkonosze Mountains Region, granite | CP-1 138.0-144.0 | Minimum | 4,470 | 2,255 | 1.70 | 0.24 | 34.6 | 31.0 | 13.0 | 5 |
| | | Maximum | 4,767 | 2,798 | 1.98 | 0.33 | 49.6 | 37.1 | 20.0 | 5 |
| | | Average/Standard deviation | 4,667/103.76 | 2,559/194.15 | 1.83/0.11 | 0.28/0.04 | 43.1/5.28 | 33.3/2.17 | 16.9/2.52 | 5 |
| | CP-1 155.0-184.0 | Minimum | 5,381 | 2,871 | 1.75 | 0.26 | 57.0 | 43.1 | 21.6 | 7 |
| | | Maximum | 5,627 | 3,188 | 1.95 | 0.32 | 67.3 | 53.6 | 26.6 | 7 |
| | | Average/Standard deviation | 5,533/85.61 | 3,103/103.25 | 1.78/0.07 | 0.27/0.02 | 63.9/3.28 | 46.4/3.30 | 25.2/1.62 | 7 |
| Gorzów Block, rhyolite | GW-2 3,348.0-3,356.0 | Minimum | 3,805 | 2,093 | 1.72 | 0.24 | 27.4 | 19.6 | 10.6 | 3 |
| | | Maximum | 3,826 | 2,216 | 1.83 | 0.29 | 30.0 | 21.4 | 12.1 | 3 |
| | | Average/Standard deviation | 3,814/8.60 | 2,149/50.68 | 1.78/0.04 | 0.27/0.02 | 28.6/1.09 | 20.5/0.71 | 11.3/0.58 | 3 |
| | J-4 3,264.0-3,277.0 | Minimum | 3,520 | 1,920 | 1.55 | 0.15 | 23.3 | 16.1 | 9.0 | 6 |
| | | Maximum | 4,958 | 3,192 | 2.09 | 0.35 | 60.0 | 39.4 | 26.2 | 6 |
| | | Average/Standard deviation | 4,142/555.15 | 2,406/397/86 | 1.74/0.18 | 0.23/0.07 | 35.2/11.69 | 22.6/8.58 | 14.5/5.43 | 6 |
| Mogilno-Łódź Trough, sandstone | PT-1 3,912.5-3,977.0 | Minimum | 2,646 | 1,554 | 1.52 | 0.12 | 15.4 | 8.1 | 6.2 | 6 |
| | | Maximum | 2,989 | 1,879 | 1.71 | 0.24 | 21.4 | 10.9 | 9.1 | 6 |
| | | Average/Standard deviation | 2,756/111.18 | 1,691/117.74 | 1.63/0.07 | 0.20/0.04 | 17.6/1.99 | 9.7/0.83 | 7.4/1.03 | 6 |
| | PT-1 4,189.5-4,286.0 | Minimum | 1,826 | 1,146 | 1.52 | 0.12 | 7.6 | 3.9 | 3.2 | 6 |
| | | Maximum | 2192 | 1426 | 1.67 | 0.22 | 11.4 | 6.2 | 5.0 | 6 |
| | | Average/Standard deviation | 2044/138.56 | 1279/112.38 | 1.60/0.06 | 0.18/0.04 | 9.6/1.49 | 5.0/0.69 | 4.1/0.73 | 6 |

**Table S4**. Mineral composition of reservoir rocks from selected EGS sites in Europe.

| Rock type | Soultz-sous-Forêts rockbody, granite (Ledésert and , 2012) | Groß Schönebeck GtGrSk4/05 well, Rotliegend, volcanic (Regenspurg et al., 2016) | Groß Schönebeck GtGrSk4/05 well, Rotliegend, sedimentary (Regenspurg et al., 2016) | Groß Schönebeck area, Dethlingen formation (Rotliegend sandstone) (McCann, 1998) |
|---|---|---|---|---|
| Quartz | 28.4 | 10-60 | 30-80 | 70-78.3 |
| Plagioclase | 39.9 (Oligoclase) | 30-60 | 0-30 | 1.7-7.5 |
| K-feldspar | 18.8 | No data | No data | $\leq 0.5$ |
| Biotite/Mica | 8.4 | $< 10$ (Mica) | $< 10$ (Mica) | No data |
| Carbonate | $\leq 1.8 - 18$ | $< 10$ (Calcite) | 0-30 (Calcite) | $\leq 13.3$ |
| Chlorite/Clay | $< 1$/- | -/$< 10$ | -/$< 10$ | No data |
| Sericite | Up to several % (Illite) | No data | No data | No data |
| Pyroxene | 4.5 (Amphibole) | No data | No data | No data |
| Epidote | $< 1$ | No data | No data | No data |
| Anhydrite | 0 | $< 10$ (Celestine/Anhydrite) | No data | $\leq 1.33$ |
| Hematite | No data | $< 10$ | $< 10$ | No data |

Notes: Data from Soultz-sous-Forêts concern composition of the main rock body. The composition of fractured and altered zones is strongly modified, especially by the dissolution of quartz and the increase in the amount of clay minerals.

**Table S5**. Comparison of selected tectonic and geomechanical parameters from Western European EGS sites and prospective EGS areas in Central Europe.

| EGS site, rock type | Target zone depth (m) /temperature (°C)/stress regime | $S_V$, $S_H$, $S_h$, $P_p$ (MPa) | $V_P$, $V_S$ (m/s) | $E$ (GPa); $v$ |
|---|---|---|---|---|
| Soultz-sous-Forêts (France), granite | 5,200.0/200/ Mixed, normal and strike-slip (Baujard et al., 2017) | At 2,200.0 m: $S_V$ is 54.8; $S_V$ >or< $\sigma_H$; $S_h$ is 29.6; $P_P$ is 22.5; calculated, based on equations from (Lengliné et al., 2017) | $V_P$, 4,390-5,200, for coarse-grained, biotite–muscovite-bearing granite from Saint Pierre Bois quarry (Kushnir et al., 2018) | Estimated $E$ for pure granite at the target zone-up to 80 GPa, in zones of increased hydraulic conductivity, and clay content, may be significantly lower. (Meller and Ledésert, 2017), from 1-2 for fractured zones up 40 GPa for intact rock (Villeneuve et al., 2018). |
| Soultz-sous-Forêts (France), granite | 5,200.0/200/Mixed, normal and strike-slip (Baujard et al., 2017) | At 2,200.0 m: $S_V$ is 54.8; $S_V$ >or< $\sigma_H$; $S_h$ is 29.6; $P_P$-22.5; calculated, based on equations from Lengliné et al. (2017) | $V_P$, 4,390-5,200, for coarse-grained, biotite-muscovite-bearing granite from Saint Pierre Bois quarry (Kushnir et al., 2018) | Estimated $E$ for pure granite at the target zone-up to 80 GPa, in zones of increased hydraulic conductivity, and clay content, may be significantly lower. (Meller and Ledésert, 2017), from 1-2 for fractured zones up 40 GPa for intact rock (Villeneuve et al., 2018). |
| Groß Schönebeck (Germany), volcanite | 4,100.0/149/ Normal-strike-slip $S_h \geq 0.55 \cdot S_V$, $S_H \leq 0.78 - 1.00 \cdot S_V$ (Moeck et al., 2009) | $S_V$ is 100, $S_H$ is 78-100, $S_h$ is 55 (Moeck et al., 2009), $P_P$ is 44.9 at 4,220.0 m (Huenges et al., 2007) | No data available | $E$ is 55, $v$ is 0.20 (Zimmermann et al., 2010) |
| Groß Schönebeck (Germany), sedimentary | 4,100.0/149/ Normal-strike-slip $S_h \geq 0.55 \cdot S_V$, $S_H \leq 0.78 - 1.00 \cdot S_V$ (Moeck et al., 2009) | $S_V$ is 100, $S_H$ is 78-100, $S_h$ is 55 (Moeck et al., 2009), $P_P$ is 44.9 at 4,220.0 m (Huenges et al., 2007) | No data available | $E$ is 55, $v$ is 0.18 (Zimmermann et al., 2010) |
| Karkonosze Mountains Region (Poland), (granite) | 4,000.0/165/ Normal-strike slip (Jarosiński, 2005; Zuchiewicz et al., 2007) | Based on average rock density $S_V$: 96 (Jarosiński, 2005) | Depending on the depth of the sampling and individual sample conditions: $V_P$ is 4,470-5,628, $V_S$ is 2,254-3,188 (this study) | Depending on the sampling depth and individual sample conditions: $E$ is 34.6-67.3, $v$ is 0.24-0.33 (this study) |
| Gorzów Block (Poland), volcanite (rhyolite) | 4,300.0/160/ Normal-strike slip (Jarosiński, 2005; Zuchiewicz et al., 2007) | Based on average rock density $S_V$: (Jarosiński, 2005) | Depending on the well and depth of samples collected: $V_P$ is 3,802-4,958, $V_S$ is 1,920-3,191 (this study) | Depending on the well and sampling depth: $E$ is 7.5-23.3-60.0, $v$ is 0.15-0.35 (this study) |
| Mogilno-Łódź Trough (Poland), sedimentary (sandstone) | 5,000.0-6,500.0/165-195/Normal-strike slip (Jarosiński, 2005; Zuchiewicz et al., 2007) | Based on the average rock density $S_V$: (Jarosiński, 2005) | Depending on the depth of the sampling and individual sample conditions: $V_P$ is 1,826-2,989, $V_S$ is 1,146-1,879 (this study) | Depending on the sampling depth and individual sample conditions: $E$ is 7.5-21.5, $v$ is 0.12-0.24 (this study) |

## References

Baujard, C., Genter, A., Dalmais, E., et al. Hydrothermal characterization of wells GRT-1 and GRT-2 in Rittershoffen, France: Implications on the understanding of natural flow systems in the rhine graben. Geothermics, 2017, 65: 255-268.

Huenges, E., Holl, H., Bruhn, D., et al. Current state of the EGS project Groß Schönebeck-drilling into the deep sedimentary geothermal reservoir. Paper Presented at Proceedings European Geothermal Congress, Unterhaching, Germany, 30 May-1 June, 2007.

Jarosiński, M. Recent tectonic stress field investigations in Poland: A state of the art. Geological Quarterly, 2005, 50: 303-321.

Kushnir, A., Heap, M., Baud, P., et al. Characterizing the physical properties of rocks from the Paleozoic to Permo-Triassic transition in the Upper Rhine Graben. Geothermal Energy, 2018, 6: 16.

Ledésert, B., Hébert, R. The Soultz-sous-Forêts' enhanced geothermal system: A granitic basement used as a heat exchanger to produce electricity, in Heat Exchangers-Basics Design Applications, edited by J. Mitrovic, InTech, Rijeka, pp. 477-504, 2012.

Lengliné, O., Boubacar, M., Schmittbuhl, J. Seismicity related to the hydraulic stimulation of GRT1, Rittershoffen, France. Geophysical Journal International, 2017, 208(3): 1704-1715.

McCann, T. Sandstone composition and provenance of the Rotliegend of the NE German Basin. Sedimentary Geology, 1998, 116(3-4): 177-198.

Moeck, I., Schandelmeier, H., Holl, H. The stress regime in a Rotliegend reservoir of the Northeast German Basin. International Journal of Earth Sciences, 2009, 98(7): 1643-1654.

Regenspurg, S., Feldbusch, E., Norden, B., et al. Fluid-rock interactions in a geothermal Rotliegend/Permo-Carboniferous reservoir (North German Basin). Applied Geochemistry, 2016, 69: 12-27.

Villeneuve, M., Heap, M., Kushnir, A., et al. Estimating in situ rock mass strength and elastic modulus of granite from the Soultz-sous-Forêts geothermal reservoir (France). Geothermal Energy, 2018, 6: 11.

Zimmermann, G., Moeck, I., Blöcher, G. Cyclic waterfrac stimulation to develop an enhanced geothermal system (EGS)-conceptual design and experimental results. Geothermics, 2010, 39(1): 59-69.

Zuchiewicz, W., Badura, J., Jarosiński, M. Uwagi o neotektonice Polski: Wybrane przykłady. Biuletyn Państwowego Instytutu Geologicznego, 2007, 425: 105-128. (in Polish)

**Artykuł IV: Potencjalne systemy geotermalne w zachodniej Polsce – zagadnienia petrotermalne i geochemiczne – artykuł IV.**

energies

MDPI

*Article*

# Potential Enhanced Geothermal Systems in Western Poland—Petrothermal and Geochemical Issues

**Krzysztof Labus [1], Rafał Moska [2] and Małgorzata Labus [1,*]**

[1] Department of Applied Geology, Silesian University of Technology, 2 Akademicka Str., 44-100 Gliwice, Poland; krzysztof.labus@polsl.pl
[2] Oil and Gas Institute—National Research Institute, 25A Lubicz Str., 31-503 Krakow, Poland; moska@inig.pl
* Correspondence: malgorzata.labus@polsl.pl

**Abstract:** This study evaluates the potential of enhanced geothermal systems (EGSs) in Poland, focusing on formations composed by igneous rocks, such as crystalline rocks of the Karkonosze pluton and volcanic rocks of the Gorzów Block. A total of 57 rock samples, including granites and rhyolites from these formations, were analyzed for their thermal and geochemical properties to assess their suitability for EGS development. The results highlight the importance of thermal parameters, such as conductivity and diffusivity, in optimizing geothermal exploitation. The measurements reveal that Karkonosze granite exhibits high thermal diffusivity and conductivity, making it a prime candidate for heat extraction. Although the Gorzów Block rhyolites show slightly lower values, their high initial temperatures still promise long-term geothermal viability. Geochemical modelling indicates that mineral precipitation that causes permeability damage is unlikely in these reservoirs. Instead, minor increases in porosity due to mineral dissolution can reduce hydraulic resistance, potentially affecting the performance of the system.

**Keywords:** geothermics; EGS; HDR; granite; rhyolite; Karkonosze; Gorzów block; thermal parameters; geochemical modelling

check for updates

Academic Editors: Efstathios E. Michaelides and Dameng Liu

Received: 5 December 2024
Revised: 8 January 2025
Accepted: 8 February 2025
Published: 12 February 2025

**Citation:** Labus, K.; Moska, R.; Labus, M. Potential Enhanced Geothermal Systems in Western Poland—Petrothermal and Geochemical Issues. *Energies* **2025**, *18*, 876. https://doi.org/10.3390/en18040876



## 1. Introduction

Among renewable energy sources, the so-called enhanced geothermal systems (EGSs) have great potential and are based on the petrothermal energy of hot rocks located at great depths. Crystalline rocks, such as granite and graniodiorites, characterized by low porosity and permeability, are the largest reservoirs of thermal energy that can be exploited using this technology [1–3]. Site selection is typically, but not exclusively, based on an analysis of the thermal gradient, thermal conductivity, and rock composition in a given area. The depth of these systems is in the range of 2000–6000 m.

The (EGS) concept refers to engineered geothermal systems where the permeability of hot rock has been artificially increased to allow fluid circulation, while hot dry rock (HDR) technology is specifically targeted at impermeable, high-temperature rocks without natural fluid paths. Not all EGS designs are limited to HDR conditions and may also include naturally permeable hot rocks. The primary difference is that HDR focuses on completely dry, impermeable rocks, while EGS covers a wider range of geological conditions. The need to artificially create hydraulic conductivity between the injection and production wells in the rock mass is a significant difference between conventional geothermal energy and EGS-type geothermal energy [4–6].

In most HDR projects worldwide, reservoir rocks are igneous rocks, mainly granites. Systems that use the energy of hot, dry sedimentary rocks are less common.

Efficient heat extraction from hot rock formations can be achieved when reservoir rocks possess minimal porosity and permeability along with maximum thermal conductivity.

Thermal parameters of rock formations are of fundamental importance for HDR projects [7] and have, therefore, been the subject of numerous studies worldwide, e.g., [8–13]. Some examples of determining thermal parameters for structures in Poland were presented by Bujakowski et al. [14] for granites, and for sedimentary rocks by Sowiżdżał and Kaczmarczyk [15] and Labus et al. [16].

The objective of our research was to evaluate the fundamental thermal properties of igneous rocks, including their diffusivity and effusivity, representing selected structures of the geothermal potential of Poland, and to investigate changes in temperature and the range of cooling distance of the formation during heat exploitation. Based on the results of experimental and modelling works, performed by Wójcicki et al. [17] and Bujakowski et al. [14], two prospective areas were selected, located in the western part of Poland. The Karkonosze pluton is a geothermal system with potentially favorable conditions for the use of HDR and/or EGS technologies, mainly due to the lithological nature of the granite formations of which it consists, which are most susceptible to fracturing processes. The second region considered in this publication is the Gorzów block, which, as a result of modelling conducted by Wójcicki et al. [17], was classified as prospective in terms of HDR technology. The north-western and western parts of the Gorzów Block (Dębno region) are particularly attractive in this context, owing to the regionally elevated temperatures and the significant thickness of volcanic formations. These findings contribute to a greater understanding of geothermal potential in Poland and offer a foundation for future exploration and development of HDR technologies in similar geological settings. However, based on the available information, a research gap was identified in determining diffusivity and effusivity as key properties influencing temperature changes and the degree of formation cooling, as well as in assessing geochemical reactions within potential EGS systems in the analyzed formations during geothermal heat exploitation.

To obtain geothermal heat from low-permeability HDR systems, a cool working fluid is injected into the geothermal reservoir, which flows through a network of natural and induced fractures, absorbing heat from contact with the reservoir rock, and then, after extraction to the surface, recovers its energy. Interaction of the working fluid with the rock can lead to the dissolution or precipitation of minerals, which can modify the original porosity and permeability of the fracture system. This is one of the key phenomena that determines the efficiency of the geothermal energy extraction process. To assess the possibility of potential geochemical reactions in the EGS collectors selected in this study, geochemical modelling was performed, taking into account the rock petrography and the different reactivity of the injected working fluid. Research in this area has not been performed in Poland before, but it can help to determine the appropriate operating parameters for the optimal use of available geothermal energy resources in potential EGS systems.

## 2. Geological Setting

### *2.1. Research Area*

The prospective EGS areas in Poland, taking into account the density of the heat flow of the Earth, are the Karkonosze Mountains, Gorzów Block, Mogilno-Łódź Trough, Szczecin Trough, and Upper Silesian Block [5,16]. In this study, igneous rocks occurring in two of the abovementioned areas were examined: (1) the Karkonosze granitoid pluton and (2) the Gorzów Block (Figure 1a,b).

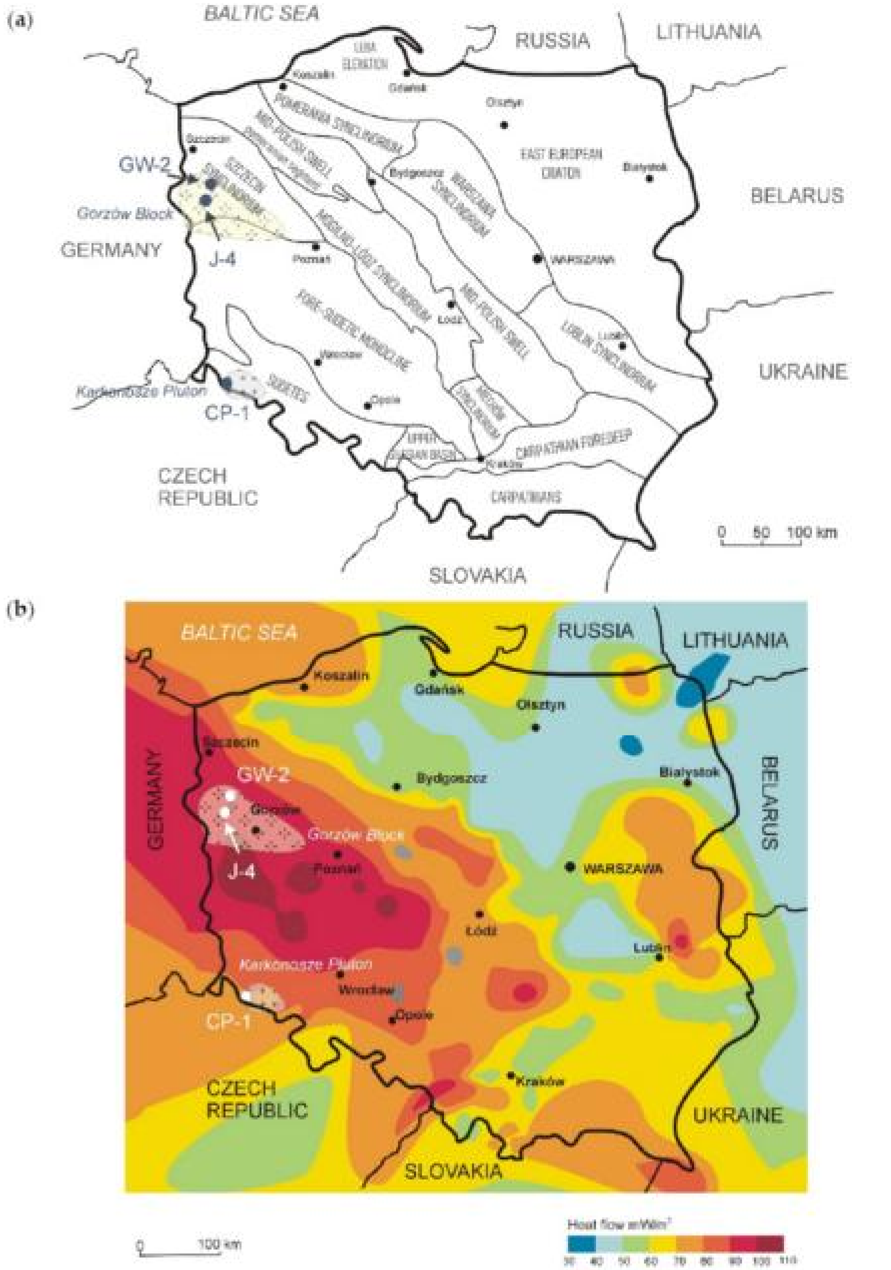


**Figure 1.** Simplified maps of the geologic provinces (**a**) and heat flow (**b**) in Poland (based on [18,19]). Symbols indicate drill wells.

### 2.1.1. Karkonosze Mountains

The Karkonosze pluton, described in detail by Cloos [20] is part of the Sudetes (Figure 1a,b). Igneous rocks (mainly granites) outcrop the surface, forming part of the Karkonosze ridge. The surface area of Karkonosze Mts. within the borders of Poland, it is ca. 185 $km^2$, with an estimated depth exceeding 10 km [14]. The granitoid intrusive rocks are dated as Carboniferous (Pennsylvanian) and upraised during the Variscian orogenic cycle. The granite of the Karkonosze Mountains is cut by numerous Variscan veins of pegmatite, aplite, microdiorite, and lamprophyre. The Karkonosze block is also rich in fractures that formed in the Neogene period, probably reaching considerable depths of about 10–20 km [21].

They are thought to be the primary pathways for heat transfer from the Earth's depths. In this region, a considerable amount of heat is also produced through the radioactive decay of specific rock-forming minerals. Research by Bujakowski et al. [14] reveals that the average radiogenic heat production in the granites of the Karkonosze Mountains is significant, reaching approximately 6 $\mu W/m^3$.

The geothermal gradient in this region is approximately 4 °C per 100 m, with temperatures reaching up to 165 °C at a depth of 4000 m below ground level.

Within the Karkonosze massif, three lithological types of granite have been distinguished. These types exhibit a variety of grain sizes and mineral compositions [22]. The most common is the porphyritic coarse- and medium-grained granite with an uneven grain size. The large potassium feldspar crystals are surrounded by plagioclase, making Karkonosze granite similar to rapakivi granites. A notable characteristic of this type is the presence of numerous biotite schliers and mafic enclaves. The second form is the medium-grained, so-called range granite, which does not contain hornblende or dark biotite schliers. The least numerous are the granophyre granites (aplogranites), which occur mainly on the north-eastern periphery of the massif.

The total porosity in the upper part (up to 100 m BGL) of the Karkonosze pluton, within the lower section of the coarse-grained granite, ranges from 3.94% to 0.86%, while in the lower part (100–200 m) of the medium-grained granites, it ranges from 1.2% to 0.47% [14]. Thermal conductivity was found to increase with depth, exceeding 3 W/mK below 180 m, and the average value of 3.5 W/mK was assumed by Bujakowski et al. [14] to create the structural–thermal model of the Karkonosze pluton.

#### 2.1.2. Gorzów Block

The Gorzów Block (Figure 1a,b) is located about 100 km east of the Groß Schönebeck region (near Berlin, Germany), where a research project on the use of heat from volcanic rocks has been conducted since 2006. The geological structure in this region is similar to that of the Gorzów Block. The reservoir rocks there are mainly volcanic rocks (rhyolites and andesites), occurring in the lower part of the reservoir. Sedimentary rocks (clastic and with poor reservoir properties) are found in the upper section of the reservoir [23]. In this structure, the geothermal gradient ranges from 3.5 to 4.0 °C per 100 m, with temperatures reaching up to 150 °C [24,25].

The Gorzów Block, being an eastern extension of the Groß Schönebeck reservoir, is built of Permian volcanic rocks, located below 4300 m, with a temperature of about 160 °C. The rock complex is heterogeneous. It is composed mainly of extrusive rocks, such as trachyandesites, andesites, rhyodacites and dacites, sporadic rhyolites, and basalts. Volcanoclastic breccias and tuffs occur in subordinate amounts.

## 3. Materials and Methods

### 3.1. Samples

The analyzed geological structures are located at depths greater than 4000 m and are characterized by typical HDR petrophysical parameters, including low porosity and permeability. Since the structures located at depths below 4000 m were not accessible by drilling, rock samples representing shallower depths in existing wells were used in this work. The Karkonosze granitoid was taken from the CP-1 well and represents grey–pink granite with medium to coarse crystals, cracked in places, with pegmatite veins. Samples of volcanic rocks representing the Gorzów Block were collected from the GW-2 and J-4 wells.

They are red–pink rhyolite (GW-2) and brownish rhyolite (J-4) with white calcite veins. The locations of the drillings are shown in Figure 1, basic data on the samples are included in Table 1, and the sample photographs (examples) are provided in Figure 2.

**Table 1.** Basic data on the samples.

| Well | Depth Intervals (m) | Temperature (°C) | Number of Samples | Stratigraphy | Litology |
|---|---|---|---|---|---|
| | | Karkonosze Mts. | | | |
| CP-1 | 137.80–138.06<br>140.10–140.23<br>143.80–143.93<br>154.50–154.76<br>181.80–182.06<br>183.60–183.86 | 165 | 38 | Pennsylvan | Granite |
| | | Gorzów Block | | | |
| GW-2 | 3348.0–3356.0 | 130 | 8 | Rotliegend | Rhyolite |
| J-4 | 3264.0–3277.0 | 130 | 11 | Rotliegend | Rhyolite |

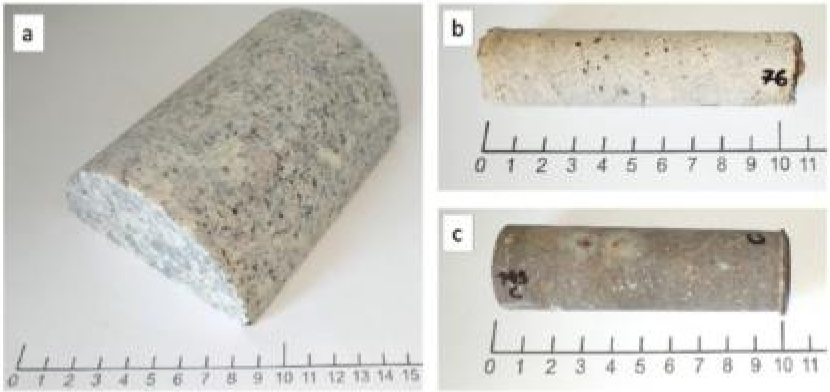


**Figure 2.** Rock samples: (**a**) granite from the Karkonosze Mountains (borehole CP-1) and (**b**,**c**) rhyolite from Gorzów Block (boreholes GW-2 and J-4, respectively). Scale in centimeters.

### 3.2. *Research Methods*

#### 3.2.1. Determination of the Mineral Composition

The mineral composition was determined using the X-ray method, with the use of a Bruker D2 Phaser Advance spectrometer. The measurement parameters were as follows: CuK$\alpha$ lamp, voltage 30 kV, current 10 mA, $2\Theta^\circ - 62^\circ$, and step 0.020°. HighScore Plus v5.2 software was used for semi-quantitative analysis, using the Rietveld method [26].

#### 3.2.2. Determination of Petrophysical Parameters

The value of the effective porosity coefficient of rocks was determined based on measurements with the use of an HGP-100 helium porosimeter and a mercury balance. The determination of pore volume consists of expanding a given volume of helium (according to Boyle's law) into the pore space and observing the pressure drop. Helium penetrates all pore spaces that are accessible to flow, i.e., all interconnected pores. Porosity calculations based on this measurement allow researchers to determine the effective porosity. On the basis of the porosity measurements, the density (grain density and bulk density) of the sample was determined.

3.2.3. Thermal Measurements and Calculations

Thermal parameters, including thermal conductivity and diffusivity, are essential data for determining heat flow, evaluating the thermal regime, and identifying geothermal systems [9,27].

Thermal conductivity ($\lambda$ or $k$) measures a material's ability to conduct heat (Q). It is expressed by the following formula [28]:

$$k = \frac{Q \cdot l}{s \cdot (T_0 - T_1) \cdot t} \quad (1)$$

where $Q$ represents the amount of heat [J], $l$ is the thickness of the material, representing the distance between the surfaces with different temperatures $T_0$ and $T_1$, ($T_0 > T_1$) [m], $t$ is time [s], and $s$ is the area [m$^2$].

Thermal effusivity, or responsivity (e), indicates a material's ability to exchange heat with its surroundings, either storing or dissipating heat [29]. It is defined as follows:

$$e = \sqrt{\rho c_p k} \quad (2)$$

where $e$ is thermal effusivity [W·s$^{½}$ m$^{-2}$ K$^{-1}$], $\rho$ is material density [kg m$^{-3}$], $c_p$ is specific heat capacity [J·kg$^{-1}$ K$^{-1}$], and $k$ is the thermal conductivity coefficient [W·m$^{-1}$K$^{-1}$].

Thermal diffusivity ($\alpha$), also referred to as the temperature compensation coefficient, represents how swiftly a material responds to temperature changes. It quantifies the rate of temperature variation within a unit volume of material due to heat transfer per unit time across an object with a unit area, unit thickness, and a unit temperature difference between its surfaces. Simply put, thermal diffusivity is the ratio of thermal conductivity to volumetric heat capacity. The connection between thermal diffusivity and thermal conductivity is expressed as follows:

$$\alpha = \frac{k}{\rho \cdot c_p} \quad (3)$$

The relationship between thermal diffusivity and effusivity is described as follows:

$$\alpha = \frac{k^2}{e^2} \quad (4)$$

The thermal conductivity and effusivity were determined using the C-Therm TCi thermal analyzer. The other parameters were calculated on the basis of the aforementioned parameters. The measurement method is described by Di Scipio [7] and Labus et al. [16].

To assess the impact of the determined thermal parameters on rock behavior during the potential exploitation of geothermal heat, analytical calculations were carried out based on the methodology outlined by Labus et al. [16]. This approach enabled the determination of temperature evolution and the depth of heat penetration into the formation as it cools during operation. The formation model was simplified to a one-dimensional half-domain, extending infinitely in one direction ($z \rightarrow \infty$) (Figure 3).

The temperature drop at distance $z$ from the boundary, after a decrease from the initial temperature, can be calculated using the analytical solution derived from the heat conduction formula, as in the following Formula (5) [30]:

$$T(\mathrm{t}, z) = T_\mathrm{i} + (T_0 - T_\mathrm{i})\, erfc\left(\frac{z}{\sqrt{4\alpha t}}\right) \quad (5)$$

where $T$(t,z) represents the temperature [°C] at time $t$ [s] and distance $z$ [m] from the half-domain boundary, $T_i$ is the initial temperature [°C], $T_0$ is the surface temperature at time $t$ = 0 [°C], $\alpha$ is the thermal diffusivity [m$^2$/s], and erfc represents the complementary error function.

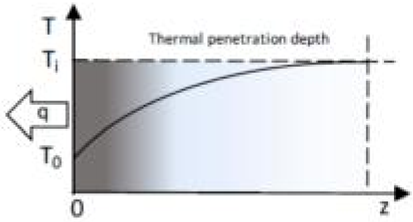


**Figure 3.** Heat conduction in a one-dimensional half-domain; $q$—heat flux (modified after [16]).

For the described 1D half-domain, the temperature drop ($T$(t,z)) at a distance ($z$) from the boundary, related to the heat outflow ($q$), can be calculated using the following formulas:

$$\frac{T(t,z) - T_0}{T_i - T_0} = \mathrm{erf}\left(\frac{z}{\sqrt{4\alpha t}}\right) \quad (6)$$

$$q = \frac{k(T_0 - T_i)}{\sqrt{\pi \alpha t}} \quad (7)$$

leading to the following solution:

$$T(t,z) = T_i + \left(\frac{q\sqrt{\pi \alpha t}}{k}\right) erfc\left(\frac{z}{\sqrt{4\alpha t}}\right) \quad (8)$$

where $q$ is heat flux density [W·m$^{-2}$], $erf$ is the error function, and the other symbols are as defined in Formula (5).

### 3.2.4. Geochemical Modelling

To assess potential geochemical interactions and their impact on the analyzed EGS collectors, geochemical modelling was carried out using the React program, which is part of the Geochemist's Workbench 11 simulator [31].

It was assumed that the injected working fluid would be raw water with low mineralization and a temperature of 40 °C (Table 2). For each of the collector rocks, two cases were analyzed: water with a pH of 7.5, and water of the same composition, energized with $CO_2$ to a fugacity level of 100 bar, to avoid mineral precipitation. The latter case also allows for an approximate analysis of the phenomena that could occur in the collector, in the case of $CO_2$ being added to it as a working fluid, in the presence of certain amounts of formation water. The water reacts with the rock for 20 days, as it flows through a network of fractures, and during this time it heats up from 40 °C to the formation temperature (Table 3).

**Table 2.** Primary composition of water.

| T (°C) | pH | Concentrations (mg/kg) | | | | | | | | | |
|---|---|---|---|---|---|---|---|---|---|---|---|
| | | $Cl^-$ | $SO_4^{2-}$ | $HCO_3^-$ | $Ca^{2+}$ | $Mg^{2+}$ | $Na^+$ | $K^+$ | $Al^{3+}$ | $SiO_{2(aq)}$ | $Fe^{2+}$ |
| 40 | 7.5 | 150 | 10 | 20 | 15 | 1 | 75 | 5 | 0.1 | 15 | 0.1 |

**Table 3.** Formation temperature, mineral composition, reaction rates, and specific surface of minerals used in the modelling. Mineral formulas are provided in Appendix A.

| | Sample | | | Reaction Rate $k_{25}$ (mol/cm² s) | | Specific Surface (cm²/g) |
|---|---|---|---|---|---|---|
| Temperature | CP-1 | GW-2 | J-4 | | | |
| (°C) | 165 | 135 | 135 | | | |
| | Mineral Composition (% vol.) | | | Neutral Mechanism | Acid Mechanism | |
| Quartz | 21.0 | 36.7 | 28.2 | $3.98 \times 10^{-18}$ | $3.98 \times 10^{-18}$ | 10 |
| K-feldspar | 34.7 | 42.1 | 21.3 | $3.89 \times 10^{-17}$ | $8.71 \times 10^{-11}$ | 10 |
| Albite | 33.7 | 16.8 | 22.4 | $2.75 \times 10^{-17}$ | $6.90 \times 10^{-15}$ | 10 |
| Biotite | 0.6 | 0.6 | 0.0 | $2.81 \times 10^{-17}$ | $1.44 \times 10^{-14}$ | 10 |
| Enstatite | 0.0 | 0.0 | 2.7 | $9.55 \times 10^{-14}$ | $9.55 \times 10^{-14}$ | 10 |
| Antigorite [a] | 0.0 | 0.0 | 8.3 | $4.00 \times 10^{-17}$ | $2.00 \times 10^{-10}$ | 10 |
| Lawsonite [b] | 0.0 | 0.0 | 2.0 | $7.59 \times 10^{-14}$ | $3.16 \times 10^{-8}$ | 10 |
| Kaolinite | 0.9 | 0.0 | 3.8 | $6.61 \times 10^{-18}$ | $4.90 \times 10^{-16}$ | 150 |
| Illite | 4.1 | 2.8 | 0.0 | $1.66 \times 10^{-17}$ | $1.66 \times 10^{-17}$ | 150 |
| Clinochlore-14A | 5.0 | 0.8 | 4.4 | $3.02 \times 10^{-17}$ | $7.76 \times 10^{-16}$ | 150 |
| Calcite | 0.0 | 0.0 | 2.1 | $1.55 \times 10^{-10}$ | $5.01 \times 10^{-5}$ | 10 |
| Hematite | 0.0 | 0.0 | 0.8 | $2.51 \times 10^{-19}$ | $4.07 \times 10^{-14}$ | 100 |
| Magnetite | 0.0 | 0.2 | 0.0 | $1.66 \times 10^{-15}$ | $2.57 \times 10^{-13}$ | 10 |
| Phlogopite | 0.0 | 0 | 4 | $4.00 \times 10^{-17}$ | $4.00 \times 10^{-17}$ | 10 |

[a] based on lizardite; [b] based on anorthite.

The mineralogical composition of the rocks was analyzed using XRD diffractometry and then converted to volume fractions (Table 3); it was assumed that all rocks were characterized by 20% fracture porosity. The reactions are simulated in a model with a volume of minerals equal to 12,500 cm³, in which 10,000 cm³ is occupied by minerals and the remaining part is the pore space through which the working fluid can flow.

The following simplified equation for the kinetics of dissolution/crystallization [32] was used in the calculations:

$$r_k = A_s \cdot k_T \cdot (1 - Q_a/K) \quad (9)$$

where $r_k$ is the reaction rate ([mol·s$^{-1}$]; dissolution—$r_k > 0$, precipitation—$r_k < 0$), $A_S$ is the mineral's surface area [cm$^2$], $k_T$ is the rate constant [mol·cm$^{-2}$·s$^{-1}$] at temperature T, $Q_a$ is the activity product [-], and $K$ is the equilibrium reaction for the dissolution reaction [-].

The reaction rates of the mineral phases depend on the pH at the HDR site. Consequently, different kinetic rate constants are applied for reaction mechanisms occurring under acidic and neutral conditions (e.g., [33]). In the cases analyzed in this study, for raw water, neutral conditions were assumed, and acidic conditions were only assumed for $CO_2$-energized water.

Kinetic rate constants for minerals participating in the simulated reactions were taken from the literature (e.g., [34]) and recalculated for the formation temperature; the specific surfaces were assumed approximately, based on the results of previous work (e.g., [35]) (Table 3). Since antigorite and lawsonite were not included in the thermodynamic database used in the simulations—thermo.tdat—for modelling purposes, they were replaced by their proxies, i.e., lizardite and anorthite.

## 4. Results and Discussion

### 4.1. Mineral Composition

The igneous rocks of the Karkonosze pluton were characterized using the results of XRD analyses for six samples from the CP-1 well, from a depth of 138 m to 184 m. These samples are granites (Figure 2a), in which feldspar plays the dominant role in mineral composition, including albite (28.6–35.4%), as well as orthoclase and microcline (8.5–21.1% and 15.5–24.5%, respectively). The average quartz content is 23%, while biotite, illite, kaolinite, and chlorite occur in small amounts (Table 4).

**Table 4.** Mineral composition of the samples from individual wells.

| Mineral | Granite, % (6 Samples) CP-1 | Rhyolite, % (2 Samples) GW-2 | Rhyolite, % (3 Samples) J-4 |
|---|---|---|---|
| Quartz | 18.3–28.6 | 37.1–37.8 | 18.5–29.2 |
| Orthoclase | 8.5–21.1 | 41.1–41.2 | - |
| Microcline | 15.5–24.5 | - | 21.3–27.2 |
| Albite | 28.6–35.4 | 16.5–16.8 | 14.5–22.9 |
| Biotite | 0.7–2.8 | 0.8–1.0 | 1.9–4.3 |
| Kaolinite | 0.7–1.6 | - | 3.8 |
| Illite | 3.8–4.3 | 2.7–3.0 | - |
| Chlorite | 2.9–10.7 | 0.7–0.8 | 4.6–33.0 |
| Magnetite | - | 0.2–0.3 | - |
| Hematite | - | - | 0.1–1.7 |
| Clinopyroxene | - | - | 1.1–2.6 |
| Pyrope | - | - | 0.8 |
| Anigorite | - | - | 1.3–26.1 |
| Lawsonite | - | - | 2.4 |

The volcanic rocks of the Gorzów Block have been classified as rhyolites [6]. They are composed mainly of quartz (37.1–37.8% in samples from GW-2 and 18.5–29.2% in borehole J-4), and K-feldspar. In the case of GW-2, it is represented by orthoclase (about 41%), while GW-4 rhyolite from borehole J-4 contains microcline (average 24%). Both types of rhyolite contain albite, a member of the plagioclase series. Clay minerals also occur in rhyolites, and several accessory minerals have been identified in samples from the J-4 well, such as clinopyroxene, pyrope, antigorite, and lawsonite.

### 4.2. *Rock Porosity and Density*

The studied geological formations are characterized by low effective porosity (Table 5). Bulk densities correspond to the values described for the equivalent rock formations (see e.g., [36,37]). The determined petrophysical parameters allow all the rocks studied to be classified as petrothermal formations [6]. The skeletal density of Karkonosze granite is in the range of2.61–2.64 g/cm$^3$, while that of the rhyolites of the Gorzów Block is in the range of 2.52–2.64 g/cm$^3$.

The skeletal density of Karkonosze granite is in the range of 2.61–2.64 g/cm$^3$, while that of the rhyolites of the Gorzów Block is in the range of 2.52–2.64 g/cm$^3$. The average value of the bulk density is the highest for granites (2.59) and lower for rhyolites. In the case of rhyolites from the GW-2 borehole, it is, on average, 2.45, while from the J-4 borehole, the bulk density is 2.52 g/cm$^3$.

**Table 5.** Selected petrophysical and thermal parameters of the tested samples.

| Type of the Rock/Number of Samples | Drill Hole | Location | Statistical Parameters | Effusivity e, (Ws½/m²K) | Thermal Conductivity k, (W/mK) | Effective Porosity p, (-) | Skeletal Density, $\rho_s$, (g/cm³) | Bulk Density, $\rho$, (g/cm³) | Heat Capacity Skeletal, $c_{ps}$, (J/kg·K) | Heat Capacity Bulk, $c_p$ (J/kg·K) | Diffusivity $\alpha$, (m²/s) |
|---|---|---|---|---|---|---|---|---|---|---|---|
| Granite 10 | CP-1 | Karkonosze Mountains | min | 2651.71 | 3.41 | 0.01 | 2.61 | 2.54 | 782.79 | 788.91 | $1.65 \times 10^{-06}$ |
| | | | max | 2902.53 | 3.98 | 0.03 | 2.64 | 2.62 | 809.65 | 834.00 | $1.88 \times 10^{-06}$ |
| | | | mean | 2781.25 | 3.70 | 0.01 | 2.62 | 2.59 | 798.21 | 809.82 | $1.78 \times 10^{-06}$ |
| | | | SD | 85.92 | 0.19 | 0.01 | 0.01 | 0.03 | 9.40 | 15.41 | $7.71 \times 10^{-08}$ |
| Rhyolite 5 | GW-2 | Gorzów Block | min | 2344.88 | 2.75 | 0.06 | 2.61 | 2.42 | 766.55 | 826.22 | $1.37 \times 10^{-06}$ |
| | | | max | 2563.66 | 3.22 | 0.08 | 2.63 | 2.47 | 780.70 | 837.97 | $1.57 \times 10^{-06}$ |
| | | | mean | 2510.90 | 3.10 | 0.07 | 2.62 | 2.45 | 775.62 | 831.00 | $1.53 \times 10^{-06}$ |
| | | | SD | 83.74 | 0.18 | 0.01 | 0.01 | 0.02 | 5.01 | 3.95 | $7.63 \times 10^{-08}$ |
| Rhyolite 7 | J-4 | Gorzów Block | min | 2297.99 | 2.65 | 0.01 | 2.52 | 2.46 | 759.63 | 775.39 | $1.33 \times 10^{-06}$ |
| | | | max | 2390.56 | 2.84 | 0.07 | 2.64 | 2.57 | 793.11 | 812.80 | $1.42 \times 10^{-06}$ |
| | | | mean | 2338.39 | 2.74 | 0.02 | 2.58 | 2.52 | 774.84 | 794.39 | $1.37 \times 10^{-06}$ |
| | | | SD | 30.60 | 0.06 | 0.02 | 0.04 | 0.05 | 11.89 | 14.99 | $2.81 \times 10^{-08}$ |

### 4.3. Thermal Properties

The range of variability for selected thermal parameters of the tested samples is presented in Table 5 and Figure 4. The lowest thermal conductivity (k) is characteristic of rhyolites from the J-4 well, i.e., in the range from 2.65 to 2.84 W/m·K. For samples from the GW-2 well, these values are in the range of 2.75 to 3.22 W/m·K. The highest values were observed for granites from the CP-1 well, in the range from 3.41 to 3.98 W/m·K. Similar dependencies occur for effusivity, which are in the following ranges: 2298–2391, 2345–2564, and 2652–2903 W·s½/m$^2$/K, respectively for samples from the J-4, GW-2, and CP-1 wells. The average specific heat for the entire volume of the rock is 810 J/kg K for granites, 838 J/kg K for rhyolites from the GP-2 well, and 775 J/kg K for rhyolites from the J-4 well.

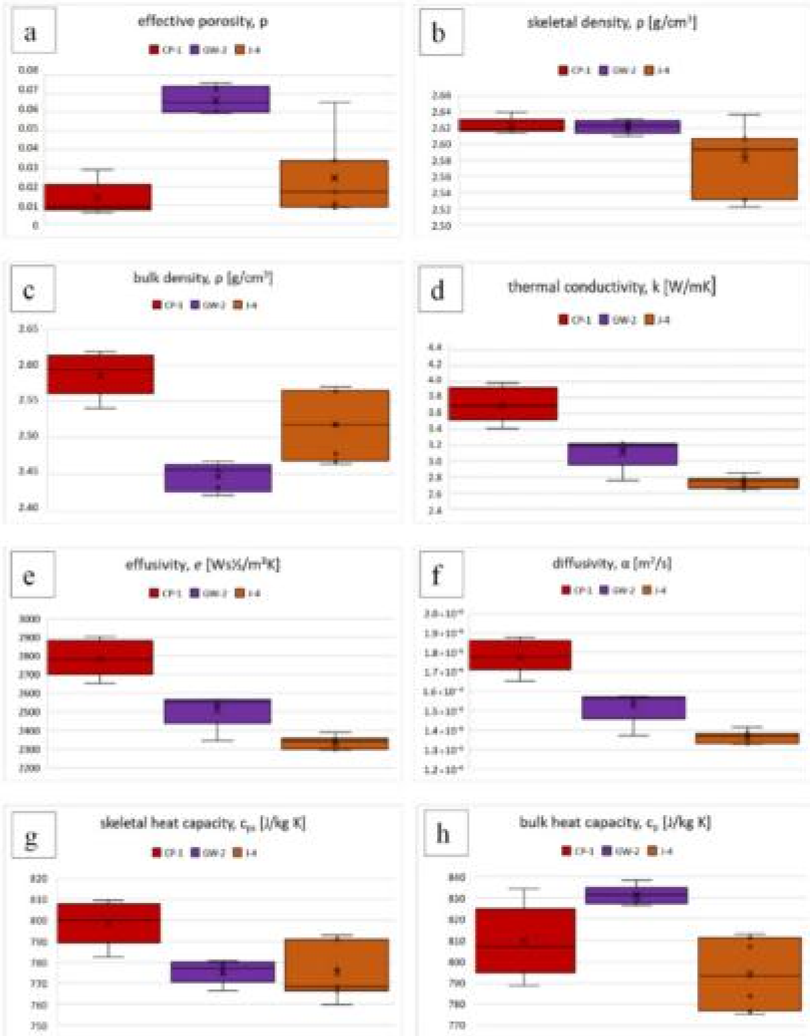


**Figure 4.** Range of variability for: (a) effective porosity, (b) skeletal density, (c) bulk density of rocks, (d) thermal conductivity coefficient, (e) thermal effusivity, (f) diffusivity, (g) skeletal heat capacity, (h) bulk heat capacity. Explanations: red—granite, Karkonosze Mountains (CP-1), purple—rhyolite, Gorzów Block (GW-2), and orange—rhyolite, Gorzów Block (J-4).

Figure 5 presents graphs of the relationships for selected petrophysical and thermal parameters of the tested samples, divided into three groups. The study of the relationship between thermal parameters and petrophysical ones has shown that the dominant influence on the differentiation of the former is exerted by rock features, such as density and porosity. Analysis of the relationships between the basic petrophysical and thermal parameters performed for the samples analyzed allows us to state that the bulk heat capacity of the rock ($C_p$) is negatively correlated with density and positively with porosity. This relationship is easily explained by the relatively low value of the specific heat for quartz, namely 741 J/kg·K, compared to the value of 1005 J/kg·K for air filling the pores of dry rock. Assuming that the rock was saturated with formation water of a seawater composition of $C_p$—3850 J/kg·K, the observed correlations could be even more significant.

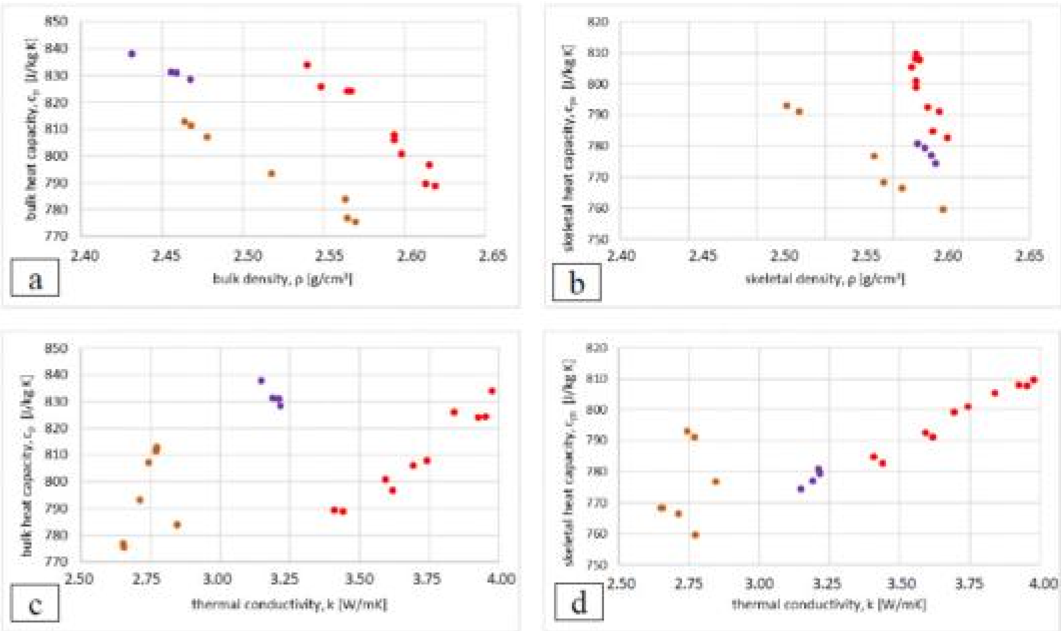


**Figure 5.** Graphic relations between thermal and petrophysical properties: (**a**) specific bulk rock heat capacity and bulk density; (**b**) skeleton heat capacity and skeleton density; (**c**) bulk rock heat capacity and thermal conductivity factor; (**d**) skeleton heat capacity and thermal conductivity factor. Explanations: red—granite, Karkonosze Mountains (CP-1), purple—rhyolite, Gorzów Block (GW-2), and orange—rhyolite, Gorzów Block (J-4).

The analysis of the parameter dependencies performed for 22 analyzed samples, for which the pore space characteristics were known, allows us to state that effusivity, thermal conductivity (k), and diffusivity are positively correlated with porosity for the analyzed rocks; therefore, in this case too, the explanation lies in the high value of the specific heat of air (filling the pores) compared to the specific heat of the rock skeleton, composed to a large extent of quartz.

Rocks with high or low thermal conductivity are always characterized by correspondingly high or low diffusivity values, as described for other examples [16]. It can, therefore, be concluded that the higher the k value of the rock (indicating greater energy extraction from the thermal source), the faster the absorbed energy is dissipated.

## *4.4. Evolution of Formation Temperature and Depth of Thermal Penetration*

Heat conduction calculations in a semi-infinite body under a specified heat flux were carried out using the values of α (average diffusivity), k (thermal conductivity), and Ti (average temperature) for the given formation (Table 5). These calculations facilitated a comparison of the behavior of different geologic formations under the same heat extraction conditions, with a heat flux of $q = -1\ W/m^2$. After 30 years of simulated heat production, rhyolites from the Gorzów Block, which had the lowest initial temperature, maintained a final temperature of no less than 108 °C and 106 °C. The resulting temperature decreases and thermal penetration depth at the domain boundary due to heat extraction for all studied formations are shown in Table 6 and visualized in Figure 6.

**Table 6.** Temperature drop and heat penetration depth for 1, 10, and 30 years of simulated heat extraction.

| Borehole | Geologic Province | Temperature Drop; Penetration Depth [°C]; [m] | | |
|---|---|---|---|---|
| | | 1 Year | 10 Years | 30 Years |
| CP-1 | Karkonosze Mts | 3; 22 | 11; 83 | 20; 160 |
| GW-2 | Gorzów Block | 4; 21 | 13; 75 | 22; 143 |
| J-4 | | 4; 21 | 14; 74 | 24; 142 |

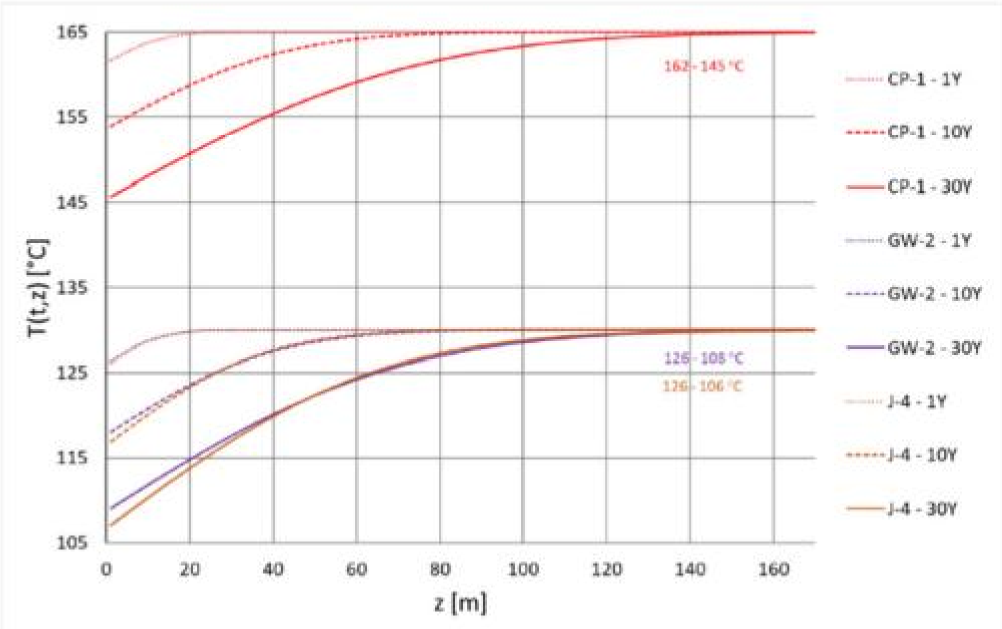


**Figure 6.** Temperature change T(t,z) depending on time and depth. Explanations: CP-1, GW-2, and J-4—names of the drilling wells; time: 1Y—1 year, 10Y—10 years, and 30Y—30 years.

The greatest thermal penetration depth is observed in geologic formations with the highest average diffusivity and thermal conductivity, such as the granites from the Karkonosze pluton, while the smallest is seen in rhyolites from the Gorzów Block (borehole J-4). After one year of cooling, the penetration depths are approximately 22 m and 21 m, respectively, and after 30 years, they reach 160 m and 142 m (Figure 6, Table 6).

The temperature drop is least significant in the Karkonosze pluton, which has the highest thermal conductivity (k) and diffusivity (α) values (Figure 6, Table 6). It is important to note that the Gorzów Block formations exhibit a relatively significant temperature drop, due to their lower $\alpha$ and k values. However, because of the formation's initially high temperature, this drop does not deplete the geothermal resources, nor does it negatively impact the possibility of continued exploitation, even over the long term. After 30 years of simulated heat extraction, the temperature remains at 106 °C and 108 °C, indicating that long-term exploitation is still feasible.

### 4.5. Geochemical Interactions

The reaction paths and amounts of reacting minerals for GW-2 and CP-1 are similar. During the reaction with raw water, K-feldspar, albite, illite and quartz decompose, while kaolinite and chlorites (clinochlore) precipitate (Table 7, Figure 7a,b). Due to the larger volume of dissolved minerals over crystallizing ones, porosity increases by 0.014 to 0.022 for GW-2 and CP-1, respectively. The pH drops slightly from 7.5 to 7.1 (Figure 8).

**Table 7.** Minerals responsible for porosity change.

| | Raw Water | | $CO_2$-Energized Fluid | |
|---|---|---|---|---|
| | **Dissolution** | **Precipitation** | **Dissolution** | **Precipitation** |
| CP-1 | K-feldspar<br>Illite<br>Albite | Clinochlore<br>Kaolinite | K-feldspar<br>Albite | Kaolinite<br>Quartz |
| GW-2 | K-feldspar<br>Illite<br>Albite | Clinochlore<br>Kaolinite | K-feldspar<br>Albite | Kaolinite |
| J-4 | Enstatite<br>Anorthite | Clinochlore<br>Illite<br>Antigorite<br>Calcite<br>Kaolinite | Calcite<br>K-feldspar | Kaolinite |

In the reaction with the $CO_2$-energized fluid, K-feldspar and albite are dissolved; the product is kaolinite. In this case, the quantity of reactants and reaction products is approximately three orders of magnitude greater than for raw water, and the increase in porosity is only slightly higher, reaching 0.016 and 0.023, while the pH of energized fluid rises from 3.5 to over 4.

The sample from the J-4 borehole, in contrast to the others, contains minerals with high reaction rates, such as calcite, enstatite, and anorthite. In reaction with raw water, enstatite and anorthite dissolve, while kaolinite, calcite, illite, and chlorite precipitate (Table 7, Figure 7c). Porosity increases by 0.013 and the final pH value reaches 7.8 (Figure 8).

Contact with the $CO_2$-energized fluid causes the rapid decomposition of calcite, which then undergoes partial recrystallization, and K-feldspar also decomposes, resulting in the precipitation of kaolinite. The quantity of reactants and reaction products is two orders of magnitude higher than that of raw water, porosity increases by 0.016, and the pH of the energized fluid stabilizes at 4.8.

Modelling the geochemical reaction path can provide a preliminary estimate of the probability and quantity of mineral deposits in the fracture network of the geothermal reservoirs that are being considered. In the analyzed cases, the permeability damage caused by mineral precipitation is unlikely. On the contrary, the observed increase in porosity may induce a decrease in hydraulic resistance and trigger an excessive flow rate, which, consequently, compromises the performance of the EGS.

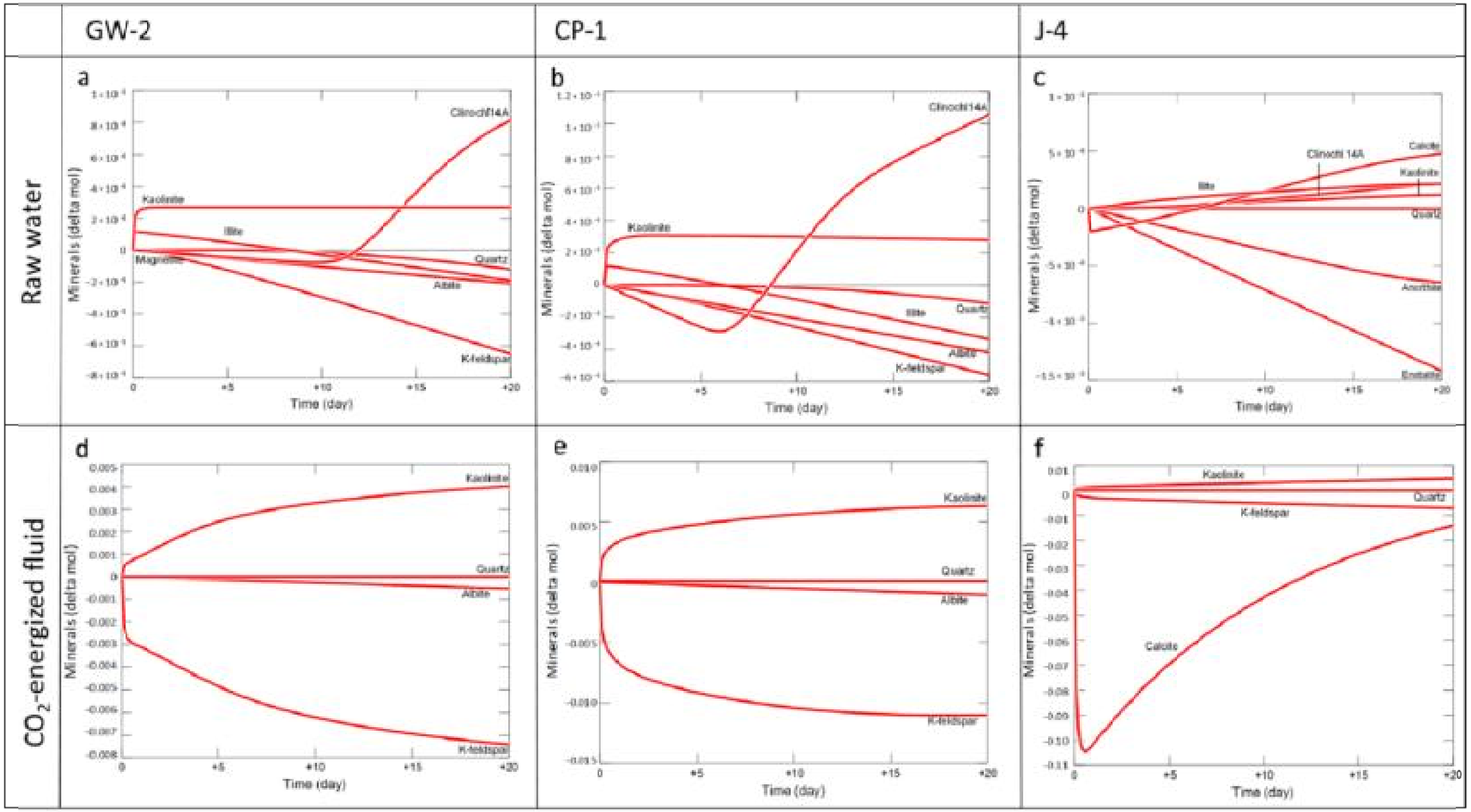


Figure 7. Changes in the mineral composition of rocks in contact with raw water: (a) sample GW-2, (b) sample CP-1, (c) sample J-4, and $CO_2$-energized fluid: (d) sample GW-2, (e) sample CP-1, (f) sample J-4 (positive values indicate precipitation; negative values indicate dissolution).

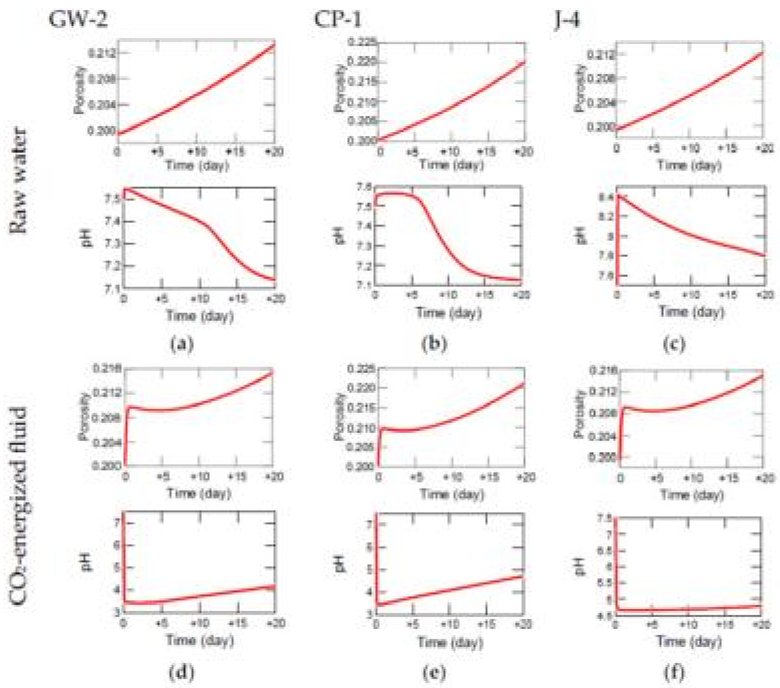


**Figure 8.** Changes in formation porosity and fluid pH due to contact of rocks with raw water: (a) sample GW-2, (b) sample CP-1, (c) sample J-4, and $CO_2$-energized fluid: (d) sample GW-2, (e) sample CP-1, (f) sample J-4.

## 5. Discussion

In recent years, there has been a noticeable increase in interest in the use of energy from enhanced geothermal system (EGS) collectors in Poland. This trend is largely driven by strict EU greenhouse gas regulations and the need to reduce the country's dependence on fossil fuels. Geothermal energy from EGS systems, including HDR, is emerging as a promising alternative. The successful implementation of EGS technology in western Europe has sparked scientific and economic discussions on the potential feasibility and profitability of adopting similar systems in the specific geological and market conditions of Poland.

In our research, we focused on geological formations formed of igneous rocks, including crystalline rocks of the Karkonosze pluton and volcanic rocks of the Gorzów Block. An important aspect of selecting these locations was the analysis of the heat flow density distribution in Poland [17,19].

An important factor in evaluating geothermal systems is the relationship between the porosity and permeability of the rocks. Generally, both permeability and porosity decrease with depth due to high static stresses and advanced diagenesis. Therefore, when assessing a potential geothermal system, the depth of the system should be considered, as it can significantly impact the long-term effectiveness of the system [38]. Based on previous studies [6], the authors classified the formations considered in this article as prospective petrothermal EGS formations.

Considering the thermal parameters determined here, it should be noted that thermal conductivity (*k*) positively correlates with diffusivity. As a result, it can be concluded that the higher the k value of the rock (indicating more energy can be extracted from the heat source), the faster the absorbed energy is dissipated, and the energy is replenished from more distant parts of the collector due to the high diffusivity. This is supported by the evolution of temperature $T$(t,z) with depth, as shown in Figure 6. In this sense, the most favorable parameters are those of the rocks belonging to the Karkonosze pluton.

Although a slightly higher temperature drop was estimated for the other rocks (Table 5), which is associated with their relatively low diffusivity and thermal conductivity, the high initial temperature of these formations makes the possibility of obtaining heat from them feasible even in the long term. For optimal geothermal system performance, it is desirable for the rocks to have high effusivity, diffusivity, heat capacity, and thermal conductivity. From this perspective, the rocks in the formations we studied possess the appropriate parameters, especially when considering their deposit temperatures.

From the perspective of hydraulic fracturing technologies, which are employed for heat recovery from HDR systems, i.e., hot, dry, and poorly permeable rocks, the thermal parameters of rocks, including thermal conductivity and thermal diffusivity, are crucial to ensure efficient heat transfer between the formation and the working fluid.

To validate the thermal parameters obtained in this study, we compare them with literature data. Typically, rocks show an increase in thermal conductivity with increasing pore water content and increasing pressure, which in turn depends on the depth and compaction-related decrease in porosity (e.g., [39,40]). On the other hand, thermal conductivity decreases with increasing temperature, which is usually positively correlated with depth, and microstructural changes, such as the appearance of microcracks and grain shifts, can reduce the heat transfer efficiency [41]. The thermal parameters we calculated are within the ranges given in the literature, at least in terms of the most popular parameter, which is the thermal conductivity. Other parameters, such as effusivity and diffusivity, are rarely determined. For example, for East and Central China granites, the mean thermal conductivity is in the range of 2.4–3.1 W/(m·K) [42], while DiScipio et al. [7] provide thermal conductivity values for dry granites from Calabria (Italy) of 1.3–3.5 W/(m·K). These values are lower than those obtained in this study for Karkonosze granites: 3.41–3.98 W/(m·K). Lim et al. [43] measured the conductivity of rhyolite from South Korea as: 3.87 W/(m·K), while Ahmed et al. [41] and Ray et al. [44] established the thermal conductivity at room temperature in the range from 2.5 to 3.3 W/(m·K). These results are applied to samples with low porosity and high density, which favor higher conductivity values. This is consistent with our results, which are in the range of 2.65–3.22 W/(m·K).

## 6. Conclusions

The novelty of this work is that it presents rarely determined rock parameters, such as diffusivity and effusivity, which are important for assessing the thermal equilibrium of geologic formations in the conditions of operation of geothermal systems in Poland. Moreover, for the first time, an assessment of the geochemical interactions of the working fluid with rock in potential EGS systems in the Karkonosze pluton and volcanic rocks of the Gorzów Block was made.

(1) The study conducted provided data on the thermal parameters of igneous rocks from two formations, namely the Karkonosze pluton and the Gorzów Block, both of which are considered potential candidates for EGS development.
(2) The low porosity and permeability values of the rocks categorize all the studied formations as potentially favorable for the development of petrothermal EGS.
(3) Karkonosze granite is characterized by the highest diffusivity, which means that during potential exploitation it can quickly regain thermal equilibrium.
(4) Geochemical reaction modelling has shown that permeability damage due to mineral precipitation is unlikely. On the contrary, due to the dissolution of some rock components, porosity may increase, which ultimately leads to a reduction in collector efficiency.

(5) Research on rocks from deep wells has revealed that the rocks of the Karkonosze pluton exhibit the most favorable parameters for energy extraction from EGS in Poland. While the rhyolites of the Gorzów Block have slightly lower diffusivity and thermal conductivity, their high initial temperature makes them a promising option for heat utilization, even over the long term.

**Author Contributions:** Conceptualization, supervision, literature review, investigation, manuscript writing, and visualization, K.L.; literature review, investigation, manuscript editing, and manuscript review, R.M.; investigation, manuscript editing, and manuscript review, M.L. All authors have read and agreed to the published version of the manuscript.

**Funding:** This paper is based on research carried out at the Oil and Gas Institute-National Research Institute (Poland), and the Silesian University of Technology, as part of the implementation doctor-ate program RJO/SDW/005-33, founded by Ministry of Education and Science of Poland.

**Data Availability Statement:** The data presented in this study are available on request from the corresponding author.

**Conflicts of Interest:** The authors declare no conflicts of interest.

## Nomenclature

| | |
|---|---|
| EGSs | Enhanced geothermal systems |
| HDR | Hot dry rock |
| $\alpha$ | Thermal diffusivity ($m^2/s$) |
| $c_p$ | Specific heat capacity of bulk rock (J/kgK) |
| $c_{ps}$ | Specific heat capacity of rock skeleton (J/kgK) |
| e | Thermal effusivity (Ws½/$m^2$K) |
| k | Thermal conductivity coefficient (W/mK) |
| l | Thickness of the material (m) |
| $\rho$ | Material bulk density ($g/cm^3$) |
| $\rho_s$ | Material skeletal density ($g/cm^3$) |
| p | Porosity (-) |
| q | Heat flux ($W/m^2$) |
| s | Sample surface area ($m^2$) |
| t | Time (s) |
| Q | Heat quantity (J) |
| $T_0$ | Temperature at the surface at time $t - 0$ (°C) |
| $T_i$ | Average formation temperature (°C) |
| $r_k$ | Reaction rate (mol/s) |
| $A_S$ | Mineral's surface area ($cm^2$), |
| $k_T$ | Rate constant ($mol/cm^2 \cdot s$) at the temperature T |
| $Q_a$ | Activity product (-) |
| K | Equilibrium reaction for the dissolution (-) |

## Appendix A

**Table A1.** Mineral phases participating in the analyzed reactions.

| Mineral Phase | Formula |
|---|---|
| Albite | $NaAlSi_3O_8$ |
| Anhydrite | $CaSO_4$ |
| Annite | $KFe_3AlSi_3O_{10}(OH)_2$ |
| Anorthite | $CaAl_2Si_2O_8$ |

**Table A1.** *Cont.*

| Mineral Phase | Formula |
|---|---|
| Antigorite | $Mg_{24}Si_{17}O_{42.5}(OH)_{31}$ |
| Calcite | $CaCO_3$ |
| Clinochlore | $Mg_5Al_2Si_3O_{10}(OH)_8$ |
| Enstatite | $MgSiO_3$ |
| Hematite | $Fe_2O_3$ |
| Illite | $K_{0.6}Mg_{0.25}Al_{2.3}Si_{3.5}O_{10}(OH)_2$ |
| K-feldspar | $KAlSi_3O_8$ |
| Kaolinite | $Al_2Si_2O_5(OH)_4$ |
| Magnetite | $Fe_3O_4$ |
| Phlogopite | $KAlMg_3Si_3O_{10}(OH)_2$ |
| Quartz | $SiO_2$ |

## References


1. Jones, C.; Simmons, S.; Moore, J. Geology of the Utah Frontier Observatory for Research in Geothermal Energy (FORGE) Enhanced Geothermal System (EGS) Site. *Geothermics* **2024**, *122*, 103054. [CrossRef]
2. Moska, R.; Labus, K.; Kasza, P.; Moska, A. Geothermal Potential of Hot Dry Rock in South-East Baltic Basin Countries—A Review. *Energies* **2023**, *16*, 1662. [CrossRef]
3. Wyborn, D.; da Graaf, L.; Davidson, S.; Hann, S. Development of Australia's first hot fractured rock (HFR) underground heat exchanger, Cooper Basin, South Australia. In Proceedings of the World Geothermal Congress, Antalya, Turkey, 24–29 April 2005.
4. McClure, M.; Horne, R. An investigations of stimulation mechanisms in enhanced geothermal systems. *Int. J. Rock. Mech. Min. Sci.* **2014**, *72*, 242–260. [CrossRef]
5. Moska, R.; Labus, K.; Kasza, P. Hydraulic Fracturing in Enhanced Geothermal Systems—Field, Tectonic and Rock Mechanics Conditions—A Review. *Energies* **2021**, *14*, 5725. [CrossRef]
6. Moska, R.; Labus, K.; Kasza, P. Dynamic elastic properties, petrophysical parameters and brittleness of hot dry rocks from prospective areas of Central Europe. *Adv. Geo-Energy Res.* **2024**, *14*, 90–105. [CrossRef]
7. Di Sipio, E.; Chiesa, S.; Destro, E.; Galgaro, A.; Giaretta, A.; Gola, G.; Manzella, A. Rock thermal conductivity as key parameter for geothermal numerical models. *Energy Procedia* **2013**, *40*, 87–94. [CrossRef]
8. Brown, D.W.; DuTeaux, R.; Kruger, P.; Swenson, D.; Yamaguchi, T. Fluid Circulation and Heat Extraction from Engineered Geothermal Reservoirs. *Geothermics* **1999**, *28*, 553–572. [CrossRef]
9. Clauser, C.; Huenges, E. Rock Physics & Phase Relations: A Handbook of Physical Constants. *Therm. Conduct. Rocks Miner. Am. Geophys. Union.* **2013**, *3*, 105–126. [CrossRef]
10. Duchane, D.V.; Brown, D.W. Hot Dry Rock (HDR) Geothermal Energy Research and Development at Fenton Hill, New Mexico. *GHC Bull.* **2002**, *32*, 13–19.
11. Heap, M.J.; Kushnir, A.R.; Gilg, H.A.; Violay, M.E.; Harlé, P.; Baud, P. Petrophysical properties of the Muschelkalk from the Soultz-sous-Forêts geothermal site (France), an important lithostratigraphic unit for geothermal exploitation in the Upper Rhine Graben. *Geotherm. Energy* **2019**, *7*, 27. [CrossRef]
12. Ollinger, D.; Baujard, C.; Kohl, T.; Moeck, I. Distribution of thermal conductivities in the Groß Schönebeck (Germany) test site based on 3D inversion of deep borehole data. *Geothermics* **2010**, *39*, 46–58. [CrossRef]
13. Zhu, Z.; Yang, S.; Wang, R.; Xie, J.; Tian, N.; Tian, H.; Zheng, J.; Jiang, G.; Dou, B. Experimental investigation on the physical-thermal properties of Nanan granite after air and water cooling for deep geothermal heat extraction. *Renew. Energy* **2024**, *223*, 119963. [CrossRef]
14. Bujakowski, W.; Barbacki, A.; Miecznik, M.; Pająk, L.; Skrzypczak, R. A Structural-Thermal model of the Karkonosze Pluton (Sudetes Mountains, SW Poland) for Hot Dry Rock (HDR) geothermal use. *Arch. Min. Sci.* **2016**, *61*, 917–935. [CrossRef]
15. Sowiżdżał, A.; Kaczmarczyk, M. Analysis of thermal parameters of Triassic, Permian and Carboniferous sedimentary rocks in central Poland. *Geol. J.* **2016**, *51*, 65–76. [CrossRef]
16. Labus, K.; Labus, M.; Leśniak, G. Thermal properties of rocks from deep boreholes in Poland in terms of obtaining geothermal energy from enhanced geothermal systems. *Adv. Geo-Energy Res.* **2023**, *8*, 76–88. [CrossRef]
17. Wójcicki, A.; Sowiżdżał, A.; Bujakowski, W. *Ocena Potencjału Bilansu Cieplnego i Perspektywicznych Struktur Geologicznych dla Potrzeb Zamkniętych Systemów Geotermicznych (Hot Dry Rocks) w Polsce*; Ministerstwo Środowiska: Warsaw, Poland, 2013. (In Polish)
18. Szewczyk, J.; Gientka, D. *Mapa Gęstości Ziemskiego Strumienia Cieplnego Polski*; Polish Geological Institute: Warsaw, Poland, 2009. (In Polish)

19. Karnkowski, P. Budowa geologiczna oraz geneza i ewolucja bloku Gorzowa. *Przegląd Geol.* **2010**, *58*, 680–688. (In Polish)
20. Cloos, H. *Einführung in die Tektonische Behandlung Magmatischer Erscheinungen (Granittektonik).Teil I. Das Riesengebirge in Schlesien; Bau, Bildung und Oberflächengestaltung*; Gebrüder Borntraeger: Berlin, Germany, 1925; pp. 1–194.
21. Mierzejewski, M.P. Denudation of the ancient Karkonosze Mts during Permo-Carboniferous and Mesosoic Era. *Geol. Sudet.* **1985**, *20*, 197–225. (In Polish)
22. Mikulski, S. Metal ore potential of the parent magma of granite—the Karkonosze massif example, Granitoids in Poland. *Arch. Mineral. Monogr.* **2007**, *1*, 123–145.
23. Huenges, E.; Holl, H.G.; Bruhn, D.; Brandt, W.; Saadat, A.; Moeck, I.; Zimmermann, G. Current state of the EGS project Groß Schönebeck—Drilling into the deep sedimentary geothermal reservoir. In Proceedings of the European Geothermal Congress 2007, Unterhaching, Germany, 30 May–1 June 2007.
24. Blocher, G.; Reinsch, T.; Henninges, J.; Milsch, H.; Regenspurg, S.; Kummerow, J.; Francke, H.; Kranz, S.; Saadat, A.; Zimmermann, G.; et al. Hydraulic history and current state of the deep geothermal reservoir Gros Schonebeck. *Geothermics* **2016**, *63*, 27–43. [CrossRef]
25. Sowiżdżał, A. Geothermal energy resources in Poland—Overview of the current state of knowledge. *Renew. Sustain. Energy Rev.* **2018**, *82*, 4020–4027. [CrossRef]
26. Rietveld, H.M. A profile refinement method for nuclear and magnetic structures. *J. Appl. Crystallogr.* **1969**, *2*, 65–71. [CrossRef]
27. Liu, S.; Feng, C.; Wang, L.L.C. Measurement and Analysis of Thermal Conductivity of Rocks in the Tarim Basin, Northwest China. *Acta Geol. Sin.* **2011**, *85*, 598–609. [CrossRef]
28. Cermak, V.; Rybach, L. Thermal properties: Thermal conductivity and specific heat of minerals and rocks. In *Landort-Börnstein Zahlenwerte und Funktionen aus Naturwissenschaften und Technik, Neue Serie, Physikalische Eigenschaften der Gesteine*; Angeneister, Ed.; Springer: Berlin, Germany; New York, NY, USA, 1982.
29. Guimarães, A.O.; Viana, D.A.; Cordeiro, T.C.; Sampaio, J.A.; da Silva, E.C.; Toledo, R.; Ribeiro, H.J.P.S.; Carrasquilla, A.A.G.; Vargas, H. On the use of photothermal methods for thermal characterization of sedimentary rocks from the Paraná Basin in Brazil. *Marine Petrol. Geol.* **2013**, *43*, 121–126. [CrossRef]
30. Hahn, D.W.; Özişik, M.N. *Heat Conduction*, 3rd ed.; John Wiley & Sons: Hoboken, NJ, USA, 2012; pp. 1–718.
31. Bethke, C.M. *Geochemical and Biogeochemical Reaction Modeling*; Cambridge University Press: Cambridge, UK, 2008.
32. Lasaga, A.C. Chemical kinetics of water-rock interactions. *J. Geophys. Res.* **1984**, *89*, 4009–4025. [CrossRef]
33. Labus, K.; Tarkowski, R.; Wdowin, M. Modeling gas—rock—water interactions in carbon dioxide storage capacity assessment: A case study of Jurassic sandstones in Poland. *Int. J. Environ. Sci. Technol.* **2015**, *12*, 2493–2502. [CrossRef]
34. Palandri, J.L.; Kharaka, Y.K. *A Compilation of Rate Parameters of Water-Mineral Interaction Kinetics for Application to Geochemical Modeling*; USGS Report 2004-1068; USGS: Menlo Park, CA, USA, 2004.
35. Labus, K.; Bujok, P. $CO_2$ mineral sequestration mechanisms and capacity of saline aquifers of the Upper Silesian Coal Basin (Central Europe)–modeling and experimental verification. *Energy* **2011**, *36*, 4974–4982. [CrossRef]
36. Bourbie, T.; Coussy, O.; Zinszner, B. *Acouistic of Porous Media*; Editions Technip: Paris, France, 1987.
37. Plewa, M.; Plewa, S. *Petrofizyka*; Wyd: Geologiczne, Warszawa, 1992. (In Polish)
38. Moeck, I. Catalog of geothermal play types based on geologic controls. *Renew. Sustain. Energy Rev.* **2014**, *37*, 867–882. [CrossRef]
39. Labus, M.; Labus, K. Thermal conductivity and diffusivity of fine-grained sedimentary rocks. *J. Therm. Anal. Calorim.* **2018**, *132*, 1669–1676. [CrossRef]
40. Joeleht, A.; Kirsimae, K.; Shogenova, A.; Sliaupa, S.; Kukkonen, I.T.; Rasteniene, V.; Zabele, A. Thermal conductivity of Cambrian siliciclastic rocks from the Baltic basin/Balti basseini Kambriumi ladestu terrigeensete kivimite soojusjuhtivus. *Proc. Est. Acad. Sci. Geol.* **2002**, *51*, 5–15.
41. Ahmed, H.M.; Hefni, M.A.; Ahmed, H.A.M.; Adewuyi, S.O.; Hassani, F.; Sasmito, A.P.; Saleem, H.A.; Moustafa, E.B.; Hassan, G.S.A. Effect of Elevated Temperature on Rhyolitic Rocks' Properties. *Materials* **2022**, *15*, 3204. [CrossRef] [PubMed]
42. Zhu, X.; Gao, Z.; Chen, T.; Wang, W.; Lu, C.; Zhang, Q. Study on the Thermophysical Properties and Influencing Factors of Regional Surface Shallow Rock and Soil in China. *Front. Earth Sci.* **2022**, *10*, 864548. [CrossRef]
43. Lim, W.R.; Hamm, S.Y.; Lee, C.; Hwang, S.; Park, I.-H.; Kim, H.C. Characteristics of Deep Groundwater Flow and Temperature in the Tertiary Pohang Area, South Korea. *Appl. Sci.* **2020**, *10*, 5120. [CrossRef]
44. Ray, L.; Chopra, N.; Singh, S.P.; Hiloidari, S.; Rao, S.E. Thermal conductivity at elevated temperature, density and geochemical signatures for the massive rhyolites of the Bundelkhand Craton, central India. *Geophys. J. Int.* **2023**, *232*, 1742–1755. [CrossRef]

**Artykuł V: Wpływ parametrów sprężystości skał na geometrię kolektora geotermalnego w wybranych, perspektywicznych dla EGS lokalizacjach w Polsce.**

*energies*

MDPI

*Article*

# Impact of Rock Elastic Properties on Fracture Geometry in Potential Enhanced Geothermal Systems in Poland

**Rafał Moska [1], Krzysztof Labus [2,*] and Piotr Kasza [1]**

[1] Oil and Gas Institute—National Research Institute, 25A Lubicz Str., 31-503 Krakow, Poland; moska@inig.pl (R.M.); kasza@inig.pl (P.K.)
[2] Faculty of Mining, Safety Engineering and Industrial Automation, Silesian University of Technology, 2 Akademicka Str., 44-100 Gliwice, Poland
[*] Correspondence: krzysztof.labus@polsl.pl

**Abstract:** In hot dry rocks (HDRs), hydraulic fracturing is necessary to create enhanced geothermal systems (EGSs) and optimize flow rates between injection and production wells. The geometry of the induced fracture is related to numerous factors, including rock mechanical properties, especially Young's modulus and Poisson's ratio. In this paper, we show the influence of Young's and Poisson's parameters on fracture geometry in selected HDR-type prospective areas in Poland. Parameters were determined in the laboratory based on drill core samples from granite and sandstone formations using both dynamic and static methods. The results obtained reveal strong differences between dynamic and static values in granite and less diverse results in sandstone. Based on these data, numerical simulations of fracture geometry were carried out, taking into account the variability in the rocks' elastic parameters. Sensitivity analysis showed that relatively high diversity in the elastic parameters led to a relatively slight impact on the fracture geometry of the tested formations. The influence of Young's modulus did not exceed 6.5% of the reference half-length and width values for sandstone and 7.3% of the half-length for granite. Variability in the fracture width was significant in granite formation and amounted to 46.4%. The influence of Poisson's ratio was marginal in both tested types of rocks. The research results, which have not been reported previously, can be considered for the design of hydraulic fracturing operations in enhanced geothermal systems in Poland.

**Keywords:** hot dry rock; HDR; enhanced geothermal systems; EGS; rock elastic parameters; hydraulic fracturing; laboratory measurements; fracture modeling

check for updates

Academic Editor: Nikolaos Koukouzas

Received: 8 April 2025
Revised: 13 May 2025
Accepted: 27 May 2025
Published: 30 May 2025

**Citation:** Moska, R.; Labus, K.; Kasza, P. Impact of Rock Elastic Properties on Fracture Geometry in Potential Enhanced Geothermal Systems in Poland. *Energies* **2025**, *18*, 2869. https://doi.org/10.3390/en18112869



## 1. Introduction

Hot dry rocks (HDRs) are one of the most promising sources of clean, renewable energy production. Utilizing this potential may meet energy needs for many decades [1]. To extract heat from deep formations with low porosity and low permeability, it is necessary to improve the hydraulic conductivity in reservoirs [2]. Due to the use of stimulation methods to increase conductivity in rocks, these types of systems are called enhanced geothermal systems (EGSs). In EGSs, connecting two or more wells at the depth of the target zone allows one to create an underground heat exchanger, where the process fluid (most often water) circulates in the loop through the formation between injection and production wells. The fluid is heated in a conduction process and then releases energy at the surface as steam, driving electric generators. Depending on the temperature at the surface, electricity is generated in binary or direct systems. The most widely used method of HDR stimulation is hydraulic fracturing (HF), which allows engineers to create new or reopen pre-existing fractures both near and far from the wellbore [3–5]. In contrast to other reservoir stimulation methods, HF enables a permanent connection between wells spaced hundreds of meters apart in the target zone. Since the 1970s, many EGS projects in which the main method of rock stimulation was tensile fracturing or hydroshearing have been developed, e.g., Fenton Hill in the USA [6,7], Rosemanowes in the UK [3], Ogachi in Japan [8], Habanero in Australia [9], projects in Rhine Graben in Western Europe [10–14], and Phoang in Korea [15]. In these projects, HF operations were carried out in both igneous and sedimentary strata, using different types of fracking fluid, proppants, and diversified types of pumping schedules. In other regions, including Poland, extensive work is currently underway to identify and evaluate prospective areas for EGSs [16–18].

The geometry of the fracture network that makes up the HDR geothermal system is influenced by many factors, including the stress state, development of the planes of discontinuity, and petrophysical parameters of the target zone. Our study investigates how rock elastic parameters influence fracture geometry at selected prospective EGS sites in Poland. It presents preliminary recommendations for HF operations in these formations. The data, which include the impact of Young's modulus and Poisson's ratio on fracture dimensions along with a sensitivity analysis, are novel and have not been published previously. To achieve this goal, we selected two petrothermal formations in Poland: altered granite from the Karkonosze Mountains and sandstone from the Mogilno-Łódź Trough. Core samples were collected from wellbores in both regions for analysis.

Results of the laboratory petrophysical and petrographical analyses of these samples in dry conditions were presented in a previous study [18]. In this paper, we combine these data with new results from subsequent laboratory ultrasonic tests on brine-saturated samples and strength tests of dry samples. Using FracPro software (version 10.13.6.0), we analyze the impact of rock elastic parameters on fracture half-length, height, and width as well as conductivity in the considered formations and present preliminary guidelines for their enhancement through HF operations.

## 2. Geomechanical Issues of Hydraulic Fracturing in Hot Dry Formations

EGS reservoirs can be broadly classified into two main types based on the stimulation concept [19]: (1) relatively intact reservoirs with extremely low matrix permeability and poorly conductive natural fractures and (2) reservoirs where conductivity is primarily enhanced by shear failure and slippage along pre-existing natural fractures. In the first type reservoirs, HF operations are predominantly controlled by in situ stress conditions and, to a lesser extent, petrophysical and rock mechanical parameters. In these settings, the minimum principal stress largely dictates the initiation and propagation direction of fractures [2,11]. Under common stress regimes such as extensional or strike-slip, vertical fractures are primarily formed (Figure 1). Fracturing in this case is governed by a tensile mechanism, which demands high injection pressures and the use of proppants. While this produces a simpler fracture network, it results in a reduced contact area between the rock and wellbore, thereby limiting system efficiency [19]. The second type of reservoir is dominated by shear-driven fracturing mechanisms (hydroshearing), where stimulation pressures are typically lower (below the minimum principal stress) and proppant is often unnecessary. This is due to the self-propping behavior of reactivated natural fractures. These shear-activated fractures provide greater contact area, resulting in more efficient geothermal energy extraction. However, in some other EGSs, both natural and induced fractures created in both pure tensile and hydroshearing mechanisms can play a role, with induced fractures acting as connectors between natural ones [20]. The interaction mode between natural and induced fractures is mainly controlled by the confining stress, approaching angle, mechanical properties of natural fractures, injection rate, and fluid viscosity [21]. The injection of relatively cool treatment fluid into a hot reservoir can also induce thermally driven fractures, typically oriented perpendicular to hydraulic fractures induced by stress reduction. While this mechanism has not been directly observed in the field, it has been confirmed through laboratory-scale experimental studies [19].

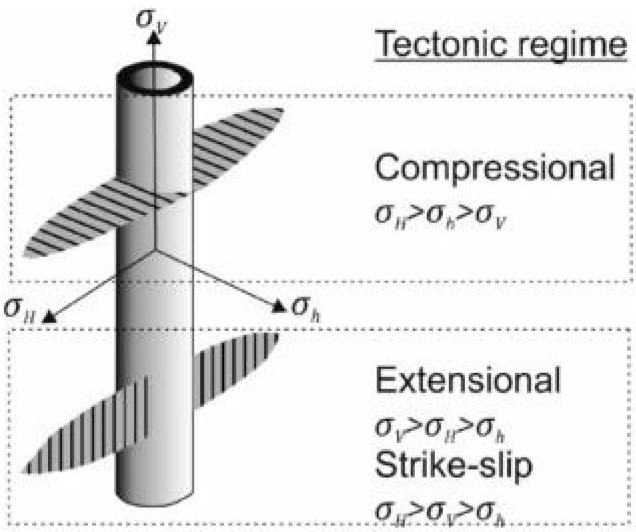


**Figure 1.** Simplified model of hydraulic fracture geometry depending on the tectonic regime. In the extensional and strike-slip regimes, vertical fractures are formed, whereas in the compressional regime, horizontal fractures dominate. $\sigma_V$—vertical principals stress, $\sigma_H$—maximum horizontal stress, $\sigma_h$—minimum horizontal stress (based on [22]).

The geological factors that influence the geometry of the induced fracture also include rock permeability/leakoff coefficient as well as the elastic properties of the target zone and the formations above and below it. The elastic parameters of the rock describe the behavior of the material, including its susceptibility to deformation and failure under applied stress of a certain magnitude. Main elastic rock parameters that must be known to design an HF system are Young's modulus ($E$) and Poisson's ratio ($v$). $E$ defines how much energy is required to complete the displacement, which is consistent with the classical concept of linear elastic fracture mechanics. According to classic fracture mechanics, as $E$ increases, the length and height of the fracture increase, while width decreases. The net pressure (fracturing and closure differential pressure ratio) also increases. Rocks with a large $E$ require more energy to experience displacement. In these formations, fractures tend to be relatively narrow, and the rock is referred to as "hard" [23]. The $E$ value of a rock typically increases with decreasing values of discontinuity and weakness planes and with increasing water saturation. $v$ determines the ability of rocks to fail under stress [24]. In practice, the influence of $v$ is lower than that of $E$. In formations with low $v$ values, the unfavorable penetration of proppant grains into the fracture walls (embedment phenomenon) increases, leading to a decrease in conductivity [25,26]. Other elastic parameters, i.e., bulk ($K$) and shear modulus ($G$), are derivatives that can be calculated from $E$ and $v$. Their influence on the fracture geometry results from the influence of $E$ and $v$; thus, they are usually not directly used for HF design.

### *2.1. Laboratory Rock Elastic Parameter Determination*

Mechanical properties play one of the most crucial roles in HF operations but also have an impact on many other aspects, especially on wellbore stability, compression/tension capacity, and the general safety of underground structures in exploration areas [27]. Two laboratory methods of rock mechanical parameter determination are commonly used: destructive and non-destructive. In the destructive method, parameters are calculated from stress-to-strain relation in the sample during uniaxial or triaxial static loading experiments. The deformation is recorded until the sample breaks, and the parameters obtained are called static. The static Young's modulus ($E_{stat}$) defines the linear relationship between applied stress $\sigma$ and strain $\varepsilon$ on the load axis (1) [23],

$$E_{stat} = \sigma/\varepsilon \tag{1}$$

whereas the static Poisson's ratio ($\upsilon_{stat}$) describes the negative ratio of transverse strain ($\varepsilon_{transverse}$) to axial strain ($\varepsilon_{axial}$) (2) [23].

$$\upsilon_{stat} = -d\,\varepsilon_{transverse}/d\,\varepsilon_{axial} \tag{2}$$

In the non-destructive method, mechanical properties are measured indirectly based on the relationship between the velocity of elastic waves (longitudinal and shear) and the bulk density of the measured sample (3) and (4) [28]:

$$\upsilon_{dyn} = \frac{1/2 - (V_S/V_P)^2}{1 - (V_S/V_P)^2} \tag{3}$$

$$E_{dyn} = \rho \frac{{V_P}^2(1+\upsilon)(1-\upsilon)}{(1-\upsilon)} \tag{4}$$

where $E_{dyn}$—dynamic Young's modulus, Pa; $V_P$—P-wave velocity, m/s; $V_S$—S-wave velocity, m/s; $\upsilon_{dyn}$—dynamic Poisson's ratio, dimensionless; $\rho$—bulk density, g/cm$^3$. The advantage of this type of testing is that the dynamic elastic parameters determined in reservoir conditions, i.e., the measurement of a saturated core sample at reservoir temperature, taking into account the influence of the effective pressure, can be correlated with the acoustic logging data. Since the samples are not destroyed during testing, they can be measured multiple times, which allows for testing before and after exposure to unfavorable environmental conditions, for example $CO_2$ [29,30]. $E$-to-$\upsilon$ relations, both dynamic and static, are also used to calculate the rock brittleness index (BI) parameter used to estimate susceptibility to fracking, mostly in natural gas reservoirs [24,31], and also may indicate prospective intervals in HDRs [18].

### 2.2. Relation Between Dynamic and Static Moduli

The discrepancy between static and dynamic rock mechanical parameters has been the subject of research for many years [27,32,33]. In most published papers, researchers indicate that $E_{dyn}$ is larger than $E_{stat}$, whereas the relationship between $\upsilon_{dyn}$ and $\upsilon_{stat}$ is not so obvious. $E_{dyn}$ is typically one to two times greater than the corresponding static value [34]. However, in weak or fractured rocks, such as coal, the $E_{dyn}/E_{stat}$ ratio can significantly exceed two [35]. Furthermore, Bukowska et al. [36] showed that $E_{dyn}$ for very weak fractured coals can be several times greater than $E_{stat}$, whereas $\upsilon_{dyn}$ is comparable to $\upsilon_{stat}$. The observed variations between static and dynamic parameters are explained by complex external and internal factors like stress–strain conditions, temperature, sample mineral composition, presence of fractures or cracks, type of pore fluid, and rock anisotropy. With respect to these factors, the existence of microfractures and pores in the rock is described as the main cause of these differences. Correlations between dynamic and static parameters are usually described by several types of empirical equations. The most commonly used are linear regression-based ($E_{stat} = aE_{dyn} + b$) and power-law-based

($E_{stat} = \alpha E_{dyn}^{\beta}$). For igneous and metamorphic rocks, the optimal relationship is the power-law correlation. On the other hand, for sedimentary rocks, linear and nonlinear logarithmic correlations give better results [27].

HDRs are usually igneous or less often tight sedimentary rocks. In general, intact unaltered granite formations are characterized by significantly high $E$ values, up to 80 GPa [37,38]. However, as the number of planes of discontinuity in the rock increases, lower $E$ values and higher discrepancies between dynamic and static values are expected [39]. Igneous rocks are good examples of diversity in static and dynamic elastic moduli depending on rock alteration. In the study conducted by Lama and Vutukuri [40], in intact unaltered granite, $E_{dyn}$ and $E_{stat}$ were similar and in the range of 65.0–70.0 GPa, whereas in slightly altered granite, both $E_{dyn}$ and $E_{stat}$ decreased rapidly, and the average $E_{dyn}$ was three times higher than $E_{stat}$ (about 15.0–5.0 GPa for dynamic and static, respectively).

### 2.3. Modeling Hydraulic Fracture Geometry

The numerical modeling of synthetic EGSs is a strategy that allows for testing different operational approaches before implementation in the field [2]. In scientific and field practice, several types of models are used, differing in terms of the set of required input data and associated numerical solutions and providing different types of output data depending on the specific needs. A 2D-plane strain approximation (Khristianovich–Geertsma–De Klerk) or 3D planar fracture model with fixed height (Perkins–Kern–Nordgren) cannot take into account, among others, the impact of natural planes of weakness or the reorientation of fractures under the influence of field stresses. More advanced models (planar shear decoupled, planar elastically coupled) consider stress shadow effects and predefined fracture barriers. High-resolution fracture models (discrete fracture network, synthetic rock mass, and bonded particle models) are suitable for modeling non-planar and complex fractures when detailed petrophysical and geomechanical data are available, whereas continuum models are advantageous in simulating large-scale problems [41]. For modeling HF operations in HDRs, both 3D planar fracture models [10,11,42,43] and more advanced models, e.g., multiple, cluster and discrete fracture models [2,44], thermo-hydro-mechanical damage models [45–47], and coupled thermo-poroelastic finite element models [48], have been used so far. Recently, advanced models integrating thermal, hydraulic, mechanical, chemical, and wellbore dynamics effects have been developed to evaluate, among others, various fracture network scenarios and consequently predict heat extraction performance [49].

## 3. Materials and Methods

### 3.1. Research Area

For this study, two potential EGS locations in Poland were defined, differing in terms of lithology and petrophysical properties: low-porosity and permeable sandstones from the Mogilno-Łódź Trough and granites from the Karkonosze Mountains area. The core samples were collected from two boreholes: Piotrków Trybunalski IG-1 (PT-1) (sandstones) and Czerwony Potok PIG-1 (CP-1) (granites). Following the method suggested by ISRM [50], cylindrical samples with a diameter of 2.54 cm (1 inch) and a length of 5.08 cm (2 inches) were cut in the vertical direction (along the borehole axis).

### 3.2. Determination of Dynamic Elastic Parameters

Dynamic elastic parameters were determined using the Acoustic Velocity System AVS-700 produced by Vinci (Nanterre, France). Before testing, the samples were fully saturated with 2% KCl brine in a vacuum container for 24 h. The samples were tested at 140 °C under triaxial conditions, with the hydrostatic confining pressure increasing from ambient pressure to 550 bar. The pore pressure in the samples was maintained at up to

20 bar throughout the tests; therefore, with increasing confining pressure, the effective pressure also increased. The methodology of determining the dynamic elastic parameters for dry samples, as well as a detailed description of the device and sample preparation, is presented by Moska et al. [18].

### 3.3. Determination of Static Elastic Parameters

Stress–strain experiments were carried out on an MTS-810 universal testing machine (MTS Systems, Eden Prairie, MN, USA). Sixteen core samples were tested under conventional triaxial conditions based on ISRM recommendations [50]. The aim was to determine the stress–strain characteristics of the sample during uniform loading until failure. $E_{stat}$ was measured based on precritical stress–strain characteristics as a tangent of the straight line slope to the strain axis. This straight line is a linear approximation of the failure curve in the precritical part of the stress–strain curve. The tests were carried out at ambient temperature and a radial pressure of 150 or 300 bar. Initially, it was assumed that $E_{stat}$ would be compared with $E_{dyn}$ at both pressures separately; however, due to the small number of samples and the average difference between the confining pressures in $E_{stat}$ of 14% for granites and 9.5% for sandstones, it was decided to combine the results from both confining pressures and compare them with the corresponding $E_{dyn}$. Due to the limitations of the pressure chamber, the values of $v_{stat}$ were determined only under uniaxial conditions (additional eight samples) using transverse extensometer set and were compared to $v_{dyn}$ measured in triaxial tests.

### 3.4. Numerical Modeling of Fracture Geometry

Planar 3D fracture geometry was simulated using Carboceramics FracPro software (version 10.13.6.0). The chosen model was the default model in the software (3D shear decoupled), which calculates the fracture growth with the composite layering effect. An important feature of the used model is that it does not take into account the presence of natural planes of discontinuity (natural fractures, cracks of fault planes), which may be prospective zones for hydraulic stimulation, especially in igneous HDRs. In other words, the model assumes the propagation of the newly induced fracture in an intact rock layer. As a result, the model also does not include the effect of the mixed stimulation mechanism or the related connection of natural fractures with induced fractures [20,21]. These simplifications in the use of the model were adopted due to the lack of available data, especially information on the presence of natural fracture zones in the analyzed locations, and because of discontinuities on a macro scale. Therefore, the results obtained for igneous rocks are intended to show how the geometry of the induced fracture changes depending on the variability in the elastic parameters of the intact rock layer. To better reflect the desirable natural fracture zones in the igneous formation, in the pay zone, slightly increased porosity and permeability were assumed with respect to adjacent zones. Due to the mentioned features of the used model, especially in the igneous formation, the showed results should be considered preliminary information on the variability in the geometry of the induced fracture as a function of elastic parameters. More precise results can be obtained by modeling natural fractures and their interactions with induced ones. A broader set of input data would enable the use of specialized thermal–hydraulic–mechanical simulators, leading to more accurate and reliable results. In practice, an analysis of the treatment parameters and reservoir responses is performed after each HF simulation. The conclusions allow one to improve the calibration of the assumed model and the design of the next treatment.

The first step in the modeling process is to define the general geological conditions in the considered locations, as well as the assumptions for the HF operation. These assumptions were based on the HF effects obtained in previously conducted EGS projects in

Western Europe, in particular those in Rhine Graben (Soultz-sous-Forêts, Landau, Rittershoffen) and Groß Schönebeck [11,43,51,52]. Based on above-mentioned literature data, the depth, thickness, and lithological profile in selected locations were defined. The porosity and permeability coefficients, as well as elastic parameters, of the target zone rocks were adopted from laboratory tests on the core samples [18], while for the overlying rocks, the literature values for the relevant lithological types were assumed. The vertical principal stress $\sigma_V$ was calculated based on the assumed average density of the overburden. Analyzed fracture dimensions were defined as follows: fracture half-length: radial distance from the wellbore to the outer tip of a fracture, fracture height: vertical distance of the fracture, fracture width: opening width of the fracture along the normal direction, propped half-length/height: length/height of the propped part of the fracture.

#### 3.4.1. Mogilno-Łódź Trough Area, Sandstone Formation

The lithological model for the sandstone formation was based on the simplified model of the Piotrków Trybunalski IG-1 well. The pay zone in the Rotliegend sandstone was assumed to exist at a depth of 4030 to 4101 m. Due to the incomplete information on the construction of the wellbore, in the model, we used the selected data from the Gt GrSK 4/05 wellbore in the Groß Schönebeck EGS project [12], as well as construction data from other wellbores in the Rotliegend formation in Poland. Figure 2 shows a schematic view of the wellbore construction, including the depths and diameters of the tubing and casing. The design of the well construction, including casing and tubing, was adapted to the ranges of formation pressure, ensuring safe operation (400 and below 600 bar for reservoir and maximum wellhead pressure, respectively). The perforation was assumed from 4060 to 4080 m in the Rotliegend formation.

The principal petrophysical parameters of the pay zone and the adjacent over- and underlying zones (40 and 88 m thick, respectively) were taken from laboratory core sample measurements presented by Moska et al. [18]. The pay zone was characterized by slightly higher porosity and permeability relative to adjacent zones. For the elastic modulus sensitivity analysis, it was assumed that the applied $E$ and $v$ in the pay zone ranged from the lowest to the highest, including the average, values obtained for this formation in the dynamic laboratory tests presented by Moska et al. [18] and static tests described in this study. The range of considered $E$ values was from 14.8 GPa (minimum value obtained in static tests) to 31.4 GPa (maximum obtained in dynamic tests for saturated samples). The hypothetical elevated value for hard sandstone (50.0 GPa) was also added to show the influence the higher $E$. The reference point (100%) for $E$ was assumed to be 19.2 GPa. The remaining petrophysical parameters of the model, including $v$, were not changed. $v$ was assumed as the average value from dynamic tests for dry samples and was equal to 0.19. The range of $v$ in sensitivity analysis ranged from 0.12 to 0.22 (values obtained in the performed tests) and additionally included hypothetically elevated values of 0.30 and 0.35, wherein $E$ was fixed as the average value from the dynamic tests of the dry samples and equaled 19.2 GPa.

The pumping schedule was designed based on information available in the literature [11,12,43]. It was divided into 10 steps. In the first step, 30 lb/1000 gal linear polymer fluid (so called pad) was pumped. This concentration of the fluid provides enough viscosity to open and propagate the fracture under the assumed conditions. In the second step, fluid with the same polymer concentration was used in addition to 100-mesh quartz sand. The addition of very-small-grain sand allows for the widening of perforation holes and reduces the fluid flow resistance in the near-wellbore zone. In the next steps, the transport of the proppant to the created fracture was scheduled. For this purpose, high-viscosity fluids based on cross-linked polymer bonds, are usually used. This allows for the transport of a proppant of relatively high strength and density deep into the created fracture. In these steps, 30 lb/1000 gal cross-linked polymer fluid with 20/40 high-strength ceramic proppant was used. Typically, during HF operations, proppant injection begins from the lowest concentrations and gradually increases during the process. This technique allows for more efficient propping. The pumping rate depends on the type of liquid and the concentration of proppant. The rates were assumed to be 2.0 $m^3$/min in the pad, 3.0 $m^3$/min in the clean perforation step, and 4.0 $m^3$/min in the slurry steps. The proppant concentration increased between the first and last slurry steps from 150 to 800 kg/$m^3$. The model net pressure for the last frac step was 49.5 bar. Details of the pumping schedule in the Mogilno-Łódź area are shown in Figure 3.

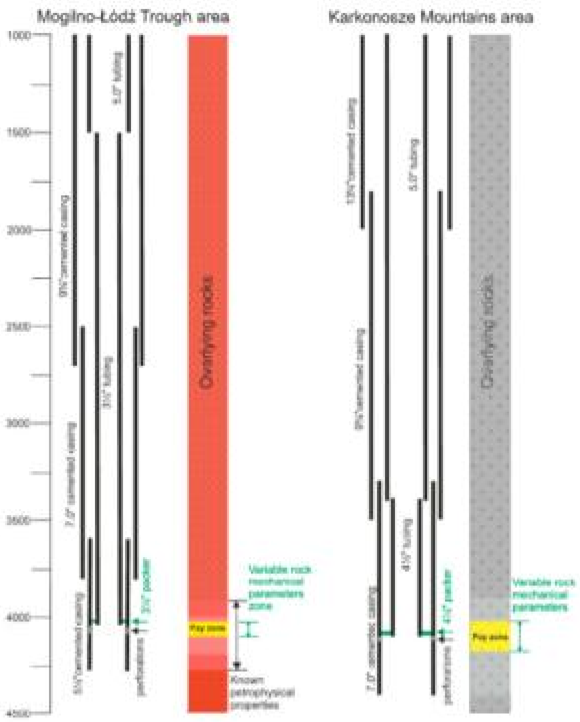


**Figure 2.** Schematic view of the borehole tubing, casing, perforation, and lithology profiles of the Mogilno-Łódź and Karkonosze Mountains area models.

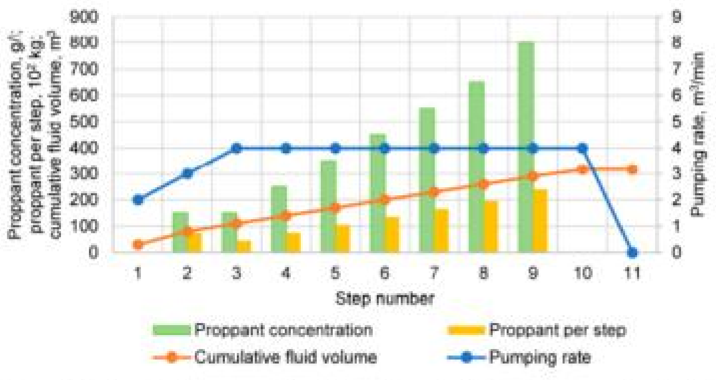


**Figure 3.** Design of the treatment schedule of the hydraulic fracturing operation in the Mogilno-Łódź area.

3.4.2. Karkonosze Mountains, Granite Formation

In the Karkonosze Mountains area, the lithology is confirmed from drilling data only to a depth of about 2000 m [53]. Below this depth, only assumptions based on the literature are possible. For the purposes of this work, we assumed that the lithological profile consists of granitoid pluton along its entire considered depth. The pay zone was placed at a depth of 4020 to 4180 m (160 m thick). The perforation was assumed to be at a depth of 4100 to 4112 m.

Similarly to the case of the considered sandstone formation, the pay zone parameters were assumed based on laboratory core sample measurements presented by Moska et al. [18] and from this study, whereas the parameters of the overburden were taken from the software database. We assumed that the pay zone is characterized by increased porosity (2.5%) and permeability (0.5 mD) with respect to adjacent zones (0.79% and 0.001%, respectively) to reflect the desirable tightened natural fracture zone of higher alteration.

The applied $E$ and $\upsilon$ values in the pay zone were assumed to include the lowest, average, and highest values obtained for the formation in dynamic laboratory tests presented by Moska et al. [18] and static tests described in this study. The considered $E$ ranged from 16.75 GPa (average value obtained in static tests for naturally fractured samples) to 62.9 GPa (average from dynamic tests for dry intact samples); 80 GPa, a value for intact granite obtained from the literature [37,38]; and several intermediate values. The reference point (100%) for $E$ was assumed to be 62.9 GPa, while $\upsilon$ was fixed at the average value obtained from dynamic tests (0.28). The range of $\upsilon$ in sensitivity analyses was from 0.07 (minimum obtained in static tests) to 0.37 (hypotethical elevated value), including intermediate values obtained in the static and dynamic tests, wherein $E$ was fixed as the average value from dynamic tests for naturally fractured samples and equaled 43.8 GPa. It was assumed that the reference point for $\upsilon$ (100%) was 0.28.

The pumping schedule was divided into 16 steps. In steps 1–10, 20 lb/1000 gal of slickwater fluid was used to open the formation. This type of fluid is characterized by a viscosity slightly higher than that of water because of a very low polymer concentration, enough to create and propagate the fracture. Furthermore, the friction-reducing additive reduces the flow resistance, which is especially important at high pumping pressures. In the simulation performed, we decided to use 40/70-mesh ceramic proppant during three stages in the final part of the treatment. The low viscosity of the liquid enables the transport of the low-density and small-grain-size proppant. The detailed pumping schedule for the Karkonosze Mountains area is shown in Figure 4.

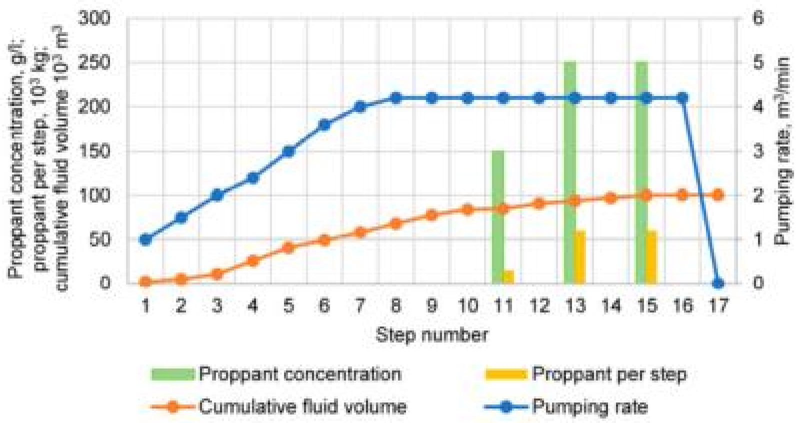


Figure 4. Design of the hydraulic fracturing operation in the Karkonosze Mountains area.

## 4. Results

Figure 5 shows a comparison of dynamic and static $E$ and $\upsilon$ parameters for dry samples from the Mogilno-Łódź Trough (sandstone) and Karkonosze Mountains (granite).

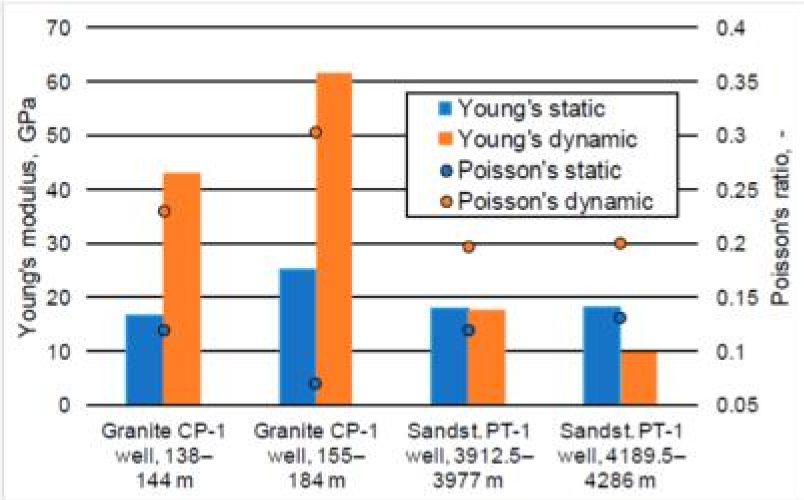


**Figure 5.** Comparison of the average static and dynamic Young's moduli and Poisson's ratios of dry rock samples from selected prospective HDR areas in Poland. Dynamic parameters were published by Moska et al. [18].

The average $E_{stat}$ values of the granite samples (16–25 GPa) were relatively low compared to the literature data [37,38] and confirmed the behavior observed for altered granite [40]. Altered granites with more developed natural fracture networks, collected from a shallower interval (138–144), exhibit lower $E_{stat}$ than deeper ones, which can also be explained by the elevated amount of clay minerals in the mineral composition (chlorite, kaolinite, illite) [18]. The $\upsilon_{stat}$ of granites from deeper intervals is slightly lower; however, it should be remembered that $\upsilon_{stat}$ was measured in uniaxial conditions, which influenced the results. According to Lógó and Vásárhelyi [54], for hard intact rocks, it can be expected that $\upsilon_{stat}$ will increase with increasing confining pressure. Sandstone samples collected from both intervals present average $E_{stat}$ values in the range of 17.9–18.2 GPa and $\upsilon_{stat}$ values of 0.12–0.13, which correspond to values for medium-strength sandstones in the literature, e.g., [55,56].

Granite samples showed a strong variability in elastic parameters depending on the measurement method (Figure 5). The average $E_{dyn}$ was more than twice the static value in both intervals, whereas $\upsilon_{dyn}$ was about four times greater than the static one measured in uniaxial conditions in the case of samples collected from a 155–185 m depth interval. On the other hand, the $E$ values of the sandstones were comparable regardless of the measurement method (in the range of 9.6–18.1 GPa for both methods), and the $\upsilon$ ratios were higher in the dynamic method. Differences between $E_{dyn}$ and $E_{stat}$ in granite samples can result from alteration, similar to the results presented in literature [40], and/or from the presence of microcracks in the samples, which do not cause elastic wave attenuation but significantly reduce the strength of the sample during static tests. Figure 6 shows the correlation between dynamic and static $E$ for measured samples. Despite the small amount of data due to the small number of undamaged samples that could be directly compared with each other, the correlation is good for both sandstone ($R^2 = 0.84$) and granite ($R^2 = 0.89$). For both data sets, the linear trend line gives the best $R^2$ coefficient, although the literature indicates the best matching of the power-law correlation for igneous rocks [27]. A flatter trend line of granite samples compared to the sandstone one indicates that the increase in $E_{dyn}$ in granites is not highly reflected in $E_{stat}$ growth. This can result from the presence of microcracks and microfractures that cause a reduction in the strength of the samples in static tests.

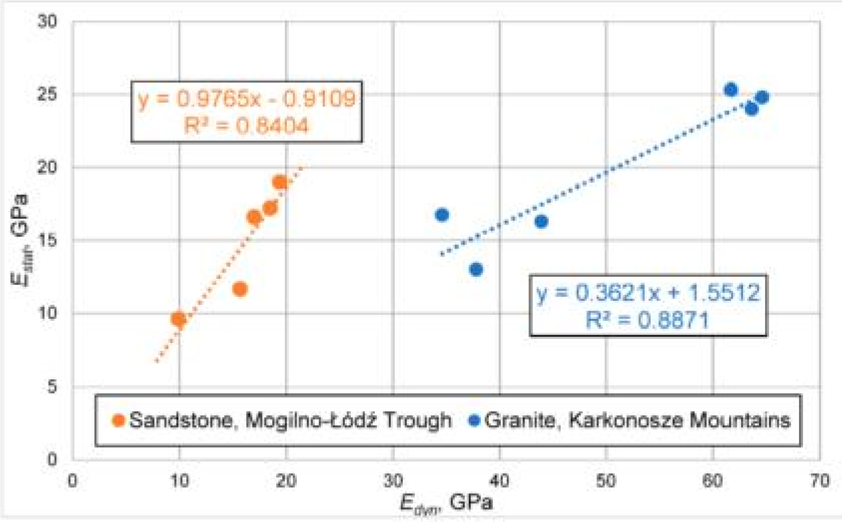


**Figure 6.** Relationship between the static and dynamic Young's moduli of granite from the Karkonosze Mountains and sandstone from the Mogilno-Łódź Trough. Results for dry samples tested under triaxial conditions. Dynamic parameters were published by Moska et al. [18].

It is also important to note that differences in testing temperature between ultrasonic measurements (conducted at 140 °C) and strength tests (conducted at ambient temperature) can influence the results. In general, elevated temperatures lead to thermal cracking in rocks due to differential thermal expansion between mineral grains, resulting in a reduction in the static Young's modulus of $E_{stat}$. However, in low-porosity rocks such as granite, the P-wave velocity typically decreases by less than 5% for a temperature increase of approximately 100 °C [57]. The rate of decrease in $E_{stat}$ with temperature is generally higher than that of the dynamic modulus ($E_{dyn}$) [58]. Nevertheless, within the temperature range from ambient to about 150 °C, changes in mechanical properties reported in the literature usually remain within a few percent of their reference values, depending on rock type [59,60]. Therefore, it can be assumed that the variation in testing temperature in this study should have only a minor effect on the results.

HDRs are usually described as formations that contain little or no water. However, the presence of water in the pore space or fractures significantly influences the elastic parameters, especially $E$, which is presented in Figures 7 and 8. Both in granite and sandstone samples, P-wave velocities increase in saturated samples because the $K$ modulus of the water is higher than the gas modulus [57]. The S-wave velocities increase slightly as a result of the increase in bulk density. This relation results in a significant increase in $E_{dyn}$ in both types of samples, though it is especially noticeable in weak sandstones. The saturation of the sandstone samples also results in a significant increase in deformation in the directions perpendicular to the direction of loading. The influence of water saturation on fracture propagation is described in the discussion section.

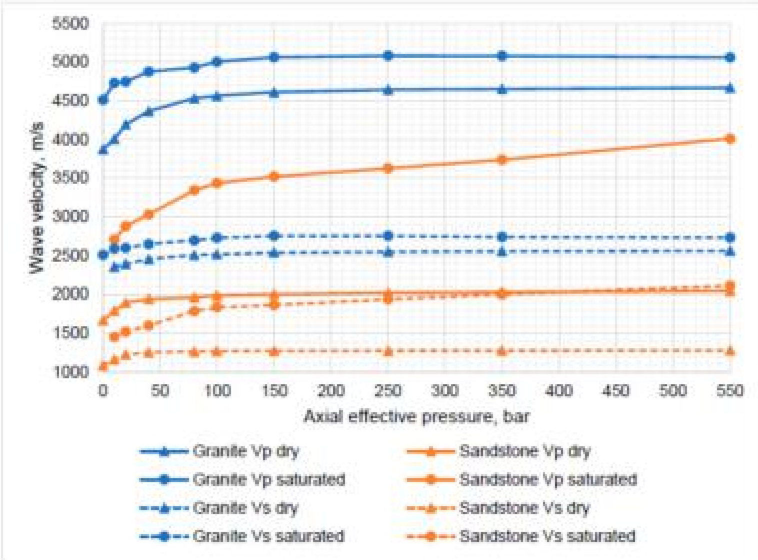


**Figure 7.** A comparison of wave velocities of dry (from [18]) and fully saturated (this study) granite from the Karkonosze Mountains and sandstone from the Mogilno-Łódź Trough in triaxial tests.

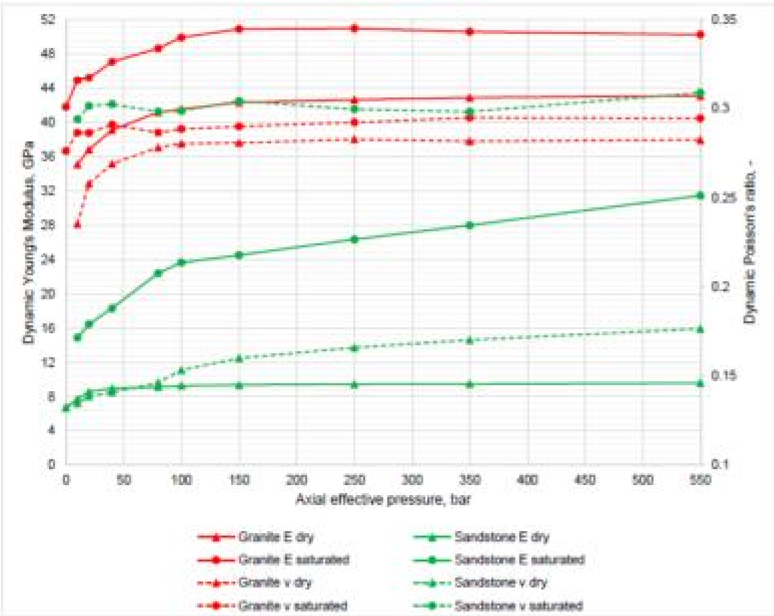


**Figure 8.** A comparison of dynamic Young's moduli and dynamic Poisson's ratios of dry (from [18]) and fully saturated (this study) granite from the Karkonosze Mountains and sandstone from the Mogilno-Łódź Trough in triaxial tests.

The sensitivity analysis for Mogilno-Łódź HDRs showed that an increase in $E$ in the target zone from 14.8 to 50.0 GPa leads to an increase in fracture height by 3.0 m, a decrease in half-length also by 3.0 m, and a decrease in width by 0.09 cm (Figure 9). Similar-scale variability was observed for the propped fracture half-length and propped height. The average fracture conductivity increased by 65 mDm and the average surface pressure by

24 bar, while the embedment phenomenon decreased from 0.031 to 0.011 cm (Figure 10). The variability in $E$ in the range mentioned above had the greatest impact on average fracture conductivity (increase from −4.3 to +8.4%) in relation to the value corresponding to the average $E$ (Figure 11). A lower impact was observed for the half-length, height, and width (decrease from +3.3 to −1.6%, increase from −1.2 to 2.5%, and decrease from 0.7 to −5.7%, respectively). Therefore, the increase in $E$ in the considered range caused a change in the half-length, height, width, and conductivity of the fracture to 4.9%, 3.7%, 6.4%, and 12.7%, respectively, which can be seen in Figure 11. Variability in fracture geometry with increasing Young's modulus in the pay zone of the Mogilno-Łódź HDR area can be seen in Figure 12.

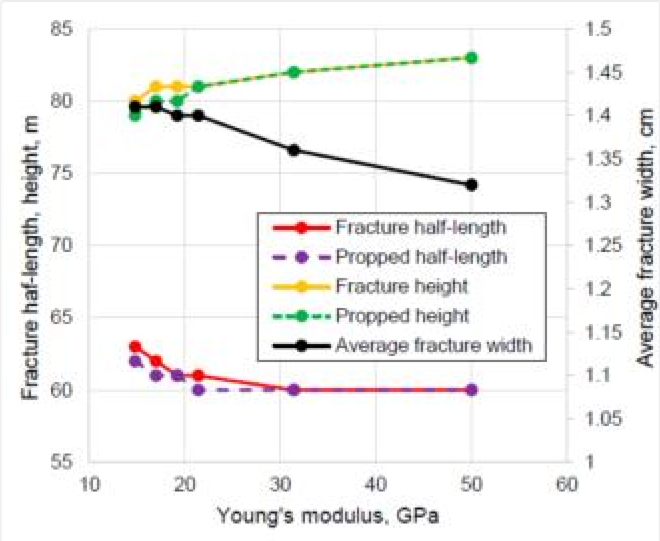


**Figure 9.** Variability in the selected fracture geometry parameters as a function of Young's modulus in the Mogilno-Łódź sandstone formation.

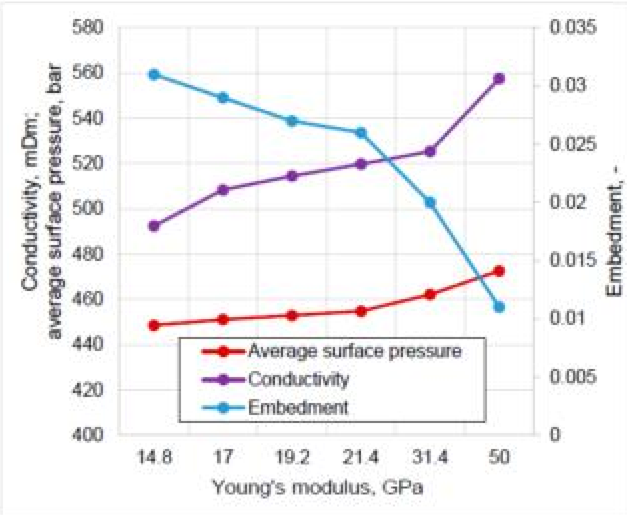


**Figure 10.** Variability in fracture conductivity, average surface pressure, and embedment as a function of Young's modulus in the Mogilno-Łódź sandstone formation.

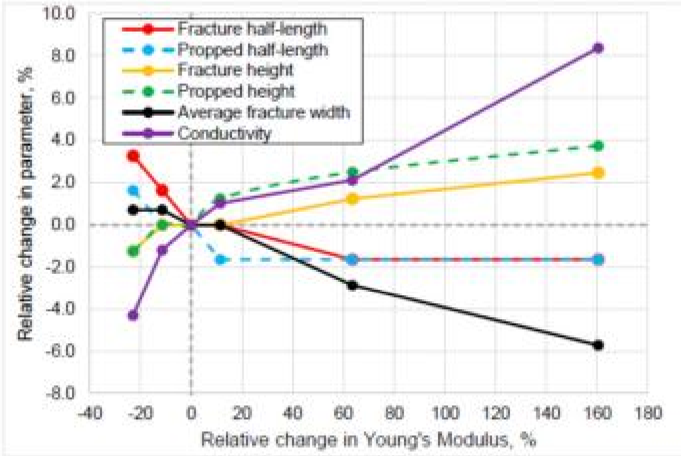


**Figure 11.** Influence of Young's modulus on hydraulic fracture characteristics in the Mogilno-Łódź sandstone formation.

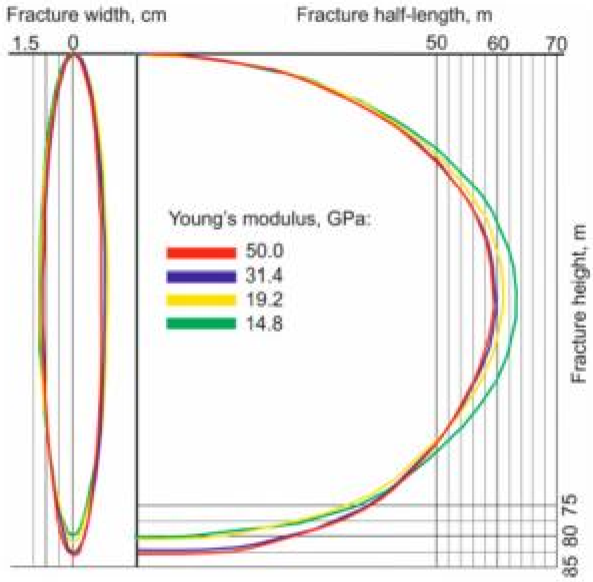


**Figure 12.** Variability in fracture geometry with increasing Young's modulus in the pay zone of the Mogilno-Łódź HDR area. Fracture shape colors correspond to the following values: green—minimum $E_{stat}$, yellow—average $E_{dyn}$, navy blue—maximum $E_{dyn}$ for brine-saturated sample, red—hypothetical $E$ for hard sandstone rock above values obtained in the tests (for comparision).

The sensitivity analysis of $\upsilon$ for the considered formation shows that at a fixed average $E$ of 19.2 GPa, the variability in $\upsilon$ from 0.1 to 0.35 did not affect the fracture length, height, or width and had a negligible impact on the propped length and height. The impact on the fracture conductivity did not exceed 2.5%. The proppant concentration in the fracture for the average values of $E$ and $\upsilon$ are shown in Figure 13. The proppant is concentrated in the middle and lower part of the fracture due to the settling proppant transport type.

Sensitivity analysis on the granite from the Karkonosze Mountains showed that an increase in $E$ in the pay zone from 16.7 to 80.0 GPa did not influence the height of the fracture. The fracture half-length decreased from 345 to 334 m (11 m decrease), while the width decreased from 0.82 to 0.55 cm (0.27 cm decrease). However, the propped half-length increased from 307 to 320 m (13 m), and the propped height also increased from 142 to 153 m (11 m) (Figure 14). The impact on fracture conductivity was not clear in this case. Conductivity increased at low $E$ values and stabilized with a tendency to slightly decrease below 34.6 GPa (Figure 15). However, it is important to mention that in the real formation conditions, conductivity may be varied due to interactions between natural and induced fractures [21], which cannot be simulated in FracPro. Therefore, the variability in fracture half-length, propped half-length, and propped height did not exceed 7.3% of the assumed reference values (Figure 16). The variability in fracture width was much more significant (from about +41.4% for the lowest assumed $E$ to about −5% for the highest). The embedment phenomenon occurred only in the lowest $E$ values and reached a maximum of 0.013 cm for the lowest assumed $E$. Variability in fracture geometry with increasing Young's modulus in the pay zone of the Karkonosze Mountains HDR area can be seen in Figure 17.

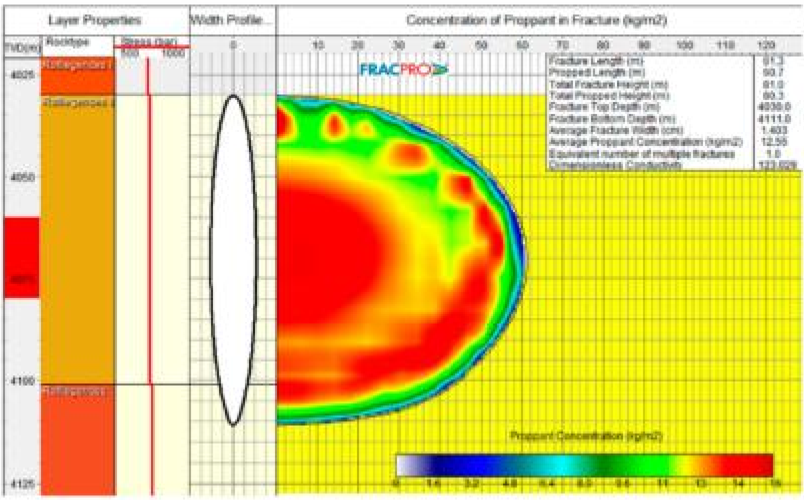


**Figure 13.** Fracture geometry and visualization of the proppant concentration for a hydraulic fracturing operation in the Mogilno-Łódź sandstone formation, assuming mean values of $E$ and $v$ in the pay zone.

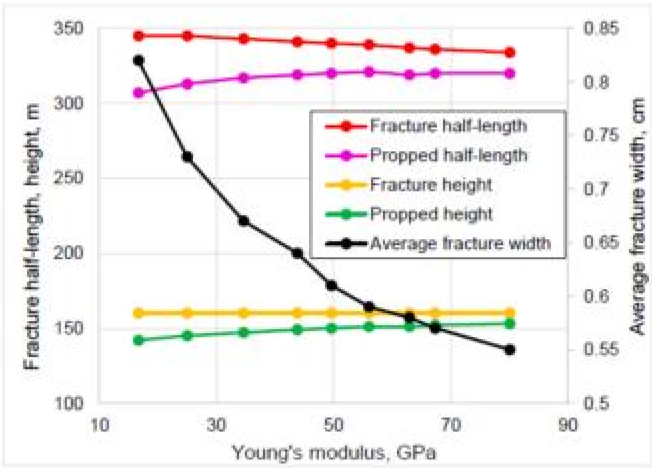


**Figure 14.** Variability in the selected fracture geometry parameters as a function of Young's modulus in the Karkonosze Mountains granite formation.

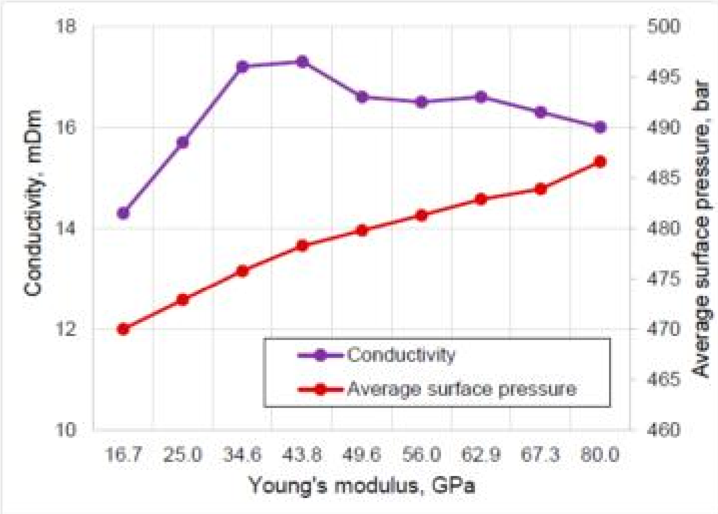


**Figure 15.** Variability in the fracture conductivity and average surface pressure as a function of Young's modulus in the Karkonosze Mountains granite formation.

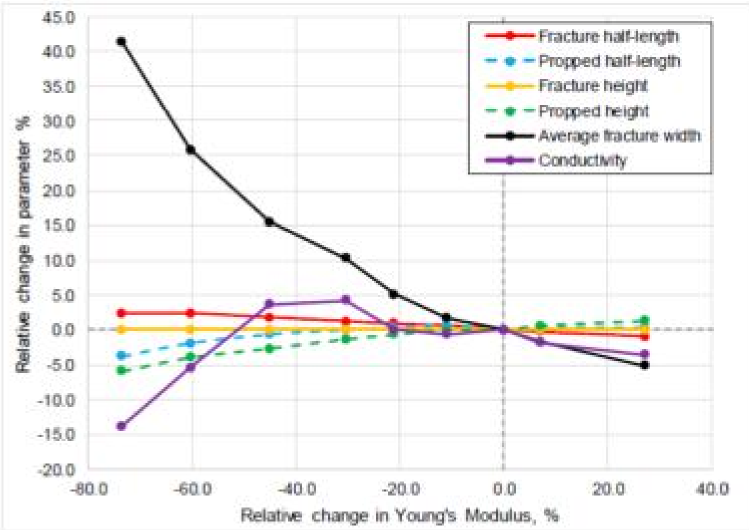


**Figure 16.** Influence of Young's modulus on hydraulic fracture characteristics in the Karkonosze Mountains granite formation.

The influence of $v$ on the fracture dimensions in the granite formation was much less significant than that of $E$, especially in the case of half-length and height. The variation in $v$ from 0.7 to 0.37 led to a change in the half-length and height of the propped fracture in the range below 2.6%. The fracture half-length changed in the range of below 1%, whereas fracture width varied more significantly (7.9%). Embedment was not observed. The influence on the fracture conductivity was unclear, but, in general, it was stable for the entire range of $v$ analyzed. The proppant concentration in the fracture for the average values of $E$ and $v$ are shown in Figure 18.

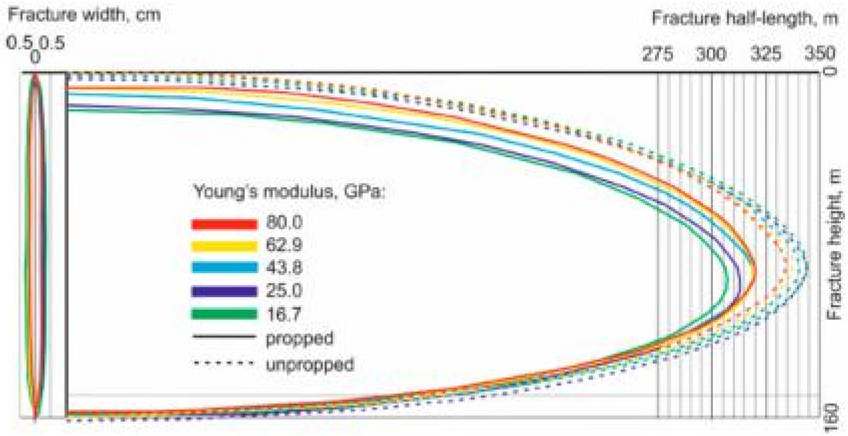


**Figure 17.** Variability in fracture geometry with increasing Young's modulus in the pay zone of the Karkonosze Mountains granite formation. Fracture shape colors correspond to the following values: green—minimum $E_{stat}$, navy blue—average $E_{stat}$, blue—average $E_{dyn}$ of fractured samples, yellow—average $E_{dyn}$ of intact samples, red—E of intact granite from the literature [37] for comparision.

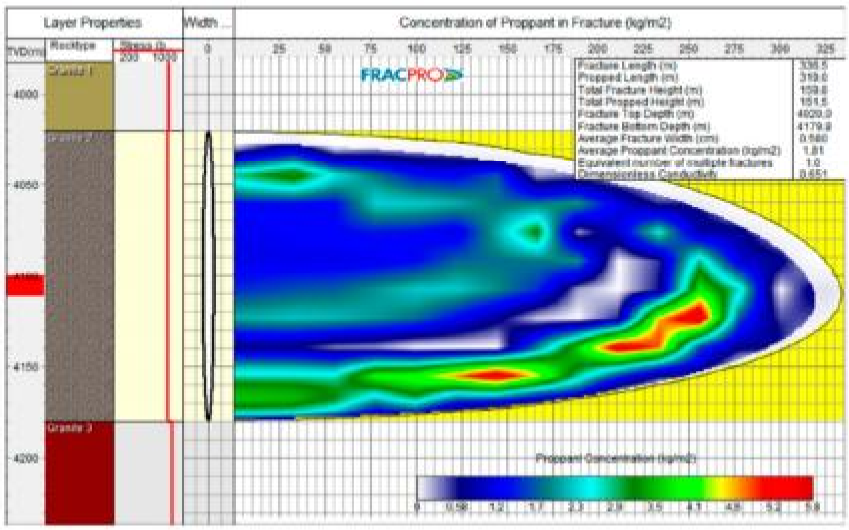


**Figure 18.** Fracture geometry and visualization of proppant concentration for an HF operation in the Karkonosze Mountains granite formation, assuming average values of $E$ and $\upsilon$ in the pay zone.

## 5. Discussion

No studies have been published to date on the influence of rock elastic parameters on fracture geometry in European HDRs, but data from other locations and rock formations are available. Lei et al. [2] discuss the influence of $E$ and $\upsilon$ on the fracture aperture and area in igneous formations. The results show that the fracture aperture decreases significantly with increasing $E$. Within the tested parameter range of HDRs in the Gonghe Basin (Northwest China), a change in $E$ relative to the average value alters the fracture aperture by 23–52% (decrease with increasing $E$). The effects of $\upsilon$ on the fracture aperture are minor; it does not change the fracture aperture by more than 6% in the ranges of the tested parameters. Fracture area increases by a maximum of approximately 15% with an increase in $E$ and insignificantly with a change in $\upsilon$. Modeling for shale rocks shows that the lower the $\upsilon$ or $E$

obtained, the less the fracture length propagates, while the fracture width increases [61]. Similar results are shown by Suryadinata et al. [62]. Osman and Bilgesu [63] stated that high $E$ values generate shorter and smaller bi-wing fractures in shales, whereas the length of the discrete fracture network increases. Bastos Fernandes et al. [64] pointed out that the higher the $E$ value in shales, the more complicated the fracture networks around the wellbore and the more shear failures observed in natural fractures. When $E$ is relatively small, the width of the fracture decreases a little, while the length slowly increases. Increasing $E$ above 30 GPa leads to dominating shear failure in natural fractures and causes a decrease in fracture length and an increase in width. On the other hand, high $v$ inhibits the growth of shear fractures. As $v$ grows, the fracture length also grows, and its width decreases. Furthermore, $E$ also decreases as the number of thermal cycling increases in EGSs due to the transformation of microfractures into larger ones [65]. With respect to the above-mentioned data, Lei et al. [2] also pointed out that compared to the influences of the in situ stress and the level of natural fracture development, the reservoir properties had a minor effect on the results of the HF treatment.

In the case of the Mogilno-Łódź HDRs, an increase in $E$ caused a change in fracture half-length, height, and width of 4.9% (decrease), 3.7% (increase), and 6.4% (decrease), respectively, which is noticeably lower compared to the data presented by Lei et al. [2]. Differences in the scale of $E$'s influence can be explained by the different types of rock being compared: low-strength sandstone on one side and granite of relatively higher strength where the fractures propagate more easily on the other side. On the other hand, the results obtained confirmed that the influence of $v$ on the fracture geometry is minor. Therefore, the variability in $E$ over a relatively wide range leads to change in the fracture geometry parameters, at most by 6.4%, whereas the influence of $v$ can be considered insignificant. The results indicate that despite the variability in rock elastic parameters depending on the used research method and water saturation, in the analyzed sandstone formation, these differences do not strongly affect the final fracture geometry. The directions of correlation (positive or negative) between fracture parameters and rock elastic parameters are shown in Table 1.

**Table 1.** Correlations of fracture parameters and elastic rock parameters. The symbols "−" and "+" denote negative and positive correlations, respectively.

| Induced Fracture Parameters | Sandstone, Mogilno-Łódź Trough | | Granite, Karkonosze Mountains | |
|---|---|---|---|---|
| | Young's Modulus | Poisson's Ratio | Young's Modulus | Poisson's Ratio |
| Half-length | − | No influence | − | − |
| Propped half-length | − | − | + | Not clear |
| Height | + | No influence | No influence | No influence |
| Propped height | + | + | + | Not clear |
| Width | − | No influence | − | − |
| Conductivity | + | Not clear | Not clear | Not clear |
| Surface pressure | + | + | + | + |
| Embedment | − | No influence | − | No influence |

In the Karkonosze Mountains granite formation, the increase in $E$ leads to a decrease in width by 46.6%, similar to the data presented by Lei et al. [2], as well as decrease in half-length (3.3%) and does not affect the height of the fracture. However, the propped half-length and propped height increased with $E$ (4.1% and 7.3%, respectively); thus, increasing $E$ in general leads to a decrease in the unpropped part of the fracture. It is important to note that embedment phenomena were expected for $E$ values less than 34.6 GPa only and reached the maximum obtained value of 0.013 cm for the lowest tested $E$. Therefore, in the tested granite, embedment is only significant in highly altered and fractured parts of the formation characterized by reduced strength.

The variability in half-length and height, both propped and total, due to $v$ change is minor (does not exceed 2,5%), which confirms the literature results [2]. Similar to the Mogilno-Łódź formation, significant variability in elastic parameters was observed for the Karkonosze granites in geomechanical tests, depending on the method used; however, in this case, the large range of $E$ changes leads to relatively small variability in fracture half-length and height but noticeable variability in width. Additional research should be carried out to determine if a significant decrease in fracture width with increasing $E$ also occurs in the case of larger initial fracture width.

In most of the EGS studies conducted so far, the target zones were igneous formations for which available data for projects in sedimentary strata are limited. The modeling results for the Mogilno-Łódź area indicate that by assuming relatively similar parameters of the fracturing operation to those of the Groß Schönebeck project, in particular the flow rates, fluid volumes, and pumping schedule, relatively similar results can be obtained (Table 2). The average fracture length in the Mogilno-Łódź HDR, taking into account average obtained $E$ and $v$ in the target zone, is 1.0 to 4.0 m lower than that in a fracking project from 2007 in Groß Schönebeck, while the fracture height is noticeably lower. However, the width at the Polish prospective site is almost three times greater (1.4 cm compared to 0.53 cm). These differences may appear due to both the pumping parameters, which were comparable but not identical, and also the petrophysical and geomechanical parameters of the target zone. The greater length and height of the fracture and its lower width correspond to the higher brittleness index of the sandstone formation at the German site (Figure 19). Therefore, assuming a greater distance between injection and production wells, allowing for higher installation efficiency, formations with higher $E$ values are desirable at the Polish site. In the case of sedimentary HDRs, a certain amount of initial water saturation could be also beneficial in order to obtain longer fractures; however, a significant brine inflow can also lead to productivity reduction due to scaling [12] and corrosion issues. The low $v$ in the formation also leads to increased embedment phenomena that can reduce fracture conductivity [26].

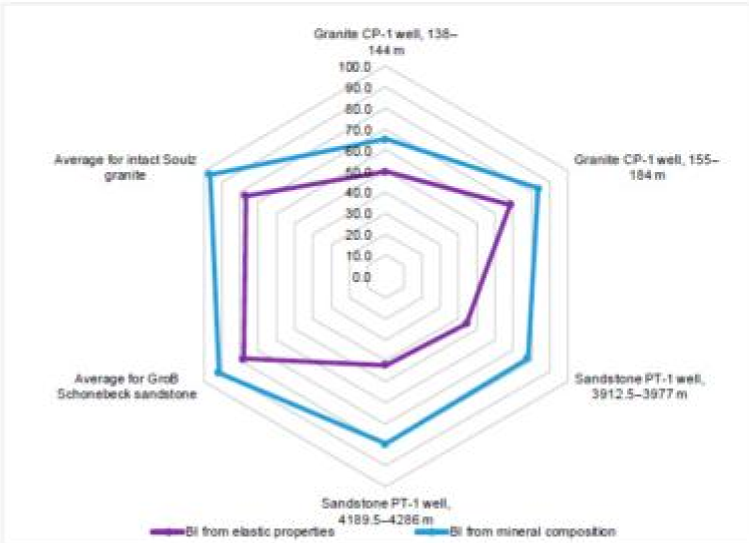


**Figure 19.** Comparison of mineral and rock mechanics-based brittleness indices of prospective formations in Poland and corresponding rocks in currently operated EGS projects in Western Europe. Based on [16,18].

Table 2. Comparison of selected data from hydraulic fracturing operations in Groß Schönebeck [12] and Mogilno-Łódź sedimentary HDR numerical modeling (this study).

| Treatment Parameter | GroßSchönebeck E GrSk 3/90 Vertical Well (2002) Gel/Proppant Frac I | Groß Schönebeck Gt GrSk 4/05 A (2) Horizontall Well (2007) Gel/Proppant Frac I | Groß Schönebeck Gt GrSk 4/05 A (2) Horizontal Well (2007) Gel/Proppant Frac II | Mogilno-Łódź Sedimentary HDR Numerical Model, Vertical Well Gel/Proppant Frac |
|---|---|---|---|---|
| Duration, h | 9.3 | 1.5 | 2 | 1.6 |
| Frac interval, m | 4140–4200 | 4204–4208 | 4118–4122 | 4060–4080 |
| Completion | Open hole | Perforated liner | Perforated liner | Perforated liner |
| Max. flow rate, $m^3/h$ | 138 | 240 | 210 | 240 |
| Cumulative volume, $m^3$ | 107 | 280 | 310 | 317 |
| Max. head pressure, bar | 452 | 350 | 400 | 533 |
| Gel type | HTU/brine | Cross-linked | Cross-linked | Cross-linked |
| Proppant type | Carbo-Lt | High strength | High strength | CarboHSP |
| Mesh size | 20/40 | 20/40 | 20/40 | 20/40 |
| Proppant mass, kg | 8796 | 95,000 | 113,000 | 103,497 |
| Fracture dimensions | | | | |
| Half-length, m | 32 | 57 | 60 | 61 |
| Height, m | 72 | 115 | 95 | 81 |
| Width, cm | 0.16 | 0.53 | 0.53 | 1.4 (average) |

Data concerning the geometry of stimulated natural fractures in European igneous EGS formations are difficult to access. Considering the low reservoir in Soultz, the distance between the bottoms of the wells suggests that the natural fracture must be conductive for a distance of at least about 600 m; therefore, it probably has to be stimulated for such a distance. In Landau, the distance between the bottoms of the wells is even greater and reaches 1200 m. The results of the simulations presented in this paper cannot be directly compared with these EGSs because the software used does not take into account the propagation of stimulated natural fractures. Reduced elastic rock parameters and increased permeability and porosity in the pay zone in the presented model constitute only an approximation of the assumed situation in the formation; thus, the presented results may therefore be an indication of how the geometry of the induced fracture depends on the variability in elastic parameters. Natural fractures may have significant initial natural conductivity, and stimulation leads to further improvement of the flow (e.g., the GPK3 well in Soultz). The Karkonosze Mountains EGS in this study can be considered a massive stimulation model containing over 10,000 $m^3$ of fluid in total (Table 3). The obtained fracture half-length would allow for keeping the distance between the bottoms of the wells at about 500–600 m assuming the connection of the fractures in the target zone after treatments in both injection and production wells. Greater fracture length in the model corresponds to lower width, which in turn is related to lower conductivity.

Lei et al. [2] indicated that the variation in the stress magnitude with depth as well as stress difference significantly affected the geometry of the hydraulic fracture network. Therefore, the choice of HF technology, including the type of fluid, proppant, and other parameters, depends on the in situ stresses and also on natural fracture development in the reservoir, as well as petrophysical parameters, i.e., $E$, $v$, porosity, and permeability. Unfortunately, concerning the analyzed HDR areas in Central Europe, there are no available data on the natural fractures in the reservoir or on detailed stress patterns. Obtaining these data is critical before designing an HF treatment. Despite incomplete data from the considered formations, and with respect to published data from Western European EGSs, it can be assumed that in the part of the formation containing intact rock or poorly developed natural fractures, gel-proppant fracturing or hybrid treatment would be applicable, while in the well-developed natural fracture network part of the reservoir, massive water fracturing would yield better results.

**Table 3.** Comparison of selected data from hydraulic fracturing operations in Soultz-sous-Forêts and Landau [52] and Karkonosze Mountains igneous HDR numerical modeling (this study).

| Treatment Parameter | Soultz GPK2 | Soultz GPK4 | Landau GtLa2 | Landau GtLa2 | Karkonosze Mountains Igneous HDR Numerical Model, Vertical Well |
|---|---|---|---|---|---|
| | Massive Fracturing | Low-Rate Injection | Hydraulic Stimulation | High-Rate Stimulation | Massive Fracturing |
| Duration, h | 144 | 84 | few hours | few hours | 55 |
| Max. flow rate, $m^3/h$ | 180 | 108 | up to 310 | up to 684 | 252 |
| Cumulative volume $m^3$ | 23,400 | 9300 | 4060 | 6600 | 10,041 |
| Max. net pressure, bar | 150 | 170 | 100 | 100 | 37 |
| Fluid type | Fresh water | Fresh water | Fresh water | Fresh water | Slickwater |
| Proppant type | - | - | - | - | High strength |
| Mesh size/proppant mass, kg | - | - | - | - | 40/70/135,000 |

The design of every HF operation in EGSs should be preceded by comprehensive well-logging data, including the stress state, presence, direction, and conductivity of natural fractures; mineral content; and elastic parameters. The research results presented in this paper indicate that while the elastic parameters of reservoir formations are important for stimulation design, they do not significantly influence the geometry of fractures as modeled in this study. From a geomechanical perspective, in sedimentary formations, the most promising target zones appear to be layers characterized by relatively high $E$ and low $v$ values, which correspond to a high brittleness index. In such rocks, the fracture network after HF operation should be more extensive, the impact of the embedment should be lower, and there should also be a lower likelihood of the unfavorable occurrence of clay minerals, which makes them the most promising. Because high-strength, high-density proppant is required in such deep formations, cross-linked fluids would be appropriate. Currently operating EGSs in igneous rocks in Western Europe indicate that natural fracture zones stimulated by a hydroshearing mechanism are a potential target. In this type of formation, it is essential to understand the orientation and propagation of natural fractures; their lengths, natural conductivities, water inflows; and the interactions between natural and induced fractures. Fractured zones typically exhibit significantly lower $E$ values than intact rock, and this is why such sections can be considered as prospective to stimulation by a hydroshearing mode. The wells drilled should intersect in the direction of the natural fractures so that after stimulation, the optimal workflow can be achieved. Since igneous formations are conducive to self-propping fractures, where the use of proppant is not necessary. The optimum fracturing fluid in this case could be fresh water or a friction-reducer-based proppant.

## 6. Conclusions

This article discusses for the first time the design of a geothermal collector in prospective hot dry rocks in Poland using the hydraulic fracturing method. For the first time, a comparison of dynamic and static rock mechanics test results in hot dry rocks is also presented, as well as a sensitivity analysis showing the influence of rock elastic parameters on fracture geometry in two different lithologies.

(1) Rock mechanics tests reveal large differences between the dynamic and static Young's modulus and the Poisson's ratio in granite formations from the Karkonosze Mountains, whereas these parameters in the sandstones of the Mogilno-Łódź Trough, especially the Young's modulus, show less variation. For both lithology types, the best fit is given by a linear trend ($R^2$ from 0.84 to 0.89 for sandstones and granites, respectively).
(2) The saturation of the samples with brine causes a significant increase in the dynamic Young's modulus compared to that of dry samples in both formations.
(3) Sensitivity analysis for Mogilno-Łódź sandstone shows that the increase in Young's modulus from 14.8 to a 50.0 GPa leads to a decrease in the half-length of the fracture by 4.9% and in the width by 6.4%, as well as an increase in the height by 3.7% and in the conductivity by 12.7%. Variability in Poisson's ratio (in the tested range from 0.1 to 0.35) leads to negligible changes in the propped fracture half-length and height, in the range below 1.6%.
(4) In the case of the Karkonosze Mountains granite formation, the increase in Young's modulus from 16.7 to a 80.0 GPa leads to decrease in half-length by 3.3% and in width by 46.4%, with an increase in propped half-length and height (4.1% and 7.3%, respectively). No influence is observed on the height of the fracture. Variability in Poisson's ratio (in tested range from 0.7 to 0.37) leads to a negligible change the fracture half-length in the range below 1%, whereas fracture width varies more significantly (decreases by 7.9%).
(5) Performing sensitivity analysis allows to determine that a relatively great variation in Young's modulus and Poisson's ratio leads to relatively little impact on fracture half-length and height in both of the hot dry formations tested. A stronger effect is observed only for fracture width in the granite formation.
(6) The results of the Mogilno-Łódź hot dry rock model indicate that using similar fracturing operation parameters to those used in the Groß Schönebeck project, similar fracture geometry results can be obtained. However, in the case of the Karkonosze Mountains area, the obtained results should be considered a preliminary approximation due to software limitations, especially the disregarding of natural fracture stimulation.

**Author Contributions:** Conceptualization, literature review, investigation, manuscript writing, manuscript editing, visualization, R.M.; investigation, manuscript editing, manuscript review, supervision, K.L.; manuscript editing, manuscript review, supervision, P.K. All authors have read and agreed to the published version of the manuscript.

**Funding:** This paper is based on research carried out at the Silesian University of Technology and the Oil and Gas Institute—National Research Institute (Poland) as a part of the implementation of doctorate program RJO/SDW/005-33, founded by the Ministry of Science and Higher Education of Poland.

**Data Availability Statement:** The data presented in this study are available on request from the corresponding author.

**Conflicts of Interest:** The authors declare no conflicts of interest.

## Nomenclature

| | |
|---|---|
| HDR | Hot dry rock |
| EGS | Enhanced geothermal system |
| HF | Hydraulic fracturing |

| | |
|---|---|
| $E/E_{stat}/E_{dyn}$ | Young's modulus in general/static/dynamic, Pa |
| $\upsilon/\upsilon_{stat}/\upsilon_{dyn}$ | Poisson ratio in general/static/dynamic, dimensionless |
| $K$ | Bulk modulus, Pa |
| $G$ | Shear modulus, Pa |
| $\sigma$ | Stress, Pa |
| $\varepsilon$ | Strain, m/m |
| $\sigma_V$ | Vertical principal stress, Pa |
| $\sigma_H$ | Maximum horizontal stress, Pa |
| $\sigma_h$ | Minimum horizontal stress, Pa |
| $\rho$ | Bulk density, g/cm$^3$ |
| $V_P$ | Compressional wave velocity, m/s |
| $V_S$ | Shear wave velocity, m/s |
| BI | Brittleness index, % |

## References


1. Lu, S.-M. A global review of enhanced geothermal system (EGS). *Renew. Sustain. Energy Rev.* **2018**, *81*, 2902–2921. [CrossRef]
2. Lei, Z.; Zhang, Y.; Zhang, S.; Shi, Y. Numerical study of hydraulic fracturing treatments and geothermal energy extraction from a naturally fractured granitic formation. *Geothermics* **2023**, *111*, 102692. [CrossRef]
3. Tester, J.; Anderson, B.; Batchelor, A.; Blackwell, D.D.; DiPippo, R.; Drake, E.M.; Garnish, J.; Livesay, B.; Moore, M.C.; Nichols, K.; et al. *The Future of Geothermal Energy-Impact of Enhanced Geothermal Systems (EGS) on the United States in the 21st Century*; Massachusetts Institute of Technology: Cambridge, MA, USA, 2006.
4. Brown, D.W.; Duchane, D.V.; Heiken, G.; Hriscu, V.T. *Mining the Earth's Heat: Hot Dry Rock Geothermal Energy*; Springer: Berlin/Heidelberg, Germany, 2018. [CrossRef]
5. Olasolo, P.; Juárez, M.C.; Morales, M.P.; D'Amico, S.; Liarte, I.A. Enhanced geothermal systems (EGS): A review. *Renew. Sustain. Energy Rev.* **2016**, *56*, 133–144. [CrossRef]
6. Duffield, R.; Nunz, G.; Smith, M.; Wilson, M. *Hot Dry Rock Geothermal Energy Development Program Annual Report, Fiscal Year 1980*; Los Alamos National Laboratory: Los Alamos, NM, USA, 1980. [CrossRef]
7. Norbeck, J.H.; McClure, M.W.; Horne, R.N. Field observations at the Fenton Hill enhanced geothermal system test site support mixed-mechanism stimulation. *Geothermics* **2018**, *74*, 135–149. [CrossRef]
8. Wakahama, H.; Mitoa, S.; Ohsumi, T.; Ueda, A.; Yajima, T.; Satoh, H.; Sugiyama, K.; Ozawa, A.; Ajima, S.; Todaka, N.; et al. A concept of $CO_2$ georeactor sequestration at the Ogachi HDR site, NE Japan. *Energy Procedia* **2009**, *1*, 3683–3689. [CrossRef]
9. Hogarth, R.; Holl, H.G. Lessons learned from the Habanero EGS project. *GRC Trans.* **2017**, *41*, 865–877.
10. Legarth, B.; Huenges, E.; Zimmermann, G. Hydraulic fracturing in a sedimentary geothermal reservoir: Results and implications. *Int. J. Rock Mech. Min. Sci.* **2005**, *42*, 1028–1041. [CrossRef]
11. Zimmermann, G.; Moeck, I.; Blöcher, G. Cyclic waterfrac stimulation to develop an enhanced geothermal system (EGS)—Conceptual design and experimental results. *Geothermics* **2010**, *39*, 59–69. [CrossRef]
12. Blöcher, G.; Reinsch, T.; Henninges, J.; Milsch, H.; Regenspurg, S.; Kummerow, J.; Francke, H.; Kranz, S.; Saadat, A.; Zimmermann, G.; et al. Hydraulic history and current state of the deep geothermal reservoir Groß Schönebeck. *Geothermics* **2016**, *63*, 27–43. [CrossRef]
13. Baujard, C.; Genter, A.; Dalmais, E.; Maurer, V.; Hehn, R.; Rosillette, R.; Vidal, J.; Schmittbuhl, J. Hydrothermal characterization of wells GRT-1 and GRT-2 in Rittershoffen, France: Implications on the understanding of natural flow systems in the Rhine Graben. *Geothermics* **2017**, *65*, 255–268. [CrossRef]
14. Vidal, J.; Genter, A. Overview of naturally permeable fractured reservoirs in the central and southern Upper Rhine Graben: Insights from geothermal wells. *Geothermics* **2018**, *74*, 57–73. [CrossRef]
15. Park, S.; Kim, K.-I.; Xie, L.; Yoo, H.; Min, K.B.; Kim, M.; Yoon, B.; Kim, K.Y.; Zimmermann, G.; Guinot, F.; et al. Observations and analyses of the first two hydraulic stimulations in the Pohang geothermal development site, South Korea. *Geothermics* **2020**, *88*, 101905. [CrossRef]
16. Moska, R.; Labus, K.; Kasza, P. Hydraulic fracturing in enhanced geothermal systems—Field, tectonic and rock mechanics conditions—A review. *Energies* **2021**, *14*, 5725. [CrossRef]
17. Moska, R.; Labus, K.; Kasza, P.; Moska, A. Geothermal potential of hot dry rock in south-east Baltic Basin countries—A review. *Energies* **2023**, *16*, 1662. [CrossRef]
18. Moska, R.; Labus, K.; Kasza, P. Dynamic elastic properties, petrophysical parameters and brittleness of hot dry rocks from prospective areas of Central Europe. *Adv. Geo-Energy Sci.* **2024**, *14*, 90–105. [CrossRef]

19. Li, S.; Wang, S.; Tang, H. Stimulation mechanism and design of enhanced geothermal systems: A comprehensive review. *Renew. Sustain. Energy Rev.* **2022**, *155*, 111914. [CrossRef]
20. McClure, M.W.; Horne, R.N. An investigation of stimulation mechanisms in enhanced geothermal systems. *Int. J. Rock. Mech. Min. Sci.* **2014**, *72*, 242–260. [CrossRef]
21. Zhang, Q.; Zhang, X.-P.; Sun, W. A review of laboratory studies and theoretical analysis for the interaction mode between induced hydraulic fractures and pre-existing fractures. *J. Nat. Gas. Sci. Eng.* **2021**, *86*, 103719. [CrossRef]
22. Dixit, N.C.; Hanks, C.L.; Wallace, W.K.; Ahmadi, M.; Awoleke, O. In situ stress variations associated with regional changes in tectonic setting, northeastern Brooks Range and eastern North Slope of Alaska. *AAPG Bull.* **2017**, *101*, 343–360. [CrossRef]
23. Economides, M.J.; Nolte, K.G. *Reservoir Stimulation*, 3rd ed.; Wiley: Chichester, UK; New York, NY, USA, 2000.
24. Rickman, R.; Mullen, M.; Petre, E.; Grieser, W.V.; Kundert, D. A practical use of shale petrophysics for stimulation design optimization: All shale plays are not clones of the Barnett shale. In Proceedings of the SPE Annual Technical Conference and Exhibition, Denver, CO, USA, 21–24 September 2008. [CrossRef]
25. Masłowski, M.; Kasza, P.; Czupski, M.; Wilk, K.; Moska, R. Studies of fracture damage caused by the proppant embedment phenomenon in shale rock. *Appl. Sci.* **2019**, *9*, 2190. [CrossRef]
26. Masłowski, M.; Labus, M. Preliminary studies on the proppant embedment in Baltic Basin shale rock. *Rock. Mech. Rock. Eng.* **2021**, *54*, 2233–2248. [CrossRef]
27. Shen, S.; Gao, Y.; Jia, L. A Comparison of the relationship between dynamic and static rock mechanical parameters. *Appl. Sci.* **2024**, *14*, 4487. [CrossRef]
28. Zoback, M. *Reservoir Geomechanics*; Cambridge University Press: Cambridge, UK, 2007.
29. AL-Ameri, W.A.; Abdulraheem, A.; Mahmoud, M. Long-term effects of $CO_2$ sequestration on rock mechanical properties. *J. Energy Resour. Technol.* **2016**, *138*, 012201. [CrossRef]
30. Moska, R. Wpływ oddziaływania $CO_2$ na dynamiczne parametry geomechaniczne w systemie geotermalnym. *Nafta-Gaz* **2023**, *79*, 199–212. [CrossRef]
31. Grieser, B.; Bray, J. Identification of Production Potential in Unconventional Reservoirs. In Proceedings of the Production and Operations Symposium, Oklahoma, OK, USA, 31 March–3 April, 2007. [CrossRef]
32. Brotons, V.; Tomás, R.; Ivorra, S.; Grediaga, A. Relationship between static and dynamic elastic modulus of calcarenite heated at different temperatures: The San Julián's stone. *Bull. Eng. Geol. Environ.* **2014**, *73*, 791–799. [CrossRef]
33. Davarpanah, S.M.; Ván, P.; Vásárhelyi, B. Investigation of the relationship between dynamic and static deformation moduli of rocks. *Geomech. Geophys. Geo-Energy Geo-Resour.* **2020**, *6*, 29. [CrossRef]
34. Eissa, E.A.; Kazi, A. Relation between static and dynamic Young's moduli of rocks. *Int. J. Rock. Mech. Min. Sci. Geomech. Abstr.* **1988**, *25*, 479–482. [CrossRef]
35. Brotons, V.; Tomás, R.; Ivorra, S. Improved correlation between the static and dynamic elastic modulus of different types of rocks. *Mater. Struct.* **2016**, *49*, 3021–3037. [CrossRef]
36. Bukowska, M.; Kasza, P.; Moska, R.; Jureczka, J. The Young's modulus and Poisson's ratio of hard coals in laboratory tests. *Energies* **2022**, *15*, 2477. [CrossRef]
37. Meller, C.; Ledésert, B. Is there a link between mineralogy, petrophysics, and the hydraulic and seismic behaviors of the Soultz-sous-Forêts granite during stimulation? A review and reinterpretation of petro-hydromechanical data toward a better understanding of induced seismicity and fluid flow. *J. Geophys. Res. Solid. Earth* **2017**, *122*, 9755–9774. [CrossRef]
38. Villeneuve, M.; Heap, M.; Kushnir, A.; Qin, T.; Baud, P.; Zhou, G.; Xu, T. Estimating in situ rock mass strength and elastic modulus of granite from the Soultz-sous-Forêts geothermal reservoir (France). *Geotherm. Energy* **2018**, *6*, 11. [CrossRef]
39. Al-Shayea, N.A. Effects of testing methods and conditions on the elastic properties of limestone rock. *Eng. Geol.* **2004**, *74*, 139–156. [CrossRef]
40. Lama, R.D.; Vutukuri, V.S. *Handbook on Mechanical Properties of Rocks*; Trans Tech Publications: Clausthal-Zellerfeld, Germany, 1978; Volume II.
41. Yadali Jamaloei, B. A critical review of common models in hydraulic-fracturing simulation: A practical guide for practitioners. *Theor. Appl. Fract. Mech.* **2021**, *113*, 102937. [CrossRef]
42. Legarth, B.; Tischner, T.; Huenges, E. Stimulation experiments in sedimentary, low-enthalpy reservoirs for geothermal power generation, Germany. *Geothermics* **2003**, *32*, 487–495. [CrossRef]
43. Zimmermann, G.; Reinicke, A. Hydraulic stimulation of a deep sandstone reservoir to develop an enhanced geothermal system: Laboratory and field experiments. *Geothermics* **2010**, *39*, 70–77. [CrossRef]
44. Lei, Z.; Zhang, Y.; Zhang, S.; Fu, L.; Hu, Z.; Yu, Z.; Li, L.; Zhou, J. Electricity generation from a three-horizontal-well enhanced geothermal system in the Qiabuqia geothermal field, China: Slickwater fracturing treatments for different reservoir scenarios. *Renew. Energy* **2020**, *145*, 65–83. [CrossRef]
45. Guo, T.; Gong, F.; Wang, X.; Lin, Q.; Qu, Z.; Zhang, W. Performance of enhanced geothermal system (EGS) in fractured geothermal reservoirs with $CO_2$ as working fluid. *Appl. Therm. Eng.* **2019**, *152*, 215–230. [CrossRef]

46. Guo, T.; Tang, S.; Liu, S.; Liu, X.; Zhang, W.; Qu, G. Numerical simulation of hydraulic fracturing of hot dry rock under thermal stress. *Eng. Fract. Mech.* **2020**, *240*, 107350. [CrossRef]
47. Aliyu, M.D.; Archer, R.A. Numerical simulation of multifracture HDR geothermal reservoirs. *Renew. Energy* **2021**, *164*, 541–555. [CrossRef]
48. Cheng, Q.; Wang, X.; Ghassemi, A. Numerical simulation of reservoir stimulation with reference to the Newberry EGS. *Geothermics* **2019**, *77*, 327–343. [CrossRef]
49. Xue, Z.; Wei, Z.; Ma, H.; Sun, Z.; Lu, C.; Chen, Z. Exploring the role of fracture networks in enhanced geothermal systems: Insights from integrated thermal-hydraulic-mechanical-chemical and wellbore dynamics simulations. *Renew. Sustain. Energy Rev.* **2025**, *215*, 115636. [CrossRef]
50. Ulusay, R.; Hudson, J. *The Complete ISRM Suggested Methods for Rock Characterization, Testing and Monitoring:1974–2006*; ISRM Turkish National Group: Ankara, Turkey, 2007.
51. Gentier, S.; Rachez, X.; Dezayes, C.; Blaisonneau, A.; Genter, A. How to understand the effect of the hydraulic stimulation in term of hydro-mechanical behavior at Soultz-sous-Forêts (France)? *GRC Trans.* **2005**, *29*, 159–166.
52. Schindler, M.; Baumgärtner, J.; Gandy, T.; Hauffe, P.; Hettkamp, T.; Menzel, H.; Penzkofer, P.; Teza, D.; Tischner, T.; Wahl, G. Successful hydraulic stimulation techniques for electric power production in the Upper Rhine Graben, Central Europe. In Proceedings of the World Geothermal Congress, Bali, Indonesia, 25–30 April 2010.
53. Bujakowski, W.; Barbacki, A.; Miecznik, M.; Pająk, L.; Skrzypczak, R. A structural-thermal model of the Karkonosze Pluton (Sudetes Mountains, SW Poland) for Hot Dry Rock (HDR) geothermal use. *Arch. Min. Sci.* **2016**, *61*, 917–935. [CrossRef]
54. Lógó, A.; Vásárhelyi, B. Theoretical Relationship between the Confining Pressure and Poisson's Ratio of Intact Rock. *Period. Polytech. Civ. Eng.* **2022**, *66*, 1114–1121. [CrossRef]
55. Molina, O.; Vilarrasa, V.; Zeidouni, M. Geologic carbon storage for shale gas recovery. *Energy Procedia* **2017**, *114*, 5748–5760. [CrossRef]
56. Lake, L. *Petroleum Engineering Handbook*; Society of Petroleum Engineers: Richardson, TX, USA, 2007.
57. Bourbié, T.; Coussy, O.; Zinszner, B. *Acoustics of Porous Media*; Editions Technip: Paris, France, 1987.
58. Yang, S.; Tian, W.; Elsworth, D.; Wang, J.G.; Fan, L.F. An Experimental Study of Effect of High Temperature on the Permeability Evolution and Failure Response of Granite Under Triaxial Compression. *Rock. Mech. Rock. Eng.* **2019**, *53*, 4403–4427. [CrossRef]
59. Guo, L.; Zhang, Y.; Zhang, Y.; Yu, Z.; Zhang, J. Experimental investigation of granite properties under different temperatures and pressures and numerical analysis of damage effect in enhanced geothermal system. *Ren. Energy* **2018**, *126*, 107–125. [CrossRef]
60. Paul, S.; Chattopadhyaya, S.; Raina, A.K.; Sharma, S.; Li, C.; Zhang, Y.; Kumar, A.; Tag-Eldin, E. A Review on the Impact of High-Temperature Treatment on the Physico-Mechanical, Dynamic, and Thermal Properties of Granite. *Sustainability* **2022**, *14*, 14839. [CrossRef]
61. Waliy, F.; Buntoro, A.; Lukmana, A.H.; Rahma, A.A. *The Effect of Poisson's Ratio and Young's Modulus on Fracture Geometry of 2D Model PKN: Case Study of Unconventional Reservoir*; IATMI: Jakarta, Indonesia, 2020.
62. Suryadinata, M.D.; Ratnaningsih, D.R.; Ariadi, I.K.; Waliy, F.; Nugroho, W.A. Rock mechanics effect on fracture geometry and dimensionless fracture conductivity of 2D model KGD (Khristianovic-Geertsma-de Klerk) in Air Benakat formation, Meruap field. *Int. J. Pet. Gas. Explor. Manag.* **2021**, *5*, 1–14.
63. Osman, T.; Bilgesu, H.I. Impact of Geo-Mechanical Properties on the Fracture Treatment of Utica Shale. In Proceedings of the SPE Eastern Regional Meeting, Morgantown, WV, USA, 13–15 October 2015. [CrossRef]
64. Fernando, B.F.; Wellington, C.; Braga, M.B.; Bothelho, M.O.A.; Freitas, A.C.D.; Braga, L.F.Q.F.; Frota, R.A. Hydraulics and geomechanics parameters for hydraulic fracturing optimization in production's developments of shale gas/shale oil in North America. *J. Pet. Environ. Biotechnol.* **2020**, *11*, 399. [CrossRef]
65. Ngoma, M.C.; Kolawole, O.; Olorode, O. Geothermo-mechanical alterations due to heat energy extraction in enhanced geothermal systems: Overview and prospective directions. *Deep Undergr. Sci. Eng.* **2024**, *3*, 256–268. [CrossRef]